

ALTERATION OF MICRORNA EXPRESSION FOLLOWING
TRAUMATIC SPINAL CORD INJURY: PATHOPHYSIOLOGY AT THE
TRANSCRIPTOME LEVEL

by

Mustafa Nadi

Submitted in partial fulfilment of the requirements
for the degree of Doctor of Philosophy

at

Dalhousie University
Halifax, Nova Scotia
September 2022

© Copyright by Mustafa Nadi, 2022

DEDICATION

To my parents, to my wife Tahani Ahmad and to my three little daughters

Razan, Serene, and Leen.

TABLE OF CONTENTS

| | |
|--|------|
| LIST OF TABLES | vii |
| LIST OF FIGURES | viii |
| ABSTRACT | xi |
| LIST OF ABBREVIATIONS USED | xii |
| ACKNOWLEDGEMENT | xiv |
| CHAPTER 1 : INTRODUCTION | 1 |
| 1.1 Overview | 1 |
| 1.2 Demographic and economic effects | 2 |
| 1.3 Minocycline as a neuroprotective agent | 4 |
| 1.3.1 Minocycline chemical structure and history of development: | 5 |
| 1.3.2 Mechanisms of action: | 5 |
| 1.3.2.1 Anti-apoptotic mechanisms: | 5 |
| 1.3.2.2 Modulation of inflammatory processes: | 6 |
| 1.3.2.3 Matrix metalloproteases (MMP): | 7 |
| 1.3.2.4 Antioxidant effects: | 7 |
| 1.3.2.5 Anti-glutamate effect: | 7 |
| 1.3.2.6 Other neuroprotective mechanisms: | 7 |
| 1.4 Anatomy and neurophysiology of the spinal cord | 8 |
| 1.5 Differences between the human SCI in clinical situations and the animal models in research | 10 |
| 1.6 Animal models of spinal cord injury in research | 12 |
| 1.6.1 Contusion models: | 13 |
| 1.6.2 Compression model: | 16 |
| 1.6.3 Transection model: | 17 |
| 1.6.4 Distraction models: | 18 |
| 1.6.5 Chemical models: | 19 |
| 1.7 Spinal cord injury pathophysiology | 19 |
| 1.7.1 Primary injury | 22 |
| 1.7.1.1 Phase description: | 22 |
| 1.7.1.2 Dissemination of primary effects and transition to the secondary phase... .. | 23 |
| 1.7.2 Secondary spinal cord injury (sSCI) | 24 |
| 1.7.2.1 Acute sSCI cellular and molecular events: | 24 |

| | |
|--|-----------|
| 1.7.2.2 Subacute stage:..... | 29 |
| 1.7.2.3 Chronic stage: | 30 |
| 1.8 Gene expression following SCI | 30 |
| 1.9 MicroRNAs (miRNAs)..... | 31 |
| 1.9.1 Ribonucleic Acid (RNA) Classification | 31 |
| 1.9.2 Biogenesis of miRNA | 33 |
| 1.9.2.1 Nuclear stage:..... | 33 |
| 1.9.2.2 Cytosolic Stage: | 35 |
| 1.9.3 MicroRNA biogenesis regulation: | 36 |
| 1.9.4 Non-canonical miRNA producing pathways..... | 38 |
| 1.10 Alteration of miRNA following tSCI | 39 |
| 1.10.1 The role of miRNA in the normal SC and nervous system pathologies | 39 |
| 1.10.2 The role of miRNAs in tSCI | 39 |
| 1.11 The practical role of miRNA in clinical situations: | 42 |
| 1.11.1 miRNA as diagnostic biomarkers for SCI: | 42 |
| 1.11.2 Potential therapeutic application:..... | 42 |
| 1.12 Aims of the study | 43 |
| CHAPTER 2 : MICRO RNA EXPRESSION FOLLOWING SCI AND AFTER MINOCYCLINE ADMINISTRATION..... | 44 |
| 2.1 Introduction..... | 44 |
| 2.2 Materials and Methods..... | 45 |
| 2.2.1 Animals and ethical approval..... | 45 |
| 2.2.2 Experimental Design..... | 45 |
| 2.2.3 Surgical procedures and setup | 47 |
| 2.2.4 Recovery and post-operative care:..... | 49 |
| 2.2.5 Preparation and administration of minocycline: | 50 |
| 2.2.6 RNA extraction and quality control..... | 51 |
| 2.2.7 Library preparation and miRNA deep sequencing: | 52 |
| 2.2.8 miRNA quantification and differential analysis | 52 |
| 2.2.9 Validating the results of miRNA Deep Sequencing and identification of miRNAs function | 53 |
| 2.2.10 RT-qPCR and ddPCR (Real time – quantitative polymerase chain reaction and droplet digital PCR) | 54 |

| | |
|--|----|
| 2.2.11 Statistical analysis..... | 56 |
| 2.3 Results..... | 57 |
| 2.3.1 Next generation sequencing (NGS):..... | 57 |
| 2.3.2 Principal component analysis (PCA):..... | 57 |
| 2.3.3 Heat maps and volcano plots:..... | 60 |
| 2.3.4 Identification of miRNAs 1 day (acute phase) following the SCI by Next Generation Sequencing (NGS)..... | 60 |
| 2.3.6 Criteria of miRNA selection for confirmation in the 1d group | 68 |
| 2.3.7 Criteria of miRNA selection for confirmation in 7d group | 74 |
| 2.3.8 Validation processes of primers sets for RT-qPCR and ddPCR experiment... | 75 |
| 2.3.9 RT-qPCR and ddPCR for the 1d survival group | 76 |
| 2.3.10 RT-qPCR and ddPCR for 7d survival group (subacute)..... | 78 |
| 2.3.11 Testing the levels of miR-21a-5p and miR-15b-5p in 7d samples | 80 |
| 2.3.12 Were all animals in the experiments exposed to a similar injury impact?..... | 81 |
| 2.4 Discussion and interpretation..... | 83 |
| CHAPTER 3 : IDENTIFICATION OF THE ROLE OF miR21a-5p AND miR15b-5p FOLLOWING SCI IN CELLULAR PATHWAYS. | 89 |
| 3.1 Introduction..... | 89 |
| 3.2 Materials and Methods..... | 90 |
| 3.2.1 Identification of miRNAs target genes and their functions | 90 |
| 3.2.2 Animals And Research Approval | 91 |
| 3.2.3 Experimental Design..... | 91 |
| 3.2.4 Surgeries | 91 |
| 3.2.5 Protein Extraction | 91 |
| 3.2.6 Western blotting..... | 92 |
| 3.2.7 Blots reading and statistical analysis | 93 |
| 3.3 Results..... | 94 |
| 3.3.1 Identification of miR-21a-5p and miR-15b-5p target genes and identification of their functions:..... | 94 |
| 3.3.2 Testing the changes in the expression levels of target proteins | 96 |
| 3.3.3 SCI impact parameters..... | 98 |
| 3.4 Discussion and interpretation..... | 98 |

| | |
|---|-----|
| CHAPTER 4 : POTENTIAL EFFECTS OF DOWNREGULATED miRNA ON THE TARGETED NEURONAL SURVIVAL PATHWAYS | 100 |
| 4.1 Introduction..... | 100 |
| 4.2 Materials and methods | 101 |
| 4.2.1 Mice and Ethics Approval | 101 |
| 4.2.2 Operative procedures | 101 |
| 4.2.3 Spinal cord harvesting and preparation..... | 101 |
| 4.2.4 Fluoro-Jade C staining and Hoechst nuclear counter staining..... | 103 |
| 4.2.5 Double labelling with immunohistochemistry nuclear anti-neuN antibody and fluoro-Jade C staining: | 103 |
| 4.2.6 Double labelling with immunohistochemistry anti-GFAP antibody and fluoro-Jade C staining: | 104 |
| 4.2.7 Imaging, histological quantification and analysis..... | 105 |
| 4.3 Results..... | 106 |
| 4.3.1 Fluoro-Jade C staining and Hoechst nuclear counter staining..... | 106 |
| 4.3.2 Double labelling with immunohistochemistry nuclear anti-neuN antibody and fluoro-Jade C staining: | 108 |
| 4.3.3 Double labeling with immunohistochemistry anti-GFAP antibody and fluoro-Jade C staining: | 109 |
| 4.3.4 Quantification analysis..... | 110 |
| 4.3.5 SCI impact parameters..... | 111 |
| 4.4 Discussion and interpretation..... | 112 |
| CHAPTER 5 : DISCUSSION..... | 114 |
| 5.1 Global miRNA pattern changes:..... | 115 |
| 5.2 miR-21a-5p: | 117 |
| 5.3 miR-15b-5p..... | 118 |
| 5.4 Lessons learned and future directions from this project: | 119 |
| 5.5 Conclusion | 120 |
| REFERENCES | 122 |
| APPENDIX A: COPYRIGHT AGREEMENT LETTER | 145 |
| APPENDIX B: SUPPLEMENTARY FIGURES AND TABLES OF CHAPTER 2 | 146 |
| APPENDIX C: SUPPLEMENTARY FIGURES AND TABLE OF CHAPTER 3 | 172 |
| APPENDIX D: SUPPLEMENTARY FIGURES OF CHAPTER 4..... | 184 |

LIST OF TABLES

| | |
|--|-----|
| Table 1.1 Stages of secondary spinal cord injury | 20 |
| Table 1.2 The size and function of different types of RNAs | 32 |
| Table 2.1 The reagents and the primers that were used in RT-qPCR and ddPCR experiments to validate the NGS findings. | 56 |
| Table 2.2 The 48 miRNA that changed by SCI and minocycline | 73 |
| Table 2.3 The subsets of miRNAs and their targets in 1 day and 7-day groups..... | 75 |
| Table 3.1 The miR-21a-5p and miR-15b-5p filtered targets by DAVID. | 95 |
| Table B-1 Significantly Expressed miRNAs in SCI+SLN vs no SCI experimental conditions in the 1d group..... | 158 |
| Table B-2 Significantly Expressed Novel miRNAs in SCI+SLN vs no SCI conditions in the 1d group..... | 162 |
| Table B-3 Significantly Expressed miRNAs in SCI+mino VS SCI+SLN conditions in the 1d group. | 163 |
| Table B-4 Significantly Expressed Novel miRNAs in SCI+mino vs SCI+SLN conditions 1d group..... | 166 |
| Table B-5 Significantly Expressed miRNA in SCI+mino vs no SCI conditions in the 1d group. | 167 |
| Table B-6 Significantly Expressed Novel miRNA in SCI+mino vs no SCI conditions at the 1d timepoint. | 168 |
| Table B-7 known miRNA in SCI+mino vs SCI+SLN condition at the 7d timepoint. ... | 169 |
| Table B-8 Novel miRNA in SCI+mino vs SCI+SLN conditions at the 7d timepoint.... | 170 |
| Table B-9 The 29 miRNAs that were excluded because they were not from the miRNAs that were found the miRNA in SCI+SLN compared to baseline. | 171 |
| Table C-1 The reagents that were used in western blot experiments | 183 |

LIST OF FIGURES

| | |
|---|----|
| Figure 1.1 Comparative anatomy of the rodent and human spinal cord cross-section. | 10 |
| Figure 1.2 Data recorded by the Infinite Horizon Spinal Cord Impactor. | 15 |
| Figure 1.3 Summary of traumatic spinal cord injury phases. | 22 |
| Figure 1.4 Biogenesis and fade of miRNA-nuclear and cytoplasmic events. | 35 |
| Figure 2.1 Experimental Design including Next Generation Sequencing, protein expression testing (western blot) and histology experiments. <i>Nadi, 2020</i> | 47 |
| Figure 2.2 Principal Component Analysis (PCA) for 1d timepoint group. | 58 |
| Figure 2.3 PCA3 vs PCA4 for 7d group. | 59 |
| Figure 2.4 Simplified heatmap: no SC vs SCI+SLN 1d demonstrating the changes of miRNAs after one day of SCI. | 61 |
| Figure 2.5 Volcano plot: SCI+SLN vs no SCI 1d illustrates the fold of changes and the magnitude of miRNA alteration after one day of SCI. | 62 |
| Figure 2.6 Simplified heatmap: SCI+mino vs SCI+SLN 1d demonstrating the miRNA changes after minocycline administration in comparison to SCI with saline control. | 63 |
| Figure 2.7 Volcano plot: SCI+mino vs SCI+SLN 1d illustrates the fold of changes and the magnitude of miRNA changes after minocycline administration measured one day after SCI. | 64 |
| Figure 2.8 Simplified heatmap: SCI+mino vs noSCI 1d demonstrates the miRNA pattern changes following minocycline administration in comparison to no SCI condition after 1d of SCI. | 65 |
| Figure 2.9 Volcano plot: SCI+mino vs noSCI 1d illustrates the miRNA pattern changes following minocycline administration in comparison to no SCI condition after 1d of SCI. | 66 |
| Figure 2.10 Simplified heatmap: SCI+SLN vs SCI+mino 7d demonstrates the changes of miRNA expression following minocycline administration and SCI (treatment) in comparison to SCI+ saline (control) tested 7 days after SCI. | 67 |
| Figure 2.11 Volcano plot: SCI+SLN vs SCI+mino 7d illustrates the magnitude and fold changes of miRNA expression following minocycline administration and SCI (treatment) in comparison to SCI+ saline (control) tested 7 days after SCI. | 68 |
| Figure 2.12 Criteria for miRNA selection in the 1d group. | 69 |
| Figure 2.13 Criteria for miRNA selection 7d group. | 74 |
| Figure 2.14 RT-qPCR miRNA results in 1d. | 77 |
| Figure 2.15 Droplet digital PCR miRNA results in 1d group. | 78 |

| | |
|---|-----|
| Figure 2.16 RT-qPCR miRNA results in 7d..... | 79 |
| Figure 2.17 ddPCR miRNA results in 7d | 80 |
| Figure 2.18 RT-qPCR for miR21a-5p&15b-5p in 7d..... | 81 |
| Figure 2.19 Actual force and SC displacement in 1d and 7d groups..... | 83 |
| Figure 3.1 A simplified illustration of filtered mi-R21a-5p targets in Jak-STAT pathway | 95 |
| Figure 3.2 Protein levels in 1d survival SCI+SLN and SCI+mino..... | 97 |
| Figure 4.1 Spinal cord specimen collected 1d after the injury. | 102 |
| Figure 4.2 Spinal cord cross section at low magnification stained with FJC stain..... | 105 |
| Figure 4.3 Fluoro - Jade C and Hoechst nuclear counter stain in three different experimental conditions. | 107 |
| Figure 4.4 Anti-neuN immunohistochemistry and FJC stains in three different experimental conditions. | 108 |
| Figure 4.5 Anti-GFAP immunohistochemistry and FJC stains in three different experimental conditions. | 110 |
| Figure 4.6 Comparison of Fluoro-Jade C positive cells in SCI+SLN and SCI+mino.... | 111 |
| Figure B1. Surgical room set up. | 146 |
| Figure B2. PCA-1 vs PCA2 of miRNA expression of three experimental conditions in the 7d group | 147 |
| Figure B3. PCA2 vs PCA3 of miRNA expression of three experimental conditions in the 7d group. | 148 |
| Figure B4. PCA3 vs PCA4 of miRNA expression of three experimental conditions in the 7d group. | 149 |
| Figure B5. PCA1 vs PCA2 of miRNA expression of two experimental conditions in the 7d group. | 150 |
| Figure B6. PCA2 vs PCA3 of miRNA expression of two experimental conditions in the 7d group. | 151 |
| Figure B7. Heatmap: no SCI vs SCI+SLN 1d demonstrating the changes of miRNAs after one day of SCI. | 152 |
| Figure B8. Heatmap: SCI+mino vs SCI+SLN 1d demonstrating the miRNA changes after minocycline administration in comparison to SCI with saline control | 153 |
| Figure B9. Heatmap: SCI+mino vs noSCI 1d demonstrates the miRNA pattern changes following minocycline administration in comparison to no SCI condition after 1d of SCI..... | 154 |

| | |
|---|-----|
| Figure B10. Heatmap: SCI+SLN vs SCI+mino 7d demonstrates the changes of miRNA expression following minocycline administration and SCI (treatment) in comparison to SCI+ saline (control)tested 7 days after SCI. | 155 |
| Figure B11. Efficiency curve in the 1d group RT-qPCR validation experiments. | 156 |
| Figure B12. Efficiency curve in the 7d group RT-qPCR validation experiments. | 157 |
| Figure C1. List of genes miR-21-5p uploaded to DAVID software..... | 172 |
| Figure C2. DAVID_ Functional Annotation Tools miR-21-5p – step 1 | 173 |
| Figure C3. DAVID_ Functional Annotation Result Summary miR-21-5p – step 2..... | 174 |
| Figure C4. DAVID output – step 3..... | 175 |
| Figure C5. Pathway miR-21-5p – step 4..... | 176 |
| Figure C6. miR-15b-5p target analysis - uploaded targets to DAVID software | 177 |
| Figure C7. miR-15b-5p target analysis – step 1 | 178 |
| Figure C8. miR-15b-5p target analysis – step 2 | 179 |
| Figure C9. miR-15b-5p target analysis – step 3 | 180 |
| Figure C10. miR-15b-5p target analysis – step 4 | 181 |
| Figure C11. SCI parameters in proteins experiment-western blot..... | 182 |
| Figure D1. SCI parameters in histology experiments..... | 184 |

ABSTRACT

Spinal cord injury (SCI) imparts permanent neurological deficits and devastates many patients' lives. The current management is not curative but focuses on blood pressure optimization, spinal cord (SC) decompression, spinal column stabilization, and rehabilitation.

Despite progress in our understanding of the pathophysiological events that occur after the injury, there have been limitations in translating the success of preclinical animal studies into clinical scenarios. Therefore, a deeper understanding of SCI mechanisms is required. The initial impact on the SC results in parenchymal and vascular disruption (primary SCI). A few minutes after the primary SCI, a complex series of biochemical reactions (secondary injury) commence and may continue for several weeks and months. These reactions are regulated by specific sets of genes accompanied by changes in micro-Ribonucleic Acids (miRNAs) that inhibit and regulate gene translation. This thesis sought to understand SCI mechanisms from the perspective of changes to miRNA expression, subsequent impact on miRNA targets, and ultimately histological findings. For the first time, a neuroprotective drug was used to modulate the miRNA changes following the SCI. It was found that SCI results in extensive change in miRNA expression, primarily in the acute stage. Furthermore, administration of minocycline resulted in a further modulation of 81 miRNAs in the acute stage. The miRNAs most predicted to regulate genes participating in survival and apoptotic pathways were pursued. The miR-21a-5p and miR-15b-5p were upregulated by the injury and then downregulated following administration of minocycline. These two miRNAs target Akt, Bcl2, and PI3K genes, which are important for cell survival. An increased expression of these proteins was observed following downregulation of miR-21 and miR-15b. These findings were then correlated with enhanced neuronal survival in the injury penumbra. Modulation of miRNA expression by a neuroprotective agent may highlight the importance of miRNAs in this complex environment following SCI. Adopting such an approach may open novel pathways to potential SCI therapeutics to improve the SC healing process and eventually functional outcome.

LIST OF ABBREVIATIONS USED

| | |
|---------------|--|
| 3UTR | 3'-untranslated region |
| AGO | Argonaut |
| ALS | Amyotrophic lateral sclerosis |
| AMPA | Alpha-Amino-3-Hydroxy-5-Methyl-4-Isloxazole Propionic Acid |
| ASIA | American Spinal Injury Association |
| ATP | Adenosine triphosphate |
| BBB | Basso, Beattie and Bresnahan |
| BP | blood pressure |
| Bp | base pair |
| BSA | Bovine Serum Albumin |
| C | cervical |
| CAM | cell adhesion molecules |
| cDNA | complementary DNA |
| CNS | central nervous system |
| Co | coccygeal |
| COX2 | cyclooxygenase-2 |
| CSF | cerebrospinal fluid |
| CST | corticospinal tract |
| DAVID | D atabase for A nnotation, V isualization, and I ntegrated D iscovery |
| ddPCR | Droplet digital PCR |
| DNA | deoxyribonucleic acid |
| dsRNA | Double strand RNA |
| ECM | extracellular matrix |
| EXP5 | Exportin 5 |
| FJC | Fluoro-Jade C |
| ICU | intensive care unit |
| IHI | Infinite Horizon Impactor |
| IL-1 β | Interleukin 1 beta |
| IP | Intraperitoneal |
| IFN- γ | gamma interferon |
| KEGG | Kyoto Encyclopedia of Genes and Genomes |
| L1 | first lumbar vertebra |
| LPS | lipopolysaccharide |
| MAP2 | microtubule-associated protein 2 |
| MCPIP1 | monocyte chemotactic protein-induced protein 1 |
| miRNA | microRNA |
| MMP9 | metalloproteinase 9 |
| mRNAs | messenger RNAs |

| | |
|--------------|--|
| <i>NF-κB</i> | nuclear factor kappa-light-chain-enhancer of activated B cells |
| Nm | nanometer |
| NMDA | N-methyl-D-aspartate |
| Nt | nucleotide |
| Nts | nucleotides |
| OSU | Ohio State University |
| PBS | phosphate buffered saline |
| PCA | Principal component analysis |
| piRNA | PIWI- interacting RNA |
| PIWI | P-element Induced Wimpy testis in <i>Drosophila</i> |
| Pol II | RNA polymerase II |
| pre-RISC | pre-RNA-induced silencing complex |
| pri-miRNA | primary miRNA |
| PGE2 | Prostaglandin E ₂ |
| Pw | pathway |
| RIN | RNA integrity number |
| RISC | RNA-induced silencing complex |
| RNA | ribonucleic acid |
| Rpm | revolutions per minute |
| RQI | RNA quality indicator |
| RT-qPCR | Real time-quantitative polymerase chain reaction |
| SC | Spinal Cord |
| SCI | Spinal Cord Injury |
| SCI+mino | SCI+ minocycline |
| SCI+SLN | SCI+ saline |
| SCs | Spinal cords |
| SEM | standard error of mean |
| siRNA | small interfering RNA |
| SNPs | Single nucleotide polymorphisms |
| sSCI | secondary SCI |
| T | Thoracic |
| TFs | transcription factors |
| TNF-α | Tumour Necrosis Factor alpha |
| tSCI | Traumatic Spinal Cord Injury |
| TUT | Terminal uridylyl transferases |
| V | Volt |
| W | Watt |

ACKNOWLEDGEMENT

I will forever be thankful to the people who have supported me during this entire journey. This work would not be accomplished without your help.

Dr. Sean Christie (Supervisor): first, I would like to thank you for all your support in this endeavor. Navigating a Ph.D. project in a relatively new field is not a straightforward mission. Things became more complicated when we were hit by the pandemic COVID-19 at the beginning of March 2020. However, you were always there, guiding, supporting, and encouraging me to keep going forward relentlessly. Outside the lab, you have been helping me to balance between my Ph.D. work and maintaining the clinical skills during all these years. I will continuously look back on these years with deep fondness.

Dr. Kazue Semba (Chair of the advisory committee): I can't find the words that express my sincere appreciation for everything you have done for me. You were so supportive, kind, and nurturing me since I started the classes in the 1st year of the program. I will never forget when I was coming to you with a pile of issues, and then leaving your office with a heap of hope, self-confidence, and happiness. Knowing you and being one of your students is a milestone in my life. I will not keep this great experience to myself only, I will pass it to the next generations of students, residents, and researchers.

Dr. Sultan Darvesh (committee member): I enjoyed your classes and teaching style. Whenever you ask a question, I learned from you that the correct answer could be two or three words, and not necessarily to be a half-page. To be concise and complete in doing tasks are skills not easy to emulate. I tried to learn this adroitness from you, and I have been exercising them, but I am not 100% sure that I am there yet. Thank you for all your guidance and unforgettable support.

Dr. Victor Rafuse (committee member): your comprehensive thinking and thoughtful ideas have helped me a lot. Your suggestions have made the project more rounded. I am grateful for all your support, particularly in histology slides production.

Dr. William Baldrige (the head of department of Medical Neuroscience): thank you, Dr. Baldrige, for being around and listening to all graduate students in the department. The departmental discussion platform that you created during the pandemic was really supportive and inclusive.

Dr. Saranyan Pillai, our research associate. I cannot thank you enough for the many things you have helped me with. Thank you for your help in my surgeries, presentations, and preparation for all meetings. Your discussion about the chemistry of the compounds in different stages of the project will not be forgotten. Last but not the least, you were there during COVID closure discussing with me the project and the presentations.

Friends and colleagues: I would like to acknowledge the help of the network of the graduate students and especially Olivier D. Laflamme who helped me to analyze the NGS data. I want to thank other graduate students Gracious Kasheke from the Robertson lab (who helped me count the cells), Jonathan Tjong from the Frampton lab (who helped me with cell counting as well), Alexander Edgar from the Marshall lab, who taught me and supervised my work in ddPCR and RT-qPCR experiments, and Aurelio Lobo from the Robertson lab who taught me the principles of RT-qPCR.

To my parents, my wife Tahani Ahmad, and my three little daughters: Razan, Serene, and Leen. Thank you for tolerating my absence. I had to be there for you. But you were there supporting me and embracing me with love and passion.

CHAPTER 1 : INTRODUCTION

Traumatic Spinal Cord Injury and The Role of miRNA

1.1 Overview

The spinal cord (SC) is a part of the central nervous system that is responsible for transmitting neurological signals to and from the brain and peripheral organs. It also carries on specific functions processed via different neuronal centers within the SC parenchyma such as spinal reflexes and urogenital parasympathetic control. Therefore, SCI can lead to extremely devastating consequences. The sequelae of an acute SCI were first documented in ancient Egypt approximately 4000 years ago (1). However, to this day, there remains no curative treatment for SCI. Current medical and surgical strategies focus on minimizing or treating the ramifications of this injury such as: preventing further SCI from potentially unstable vertebral column by spinal stabilization (1, 2), managing spasticity, bowel and bladder training and rehabilitation, treating the symptoms of sympathetic dysreflexia and lifestyle modifications due to motor and sensory loss. Additionally, SCI results in cardiac, respiratory, psychological, and social consequences that must be considered in the management plan.

In general, there are two main mechanisms implicated in SCI. Firstly, the primary injury mechanism, which is also referred to as the initial impact. This transfer of kinetic energy results in mechanical disruption of spinal cord tissue and its vascular network. The primary impact can be a shearing force, compression and/or contusion (2). Following this the spinal cord experiences a secondary injury mechanism, which is a progressive series of cellular and biochemical events that start after the primary insult. It usually starts a few minutes after the primary injury and may last for many weeks or months. It is also usually responsible for the deterioration in neurological function beginning within 8 to 12 hour of the injury(2).

Presently, research is moving towards finding a curative intervention for SCI (1). The loss in neurological function in SCI patients is directly related to both the primary and secondary insults. From a mechanistic point of view, the secondary injury mechanism is responsible for further deterioration in function and there is more time to intervene to prevent the deleterious pathophysiological changes that occur in this phase. Modulating reactions in this phase may improve the outcome of SCI. In fact, there are several studies that employed novel approaches such as gene therapies, cellular modulation and tissue replacement or engineering to overcome the consequences that preclude re-innervation, axonal reconnection, and neuronal cell regeneration to replace the injured/dead cells following SCI (3). For the past two or three decades, laboratories interested in SCI have extensively studied cytokines, chemokines, calcium, and sodium channel molecular behavior following injury (1, 4, 5). These targets are the downstream products of genes including apoptotic and inflammatory genes that respond to trauma. The translation of messenger RNAs (mRNAs) of these molecules is likely controlled by microRNAs (miRNA) (6). Understanding the miRNA response to injury can further elucidate the molecular reactions that occur after the primary injury and potentially pave the road to discovering therapeutic targets for the treatment of SCI. Thus, further understanding the molecular mechanisms of the spinal cord's response after trauma may facilitate new avenues to explore and implement novel treatment modalities for SCI. Within this thesis I will: first, demonstrate the effect of SCI injury on patients and communities. Secondly, the basic spinal cord anatomy and SCI pathophysiology will be discussed. Lastly, the response of miRNAs following SCI will be explored to demonstrate the importance of studying changes in miRNA expression following SCI, in the hope of exploiting their therapeutic potential in the future.

1.2 Demographic and economic effects

SCI impacts the lives of thousands of people around the world every year. The sequelae of SCI are not limited to the affected individuals, these injuries also impact the quality of life for the patients' family and the economy of the whole society, as well as the healthcare system (3, 7). Although disability is the major consequence, in some patients SCI may result in death. Mortality rates depend on several factors such as patient age,

frailty, comorbidities, multisystem injuries, and level and completeness of injury (cervical SCI results in the highest mortality compared to thoracic or lumbar injuries) (8). The mortality rate for acute in-hospital admission is between 4-17% (8). Severity of SCI also reduces the life expectancy, for example, a 40-year-old patient with an injury below C5 is expected to live at least 23 years after injury, whereas a higher level, ventilator-dependent patient may only be expected to live approximately 8.5 years only (8). However, generalization is difficult due to the retrospective nature of data typically reported in epidemiological manuscripts; as well there is variability in the incidence rates among countries likely due to inherent societal differences (9). With reliable data from Canada, USA, a few countries in Europe and Australia (9, 10), the yearly global incidence of SCI approximates 130,000 cases and the worldwide prevalence approaches 2.5 million (2). In North America, SCI affects more than one million individuals (11) and the yearly incidence in the USA is > 10,000 cases (1, 2), with the majority of them younger than 30 years of age. A recent 2018 estimation by National Spinal Cord Injury Statistical Center, University of Alabama at Birmingham, reported a national incidence > 17,000 cases per year (12). In other words, the global incidence varies between 8 and 246 cases per million individuals per year, while the global prevalence ranges between 236 and 1,298 per million individuals (13). The cost attributed to medical care for each patient approximates US\$1.1 to 4.6 million and is dependent upon level and severity of injury (11). In general, SCI epidemiology demonstrates two peaks, the first in young adults where the injuries result from motor vehicle accidents in 38% of all cases of SCI (1, 11). Other causes of injury in this age group are sport-related and penetrating injuries. The second peak is in the elderly group where SCI usually results from falls and typically occurs in the presence of pre-existing spinal stenosis (11). Statistical analyses demonstrate that falls are responsible for between one-fifth and one-third of SCI cases, although there is again variability from country to country (1, 14, 15). Males are commonly more affected by traumatic SCI (tSCI) (79.8%) than females (20.2%) (16). Cervical level SCI (circa 60%) is more common than thoracic (32%) or lumbar (9%) injuries (16). It is worth noting that during the 1990s the annual expense of surgical and rehabilitation care for SCI in the USA approximated \$4 billion and this figure is significantly much higher today (2). This emphasizes the significant socioeconomic

impact that results from this condition, and the dire need to attain a efficacious therapeutic intervention.

1.3 Minocycline as a neuroprotective agent

Neuroprotection is a broad term primarily referring to strategies that maintain the structural integrity and/or function of neuronal tissue after an insult and may encompass both medical and surgical measures. The insult can be physical, such as SCI, head injury and stroke, or a progressive neurodegenerative disorder such as Huntington's disease and Parkinson's disease(17). Although the span of disorders and insults to neural structures are wide and vary from acute to chronic and from exogenous to endogenous, they share some common pathways that lead to neuronal cell death, such as apoptosis, excitotoxicity, inflammatory cascades, mitochondrial failure, and oxidative stress (17-19). Neuroprotective agents are pharmaceuticals capable of preventing or slowing the rate of neuronal death overtime (minimize secondary injury) or promoting regrowth and function of the insulted neuronal tissues (20).

There are multiple classification schemes for neuroprotectants. Some have classified them according to their role in mechanisms of secondary SCI, such as antioxidants, anti-apoptotic (21), neuro-stimulants (17) or anti-inflammatory (2). Whereas others, recognizing drugs often have multiple sites of action, have approached this more broadly:

1. Agents with protective activities-preserving SC cellular population
2. Medications enhancing neuronal regrowth
3. Medications counteracting inhibitory molecules that hinder spinal cord recovery (1).

This understanding has led to a litany of pharmaceuticals, each utilizing one of more mechanisms, employed to mitigate the impact of SCI. Despite considerable effort, and notable laboratory successes, no drug thus far has gained universal acceptance as a protective treatment following SCI (22-24). Minocycline is one such agent known to modulate multiple pathways of secondary SCI (sSCI) (1, 25-27). Therefore, it was thought that this drug could be a good option to modulate the expression of miRNA in this thesis.

1.3.1 Minocycline chemical structure and history of development:

Minocycline hydrochloride is a semisynthetic, second-generation, derivative of tetracycline (27). In essence, tetracyclines are a group of bacteriostatic antibiotics first discovered in the 1940s as isolates from *Streptomyces* spp. bacteria. This name was dubbed because all members of the group share four hexagonal hydrocarbon rings (27, 28). Minocycline, a lipid-soluble derivative of Tetracycline, has a broader spectrum of action than doxycycline and tetracycline, better CNS penetration, longer half-life (16 hours) and 2-4 times serum levels in comparison to tetracycline. It was patented in 1961 and commercialized at the beginning of the 1970s. It has several biological activities: antimicrobial, anti-inflammatory, antioxidant, anti-apoptotic properties (21, 27). Moreover, it is an approved drug for other disorders such as skin acne (29).

1.3.2 Mechanisms of action:

The positive results of this medication were initially observed in animal models for stroke (27). Subsequent experiments *in vivo* and *in vitro* were conducted by different laboratories to investigate other neurological disorders such as SCI, head injury and neurodegenerative diseases (21). Further observations elucidated its interference at multitude levels of cellular cascades of sSCI.

1.3.2.1 Anti-apoptotic mechanisms:

Minocycline reduces the expression and activation of caspases following CNS insults (27, 30). Broadly speaking, minocycline inhibits the release of pro-apoptotic mediators and enhances the expression of anti-apoptotic molecules as follows:

1. Reduces the activity of caspase-3 in several CNS pathologies including SCI (30-33).
2. Diminishes the swelling depolarization of mitochondria, as well as cytochrome c release from the mitochondria whether Bid or Ca²⁺ dependent (27).
3. Reduction in apoptosis-inducing factor (AIF) release to the cytoplasm as well as its nuclear translocation (34).

4. Increased expression of anti-apoptotic factors and up-regulates Bcl-12 protein and mRNA (35).
5. Up-regulation of the expression of XIAP (X-linked inhibitor of apoptosis protein) which suppresses caspase activation (36).
6. Downregulation of the expression of caspases 1, 3, 7, 8, 9 and 12 below normal levels under normal cellular conditions (27).

1.3.2.2 Modulation of inflammatory processes:

Pro-inflammatory and anti-inflammatory cytokines are typically released following the SCI. Minocycline decreases the production of the pro-inflammatory IL-1 β by reducing expression of caspase-1, which is required for IL-1 β maturation (32, 33). It also minimizes TNF- α mRNA expression by interfering with lipopolysaccharide, which is needed in TNF- α processing (37). Minocycline can alter the expression of the chemokines or their receptors. For instance, minocycline reduces the expression of CXCR3 receptor (38) which is expressed in CD4+ T-helper 1 (Th1) cells, involved in microglia and macrophage activation as well as demyelination (39). Furthermore, minocycline inhibits phospholipase A2 (PLA2) and its multiple isoforms, including cytosolic PLA2 (cPLA2), secretory PLA2 (sPLA2), lipoxygenases and cyclooxygenases (21, 40). *In vivo*, minocycline inhibits PGE2 and COX2 levels in microglia and monocytes (41-44).

Minocycline decreases resident microglia activation. Microglia release chemokines, cytokines, lipid inflammatory compounds as well as different members of matrix metalloproteases (27). Moreover, minocycline diminishes activation of macrophages (27) and astrocytes after CNS insults including SCI (45, 46), which may reduce glial scar formation. Inhibition of microglial pro-inflammatory cytokines reduces their interaction with T-cells (47). Moreover, minocycline reduces microglial activation by inhibiting nuclear translocation of NF-kappa B (43). Of note, this transcription factor is upregulated within 24 hours post-injury and has been implicated in the expression of pro-inflammatory factors and apoptosis (48, 49)

1.3.2.3 Matrix metalloproteases (MMP):

Minocycline has been shown to diminish MMP2 levels in animal models of multiple sclerosis (50). In a cultured T-cell study, minocycline reduced MMP2 and 9 levels and activities that impact T-cell migration (51). It also reduces the expression of MMP12 (52), which increases after mice SCI (53). Minocycline exerts its effect on MMPs via direct interaction with Zn^{2+} which is essential for MMP activities (21).

1.3.2.4 Antioxidant effects:

Minocycline diminishes the production of NO (nitric oxide) after hypoxia in a microglia cell culture (54, 55) as well as macrophages (56). Moreover, it downregulates iNOS (inducible Nitric oxide synthase-2), mRNA expression and protein activity after exposure to pro-inflammatory cytokines (LPS, IFN- γ and IL-1 β) (57). In microglia, minocycline inhibits Zinc and thrombin-induced activation of NADPH oxidase (21). In animal SCI model, it increases expression of glutathione (GSH an antioxidant) (58) and glutathione peroxidase (GSH-Px) in addition to promoting superoxide dismutase (SOD) activity(59).

1.3.2.5 Anti-glutamate effect:

Minocycline acts as a neuroprotective agent by abrogating the toxic glutamate effects via:

1. Chelating metallic ions including Ca^{2+} , Fe^{2+} , Fe^{3+} , Zn^{2+} and Mg^{2+} .
2. Inhibit Calcium influx in via NMDA receptors (60).

1.3.2.6 Other neuroprotective mechanisms:

Minocycline inhibits poly (ADP-ribose) polymerase-1 (PARP-1) enzymatic activity. It is a nuclear enzyme activated after SCI via DNA damage. PARP-1 activity leads to energy consumption and mitochondrial failure and further cellular damage (21, 61).

Furthermore, minocycline inhibits blood-derived iron toxicity (lipid peroxidation) via direct scavenging effect, Ferric and Ferrous ion chelation and increases expression of ferritin which buffers local iron levels(21).

Given these multiple sites of action and promising early clinical results (62, 63) minocycline remains a useful agent in the investigation and mitigation of secondary injury, particularly when exploring upstream initiators of apoptosis and neuronal survival.

1.4 Anatomy and neurophysiology of the spinal cord

The human spinal cord (SC) is an approximately 30 g, semi-cylindrical, gray-white neural continuation of the medulla oblongata. It starts at the level of the foramen magnum and ends with a cone-shaped structure called conus medullaris at the lower border of the first lumbar vertebra (L1) (64) in humans. In rats it terminates at the L3 vertebral body (1) and at the L4 vertebral body in mice (65). The spinal cord length in human adults is approximately 42 to 45 cm (66), with an average diameter of 1 to 1.5 cm (64). Although it maintains its embryonic segmental organization histologically and functionally, the exterior appearance of the spinal cord is smooth and uniform. It has two fusiform enlargements, the upper one is the cervical enlargement where it gives off the brachial plexus and the lower one is the lumbar enlargement where it gives off the lumbosacral plexus. Along the spinal cord, two longitudinal furrows can be identified, a deep anterior median fissure and a shallow posterior median sulcus.

The spinal cord substance is a soft gelatinous structure which is protected at multiple levels. It is surrounded by a bony spinal canal from all directions. It is covered also by three layers of the meninges (the dura mater, an arachnoid membrane and the pia mater which is adherent to the cord itself). Moreover, the cerebrospinal fluid between the pia and arachnoid layers functions as a cushion and shock absorber. Furthermore, the SC is fixed to its surroundings by several structures which include 31 pairs of nerve roots, 21 pairs of dentate ligaments and the filum terminale. The epidural space between the dura and vertebral periosteum is filled with loose fibrous and adipose connective tissues (67, 68); these act as another protective layer to the SC.

Functionally, the SC serves as a means of communication (a conduit) between the brain and the peripheral nerves. It also contains local circuitry including the spinal reflexes. Furthermore, the sacral segments of the SC (S2-S4) contain the parasympathetic centre that supplies the urinary bladder, genitalia, and the distal colon below the left colonic

flexure. Sacral segments also contain Onuf's nucleus which is a collection of motor nuclei and the origin of pudendal nerve. Thus, it is directly involved in processes of urination control, erection and sexual function as well as defecation regulation (66).

Histologically, the spinal cord substance is arranged such that the white matter surrounds the centrally located gray matter. The gray matter is made up of cell bodies of lower motor neurons, interneurons, and glial cells. It also includes the dendrites and synapses of efferent and afferent neurons. The white matter is comprised of ascending and descending bundles of fibers containing myelinated axons that relay the impulses in both directions between the brain and the peripheral end organs (1).

Axons of the motor neurons (efferent fibers) exit ventrally to form ventral rootlets, whilst the sensory (afferent) fibers that project from the dorsal root ganglia enter the SC via the dorsal roots. Anatomically, the ventral and dorsal roots of the same spinal segment unite within the spinal foramen to form the peripheral spinal nerve. In humans, there are typically 8-cervical (C), 12-thoracic (T), 5-lumbar (L), 5-sacral (S) nerves and 1 coccygeal (Co) nerve, which innervates the skin over the coccyx. The C and L nerves supply mainly the upper and lower limbs respectively, whereas the T nerves innervate the trunk, and the S nerves supply the viscera below the left colonic flexure and the genitourinary system.

Comparatively, the mouse (and rat) spinal cords are made up of 34 segments: 8-cervical (C1 to C8), 13-thoracic (T1 to T13), 6-lumbar (L1 to L6), 4-sacral (S1 to S4), and 3-coccygeal (Co1 to Co3). There are two enlargements, the cervical and lumbar (lumbosacral) enlargements (69) and they exert similar functions to humans (1).

Of note, the presence and location of various spinal cord tracts, and their functional relevance varies between species. For instance, the corticospinal tract (CST- the motor tract) in rodents (1, 70) differs in position compared to humans. In humans, the CST is located mainly in the lateral funiculus, while in rodents it runs in the ventral portion of the dorsal column (Figure 1.1). Further details about the rodents' spinal cord tracts are discussed by Watson, Paxinos and Kayalioglu et al. (71-73).

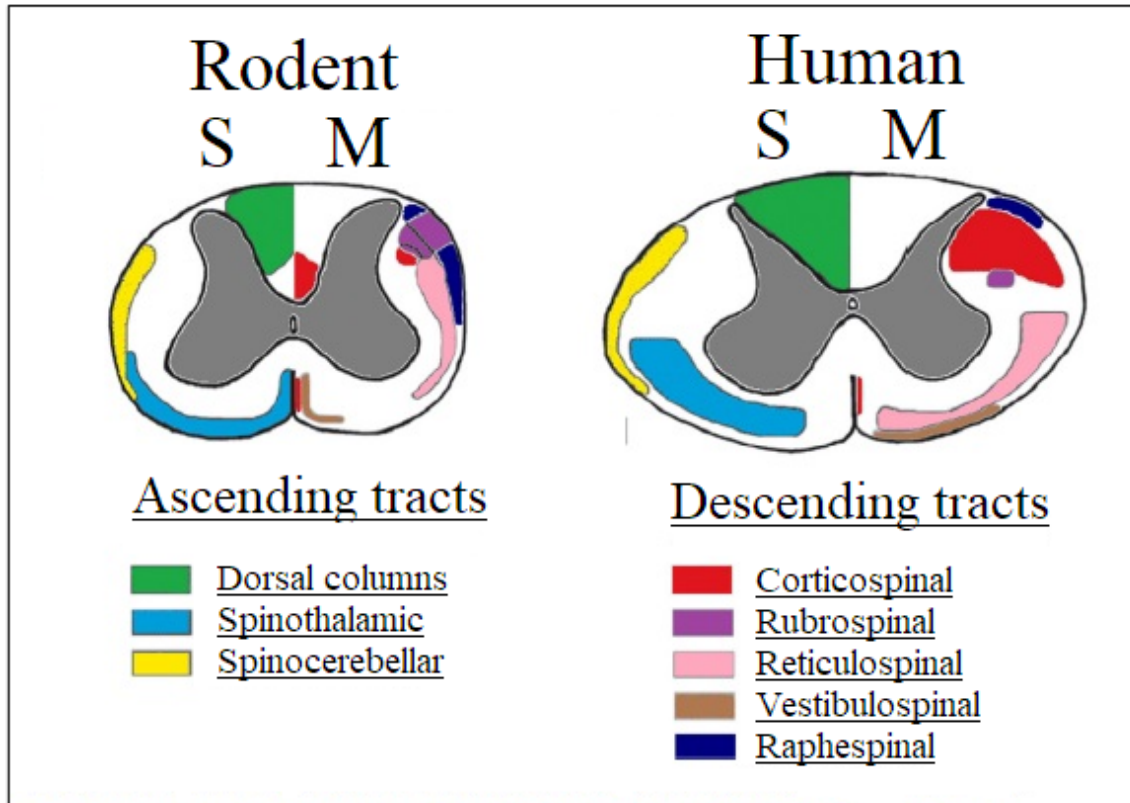


Figure 1.1 Comparative anatomy of the rodent and human spinal cord cross-section. The drawing depicts the approximate locations of ascending and descending tracts in each species. The descending cortico-spinal tract in the rodent is located in the ventral portion of the dorsal column vs the dorsal part of the lateral funiculus in human. M= motor; S=sensory. Modified with permission from Silva et al., *Progress in Neurobiology* 114 (2014); 25-27. (Appendix A)

1.5 Differences between the human SCI in clinical situations and the animal models in research

Several aspects of SCI have been extensively studied in animal models for more than 40 years (74). There has been marked progress in understanding the pathophysiology of SCI and preclinical experiments, yet the translation of the basic science success into clinical trials has been difficult and remains disappointing. There are several caveats that should be addressed to assess the gap between the clinical SCI and research models. These may include but are not limited to the following points:

1. To begin, clinically there are several classifications for SCI based on functional or anatomical assessment (75, 76). The scale most commonly used currently by medical community is the International Standards for Neurological Classification of Spinal Cord Injury (ISNCSCI). Developed by the American Spinal Injury Association (ASIA), it includes a standardized assessment of key myotomes and dermatomes enabling the calculation of a motor score, sensory score, and hence an ASIA Impairment Scale grade (77). Conversely, various scales and methods have been described to assess SCI and recovery in animal models. For example, locomotor function tests (open-field locomotor assessment such as Basso, Beattie and Bresnahan or BBB scale, Staircase test, digital systems and ladder-wire grid test); limb strength (forelimb grip and inclined plane tests); Sensory function (the Hargreaves assay, tail-flick test and Von Frey filaments) (8).
2. In experimental animal models, the SCI is produced in a controlled fashion and typically exploit a single insult such as contusion, compression or transection. Furthermore, there are different methods to produce each one of these three types of injuries (78). In contrast, pre-operative neuro-imaging and surgical exploration in humans suggests that SCI results from a combination of these mechanisms.
3. The true severity of trauma impact: in animal models, the force delivered to the spinal cord is structured to generate solely SCI while avoiding other organ damage. Additionally, the delivered force is precisely controlled and graded as a mild, moderate or severe injury (79, 80). In contrast, a significant number of clinical cases of SCI result from either motor vehicle accidents or falls from a height. The energy of the impact from these injuries extends beyond the SC to other body organs. Therefore, in the clinical scenario, the overall impact of the traumatic forces resulting in SCI are more extensive than those observed in research models.
4. Inconsistency within SCI clinical research: because of heterogeneity in the mechanisms of injuries, underlying pathophysiology and patient population, the discrepancies extend from methods of diagnostic tools to several elements of management such as performing urgent MRI, administration of methylprednisolone, the type and time of surgical decompression and stabilization

(11). All these variables influence the outcomes and consistency of clinical research.

5. Rodents have been the most common species used in SCI animal models (92% in total, rats constitute 72.4% and mice 16%) (81). Cellular and molecular responses to SCI, although they share some similarities, are different amongst human, non-human primates and rodents. (82-84). In humans, the site of SCI is filled with fibrous tissue, whereas in mice the lesion centre displays fibroblast-like cells that express CD11b, CD13, CD45, collagen, and fibronectin. Additionally, the inflammatory response lasts longer in primates than rodents. Pro-inflammatory cytokines expression in the common marmoset, for instance, returns to basal level after 14 days of SCI, whereas in mice these cytokines return to basal level at 1 week after SCI (84).
6. Finally, from the results of clinical trials, the SCI response to neuroprotective agents varies according to the anatomical level of injury namely, cervical vs thoracic. This observation is under active research (25). This is relevant as the majority of clinical cases of SCI are at the cervical level (60%) (8), whereas, most experimental SCI have been conducted at thoracic level (81%) followed by cervical area (12%) (81).

These factors have contributed to the limited progress in translating basic science successes into viable clinical therapies. Therefore, studying SCI pathophysiology at the molecular level namely, gene expression and miRNA changes, which are conserved among species might bridge this gap and represent a shared intersection point. The next section will further explore these concerns, including the pathophysiology of animal models of SCI and the role of gene expression and miRNA in SCI.

1.6 Animal models of spinal cord injury in research

Various distinct methodologies that have been used to generate SCI in several species of animal. These modalities were developed to create an injury for a specific purpose or to emulate a specific clinical scenario. Regarding model species, the rat is the most popular,

mainly due to their access at a reasonable cost, a size that is easy to handle pre and postoperatively, and the presence of several validated functional and behavioral tests to assess injury outcomes (1, 78). Mouse SCI model is the second most common in practice (78, 81). Mice have been used to study the extensive molecular cascades and reactions of secondary SCI (sSCI) because of the commercially available genetically modified mice (transgenics) with reasonable costs (1, 85). Practically, the primary difficulty with using mice is their small size, which requires more skill to create a reproducible model of SCI compared to rats and larger sized animals. Additionally, their limited blood volume mandates that researchers be meticulous with their surgical technique so as to minimize blood loss that may precipitate global hypoxia or ischemia. These augmented effects can complicate the sequence of secondary reactions and influence gene expression and may confound the results of the study. Non-primate species such as pigs and dogs have also been used and their neuroanatomy, physiology, and size are closer to human than rodents (85). However, high cost, limited supply and requirement for specialized personnel and facilities have hindered their utilization in SCI research. Notwithstanding, they constitute a valid translational option to refine potential therapeutic results from rodents studies prior to proceeding to human clinical trials (1, 85). Regardless of animal species used, all studies employ one of a variety of SCI models:

1.6.1 Contusion models:

The contusion SCI model is currently the most widely used to study SCI (904 out of 2209 articles included in the analysis, or 41%) (81). The concept of this method is to produce a contusion by applying a transient force or tissue displacement with an attempt to preserve the covering membranes of the SC after removing some of the laminae. In the literature, several methods to deliver a contusion SCI have been described:

- A. The freefall of a fixed weight onto the SC in a rat model; this modality was described by researchers at New York University (86). It consists of a 10 g weight that falls freely by the effect of gravity from different heights to produce distinct impact severity and various levels of SCI in the thoracic level. Ideally, the spinal column is fixed by clamps for accurate impact delivery. The main downside of this method is the potential for a rebound impact from the weight producing a

second trauma to SC. Although the developers of this method have minimized the importance of repetitive trauma to the SC, they suggest that the model does not adequately simulate the clinical scenarios.

- B. Electromechanical tissue displacement model: this modality was described by Behrmann et al. in 1992 using a solenoid device to exert mechanical SC tissue displacement at various levels, 0.8 mm, 0.95 mm and 1.1 mm (87). The phenotype and histological features were reproducible and accurate at the T9 level in a rat model. Although this tissue displacement model may mimic some of the clinical features of SCI, the major downside of this model is that the tissue displacement is temporary, whereas in the clinical setting tissue displacement/compression persists until surgical decompression is achieved. The lack of sustained tissue displacement may explain why such an experimental SCI demonstrates recovery rates that differ from those seen clinically.
- C. Computerized impactor: Currently, an impactor is one of the most popular devices used in experimental SCI laboratories (81, 88). The Infinite Horizon Impactor (IHI, Precision Systems and Instrumentation, Lexington, KY, USA) is one of broadly available machines. It consists of two main parts: an impactor device which is contained within the surgical field and a separate, but connected, computer system which drives the impact. It delivers a measurable force that can be pre-determined through the software prior to producing the injury. This device also records all mechanical parameters and events that occur during the process of SC impact, such as the actual force delivered, magnitude of tissue displacement and impactor velocity (Figure 1.2). It has been used in mice and rats to create cervical and thoracic SCI (88-90). These technical features render this device capable of producing a reproducible and accurate SCI (1). It is thought that using the IHI device to create a SCI produces one of the closest models to the clinical scenario.

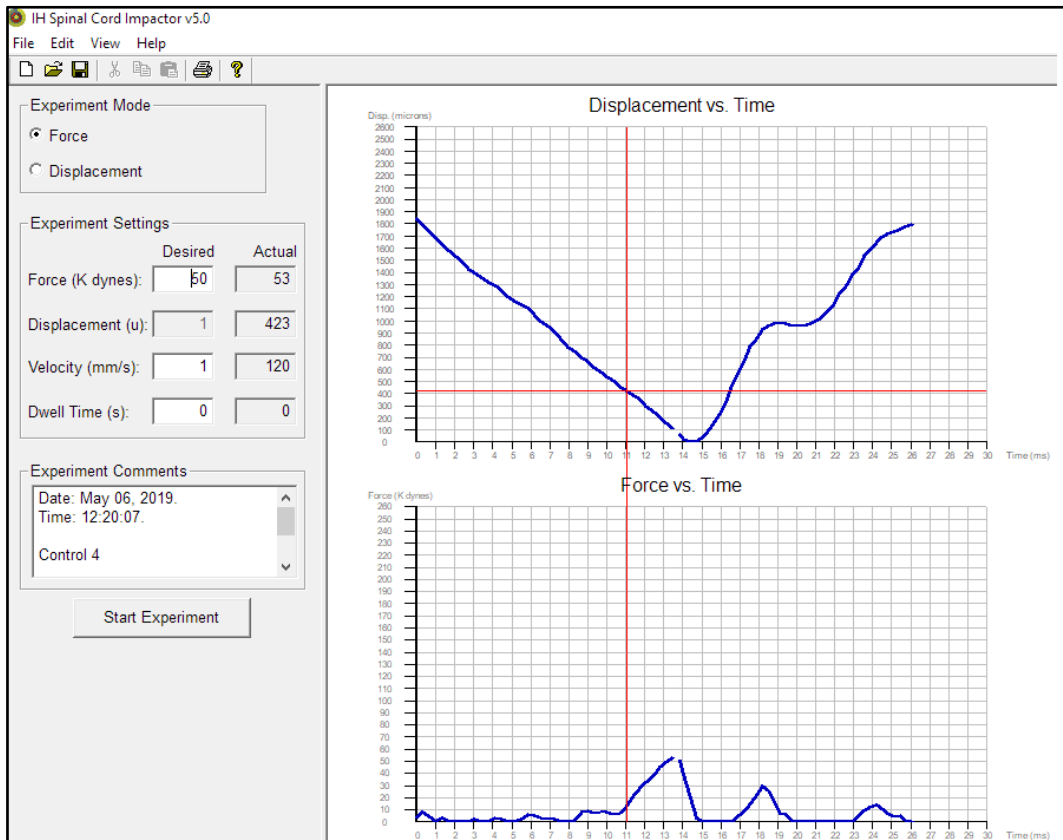


Figure 1.2 Data recorded by the Infinite Horizon Spinal Cord Impactor.

The device is designed to deliver repeatable and graded injury. The computer allows for setting the desired parameters like force, duration of impact, and records the actual delivered force (k dyne) and tissue displacement (in micrometer). The device also displays the relationship between time, tissue displacement and delivered force. *Nadi, 2019.*

D. Air gun impactor: this device produces SCI by applying a high-pressure air stream directed to the SC via a 2 mm hole through the lamina. Different severity of SCI can be created by changing the air stream pressure and the duration. Further work is still required to validate this device (88, 91).

E. Ohio State University (OSU) impactor : it is a computer-controlled device that has been upgraded and modified since it is first developed in the late 1980s (92). It requires laminectomy at the intended SC level. The impactor probe touches the SC tissue to set up the start point and then deliver a predetermined displacement

distance over a period of time. The instrument records the displacement distance as well as the force delivered to the SC (88).

1.6.2 Compression model:

This model has been utilized in 19.4% of experiments (428 out of 2209 SCI model studies) (81). In this model, a crush or a compression is applied to SC by using different methods. The most common are:

- a. Aneurysm clip application: a cerebrovascular aneurysm clip is utilized to deliver a compression force on the SC to create local injury. Originally, the clips were modified by altering the closing strength of the clip to deliver compression force measured by grams, such 2, 5 and 10 grams, and the force was left for a measurable period of time. By altering the time and strength of the clip distinct levels of SCI severity were created (93). This was developed in 1978 by Rivlin and Tator (74) and a significant number of papers have been published since then by using this method.
- b. Balloon compression model: the balloon is affixed to the tip of a catheter that can be inserted in the spinal canal after performing laminectomy caudal to the intended site of the lesion. Air or saline can be used to inflate the balloon to create SC compression (88). The severity of compression can be altered by varying the volume and/or the duration of inflation. Although it is an easy and inexpensive method to create an injury, it has limitations. The amount of applied compression and the velocity of force application on the SC cannot be precisely evaluated. Therefore, it can be difficult to reproduce the same severity of SCI each time making this technique less popular than clip compression method. It was first used in 1953 and has been applied to different animal models (88, 94-96).
- c. Forceps compression: this model employs a pair of surgical forceps equipped with a spacer, to calibrate the force of the compression (88). Following laminectomy, the forceps are applied around the SC. The severity of an injury can be determined by changing the applied force and the duration of

compression. The advantage of this model is that it is simple and inexpensive. However, the lack of acute compression application on the SC and inability to record the force during compression makes this method incomparable and less common than clip application. It was described in 1991 and used in several animal models (97, 98).

- d. Strapping technique: in this method, the injury is created by using a suture wrapped around the SC. For this purpose, a curved surgical needle with a suture is inserted directly through the skin from the back without laminectomy (99). While one end of the suture is attached to a fixed point, the other end is passed around a pulley and connected to a mass. The freefall of the mass creates compression around the SC, and it is usually left for one minute to produce circumferential injury. Different grades of SCI severity can be created by changing the mass weight (88). Although it is relatively less invasive than the previously mentioned methods above, the certainty around its reproducibility is undetermined rendering this technique less popular than the clip compression methods.

1.6.3 Transection model:

The transection model is the second most common method (32.5%) reported in SCI experiments (718 studies in an analysis of 2209 papers) (81). The injury can be delivered by using a small blade. The transection can be a complete or partial transection (88). Although this technique does not exactly simulate the clinical situation, it has unique experimental benefits. It is easy to perform and inexpensive. This approach can be used to study axonal regrowth and functions of certain SC circuits. A complete transection is easy to reproduce and somatosensory evoked potential or retrograde labeling can be used as an index for partial transection consistency (100). It is a popular technique and has been validated on several species of animals (88).

1.6.4 Distraction models:

In this model, the SC is exposed to a stretching process similar to what might happen during a flexion mechanism causing human SCI. Several animal species have been used in this model including cats, dogs and pigs (88). A number of devices have been developed:

- A. Harrington distractor: this model was described in 2004 in the rat thoracic spine (101). It involves target level laminectomy and insertion of two Harrington hooks under the rostral and the caudal laminae. The hooks are attached to a motorized spacer that controls the speed, duration, and span of the distraction via a computer software. The facet capsules and ligaments are generally dissected free. Distraction by 3, 5, or 7 mm usually results in graded levels of SCI. There are limitations to this method which include:
 1. Variability within each grade
 2. Slow distraction speed (1 cm/s), while in human clinical scenario the speed is thought to be 100 cm/s
 3. Lack of validation
- B. University of Texas distractor: This device produces distraction in two directions - rostral and caudal to the target level (102). No laminectomy is required, rather clamps are fixed to the vertebral body and a computer controlled rostral-caudal distraction by 3, 5, or 7 mm produces mild, moderated, and severe SCI, respectively. Limitations of this technique include:
 1. Inconsistency of behavioral assessment for the injury
 2. Slow and does not mimic the human SCI speed
 3. Requires validation
- C. University of British Columbia (UBC) multi-mechanism device: This device delivers SCI by contusion, distraction and dislocation at different stages (103). It was developed to create cervical SCI in rats. It requires laminectomy of the target level and bilateral facetectomy for the realignment after dislocation. It is reported to be as fast as the human SCI may happen. Thus, the extension of

injury is the farthest amongst other models. Graded injuries can be produced. Limitations of this include:

1. It requires a longer surgical time than contusion injury alone, which may introduce confounders
2. A greater degree of surgical skill is required
3. Locomotor tests are required to validate this method

1.6.5 Chemical models:

Chemical models of SCI entail injection of chemical reagents into the SC substance to study specific reaction pathways of SCI (88). There are many reagents that have been used for this purpose. In broad terms, chemicals causing demyelination, ischemia (104), inflammation (105) and excitotoxicity(106) have been applied to understand these specific elements of secondary SCI mechanisms and to evaluate the efficacy of therapies directed towards SCI healing processes. It is apparent that these models do not simulate clinical SCI, nor can the exact location and the extent of the injury be tightly controlled. Notwithstanding, these approaches may continue to serve a role in the understanding of discrete secondary injury mechanisms.

1.7 Spinal cord injury pathophysiology

Spinal cord injury refers to SC tissue destruction following exposure to an insult. In trauma this involves the transfer of kinetic energy. Within a few minutes after the initial insult, SC physiological and biochemical responses are initiated (48). Both the nature of the initial injury and the pathophysiological responses secondary to the insult determine the ultimate histological damage and the phenotypic neurological deficits. To understand the complex histological, cellular and molecular processes that influence the neural, vascular and immune components of SCI (48), these events can be divided into primary injury and secondary injury. The latter is subdivided temporally into acute, subacute, and chronic stages. Some of the reactions start in the acute stage and persist to the subacute stage (Table 1.1 and Figure 1.3) (107).

| Stage | Descriptions (Rodents) (85, 107-109) |
|---|--|
| Acute | 0 - 48 hr – vascular and endothelial cell injury, hemorrhage, edema, ischemia, ionic imbalance, necrotic and apoptotic cell death, calcium influx, excitotoxicity, oxidative stress reactions, lipid peroxidation, inflammatory cell infiltration. |
| Subacute | 48 hr - 6 wks – demyelination of surviving axons, axonal dieback, apoptosis, inflammatory cell infiltration, Wallerian degeneration, matrix remodeling, evolution of glial scar. |
| Chronic | > 4-6 wks – Mature glial scar formation, more axonal die-back, cystic cavity formation. |
| hr = hour; wks = weeks. Different authors refer to different durations to determine these temporal stages. There is no consensus on these periods. The above-mentioned durations are most common. | |

Table 1.1 Stages of secondary spinal cord injury

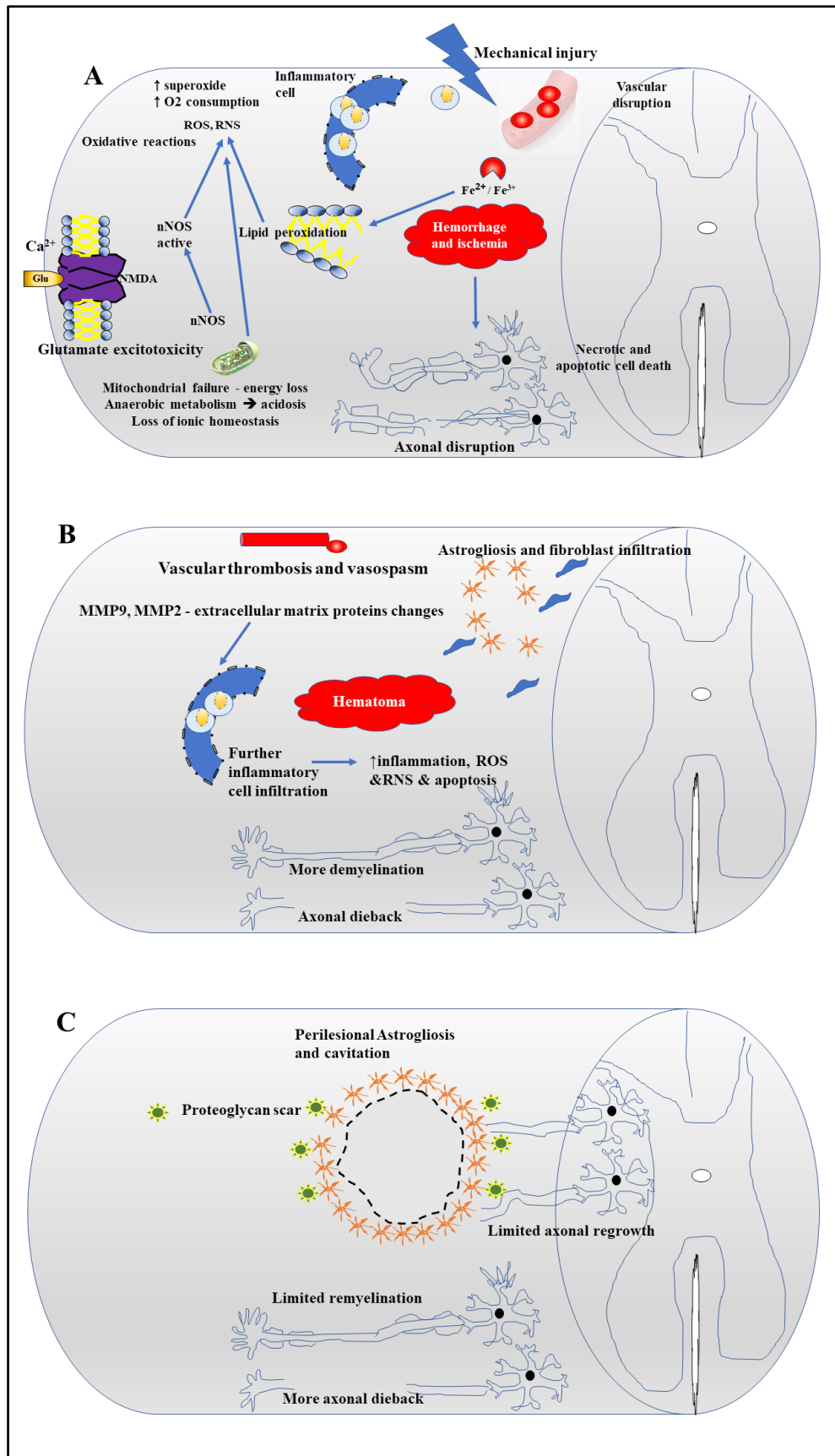


Figure 1.3 Summary of traumatic spinal cord injury phases.

- a.** The initial mechanical trauma to the spinal cord initiates the secondary injury cascade that is characterized in the acute phase by vascular disruption, haemorrhage, ischemia, inflammatory cell infiltration, the release of cytotoxic products and cell death. This secondary injury leads to necrosis and/or apoptosis of neurons and oligodendrocytes.
- b.** In the subacute phase further ischemia occurs owing to vessel thrombosis and vasospasm. Persistent inflammatory cell infiltration causes further cell death. Astrocytes proliferate and deposit extracellular matrix molecules into the perilesional area.
- c.** In the chronic phase an astro-glial scar matures to become a potent inhibitor of axonal regeneration. Cystic cavities can coalesce to further restrict axonal regrowth. *Nadi, 2020.*

1.7.1 Primary injury

1.7.1.1 Phase description:

SCI occurs when the force of the impact exceeds SC tissue resistance and/or the impact displaces the tissue beyond its resilience. Causes other than trauma, such as tumors (48) can result in SCI with different mechanisms taking into consideration the gradual progress that allows for SC adaptation. This neurological adaptation, with the long-standing presence of an insult, eventually fails to preserve the structural and functional integrity of the SC.

Pathophysiology of chronic SC insults is beyond the scope of this thesis and discussed in detail in several reviews (110-112).

The primary injury starts from the moment of SC exposure to the insult, which could be either an open/penetrating or closed/blunt injury, the latter the most common. The type of initial force ultimately dictates the nature of the injury and that might be either contusion (from impact and momentary compression), compression, transection or laceration, distraction or any combination of these (1, 107). Contusion-compression mechanisms are the most frequently observed clinical mechanism. Displaced fragment(s) of the spinal column can exert persistent compression on the SC parenchyma (113). The initial forces delivered to the SC also impacts the severity of the injury. Practically, there is no treatment

for the primary injury (yet there are precautions to avoid its occurrence) and its time span is short.

1.7.1.2 Dissemination of primary effects and transition to the secondary phase:

Traumatic SCI initiates immediate local and systemic responses that may synergize each other to shape the reactions at the injury epicenter. At the systemic level, the impact causes a sudden and temporary surge in systemic blood pressure (BP). This is followed by a prolonged period of a drop in body BP (48). The drop in BP subjects the SC to hypoxia. At the injury site, vascular damage, in particular the small vessels in the gray matter zone, causes hemorrhage, blood-SC-barrier disruption, vasospasm, thrombosis, SC edema, and further local hypoxia and cellular death (48, 114). In addition to axonal disruption, neurons, astrocytes, oligodendrocytes, and endothelial cells die due to cellular membrane shear and hypoxia. This results in local ionic imbalance. Moreover, the local surviving neurons fire action potentials complicating the ion imbalance and causing neurotransmitters to accumulate. The toxic ionic concentrations induce death in nearby cells; as well, the abnormal levels of neurotransmitters cause prolonged neuronal stimulation, cellular edema, and excitotoxicity. This cascade induces further neuronal and glial cell loss (48). Moreover, the damage to small vessels and blood-SC barrier leads to extravasation of RBCs and plasma-borne molecules into the injury site (115). Given the gray matter has a richer capillary network than white matter, it demonstrates more dramatic hemorrhagic events. Hemorrhage and swelling cause further mechanical damage and may extend beyond the injury epicenter (116). Hemorrhage, ischemia and cell death lead to the release of pro-inflammatory cytokines and recruit peripheral immune cells and stimulate the resident microglia (117). All these events, within minutes after the injury, initiate a series of cellular reactions which is known as secondary injury (48).

1.7.2 Secondary spinal cord injury (sSCI)

sSCI is the cascade of reactions that evolve within a few minutes following the primary injury and continue for several weeks to months. Given the time span and because of the significant insult that occurs during this phase, it is proposed that this stage of injury is the period whereby a therapeutic intervention can have a significant impact on the eventual course of disease and improve the ultimate clinical outcome of the SCI. Cells and molecules from nervous, immunological, and circulatory systems participate in these reactions at different stages of secondary reactions. sSCI can be further classified into acute, sub-acute and chronic stages (Figure 1.3, Table 1.1).

1.7.2.1 Acute sSCI cellular and molecular events:

The notion of sequential reactions that occur after the initial injury was first suggested in 1911 by Dr. Allen during his research in the canine SCI model (1). His findings were then supported by the work of many other researchers who came later. During secondary injury, further cellular damage occurs and lesion size expands, worsening the clinical outcome (48). Therefore, manipulation of these cellular and molecular reactions has the ability to minimize the extent of the lesion, preserve the cellular population, improve axonal regeneration, and eventually improve the neurological outcome. The major events during acute stage of sSCI encompass:

1. **Vascular events:** the initial trauma disrupts the blood vessels, particularly the small blood vessels in the gray matter, which leads to hemorrhage (1, 48). This is followed by vasospasm and local thrombosis leading to loss of vascular autoregulation and loss of the integrity of blood-SC-barrier that extends beyond the injury site for several weeks. These events lead to ischemia, local tissue necrosis, SC edema. The hypoperfusion status will be followed by reperfusion, which enhances free radical production and induces further cytokine production, increasing blood vessel permeability to SC parenchyma. These vascular events stimulate endothelial cell production of selectins and cell adhesion molecules

(CAM). Cumulatively these factors induce inflammatory and immune cells infiltration to the site of injury (1, 48).

2. Inflammatory reactions: Inflammation is a homeostatic response to an insult causing tissue damage by trauma, invading microorganisms or toxic chemical agents. This response entails activation of immune body systems, both humoral and cell-mediated pathways (118). The first cells that get activated after SCI are resident microglia (microglia are the local source of central nervous system, CNS, macrophages; circulating monocytes are the external origin migrating macrophages) (27, 119). These cells are the initial source of pro-inflammatory factors that include IL-6, IL-1 β , TNF- α . This stage is followed by neutrophil infiltration, which reaches its highest level between day 1 and day 3 post injury, although their activity can persist for several weeks (27, 120). Neutrophils release proteases, nitrogen and oxygen radicals which cause protein nitration and peroxidation of lipids that can negatively impact neurological outcome (4). Hence interfering with neutrophils reactions can inhibit their early detrimental consequences. The circulating macrophages then invade the lesion site. Popovich et al. 1997, reported that leukocyte infiltration to the site of injury results in more cytokines and cytotoxic factor release which can be destructive and also attract more leukocytes to the injured area (1, 121, 122). Several groups have demonstrated in different experimental animal models that depletion of peripheral macrophages reduces activated macrophages at the trauma epicenter, preserves myelinated axons, reduces cavitation and improves functional outcome (123, 124). In conclusion, resident microglia are activated first. Their cytokines attract neutrophils and macrophages are attracted later. Moreover, the inflammatory response has two different effects: a deleterious effect in the first few days of injury that causes further tissue damage (125) and a beneficial effect as it participates in the repair of SC tissue that occurs at later stages (27, 126). Hence, the mitigation of inflammation in acute stages can be beneficial. Klusman et al 1997, for instance, showed that modulation of the inflammatory process at different time points can have effects on tissue damage or repair (127). This group

used pro-inflammatory cytokines at day 1 and day 4 post-SCI. They observed more tissue loss in day 1 compared to day 4.

- 3. Programmed cell death:** Programmed cell death which is also known as apoptosis is a tightly- controlled and active process of cell death. It differs from necrosis in that the apoptotic cells are cleared by phagocytosis and there is no inflammatory reaction (27). There are two main pathways, the intrinsic or mitochondrial pathway and extrinsic or death receptor pathway that mainly recruits caspases in downstream reactions. Apoptosis can affect neurons, oligodendrocytes and other cells in the SC. Apoptosis, in addition to necrosis can expand the lesion area after SCI (128). Far from the injury site, pontine and corticospinal neurons may undergo apoptosis following SCI (129, 130). Apoptosis in oligodendrocytes can happen within 24-hours after trauma at the injury epicenter. It can also occur several weeks after SCI outside the epicenter of the injury with a maximal loss of oligodendrocytes observed 6 weeks after injury. This period of time is the longest duration after which the oligodendrocyte population in a SCI model was examined (131). Hence, this type of cellular loss suggests that apoptosis participates in demyelination of axons by affecting oligodendrocytes (132). While microglia after SCI undergo apoptosis, astrocytes usually do not go through this pathway (30). Finally, there is a relationship between microglia activation and oligodendrocyte apoptosis (128). After SCI, activated microglia are found accumulated rostral and caudal to the injury epicenter, along white matter tracts concomitant with apoptotic oligodendrocytes.
- 4. Generation and release of free radicals:** The initial local vascular changes and systemic hypotension contribute to local hypoperfusion and ischemia. These events are followed by the improvement of local perfusion and oxygen delivery that leads to the generation of free radicals such as peroxynitrite, superoxide and nitric oxide (48). In fact, the generation of free radicals starts during the ischemic stage and increases during reperfusion periods (133). This leads to several other downstream oxidative reactions that cause further cell death. For instance, these

radicals can disrupt cellular membranes and other cellular organelles by reacting with the membranous polyunsaturated fatty acids through the process of peroxidation. Moreover, fatty acid peroxidation leads to the production of malondialdehyde that disrupts neuronal Na-K ATPase enzymes and eventually leads to further cellular ionic imbalance and neuronal cell loss (1, 134).

- 5. Cellular excitotoxicity:** SCI leads to release of an excessive amount of glutamate (the primary excitatory neurotransmitter in the CNS) to the extracellular space within and around the injury epicenter (for the mechanisms of glutamate accumulation see Box 1) (21, 85, 107). Glutamate levels rise rapidly and can be detected within 30 minutes following injury, returning to normal levels within 60 minutes (85). This surge leads to a prolonged activation (135) of glutamate receptors on neurons, oligodendrocytes, and other glial cells (85, 136, 137). Glutamate stimulates metabotropic receptors for Ca^{2+} intracellular influx and the ionotropic AMPA, NMDA, and kainate receptors (138). Binding of glutamate molecules to their receptors activates potassium and calcium gated receptors. Glutamate also enhances nitrogen and oxygen radical production which causes microcirculatory constriction and augments local ischemia (133). Moreover, the prolonged Ca^{2+} influx eventually leads to cell swelling and death by necrosis or apoptosis (139). Neuronal cells and oligodendrocytes express glutamate receptors on their cell membrane and as such both are vulnerable to excitotoxicity. This leads to loss of neuronal cell populations and demyelination, resulting in conduction block and loss of sensorimotor function.

Box 1. Mechanisms that increase glutamate level in SC parenchyma after the injury:

1. Direct local cellular damage
2. Indirect cellular damage by hypoxia and ischemia
3. Decrease in the efficiency of activated astrocytes to re-uptake the excess glutamate locally. Phospholipase A2 and NO play key role in preventing re-uptake by astrocytes.
4. High intra-astrocyte Ca^{2+} levels induce these cells to release the glutamate into the interstitial space.

- 6. Cellular ionic imbalance:** Failure of Na^+/K^+ ATPase function and alterations in cellular membrane depolarization result in Na^+ , K^+ and Ca^{+2} ion imbalance and accumulation of intracellular Ca^{+2} . This damages mitochondria and facilitates neuron and oligodendrocyte apoptotic and necrotic death.

The excess glutamate levels alter cellular membrane depolarization and ionic flux which further complicates the secondary reactions. These changes result in an increase in Ca^{2+} and Na^+ intracellular levels and depletion of intracellular K^+ concentration (140). Free Ca^{2+} levels during normal conditions in cytoplasm range between 50-100 nM versus 0.5-1.0 nM within the endoplasmic reticulum (141). An abnormal increase in Ca^{2+} concentration in cytosol, mitochondria and endoplasmic reticulum results in serious ramifications (142, 143). In fact, mitochondrial- Ca^{2+} dependent cell death plays a key role in neuronal loss in gray matter as well as oligodendrocytes, astrocytes and myelin sheath in the injured white matter (85). In gray matter, the excess glutamate leads to the prolonged activity of neuronal NMDA receptors which in turn leads to cellular Ca^{2+} overload (144). High levels of Ca^{2+} in turn enter the mitochondria via the calcium uniporter and induce mitochondrial failure which results in oxidative damage. Calcium overload also induces phospholipases, protein kinases and calpains which are calcium-dependent proteolytic enzymes that degrade proteins such as microtubule-associated protein 2 (MAP2) and neurofilament (140). Likewise, glutamate and Ca^{2+} overload activate caspase-3 and stimulate intrinsic (145) apoptosis which starts within a few hours after injury and resolves within the first week in rats. Furthermore, mitochondrial respiration failure along with local anoxia leads to ATP depletion. ATP depletion inhibits the activity of Na^+/K^+ ATPase which increases intracellular Na^+ levels (146). High intracellular Na^+ interferes with other cellular reactions. It reverses the action of $\text{Na}^+/\text{Ca}^{2+}$ exchanger and leads to an increase in Ca^{2+} influx (147). It also reverses the activity of the Na^+ -dependent glutamate transport mechanism (146, 148). This mechanism requires a preserved Na^+ gradient to transport glutamate into the intracellular compartment. Cell membrane depolarization stimulates voltage-gated Na^+ channels, which are highly condensed at the nodes of Ranvier. The resultant Na^+ influx and passive intracellular

movement of Cl^- and water culminates in cellular edema (149). Therefore, axons are more vulnerable to ionic imbalance damage compared to the neuronal body. Excess intracellular Na^+ stimulates the Na^+/H^+ exchange pump leading to increased intracellular proton levels and axonal acidosis which by itself enhances membrane permeability allowing for further Ca^{2+} influx (140, 146, 150).

1.7.2.2 Subacute stage:

The subacute stage occurs between day 2 and 4 weeks post-SCI in rodents (8, 140). Some suggest that it may extend to 6 weeks (Table 1.1) (151). As the acute stage is characterized by vascular and inflammatory events, the prominence of cellular death, demyelination, the continuation of these already initiated inflammatory process and initiation of fibroglial (glial) scar formation are the main features of this stage (140, 152). The glial scar is composed of two main regions, the periphery, and the core. At the periphery of the injury epicenter, to protect the healthy tissue of SC from the secondary reactions, astrocytes alter their gene expression, morphology and become hypertrophic (153). The core is composed of phagocytic macrophages, pericytes, vascular and/or meningeal fibroblasts, oligodendrocyte precursor (NG2^+ glia/cells), ependymal cells as well as extracellular matrix (ECM) that is formed by fibroblasts within and around the injury epicenter (140, 154). Pericytes migrate from blood vessels' periphery and occupy the core of the lesion. They are surrounded by astrocytes and their number is double the number of astrocytes (in the normal situation the ratio is 1:10 pericytes: astrocytes) (155). These pericytes are the source of the connective tissue and ECM molecules that form the scar. They begin to express fibronectin which is a fibroblast marker (155). Meningeal fibroblasts also participate in laying down inhibitory molecules, fibrosis and spinal cord tethering (156, 157). Moreover, in addition to apoptosis, necroptosis, which is programmed necrotic cell death, plays an active role in neuronal cell loss during this phase (158). Necroptosis can occur even in the presence of apoptosis inhibitors and can be inhibited by a specific blocker necrostatin-1 (159). The latter showed a neuroprotective effect via preserving mitochondrial function (160).

1.7.2.3 Chronic stage:

The chronic stage starts several weeks (Table 1.1) to years after the injury and determines the ultimate structural SC damage and severity of neurological deficits. The structural and functional damage seen can affect regions beyond the point of initial injury and even in areas within the brain (1, 161). The main structural characteristics of this phase are mature glial scar formation, demyelination of the white matter as well as a significant reduction in gray matter substance. In addition to the cellular components (astrocytes and microglia), the glial scar contains inhibitory molecules such as chondroitin sulfate proteoglycans (162, 163). The glial scar has been traditionally considered the major barrier for axonal regrowth. Yet, there are reports suggesting it enhances axonal regeneration, minimizes further cell infiltration, closes blood-SC barriers, and reduces potential infections (164, 165). Thus, it may have a positive influence in restoring the chemical and physical integrity of the injured SC segment (166). This scar typically surrounds a cystic cavity that can expand up and down from the site of the injury within SC parenchyma. This expansion, termed post-traumatic syringomyelia, can lead to progressive functional loss above the level of injury and/or other unpleasant sequelae such as autonomic dysreflexia and worsening spasticity. One of the main functional disorders during late stages of injury is a chronic neuropathic pain syndrome, which is a debilitating condition that disturbs patients' lives (167, 168). The exact mechanism of this syndrome is not completely understood and few explanations from animal models of SCI have been documented. Loss of inhibitory inputs from the thalamus has been suggested by Masri et al 2012 (168) and dorsal horn sensory neurons hyperexcitability due to lack of inhibition has been observed (169, 170). Unfortunately, this unrelenting chronic pain is frequently resistant to treatment.

1.8 Gene expression following SCI

The cellular phenotypical and functional changes after SCI are guided by activation and inhibition of many transcriptional pathways (171). Alterations in gene expression after SCI have been shown in several studies that entailed various species and strains (48).

Several clusters of genes that are responsible for specific molecular reactions have been reported. Upregulation of transcription factor *NF-κB* (nuclear factor kappa-light-chain-enhancer of activated B cells), for instance, occurs early after SCI. It promotes pro-inflammatory gene expression and persists for 24 hours after injury (49). Upregulation of inflammatory genes, such as *IL-1β*, *TNF-α*, and *IL-6*, persist for a week before returning to normal levels approximately two weeks following injury. Likewise, alterations in genes coding for pro-apoptotic and anti-apoptotic mechanisms, proteins of calcium channels and sodium and potassium pumps in neurons and astrocytes have also been reported (48). The alteration in expression of several genes is likely regulated by microRNAs (miRNA) at the post-transcriptional level.

1.9 MicroRNAs (miRNAs)

miRNAs are small endogenous non-coding RNAs that downregulate gene expression. They are composed of 18-24 nucleotides (approximately 22) (172, 173). They function by inhibiting targeted mRNAs translation through binding to the 3'-untranslated region (3UTR) of their specific mRNAs.

1.9.1 Ribonucleic Acid (RNA) Classification

RNA is an essential polymeric molecule essential for many cellular processes including coding, non-coding and regulating gene expression. There are several types of RNA that are different in their nucleotide length and function. Regarding function, RNA can be classified into coding and non-coding RNA. According to their size (174), more than one definition of large or long RNA versus small types is found in the literature. The cut-off point adopted is arbitrary and solely for the sake of differentiation. Several authors refer to RNAs that are larger than 200 nucleotides (nts) as large RNAs, while those composed of less than 200 nucleotides are small RNAs (175-178). Notwithstanding, others have defined small RNAs as those between 20-30 nts in length (172). Small RNAs are often associated with protein families such as Argonaute (AGO) or P-element Induced Wimpy testis (PIWI) in *Drosophila* and are highly conserved. Some of these small RNAs have specific silencing functions and mainly include: microRNA (miRNA), small interfering

RNA (siRNA) and PIWI- interacting RNA (piRNA) (172). Table 1.2 summarizes different types of RNAs. In somatic cells, miRNAs dominate the rest of the small RNAs.

| <u>RNA type</u> | <u>Acronym</u> | <u>Size</u> | <u>Function</u> |
|-----------------------|----------------|-----------------|--|
| Messenger RNA | mRNA | Variable (179) | Coding protein sequence |
| Ribosomal RNA | rRNA | Variable (179) | Together with specific proteins constitute ribosomes: the principal machinery system for protein synthesis |
| Transfer RNA | tRNA | < 100 nts (180) | Amino acid transportation to ribosomes |
| MicroRNA | miRNA | 18-24 nts (172) | Regulating gene expression |
| Small interfering RNA | siRNA | ~ 21 nts (172) | Regulating gene expression and transposons |
| PIWI-interacting RNA | piRNA | 24-30 nts (172) | Not well-understood, yet share in silencing of transposons |

Table 1.2 The size and function of different types of RNAs

miRNAs are highly conserved across species (173). The first miRNAs were described in 1993 in *Caenorhabditis elegans* development, namely *lin-4* and *let-7* (181). There are several families of miRNAs. Mature miRNAs with similar sequences between nucleotides 2 - 8 are considered in the same family (172). They regulate gene expression by base pairing with targeted mRNAs that leads to mRNA decay or translation repression. The region between nts 2 and 7 at the 5' end of miRNA is called the **miRNA seed** because it recognizes the bases located in the 3' untranslated region of mRNA (182). miRNAs need AGO proteins that facilitate mRNAs deadenylation and decay (183). Therefore, miRNAs are essential in all cellular and biological activities encompassing cell growth, differentiation, metabolism, and preserving cellular identity (184). Hence, they are also involved in all pathological processes. Due to their influential role at the cellular and subcellular levels, they are under strict control spatially and temporally. Over the last few years, it has been demonstrated that their dysregulation can

result in serious diseases in humans (172). miRNAs are regulated at several stages of their synthesis starting from their transcription and ending with their decay (185, 186). The cellular conditions dictate how the cell should facilitate production and turnover of these miRNAs by activating transcription factors, RNAs and protein modifying enzymes.

1.9.2 Biogenesis of miRNA

There are canonical (which is the dominant) and non-canonical pathways of miRNA synthesis. The first step of miRNAs synthesis is the initiation of miRNA gene transcription. The miRNA genes are widely distributed in humans, numbering in excess of 2500 (172). Furthermore, in mammals there are 196 families of miRNAs conserved (172, 187). In humans, miRNA sequences are mainly encoded by coding or non-coding introns, yet some of them are encoded by exons (172). Although co-transcription of several miRNAs from one cluster is the usual pattern, some of the transcribed miRNAs are individually suppressed post-transcriptionally. The transcription process is regulated by transcription factors (TFs) as well as by epigenetic regulators. TFs such as MYC, ZEB1&2, and p53 interfere with the regulation process as well as histone modification and methylation of the DNA. It's worth mentioning that miRNA promoters can be found in more than one location. The promoter of the host gene can be the same for miRNAs when the miRNA gene is located in an intron of the protein-coding gene. Yet, the miRNA promoter can be different when the miRNA gene is located at a different site (188). To proceed, the process requires RNA polymerase II (Pol II) which is regulated by RNA Pol-II TFs and epigenetic factors (189). In certain situations, RNA Pol III transcribes miRNAs (172). The miRNA sequence is included in the primary transcript, or pri-miRNA, which is usually more than 1000 bases long. Therefore, several stages of processing are required to get mature miRNAs. The first stage begins in the nucleus.

1.9.2.1 Nuclear stage:

Pri-miRNA consists of a stem (which is a dsRNA(double-stranded)), terminal loop and both 5' end and 3' end of the stem is attached to a single-stranded RNA segment (Figure

1.4). RNase III (Drosha) and its cofactor DGCR8 cleave the stem at ~ 22 nts from the loop (apical junction) which is ~ 11 nts away from the basal junction to release stem-loop of a hairpin shape with ~ 65 nts, thus referred to as pre-miRNA (172, 190). Although this step is performed precisely, as it dictates the ultimate specificity of miRNA, the mechanism of how Drosha and its cofactor recognize the site of cleavage on the pre-miRNA is not known.

The pre-miRNAs are then transported to the cytosol and further processed by Dicer. Exportin 5 (EXP5) binds to pre-miRNA and nuclear protein RAN.GTP to form a transport complex that passes through the nuclear pore complex (191). EXP5 exports pre-miRNA and protects it inside the nucleus (172).

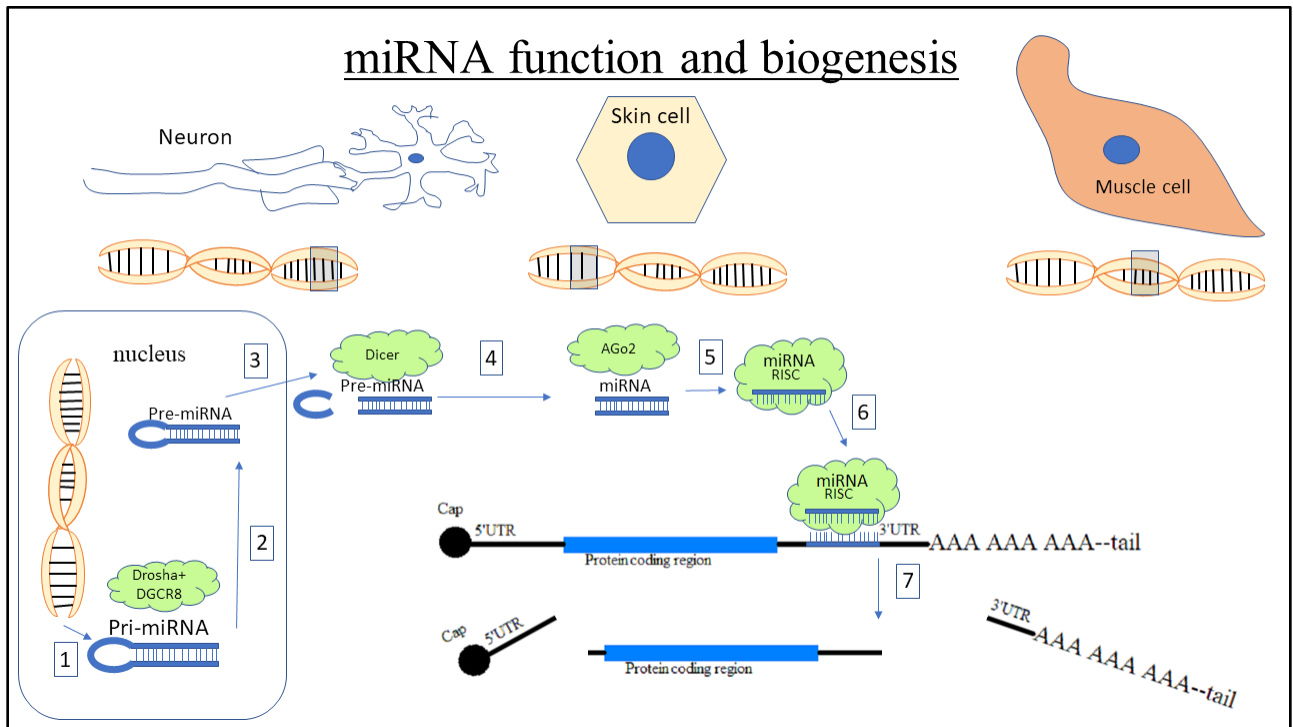


Figure 1.4 Biogenesis and fade of miRNA-nuclear and cytoplasmic events.

1. Transcription from DNA 2. Cropping. 3. Export from nucleus to cytosol 4. Dicing 5. AGO protein loading and unwinding and RISC formation. The guide miRNA strand is uploaded to the AGO protein. The passenger miRNA strand is not shown in the drawing. 6. RISC base pairing with 3' UTR of target mRNA 7. Decay of the RISC and the target mRNA. *Nadi, 2021.*

1.9.2.2 Cytosolic Stage:

In the cytosol, the complex breaks up and pre-miRNA is released via GTP hydrolysis. Dicer then crops pre-miRNA near the terminal loop to release small dsRNA (Figure 1.4) (192). Dicer binds to the pre-miRNA at 5' end and cleaves it ~ 22 nts from 5' end. As the 5' and 3' ends of pre-miRNA bind Dicer at PAZ domain simultaneously, a similar process starts from the 3' terminus (193, 194). Afterward, the generated duplex of RNA is loaded onto AGO to form pre-RNA-induced silencing complex (pre-RISC), which is an ATP-dependent process (172, 195). Immediately after pre-RISC assembly, the miRNA duplex unwinds and the passenger strand is released by ATP-independent

mechanisms (172, 196, 197). This process results in the formation of a mature RISC and the passenger strand decays quickly. The A-shape conformation of the guide miRNA seed area enhances its efficiency in detecting the sequence of the target mRNA. Additionally, there is an area within the AGO protein's structure called PIWI domain which is able to recognize and actively cleave the target mRNA (198, 199). While in *Drosophila* and *C. elegans* the structure of the small RNAs dictates their loading to the type of AGO protein (200, 201), in humans different groups of miRNAs can bind to different AGO1-4 proteins (202). Dicer is not required for asymmetric RISC formation in humans (203). Moreover, in humans, the main mechanism of passenger miRNA strand unwinding is the release without cleavage due to central mismatches of both strands (at nts 2-8 and 12-15 on the guide strand), furthermore AGO1, AGO3 and AGO4 have no cleavage features (172, 195). The second mechanism requires the cut of the passenger strand by AGO2, provided both the guide and passenger strands match (172, 204). An endonuclease enzyme, C3PO, assists in the removal of the cleaved passenger strand (205).

1.9.3 MicroRNA biogenesis regulation:

During the process of miRNA production, there are several molecular events that influence the structure, and hence the stability of miRNAs, and modulate their concentrations:

- A. Single nucleotide polymorphisms (SNPs): this event occurs within the genes of miRNAs. It may result in changes in their target specificity or may affect their production (206).
- B. miRNA tailing: refers to an addition of a nucleotide to the 3' end of the miRNA by either uridylation or adenylation. Nucleotides can be added to pre-miRNA and to mature miRNA. This can either stabilize and enhance their production or destabilize them (184). An example of tailing is the uridylation of pre-let7 through the effect of LIN28 proteins, which attach to the terminal loop of pri- and pre-let7 (207). This binding enhances decay of let-7 miRNA by blocking Dicer activity (208). On the other hand, mono-uridylation facilitates let-7 production in

LIN28 deficient cells (209). Similar to uridylation, adenylation can either stabilize or facilitate miRNAs decay (172).

- C. miRNA editing: editing is a process of changing a nucleotide sequence within an RNA structure after its generation. The changes can be either conversion, substitution, insertion, or deletion. This manifests in the stem region of a certain subset of pri-miRNA. For instance, adenosine is converted to inosine and facilitated by adenosine deaminases (ADARs) (172, 210).
- D. miRNA methylation: methylation of pre-miRNA 145 by BCDIN3D at 5' monophosphate interferes with Dicer activity. Of note, miRNA-145 has anti-tumorigenesis activity while BCDIN3D plays a role in breast cancer formation (172, 211).
- E. miRNA stability alteration via miscellaneous mechanisms/turnover mechanisms: miRNA can be degraded either early during the production process or once they are mature miRNAs after conducting their specific function (172). Several aspects of miRNA turnover and selection principles are not well understood. Conceptually, miRNAs are stable when they bind to RISC because AGO proteins protect both ends of miRNAs (212, 213). Some examples of stability modifying mechanisms are:
 1. Endoribonucleases can cleave pre-miRNAs which stop the production of miRNAs (214, 215).
 2. Active decay of miRNA by the action of exoribonucleases (216).
 3. Destabilization and decay by the effect of target mRNA. Yet this may contradict the concept of miRNA stability within RISC (217) and hence, further studies are necessary to uncover the selectivity of miRNA fate.
 4. Viral RNAs can degrade miRNAs of the infected host via a base pairing process (218).

Of note, in miRNA nomenclature, 5p and 3p means the position of the strand in the pre-miRNA hairpin (219).

1.9.4 Non-canonical miRNA producing pathways

Cells can use alternative mechanisms to generate miRNAs which are different from the canonical pathway. These alternatives produce only ~ 1% of miRNA levels, thus the canonical pathway remains the essential machinery. The alternative pathways were initially described in 2007 (220, 221). There are basically three different pathways:

- A. Drosha-independent: miRNA can be produced via a mRNA splicing process when the intron is removed from mRNA. The removed base sequence enfolds to form loop-stem pre-miRNA and this is known as mirtron (221). Similarly, a category of RNAs is known as short hairpin RNAs such as mir-320 (222). In this category, the miRNA is transcribed by either pol-II or pol-III and then the pre-miRNA is capped by 7-methylguanosine at 5' end and then will be exported to cytosol by exportin1 to get processed by Dicer. Furthermore, small nucleolar RNAs and tRNAs can be sources for miRNAs that bypass Drosha, yet require Dicer to reach maturity (223).
- B. Dicer-independent: An erythropoietic miRNA-451 is an example of this pathway. The pri-miR-451 is processed by Drosha and then transported to the cytosol by exportin5 (172, 224). The pre-miR-451 stem is short ~ 18 bp and cannot be recognized by Dicer. Instead, it is cleaved by AGO2 which produces AGO-cleaved-pre-miR-451. The latter is further processed by poly (A)-specific ribonuclease to generate mature miR-451 (225).
- C. Terminal uridylyl transferase (TUT)-dependent: Drosha and Dicer are required in this pathway. Group II pre-miRNAs that encompass let-7 members are examples of this pathway (209).

1.10 Alteration of miRNA following tSCI

1.10.1 The role of miRNA in the normal SC and nervous system pathologies

To understand the role of miRNA in the pathophysiology of spinal cord injury, it is crucial to understand the function of miRNAs in the normal spinal cord. miRNAs are highly expressed in the spinal cord of mice, rats and other mammals (6, 48, 226). The expression is conserved across species (227). As one of their several functions, miRNAs determine a specific cell's identity, hence, some miRNAs (commonly denoted miR-####) are expressed exclusively in certain cell types. For instance, miR-219 is specific to oligodendrocytes, miR-23 is expressed in astrocytes, while miR-128 and miR-124 are expressed by neuronal cells (228, 229). In addition to cell identity determination, miRNAs play a significant role in cell type differentiation and SC development. For example, miR-381 and miR-219 are involved in neuron and oligodendrocyte differentiation, respectively (230). In fact, it is estimated that more than 30% to 60 % of human genes are controlled by miRNAs (48, 231). Outside the normal SC condition and tSCI, miRNA upregulation or downregulation have been observed in several pathological conditions of CNS such as Huntington, Alzheimer and Parkinson's diseases (232). Furthermore, dysregulation of miRNA has been noticed in psychiatric disorders such as Schizophrenia as well as developmental disorders such as Fragile X syndromes (233, 234)

1.10.2 The role of miRNAs in tSCI

Evidence from different laboratories reveal the role of miRNAs in cellular reactions of several CNS pathological disorders. They participate in apoptosis and inflammatory processes. The role of miRNAs in similar cellular responses and other reactions after SCI have also been observed (235). As post-transcriptional gene expression regulators, miRNAs are the upstream molecules that could be altered after acute SCI. The first paper published in this field was in 2009 by Liu et al. (6). They used a contusion SCI model in rats to examine the changes in SC miRNAs at three different time points: 4 hours, 24 hours, and 7 days. They reported changes in 60 miRNAs with three different patterns of

alteration: 30 miRNAs were upregulated, 16 were downregulated and 14 were initially upregulated at 4 hours after SCI and then downregulated. Several other papers were published later and examined miRNA changes at different and longer timepoints such as 12 hours, 3 days, 14 days, and after 30 days (236). The pattern and the number of miRNAs were different among these studies. These differences may be due to the variation in the experimental paradigms utilized within these studies, such as different species, methods of producing SCI, SC specimen collection timings, RNA extraction and miRNA sequencing techniques. Yet, the general theme was that many of these miRNAs were upregulated and downregulated along the course of secondary reactions after the injury (227, 235, 237).

Several miRNAs participate in inflammatory and oxidative reactions by targeting the mRNA of mediators involved in these processes (238, 239). Initially, there is an increase in intracellular adhesion molecules (ICAM), this facilitates the extravasation process and immune cell infiltration into the injury site (48). Subsequently, this results in alterations in several miRNA levels. For instance, miR-30a-5p is downregulated after SCI and Neurod1 (a protein expressed in nervous system and crucial for maturation and survival of adult-born neurons) is its target. Its overexpression enhances oxygen radical scavenging and overexpression of glutathione peroxidase1 (GPX1), selenoprotein Type N1 and thioredoxin-like 1 (TXNL1) (240). Moreover, this miRNA suppresses iNOS expression (induced nitric oxide synthase) in microglia. It also reduces inflammation by decreasing the levels of IL-1 β , and TNF- α . Therefore, miR-30a-5p regulates oxidative and inflammatory reactions MAPK/ERK signaling pathway. Observations also showed that C1qb (a complement protein which participates in antigen-antibody reactions to activate the immune response) knockout mice had a better outcome. Although the C1qb protein promotes cellular debris removal, it contributes to demyelination and further cell death (48). miR-103 downregulation after SCI could have harmful effects as it releases C1qb protein expression.

Additionally, miRNAs participate in apoptosis, which is one of the hallmarks of sSCI (235). There has been discrepancy in the alteration patterns of miRNA reports related to the temporal and spatial expression of both anti-apoptotic and pro-apoptotic signals after

SCI (48). However, it has been generally observed that several miRNAs regulate apoptosis by inhibiting pro-apoptotic and anti-apoptotic gene expression. miR-9 is downregulated following SCI and has been associated with an overexpression of MCP1 protein resulting in an induction of neuronal apoptosis (241). In contrast, miR-223 is upregulated for two weeks after SCI and its suppression reduces apoptosis (242). Shen et al demonstrated that miR-137 is upregulated after SCI and inhibits neuronal apoptosis by targeting Calpain 2 (235). A further illustration of the varied effects of miRNAs on the intricate apoptotic pathway is through modulation of Bcl-2. While miR-15b upregulation decreases Bcl-2 expression and induces apoptosis (48), simultaneous downregulation of miR-138 and miR-148b enhances Bcl-2 expression in the first three days after SCI. Yet, by the end of the first week after SCI the Bcl-2 expression decreases progressively.

Considering demyelination, miR-219 minimizes demyelination by regulating monocarboxylate transporter1 expression, which is critical for the maturation of oligodendrocytes (243) and it targets ELOVL7 which induces lipid component in myelin-rich areas and disrupts the stability of the myelin sheath (244). According to Liu et al 2009 and Yunta et al 2012, miR-219 is downregulated after SCI (6, 227).

Furthermore, miRNA can regulate astrogliosis and scar formation after SCI. miR-145 upregulation targets GFAP and c-myc gene and regulates/decreases astrocyte density and size (235). Additionally, there is evidence of miRNA involvement in neuropathic pain (245). Following SCI, miR-23b is downregulated in GABAergic neurons resulting in an increase of its target expression, NADPH oxidase 4 (NOX4), which is involved in the generation of pain perception. Examination of blood samples from SCI patients with neuropathic pain, Wang et al. 2018 were able to identify the following miRNAs as biomarkers: miR-204-5p, miR-519d-3p, miR-20b-5p, miR-6838-5p. Yet, the role of these miRNAs has not been verified clinically and their molecular targets have yet to be determined (246).

Lastly, miRNA has a role in axonal regeneration. For instance, miR-133b inhibition hinders axonal regeneration by modulating RhoA expression. In mammals, this miRNA

has been shown to be downregulated during the first 7 days after SCI and this may reflect the limited regenerative capacity of the SC (6, 227).

1.11 The practical role of miRNA in clinical situations:

1.11.1 miRNA as diagnostic biomarkers for SCI:

Several studies have demonstrated that miRNAs are stable in body CSF and serum, share phylogenetic characteristics and tissue-specificity (235, 247, 248). These molecules have been used as biomarkers in traumatic brain injury and other central pathologies such as Alzheimer's disease (249, 250). There have been two animal studies showing the relationship of SCI severity with miRNAs (247, 248). Most recently, a study of 44 human SCI patients, the largest study to date, revealed a severity-dependent pattern of miRNAs in relation to SCI. However, further studies are warranted to validate these findings (247).

1.11.2 Potential therapeutic application:

Given the alterations of miRNA expression after SCI, theoretically, increasing the expression of useful miRNAs and suppressing the levels of deleterious miRNAs may modify the pathophysiological changes following SCI and improve neurological outcomes. At the clinical level, the future outlook is that miRNAs could be used for therapeutic purposes (48, 251). Yet, due to limited knowledge of their exact role(s) in pathological pathway(s), the ideal method(s) of delivering or altering these molecules, and the effect on other organ systems in vivo, much is needed to be elucidated before practical clinical applications could be explored.

SCI pathophysiology entails many cellular and molecular pathways that interconnect neural tissue, vascular and immune systems. The cascades of reactions are intertwined in a self-propagating pattern. Once a biochemical reaction is induced through trauma, it provokes and initiates several other pathways. Several animal models and species have been used to understand these mechanisms toward finding therapeutic solutions to mitigate the destructive effects of the secondary injury and to promote neural and axonal

regeneration and re-integration. I have discussed several limitations in these experiments at multiple levels. Re-visiting this subject from its genetic basis may facilitate a better understanding and potentially uncover a meaningful therapeutic intervention. miRNAs regulate gene expression. Dysregulation of miRNA may alter the course of events following SCI. Therefore, as regulators of mRNA translation, miRNAs could be viewed as (promising) therapeutic molecules to mitigate secondary injury at multiple stages following SCI, with the intent to ultimately improve neurological outcome.

1.12 Aims of the study

Currently, there is no effective pharmacological agent to mitigate the effects of sSCI. Moreover, multiple pharmaceutical agents that were experimentally promising in animal models have failed to demonstrate similar success in clinical settings. Therefore, the overall goal of this research is to better understand the molecular mechanisms of sSCI. More specifically, to determine whether further study of the alterations in miRNA expression following SCI is warranted as we pursue alternative approaches to understand the underlying mechanisms of sSCI and uncover potential future therapies.

The main hypothesis of this thesis is that modulation of miRNA expression by a neuroprotectant after SCI may attenuate the effects of sSCI.

The specific aims of this study are:

1. To examine how SCI affects miRNA expression in an animal model (Chapter 2).
2. To examine whether a neuroprotectant administered after SCI influences miRNA expression (Chapter 2).
3. To examine whether the target proteins of the effectively modulated miRNA have a role in neuronal survival (Chapters 3 and 4).

CHAPTER 2 : MICRO RNA EXPRESSION FOLLOWING SCI AND AFTER MINOCYCLINE ADMINISTRATION

2.1 Introduction

The primary cellular and vascular disruption following SCI triggers an array of complex biochemical reactions within the neuronal, immune, and vascular systems. These secondary reactions are responsible for progressive tissue damage leading to an increase in the lesion size, and ultimately have a significant impact on the final neurological outcome. Apoptosis, inflammatory and oxidative reactions are major events that further expand the lesion size. Such secondary reactions are controlled by sets of genes that are activated or inhibited following SCI (48). Furthermore, studies suggest that miRNAs are one of the major molecules that interfere with gene expression under normal (252) as well as disease conditions (227, 253). They are the upstream controllers of genes and regulate the apoptotic and inflammatory responses of sSCI (6, 237). Our molecular understanding of the multiple levels of events of sSCI remains limited. Molecular therapeutic approaches for sSCI to mitigate further damage requires further research as it is yet to be clearly addressed in the literature. Identifying pathways that can be therapeutically targeted to minimize neuronal loss might represent novel and promising approaches to enhance functional recovery.

Previously, several scientists examined the changes in miRNAs following SCI in rodents (6, 227). Microarray was the primary technique employed to study the expression of miRNA in these studies. Newly developed RNA deep sequencing technology, or what is commonly referred to as second generation sequencing, could represent an efficient method to explore a wider range of changes in miRNA expression (254). In this study, deep sequencing was used to explore changes in miRNA expression in a murine model of SCI. Furthermore, treatment with a known neuroprotective agent sought to examine whether modulation of miRNA expression after SCI is achievable. This approach may

facilitate identification of pertinent miRNAs critical to post-injury neuroprotection. Additionally, it might uncover therapeutic pathways to preserve neuronal tissues and improve functional outcome.

2.2 Materials and Methods

To achieve the above mentioned goals, the Infinite Horizon impactor was used to produce contusion SCI (see section 1.6.1.C) (81, 88). This device delivers a graded and reproducible SCI in rodents. To modulate miRNA expression following the SCI, minocycline was utilized as a neuroprotective agent. It is a known anti-microbial and anti-inflammatory drug in clinical use. In addition, it has several benefits such as anti-apoptotic and antioxidant properties (21, 27, 33, 37, 44). It has demonstrated efficacy in pre-clinical experiments and has been in SCI clinical trials for the last 5-10 years (62, 63).

2.2.1 Animals and ethical approval

In this study, C57BL/6 YFP transgenic mice were obtained from Jackson Laboratories (Charles River, PQ) and then bred in house to maintain a colony. Female mice between 10 to 20 weeks of age were used in the experiments. Mice weights range between 20 and 25 gm. Animal care, procedures and post-operative care were performed in accordance with the policies of Dalhousie University & the Canadian Council on Animal Care guidelines. Animal ethics approval was granted by the Dalhousie University Committee on Laboratory Animals_(protocols #17-136, #20-060).

2.2.2 Experimental Design

The study was designed to examine the changes of miRNA following SCI during the acute and subacute stages of sSCI (Figure 2.1). Regarding the acute stage, the animals were sacrificed 1 day (1d) following the injury. For the subacute stage, the mice were

sacrificed 7 days after SCI. In the 1d group, the mice were divided into three experimental conditions:

1. The no SCI, or sham (S) group, where T10 laminectomy was performed but no SCI was delivered.
2. The SCI + saline (SCI+SLN) or control (C) group. This group underwent T10 laminectomy followed by impact SCI. Mice in conditions 1 and 2 were given 0.5 ml IP buffered saline (vehicle).
3. The SCI + minocycline (SCI+mino) or treatment (R) group, where T10 laminectomy was performed, SCI was delivered and IP minocycline (90 mg/Kg in 0.5 ml buffered saline) was administered as a single dose for the 1d group.

In the 1d group, the mice were euthanized 1d after SCI and SCs were harvested for RNA extraction.

In 7d group there were two experimental conditions:

1. The SCI+SLN or (D7C = day 7 control): after T10 laminectomy and SCI, 0.5 ml IP buffered saline was given daily for seven days.
2. The SCI+mino (D7R = day 7 treatment): following the laminectomy and SCI, minocycline (90 mg/kg in 0.5 ml buffered saline) was administered as single IP dose daily for 7 days.

In the 7d group, the mice were euthanized 7 days after SCI and SCs were harvested for RNA extraction.

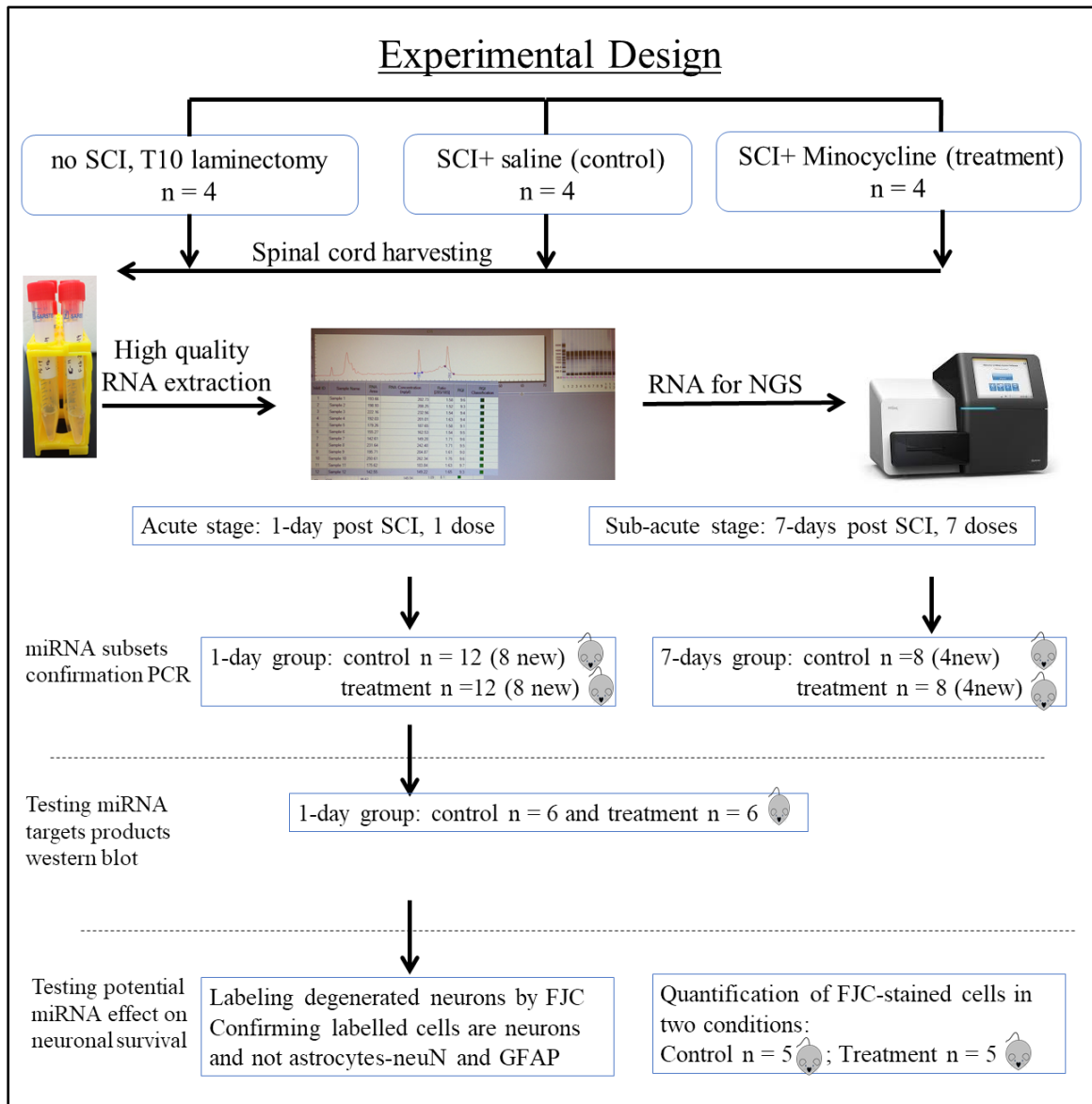


Figure 2.1 Experimental Design including Next Generation Sequencing, protein expression testing (western blot) and histology experiments. *Nadi, 2020.*

2.2.3 Surgical procedures and setup

The surgery performed T10 laminectomy to expose the lower thoracic SC (65). General inhalational anesthesia was used for all surgeries. Inhalational isoflurane (Isoflurane USP- Fresenius Kabi Canada) was delivered at a rate of 4% for anesthesia induction and

at a rate of 1.5% as a maintenance dose during the surgery with medical oxygen as carrier gas at a flow of 1.0 L/min.

At the time of surgery, a mouse was transferred from their cage to the anesthesia chamber. Once the animal was anesthetized, the fur in the surgical area was removed by using an electric clipper, centered around the dorsal midline starting from the area of the spinal column arch up to the neck. The weight of the mouse was recorded and then the mouse was transferred to the surgical platform. To prevent corneal abrasion, eye lubricant (Lacrilube) was applied to both eyes and the animal's nose was inserted into the nose cone to maintain anesthesia. The depth of anesthesia was monitored by observing the respiratory pattern and applying pressure on the nailbed of the forefoot.

The animal was kept in a prone position. To keep the mouse's nose within the nose cone that delivers the anesthesia and to restrict mouse movement during the surgery, the forefeet were gently taped to the surgical platform. The rear feet remained free. The procedure was performed under strict sterile conditions and with the aid of a binocular microscope (Leica M 651). The shaved area was wiped first with soap (GERMI-STAT GEL antiseptic soap, Chlorhexidine Gluconate 4%), then 70% alcohol (Isopropyl alcohol 70% USP) and finally by propidine microbicidal solution (Poloxamer-Iodine Complex 1%) (three times each). A subcutaneous injection of 0.1 mg/kg buprenorphine SR (slow release) was administered just before scoring the skin. A scalpel with a #11 blade was used during the procedure. An approximately 10 mm skin incision was created between the scapulae and the back bow. Upon identification of the T10 spinous process (65), the paraspinal muscles were dissected from midline spinous processes and interspinous ligaments in a lateral direction. The dissection was kept close to the bone (subperiosteal muscle elevation) to minimize the bleeding from the muscle belly. After identification of T10 lamina, a micro rongeur was used for the laminectomy. The laminectomy started from the caudal inter-laminar space and proceeded rostrally. This helped removing the inter-laminar ligaments and provided a clear visualization of the SC and minimized iatrogenic SC injury. Ligamentum flavum was identified, gently dissected, and removed. A sterile cotton swab was used to control minor bleedings by exerting some pressure for approximately 20 to 30 seconds, in addition to saline irrigation.

Upon completing the laminectomy, the spinal column was stabilized by using custom surgical platform stabilizing forceps, first placing the rostral stabilizer then the caudal one. To facilitate equal force distribution during the impact injury to the SC, the spinal column was kept straight and parallel to the surface of the surgical platform. During the spinal column stabilization, normal spinal cord pulsation was observed and maintained. Care was taken to avoid overtightening the stabilizing forceps to prevent inadvertent compression of the spinal column and obstruct venous drainage which could initiate unnecessary new bleeding.

Delivering impact injury to the SC: The Infinite Horizon Spinal Cord Impactor (Precision Systems and Instrumentation V5.0, Lexington, KY, USA) was utilized for this purpose.

The surgical platform was moved on to the impactor. The sterile impactor tip was centered over the exposed part of the SC. A moderate injury was delivered by pre-setting the impact force to 50 kilodynes, which was the desired force (255, 256). The actual delivered force to the SC as well as tissue displacement was recorded by the device sensors. After the injury, the paraspinal muscles were reapproximated by applying two silk 6-0 sutures. The skin was closed in one layer using 6-0 silk or Prolene sutures. The surgical room setup is illustrated in appendix B (Figure B.1).

Immediately following the surgical procedure, while the animal was still asleep, an IP (intraperitoneal) injection of 0.5 mL sterile buffered saline (pH 7.4-7.6) (for the sham and control groups) or 90 mg/kg minocycline dissolved in 0.5 mL same buffered saline (treatment group) were administered immediately after surgery.

2.2.4 Recovery and post-operative care:

Upon recovery, the mouse was placed in a new clean cage containing autoclaved hay, bedding, and a shallow container of mash style food. Water and food were provided continuously. The cage was placed on a heating pad in the recovery room with controlled dark-light time every 12 hour. Mice were weighed daily. Mice experiencing weight loss greater than 20% of pre-operative weight were sacrificed as per agreed humane end point. In addition to regular food and water, the 7-day group mice were provided with high

calorie diet supplement-Diet Gel Boost-72-04-5022 and purified dietary supplement - Diet Gel Recovery-72-06-5022.

The bladder of the mouse was expressed thrice daily. Mice were sacrificed if indications of severe pain or health deterioration (e.g., change in respiration pattern or rate, reluctance to be handled, disarranged fur, ruptured bladder, or appetite problem) were observed post-surgery.

The mice were excluded from the analysis if:

1. Significant bleeding from a major vessel or bone at any stage of surgery or post-operatively.
2. Dural breach and CSF leak
3. Iatrogenic SCI during the laminectomy or spinal column stabilization.
4. Animal showed features of significant stress or required to be euthanized for reasons determined by the veterinarian after surgery.

2.2.5 Preparation and administration of minocycline:

Minocycline hydrochloride (MH) crystalline- (Sigma-Aldrich M9511, code 101530966) was prepared in injectable saline (pH 7.4-7.6) buffered with sodium bicarbonate. To dissolve MH completely, the saline was heated in 55 °C water bath for 15-20 minutes. The MH solution was wrapped with foil until the time of injection or stored in the dark at 4 °C for up to two days, as per manufacturer's instructions. It was administered at a dose of 0.09 mg/gm (90 mg/kg) in 0.5 ml saline intraperitoneally (IP) (257, 258) as a single dose immediately after skin closure for the 1d group. For the 7d group, MH was given as a one dose/day total of seven doses at the same time everyday.

2.2.6 RNA extraction and quality control

At the predetermined time, the mice were euthanized by a lethal dose of pentobarbital (250 mg/kg), delivered intraperitoneally. The SC was extracted via hydraulic expulsion using an 18-gauge needle and a 5 mm length, centered on the injury epicenter, was harvested. The Animal Tissue RNA Purification Kit (Cat. 25700 Norgen Biotek Corp.) was used to extract high quality RNA. The manufacturer's instructions were followed and modified according to our tissue specimens. All buffers were supplied within the kit. In summary, the SC specimen was washed well with cold sterile PBS 1X (Gibco™ PBS 1X, pH 7.4 Catalog # 10010023). Then the specimen was moved to bead-bug tube with 300 µl Buffer RL mixed with 3 µl of 2-beta mercapto-ethanol (Sigma M-7522, EC No 200-464-6) concentration =1/100. Homogenization was conducted immediately for 30-60 seconds in an electric homogenizer. The homogenized sample was kept at room temperature for 1-2 minutes then moved to -80 °C freezer. On the day of RNA extraction, the sample was thawed gradually on ice and 600 µl of RNase-free water was added and mixed well. Proteinase K 20 µl was added and vortexed. The sample was incubated for 15-30 minutes in 55 °C water bath in a floater, then centrifuged for 1 minute at 14000 rpm. The clear supernatant was transferred to a new Eppendorf tube, the pellet was discarded, and 450 µl of 100 % ethanol was added to the lysate.

The lysate was applied to a column with collecting tube unit and spun to collect the RNA. Then, 400 µl of wash Solution A was added to the collecting tube and centrifuged as described above. Enzyme incubation Buffer A 100 µl and 15 µl of DNase I were then added to the column and centrifuged for an additional 1-2 minutes. The flowthrough was pipetted from the collection tube (the whole 115 µl) back to column and incubated for 15 minutes at room temperature. Then 400 µL of wash Solution A was added and centrifuged for 1 minute three separate times. A new elution tube was used, and the column was placed in it to add 50 µl of elution Solution A. The solution was incubated for 5 minutes at room temperature and then centrifuged for 2 minutes. After extraction, RNA concentration, purity, and integrity were tested as quality control before using the samples in the next experimental steps (259). For RNA quality control, 3-5 µl of each RNA sample was used and the rest of the sample was stored at -80 °C until further use.

The BMG LABTECH- SPECTROstar Nano system was used to test for purity and concentration. RNA concentration was measured at 260 nm, and the purity at 260/280 and RQI (RNA Quality Indicator for integrity) via microchip system (Bio-Rad).

Briefly, 2 μ l of elution solution in the first upper two wells of the microplate, followed by 2 μ l from each RNA sample was applied to the designated well. The microplate was read on a SPECTROstar reader. The RNA samples with absorbance of 260/280 between \sim 1.8 and 2 were used for further experimental processing. The RNA integrity was checked using Experion RNA StdSens Chips (Bio-Rad, catalog # 7007153), Experion RNA StdSens analysis kit (Bio-Rad, catalog # 7007154), and Experion automated electrophoresis system. The procedure was performed using microchip and following the manufacturer's instructions. Only RNA samples with RQI >8 were used for the analysis.

2.2.7 Library preparation and miRNA deep sequencing:

For miRNA library construction and deep sequencing, the RNA samples were submitted to and processed by Next Generation Sequencing Facility - The Center for Applied Genomics, The Hospital for Sick Children, Toronto, ON, Canada. First, the total RNA samples went through another quality control check by using an RNA Nano chip- Agilent 2100 bioanalyzer system following manufacturer's recommendations. RNA concentration was measured by using Qubit fluorometer and Qubit RNA (high sensitivity) HS Assay from ThermoFisher Scientific. The construction of small RNA library followed Illumina protocol- "NEBNext Small RNA Library Prep Set". The library was sequenced on an Illumina HiSeq 2500 - Rapid Run platform following the manufacturer's instruction (260).

2.2.8 miRNA quantification and differential analysis

The database miRbase (<http://mirbase.org>) (261) and sRNAbench (262) were used for known miRNA identification and quantification. Novel miRNA were predicted by using

mirdeep2 (263). Differential analyses between various 1d and 7d groups were performed. In brief, bcl2fastq2 v2.17 was used to generate the data output that was processed in FASTQ format. FastQC v.0.11.2 was used to evaluate data quality (<http://www.bioinformatics.babraham.ac.uk/projects/fastqc/>) (264). Raw reads were assessed for quality and adaptor trimming by utilizing trim-galore v0.4.1 (http://www.bioinformatics.babraham.ac.uk/projects/trim_galore/). Stringency 5 was used for adaptor trimming and minimum phred score was set at 20 to trim low-quality end reads. V21 of mature sequences from miRbase (<http://mirbase.org>) was used for known miRNAs quantification. sRNAbench (<http://bioinfo5.ugr.es/sRNAbench>) (262) was used to analyze the reads. The read length cut-off was set at 15. Reads shorter than 15 were excluded from analysis.

Reads were first mapped to mouse genome. Then genome coordinates of miRNAs were determined (<http://bioinfo5.ugr.es/sRNAbench>). Novel miRNAs were analyzed using mirdeep2 version 0.1.3 (<https://www.mdc-berlin.de/content/mirdeep2-documentation>). The counts of all mature miRNAs in all groups were uploaded into DESeq2 (<https://bioconductor.org/packages/release/bioc/html/DESeq2.html>) for differential analysis (265).

2.2.9 Validating the results of miRNA Deep Sequencing and identification of miRNAs function

To validate the results of deep miRNA sequencing, Real time-qPCR and ddPCR were used to confirm the results (6, 227). SCI experiments were repeated as described earlier for both 1-day and 7-day survival after SCI. The RNA samples that were analyzed by deep sequencing in addition to the new samples were included in the analysis. A subset of miRNA from both the one-day and seven-days groups' deep sequencing results were selected to run the qPCR because deep sequencing of miRNA resulted in expression changes in hundreds of miRNAs. The aim of the project was to identify a neuroprotection pathway, so the miRNAs that potentially target translation of proteins playing a role in neuroprotective pathways were selected. Thus, a systematic way for

selecting a subset of miRNA from both time points was developed. First, the miRNAs were reviewed in miRbase which provides essential information about the miRNA such as annotation confidence, sequence, and its cluster (266). The miRbase also has a direct link to an online database to predict the targets of miRNA. So, the miRNA targets were first reviewed in miRDB (267). This database used target scores between 0 and 100, as absolute unit of prediction or likelihood of being a real target. It has been recommended with this data set to use targets with scores between 80 to 100, which reflects the likelihood of being real targets. Then the selected targets were reviewed in another data set, the Targetscan Vert which uses different scores to minimize the false positive target selection (268). Only the miRNAs whose predicted genes were found in both datasets were selected.

2.2.10 RT-qPCR and ddPCR (Real time – quantitative polymerase chain reaction and droplet digital PCR)

The miRNA-subsets included six miRNAs from the 1-day group and four miRNAs from the 7-day group. The miSCRIPT chemistry was selected as it contains the primers for all miRNAs in the selected subsets of both groups. The kit, miRNAs primer sets and endogenous controls small RNAs are illustrated in Table 2.1. First, miRNA cDNA was synthesized using miSCRIPT II cDNA synthesis kit according to manufacturers' instructions. In brief, cDNA of 10 µl was synthesized by using 150 ng of total RNA. All primers were validated for optimal dilution and running temperature and then the RT-qPCR was performed. The miRNAs that showed different patterns of change from miRNA sequencing were processed further by doing ddPCR as another step of confirmation. The comparisons were made between SCI+SLN and SCI+mino conditions. In the 1-day group 12 samples were included in qPCR reactions, while 8 cDNA samples were included in qPCR analysis in the 7-day group. These samples include the new and all sequenced samples. For ddPCR, 11 samples from the 1-day group were analyzed and all 8 samples from the 7-day group. A C1000 Touch Thermal Cycler- CFX384 Real-Time System from Bio-Rad was programmed to run the qPCR. The steps were set up according to the protocol provided by the manufacturer. The RT-qPCR reaction was of

40 cycles that include three reaction-steps per cycle, denaturation step at 95 °C for 15 sec, annealing step for 15 sec, and extension reaction at 70 °C for 15 sec. The program for ddPCR was modified for 50 cycles as its end point reaction, denaturation 30 sec at 95 °C, annealing 30 sec at 60 °C and extension for one minute at 70 °C. The ddPCR consists of four main steps, preparing ddPCR mixture using QX200 ddPCR EvaGreen supermix (Bio-Rad, catalog # 1864034), droplet generation by using QX200 Droplet Generation Oil for EvaGreen (Bio-Rad, catalog # 1864006), then PCR amplification, and finally loading the samples into the QX200 Droplet Reader.

The reagents and primer sets used in RT-qPCR and ddPCR

All from Qiagen unless where indicated.

1. miSCRIPT II cDNA synthesis kit 50 reactions cat # 218161
2. miScript SYBR Green PCR Kit (1000) including the universal primer cat# 218075
3. Spike in control kit cat # 339390
4. Spike in control primer ce-miR-39-3p MS00019789
5. miScript Primary Assays (100)- cat#218300 includes the following primers
6. Mm-miR15b-5p gene globe ID MS00011235
7. Mm-miR-21a-5p gene globe ID MS00011487
8. Mm-miR-486a-3p gene globe ID MS00025998
9. Mm-miR-34a-5p gene globe ID MS00001428
10. Mm-miR-702-3p gene globe ID MS00002912
11. Mm-miR-3547-3p gene globe ID MS00065470
12. Mm-miR-15b-3p gene globe ID MS00011242
13. Mm-miR-200b-3p gene globe ID MS00011417
14. Mm-miR-96-5p gene globe ID MS00001456
15. Mm-miR-344c-3p gene globe ID MS00025620
16. Hs_SNORD72_11 (reference primer) gene globe ID MS00033719
17. Hs_SNORD95_11 (reference primer) gene globe ID MS00033726
18. Hs_SNORD96A_11 (reference primer) gene globe ID MS00033733
19. Hs_RNU6-2_11 (reference primer) gene globe ID MS00033740
20. From Bio-Rad: SYBR green master mix Bio-rad Cat# 172527

Table 2.1 The reagents and the primers that were used in RT-qPCR and ddPCR experiments to validate the NGS findings.

2.2.11 Statistical analysis

The data was analyzed by first drafting the results in Microsoft Excel sheet and then transferred into GraphPad Prism v 9.0.0 for Windows (GraphPad Software, La Jolla, California, USA, www.graphpad.com). Student's t-test was performed, and all results

expressed as mean \pm SEM. GraphPad prism was also used to check for normal distribution of our data.

2.3 Results

2.3.1 Next generation sequencing (NGS):

In the 1d group, miRNA analysis included RNA samples extracted from a total of 12 mice (biological replicates), 4 mice in each experimental condition (no SCI, SCI+SLN, and SCI+mino). In the 7d group, miRNA analysis included RNA samples extracted from 8 mice, 4 biological replicates each in two experimental conditions (SCI+SLN and SCI+mino). A total of 20 biological replicates were analysed by NGS. All RNA samples passed the quality control tests with minimum RNA Integrity Number (RIN/RQI) of 8.7.

2.3.2 Principal component analysis (PCA):

This multivariate method of analysis is used to depict the behavior of a large number of variables at the same time. It has been previously described in microarray analysis (227) to determine whether the behavior of a certain group of genes or miRNAs can be grouped or segregated. For the 1d groups, the PCA diagrams reflected general patterns of miRNA expression, specifically, PCA-1 and PCA-2 gave the general distribution of the miRNA expression. The miRNAs are well-clustered according to the experimental groups (no SCI, SCI+SLN, and SCI+mino) (Figure 2.2 PCA for 1d group). For the 7d group analysis, two attempts at PCA were conducted. First, 4 samples of SCI+SLN and 4 samples of SCI+mino along with the 4 baseline samples (no SCI – laminectomy only from the 1d group) were analyzed. This PCA failed to show segregated groups (Appendix B Figure B.2 through B.4). The second attempt included the samples from 7d groups only. Again, the PCA did not show well segregated groups between SCI+SLN and SCI+mino in PCA1, PCA2 and PCA3 (Appendix B Figure B5 and B6). In PCA3 vs PCA4, there was a separation between these two groups (Fig. 2.3 PCA for 7d group).

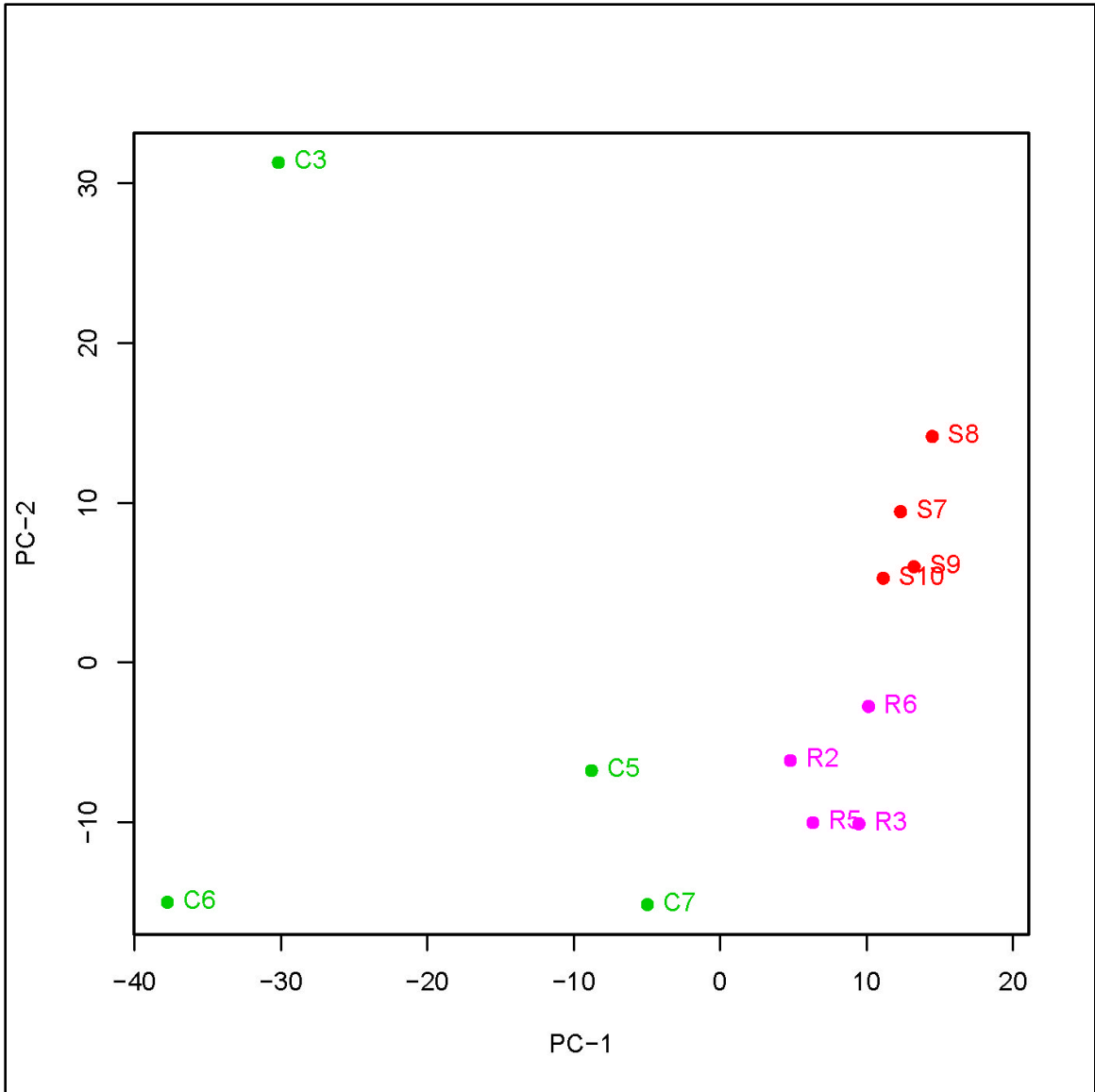


Figure 2.2 Principal Component Analysis (PCA) for 1d timepoint group.

PCA1 vs PCA2 illustrates well-clustered samples of each experimental condition in 1d survival group. S = no SCI; C = SCI+SLN; R = SCI+mino

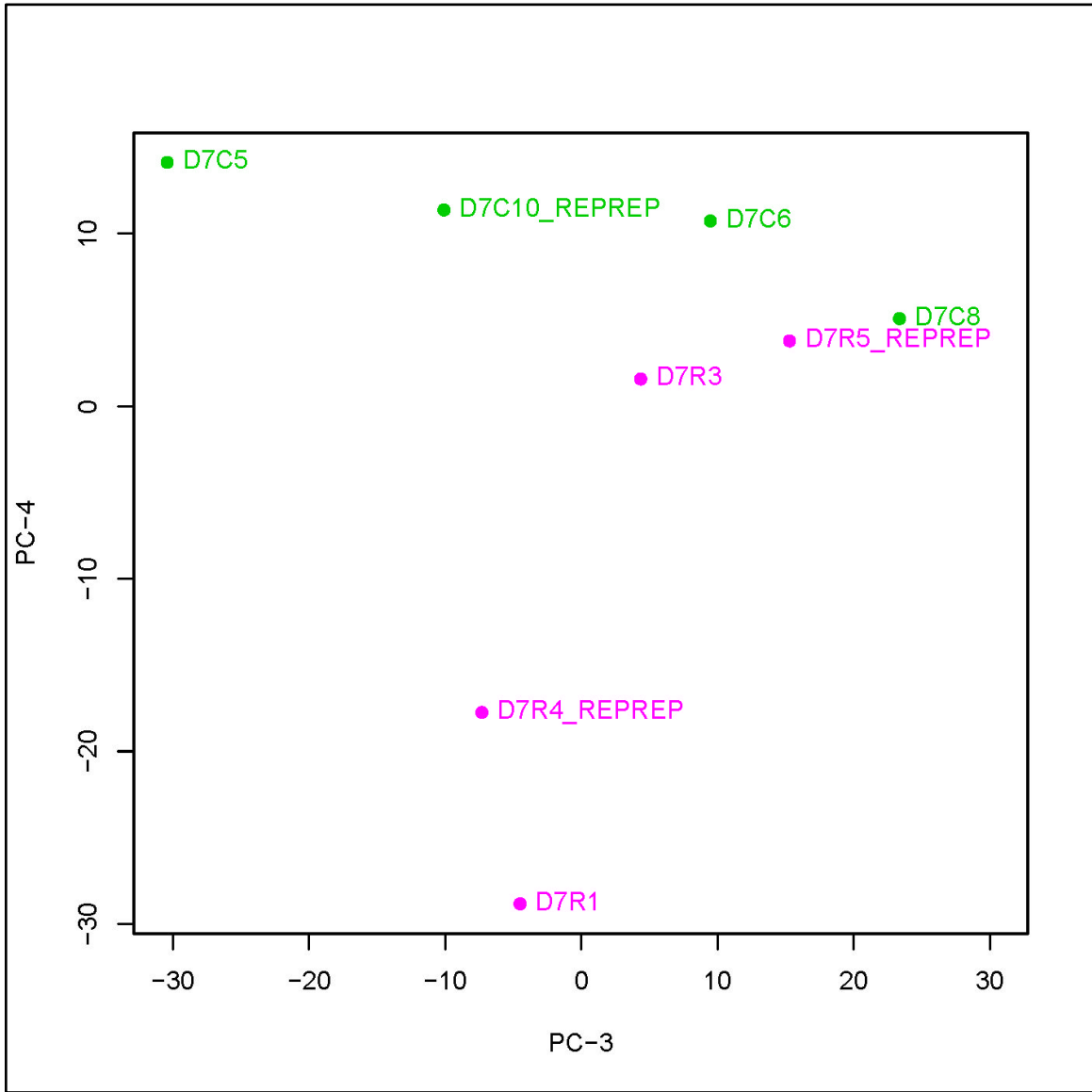


Figure 2.3 PCA3 vs PCA4 for 7d group.

This figure illustrates a pattern of segregation between the two experimental conditions in 7d group. D7 = 7day group; C = SCI+SLN; R= SCI+mino; REPREP = the cDNA samples were reprepared again for technical error and failed the initial preparation.

2.3.3 Heat maps and volcano plots:

The heat maps for the 1d group demonstrated well-clustered groups and the miRNAs were differentially expressed according to the three experimental conditions: no SCI vs SCI+SLN (Figure 2.4), SCI+ mino vs SCI+SLN (Figure 2.6), and SCI+ mino vs no SCI (Figure 2.8) for the 1d group analysis (the detailed heatmaps are in appendix B). Volcano plots for the three conditions in the 1d group illustrate the magnitude of changes of individual miRNAs: SCI+SLN vs no SCI (Figure 2.5), SCI+ mino vs SCI+SLN (Figure 2.7), and SCI+ mino vs no SCI (Figure 2.9).

Likewise, the heat map for the 7d group demonstrated well-clustered groups (SCI+SLN, and SCI+ mino). Again, the volcano plot depicted the magnitude of differentially expressed miRNAs (Figures 2.10 and 2.11 heatmap and volcano plot for the 7d group)

2.3.4 Identification of miRNAs 1 day (acute phase) following the SCI by Next Generation Sequencing (NGS)

In the 1d group, the experimental conditions were compared to each other. This group represents the acute changes seen miRNA expression following the SCI.

A. SCI+SLN compared with no SCI condition: to determine how the injury alters miRNA expression in SC, the SCI+SLN condition was compared with baseline miRNA expression in no SCI condition. There were 120 miRNAs identified which displayed significant changes after 1 day of SCI. Of these 120 miRNAs, 40 miRNAs downregulated and 80 upregulated (Figures 2.4 Heatmap and 2.5 Volcano plot; Table B.1 Appendix B). There were 10 novel miRNAs identified in SCI+SLN group (Table B.2 Appendix B). All these new miRNAs were upregulated after the injury.

B. SCI + mino group compared with SCI+SLN group: there were 81 miRNAs showing significant changes in expression. Of these, 59 miRNAs were downregulated, and 22 miRNAs were upregulated (Figures 2.6 Heatmap and 2.7 Volcano plot; Table B.3

Appendix B). By comparison, 4 novel miRNAs demonstrated a downregulation in expression following treatment with minocycline (Table B.4 Appendix B).

C. SCI + mino compared with no SCI condition: there were 27 miRNAs that showed significant miRNA expression changes within the SCI+mino condition compared with no SCI condition. Of these miRNAs, 3 were downregulated, and 24 upregulated (Figures 2.8 Heatmap and 2.9 Volcano plot; Table B.5 Appendix B). Furthermore, 7 miRNAs were novel miRNAs (Table B.6 Appendix B). Following minocycline administration, the novel miRNA - chrX_23260 was upregulated and the miR543-3p downregulated. The latter two miRNAs did not show significant expression changes following injury in SCI+SLN group. Additionally, minocycline did not influence the expression level of miR615-3p and miR218-5p that were downregulated by the injury and remained significantly downregulated after minocycline administration.

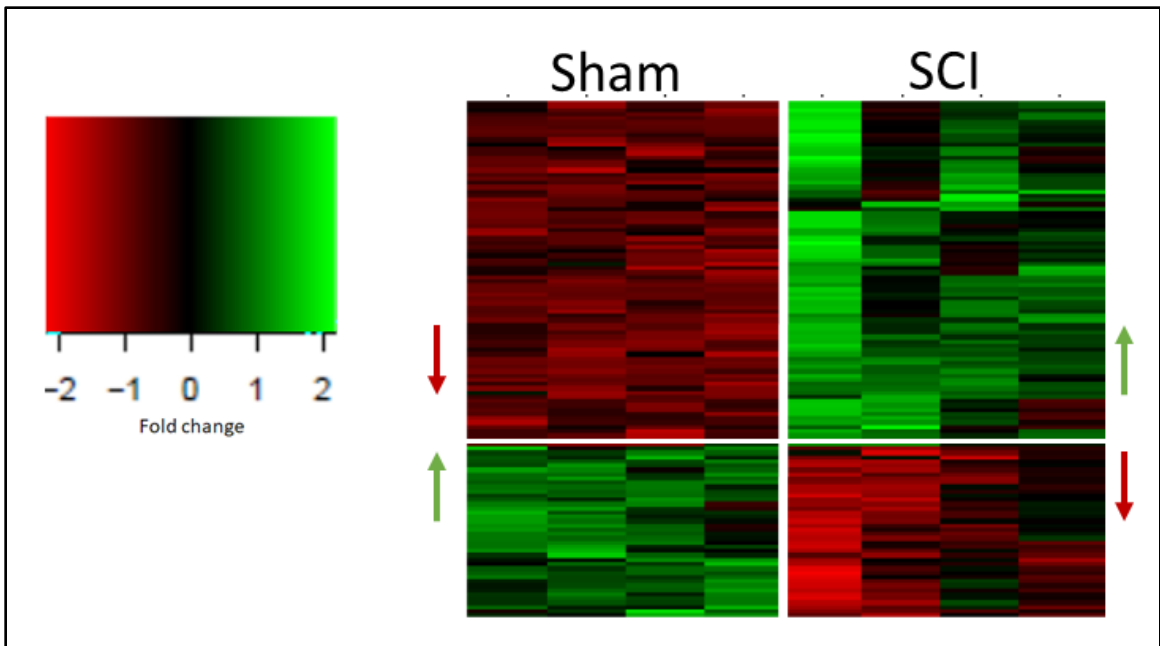


Figure 2.4 Simplified heatmap: no SC vs SCI+SLN 1d demonstrating the changes of miRNAs after one day of SCI.

The left upper colored rectangle represents the color key. The red color represents downregulated miRNAs while green color represents upregulated miRNAs. The detailed heatmap in appendix B. figure B.7.

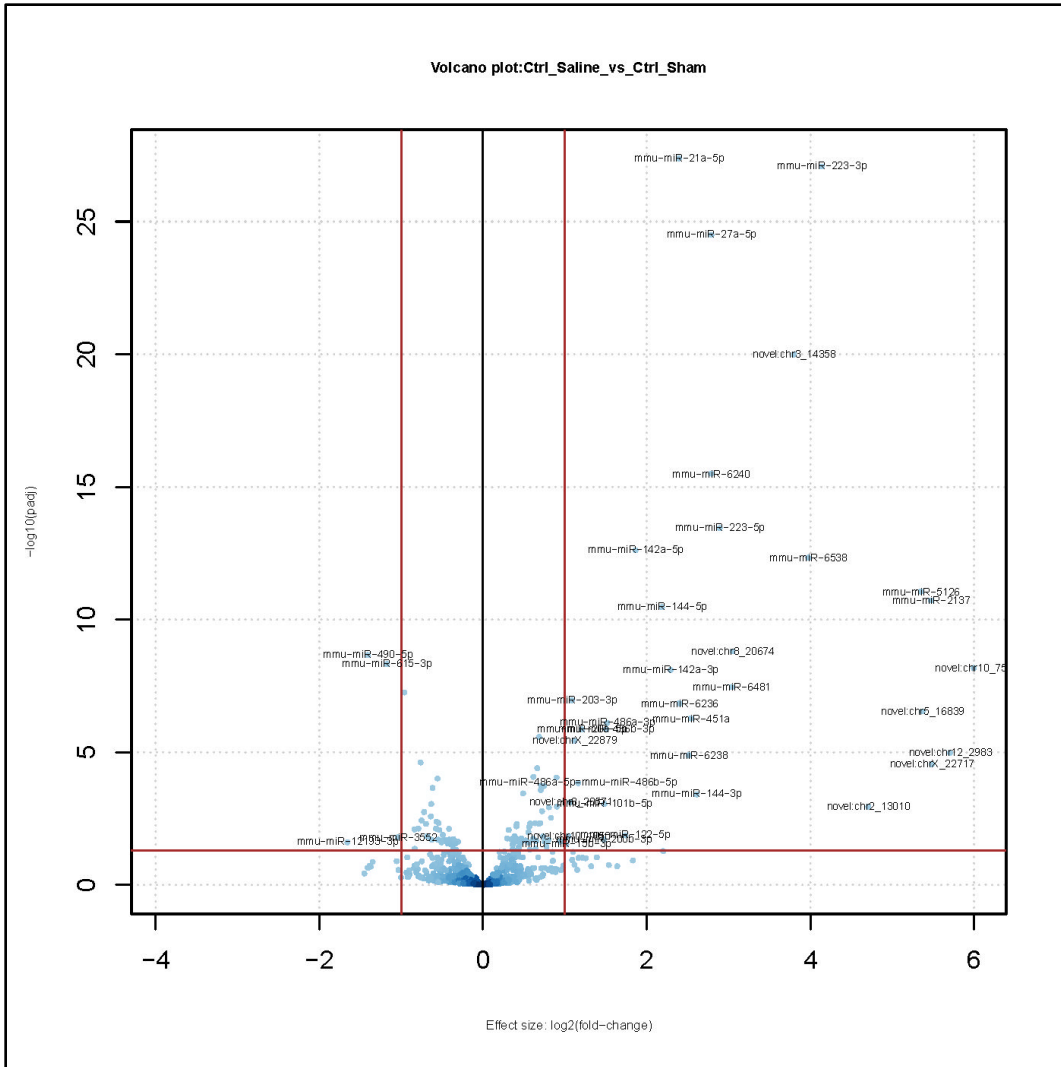


Figure 2.5 Volcano plot: SCI+SLN vs no SCI 1d illustrates the fold of changes and the magnitude of miRNA alteration after one day of SCI

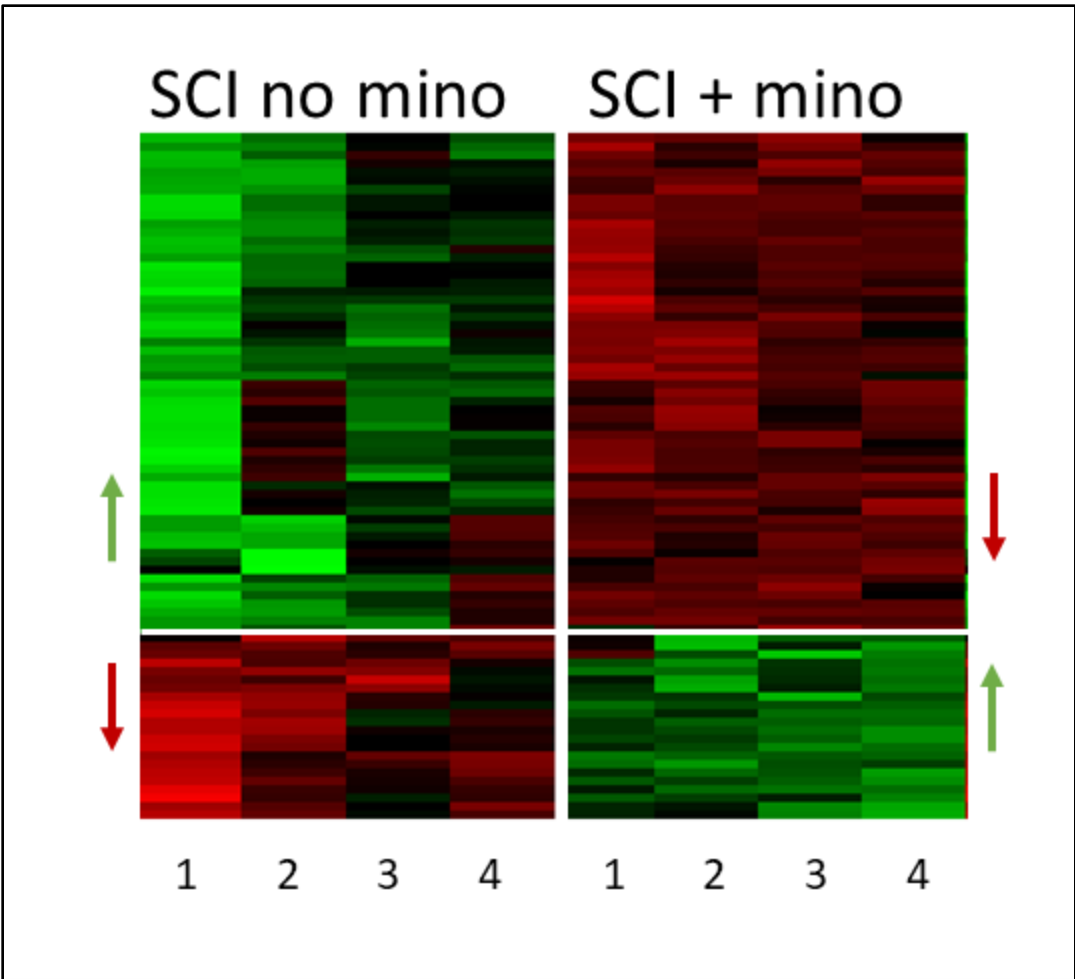


Figure 2.6 Simplified heatmap: SCI+mino vs SCI+SLN 1d demonstrating the miRNA changes after minocycline administration in comparison to SCI with saline control.

The detailed heatmap is in appendix B figure B.8.

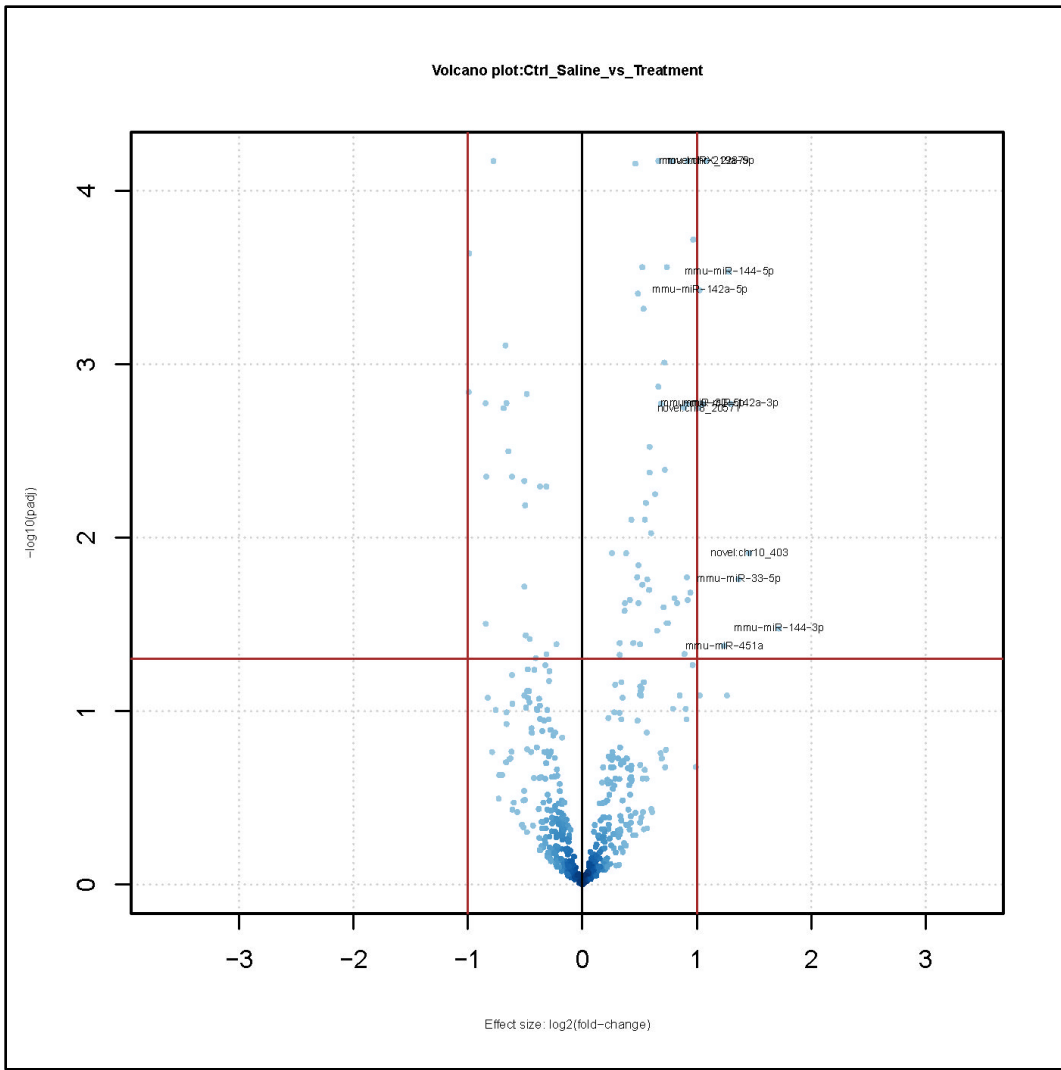


Figure 2.7 Volcano plot: SCI+mino vs SCI+SLN 1d illustrates the fold of changes and the magnitude of miRNA changes after minocycline administration measured one day after SCI.

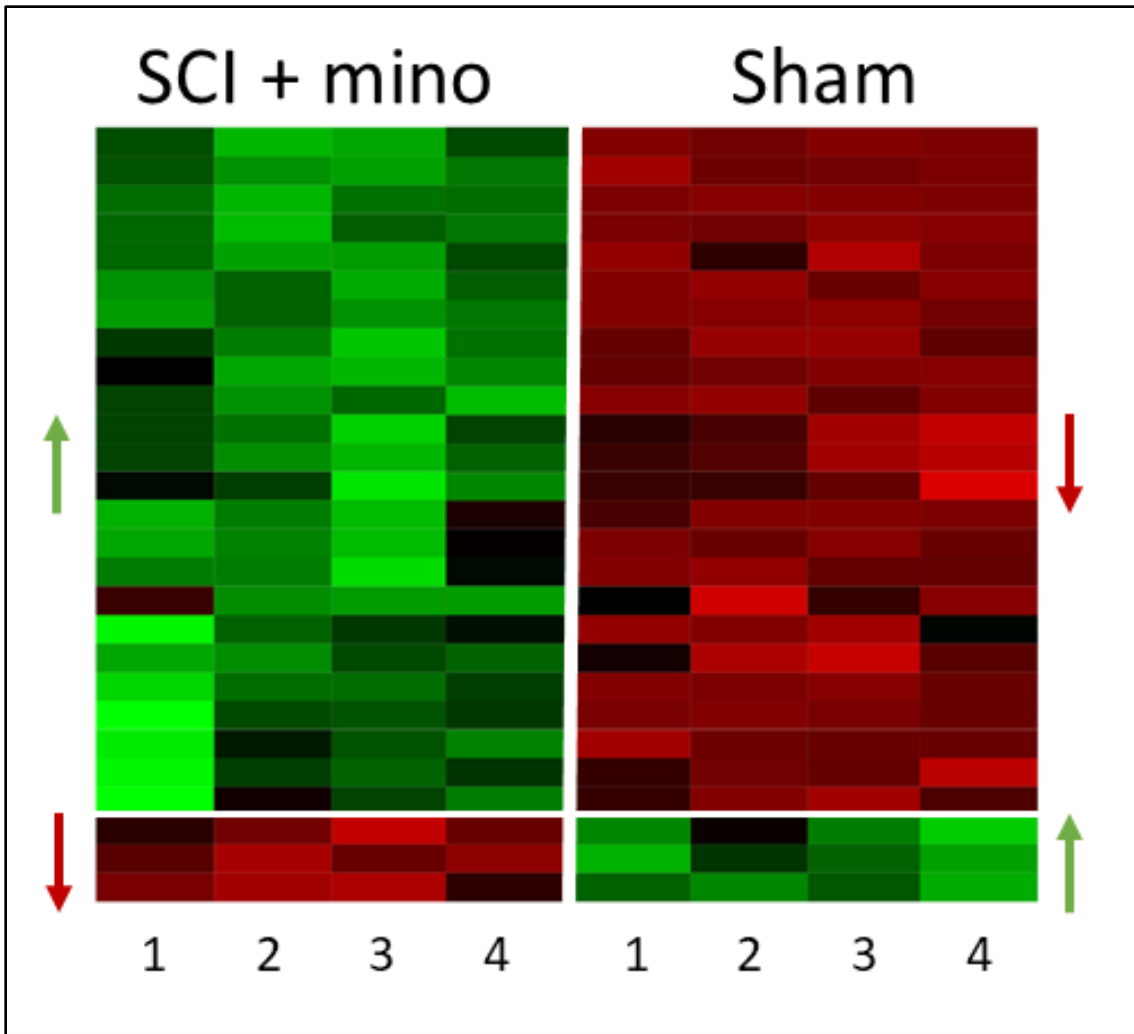


Figure 2.8 Simplified heatmap: SCI+mino vs noSCI 1d demonstrates the miRNA pattern changes following minocycline administration in comparison to no SCI condition after 1d of SCI.

The detailed heatmap is in appendix B figure B.9.

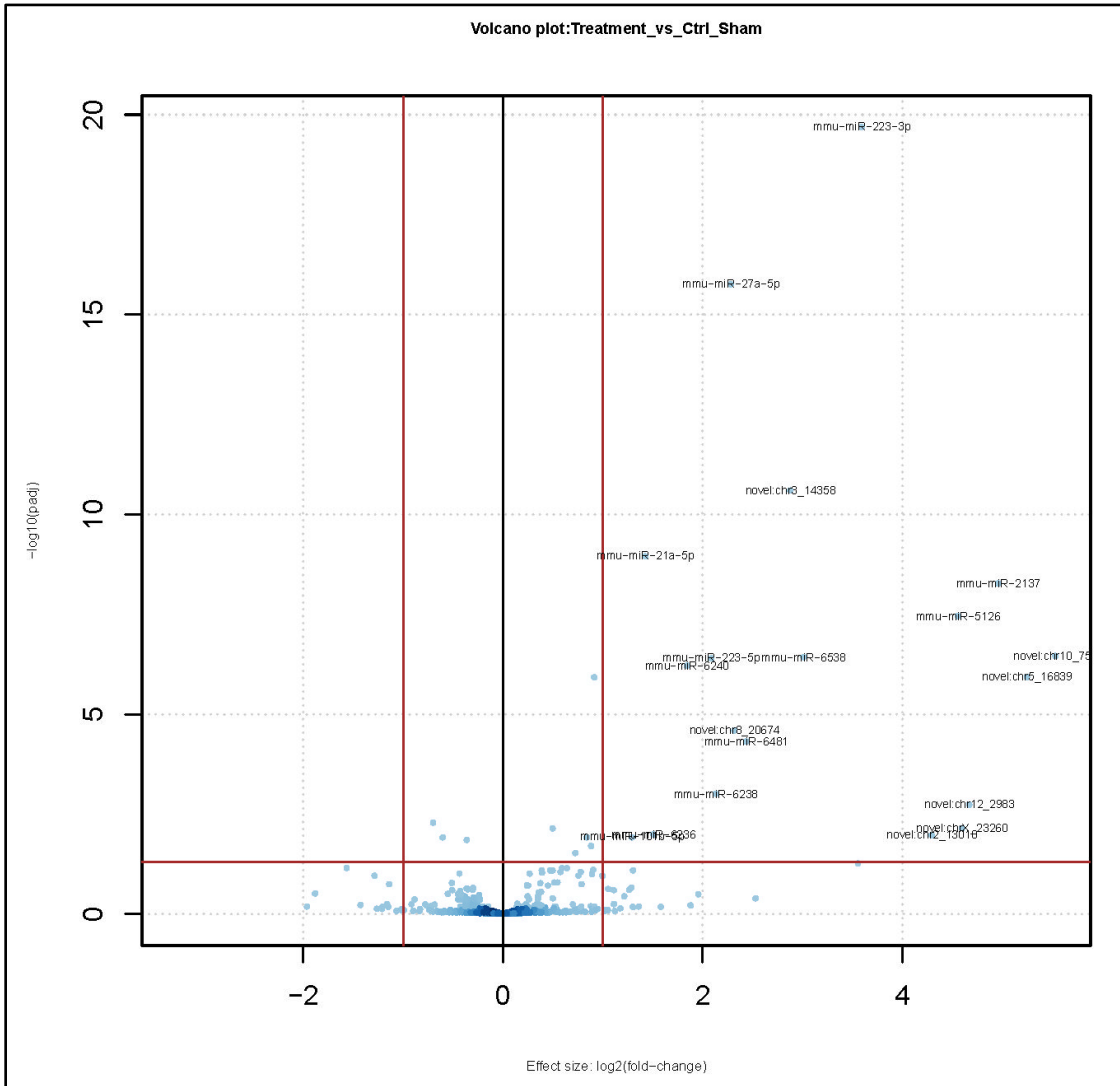


Figure 2.9 Volcano plot: SCI+mino vs noSCI 1d illustrates the miRNA pattern changes following minocycline administration in comparison to no SCI condition after 1d of SCI.

2.3.5 Identification of miRNAs 7-day (sub-acute phase) following the SCI by NGS

In the 7-day survival groups, two experimental conditions were included in the analysis, SCI+SLN and SCI + mino. The comparison of these two conditions showed significant changes in the expression of 14 miRNAs; 7 miRNAs were upregulated and 7 downregulated (Figures 2.10 Heatmap and 2.11 Volcano plot, Table B.7 known miRNA in the 7d group Appendix B). Of these 14 miRNAs, 6 were novel miRNAs (Table B.8 Novel miRNA in 7d group Appendix B).

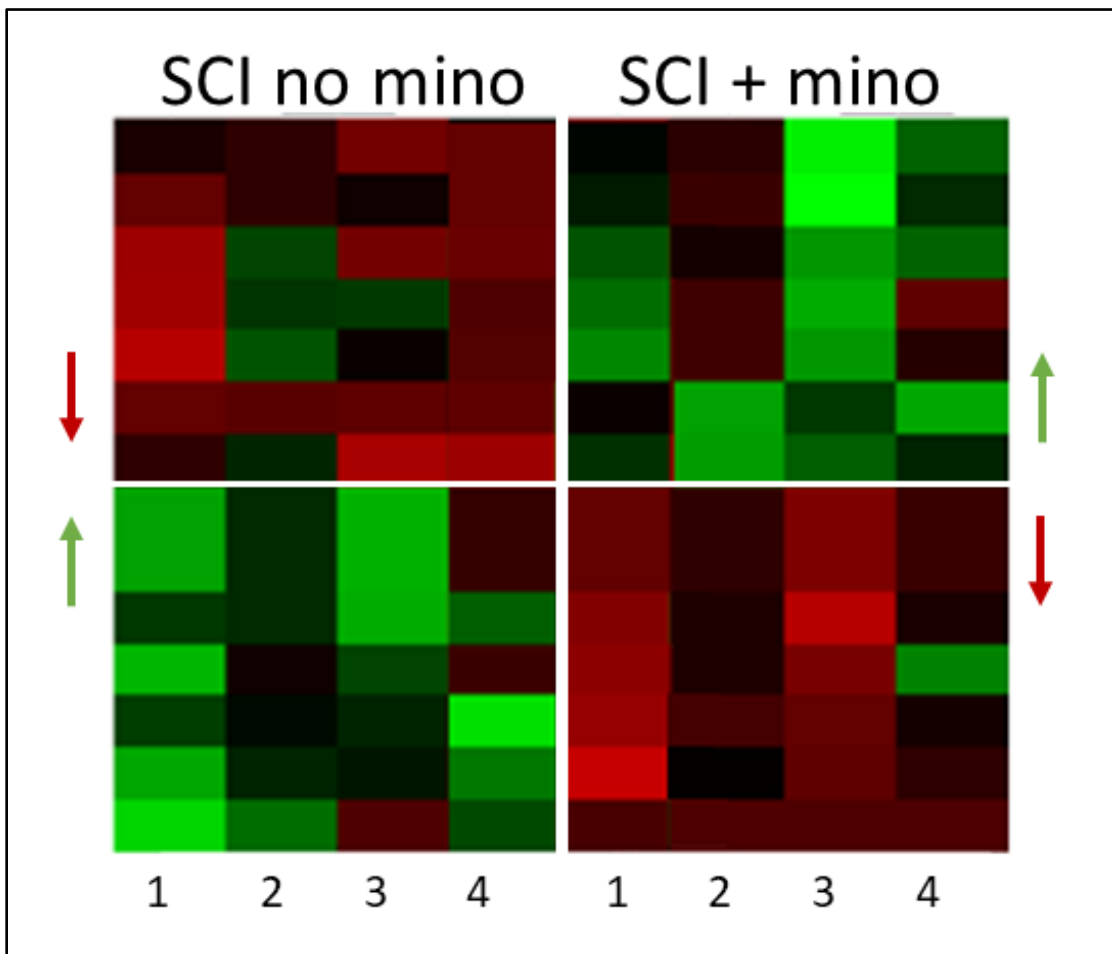


Figure 2.10 Simplified heatmap: SCI+SLN vs SCI+mino 7d demonstrates the changes of miRNA expression following minocycline administration and SCI (treatment) in comparison to SCI+ saline (control) tested 7 days after SCI.

The detailed heatmap is in the appendix B figure B.10

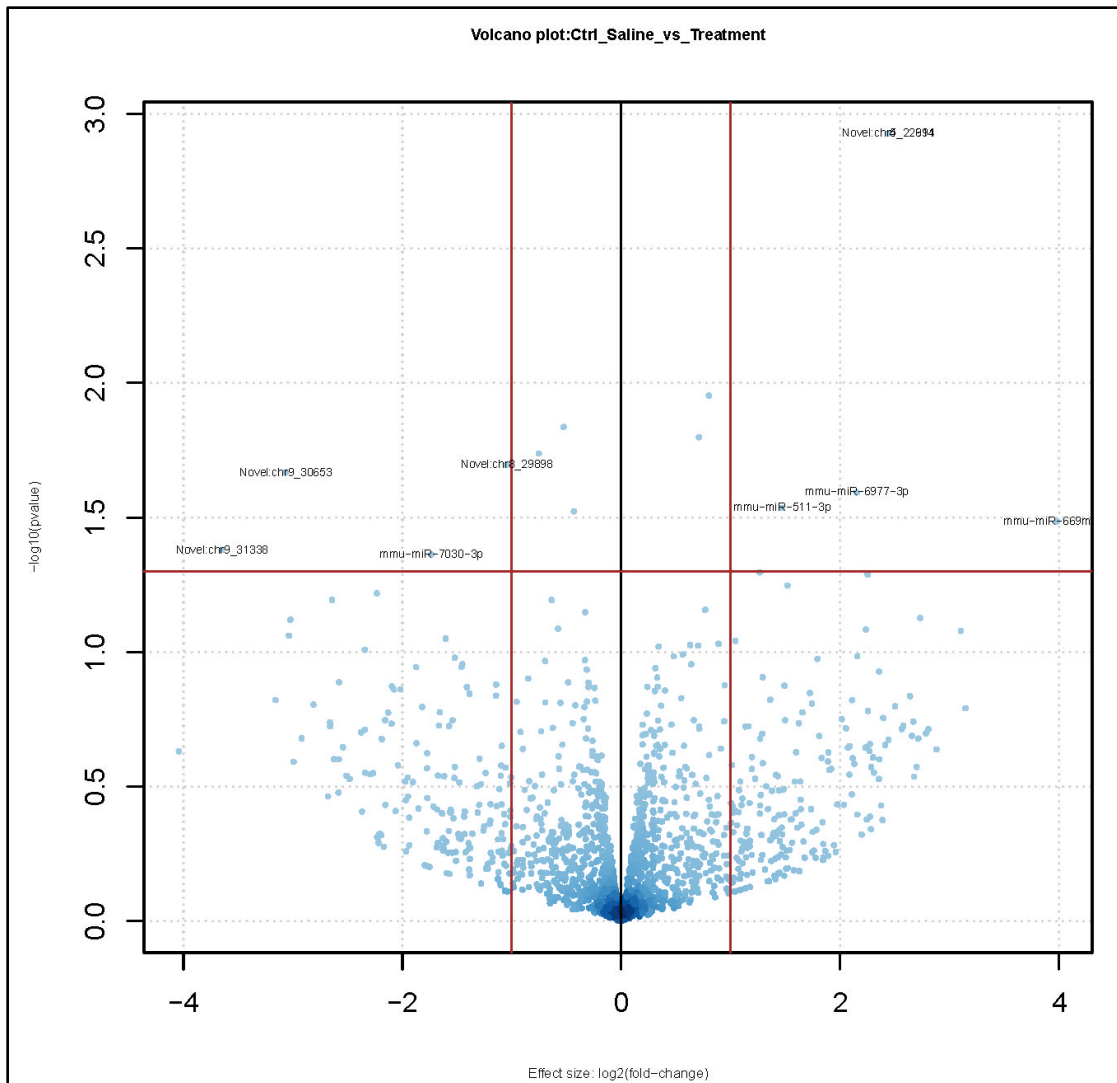


Figure 2.11 Volcano plot: SCI+SLN vs SCI+mino 7d illustrates the magnitude and fold changes of miRNA expression following minocycline administration and SCI (treatment) in comparison to SCI+ saline (control) tested 7 days after SCI.

2.3.6 Criteria of miRNA selection for confirmation in the 1d group

The results obtained from miRNA deep sequencing showed significant changes in the levels of expression of a multitude of miRNAs, either due to injury per se or due to administration of minocycline. To validate the results of deep sequencing, a subgroup of the miRNAs that were significantly changed due to injury and minocycline were selected. The selection criteria were set up to focus on the main objective of the study, which is to

understand the mechanisms of sSCI but specifically exploring neuroprotective pathways. As discussed earlier, this is the first study to analyze the effect of a known neuroprotective drug (minocycline) on miRNA expression following SCI. The criteria for selecting the subset of miRNAs in the 1d-survival group (Figure 2.12) included:

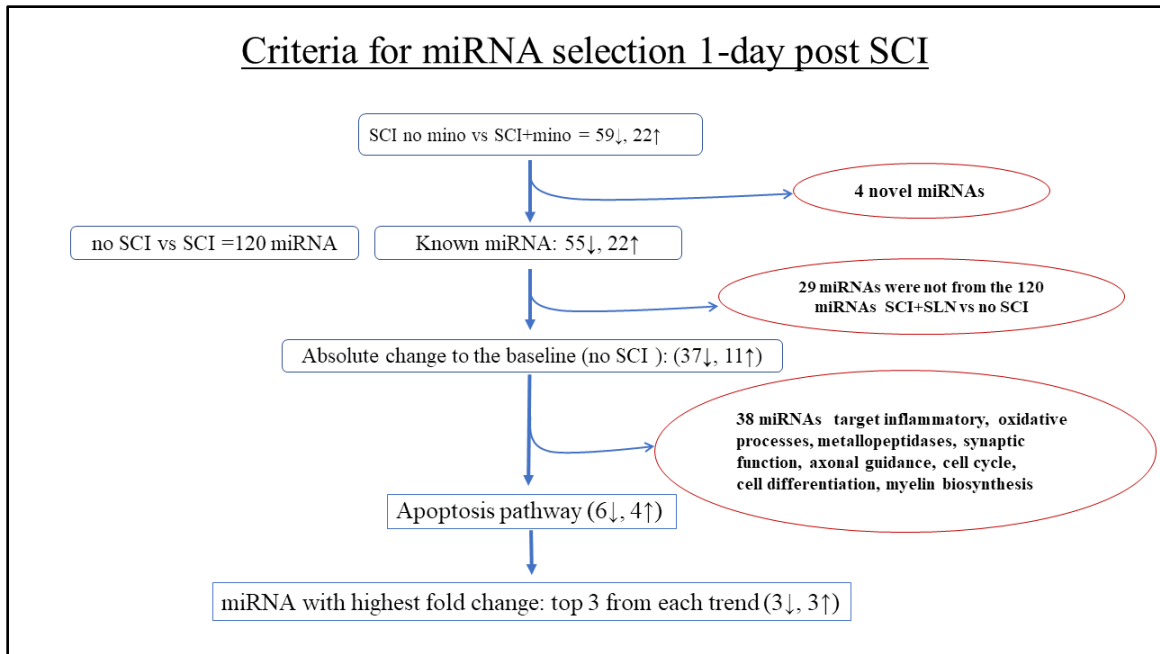


Figure 2.12 Criteria for miRNA selection in the 1d group.

1. miRNAs that significantly changed expression following administration of minocycline. In other words, the miRNAs significantly changed when SCI+mino was compared to SCI+SLN (81 miRNAs).
2. The 77 previously characterized miRNAs were retained within the selected subgroup. The novel miRNAs (4 novel miRNAs) were excluded at this stage.
3. From this group, the miRNAs that were significantly changed after injury compared to base line (SCI+SLN vs no SCI) were included. There were 29 miRNAs within this group that were significantly altered following administration of minocycline were excluded from the final list as they were not significantly changed by injury itself (SCI+SLN vs no SCI) and felt to reflect a response to or effect of minocycline not necessarily related to

SCI. Therefore, there were 48 miRNAs that changed significantly due to injury per se and after minocycline administration (Table 2.2). The miRNAs excluded at this stage are listed in Appendix B (Table B.9).

4. Given the focus of this work was directed toward miRNAs whose target proteins participate directly in cell death and survival-apoptotic pathways, 10 miRNAs contained within subset derived from #3 above were identified from available online databases. Of these 10 miRNAs, there were 6 miRNAs downregulated and 4 miRNAs upregulated.

5. The final subset to be analyzed further was based upon the magnitude of the expression change identified on the respective Volcano plots. A sample of 3 upregulated and 3 downregulated miRNAs (6 out of 10 miRNAs) were selected to confirm their expression changes with RT-qPCR in 1d survival group.

To identify the potential targets of these miRNAs, two online miRNA databases were searched. The first was the miRDB data set (<http://mirdb.org/>) (267). As recommended by the data set guidelines, the potential targets with scores of 80 and above are likely to represent a true downstream product. The targets identified were then compared with the results from another search on a second online miRNAs data base the TargetScan data set (<http://www.targetscan.org/>), which uses a scoring system close to miRDB data set (268). The targets that were shared in these two data bases were considered. In silico based miRNA-target prediction, utilizing more than one miRNA database was demonstrated to minimize the false positive predicted targets (269). The function and cellular role of the identified targets were cross-checked against the “National Center for Biotechnology Information, U.S. National Library of Medicine” gene online resource <https://www.ncbi.nlm.nih.gov/gene/>. Ultimately, targets relevant to mechanisms of SCI were considered (apoptosis, cell survival, cell death, cell cycle, inflammation, oxidative stress, neuronal migration, astrogliosis, matrix metalloproteases).

| Downregulated by mino in comparison to SCI+SLN | FC | padj | Target | Function (predicted) |
|--|--------|-------|--|--|
| mmu-miR-144-3p | -1.719 | 0.033 | Nfe2l2,Arid1a;Map3k4 | Oxidative Stress, chromatin remodeling; inflammation |
| mmu-miR-142a-3p | -1.297 | 0.002 | Ash1l;Rab2a | negative regulation of inflammatory response; Cell Cycle, Mitotic activity |
| mmu-miR-144-5p | -1.283 | 0.000 | Pcdhb11;Nrg3;Prkacb;Grin1 | cell adhesion; chemorepulsion in interneuron migration ;inflammation, Glutamate receptor activity |
| mmu-miR-451a | -1.238 | 0.042 | H2afy, Vapa | DNA repair-TF; RBC marker, SNARE and ER |
| mmu-miR-219a-5p | -1.083 | 0.000 | Zbtb18,Elov17 | neuron development, sphingolipid biosynthetic process |
| mmu-miR-32-5p | -1.051 | 0.002 | Btg2,Cpeb3 | CNS development, dendritic spine development |
| mmu-miR-142a-5p | -1.026 | 0.000 | Iltfb,Map4k3 | cytokine activity, MAPK pathway |
| mmu-miR-21a-5p | -0.971 | 0.000 | Pik3r1;Ntf3 | Apoptosis and survival pathway; negative regulation of neuron apoptotic process |
| mmu-miR-6240 | -0.946 | 0.021 | Prkg1;Ndnf | dendrite development and migration; regulated neuron projection and development |
| mmu-miR-153-3p | -0.921 | 0.000 | NeuroD6;Adam23 | Neuron differentiation; brain development and inflammation |
| mmu-let-7a-1-3p=mmu-let-7c-2-3p | -0.914 | 0.002 | Ppp1r15b;Nbea;Il4 | synaptic plasticity and neurons differentiation; regulates neurotransmitter receptor trafficking to synapses; inflammation |
| mmu-miR-6236 | -0.895 | 0.047 | first target is with score 71: 3110040N11Rik | molecular-biological function/embryonic |
| mmu-miR-24-2-5p | -0.891 | 0.002 | Cacna2d2;Cers6;Pcdh9 | calcium channel activity; sphingolipid biosynthesis and inflammation; neuronal synaptic function |
| mmu-let-7f-1-3p | -0.828 | 0.024 | Nlgn1;Itga6 | Synaptic function; cell adhesion and signaling |
| mmu-miR-223-5p | -0.807 | 0.022 | NR2B (AMPA), GluR2 (NMDA) recep | Ca ²⁺ signalling |
| mmu-miR-486b-3p | -0.750 | 0.031 | Traf3;Phb | Oxidative stress; inflammatory and immune response |
| mmu-miR-101c | -0.741 | 0.000 | Adamts17;Map3k2 | metallopeptidase activity; MAPK pathway and TNF-alpha NF-kB signaling pathway |

| Downregulated by mino in comparison to SCI+SLN | FC | padj | Target | Function (predicted) |
|--|--------|-------|--------------------------|--|
| mmu-miR-101a-3p | -0.740 | 0.000 | Map3k4,Tgfb1;Adamts17 | Inflammation, metalloendopeptidase activity |
| mmu-miR-486a-3p | -0.738 | 0.031 | Faim2; Traf3 | Apoptosis, Fas apoptotic inhibitory molecule 2 ; inflammation |
| mmu-miR-1191a | -0.722 | 0.004 | Npy5r;Bmp7 | neuropeptide Y receptor activity, bone morphogenetic activity |
| mmu-miR-96-5p | -0.719 | 0.001 | Cacnb4; Oxsr1;Prkce | Presynaptic depolarization and calcium channel opening; inflammatory processes; inflammatory process and oxidative reactions |
| mmu-miR-467a-5p | -0.711 | 0.025 | Clock; Nbea | regulation of circadian rhythms; regulates neurotransmitter receptor trafficking to synapses |
| mmu-miR-30e-5p | -0.667 | 0.000 | Limch1;Av19 | neuronal projection(excitatory);cell migration |
| mmu-miR-381-3p | -0.666 | 0.001 | Arid4b;Gad1 | embryonic stem cell differentiation; catalyzes the production of GABA |
| mmu-miR-203-3p | -0.637 | 0.006 | Ptp4a1;Nufip2;Lrrtm2 | Oxidative stress; active_in cytoplasmic stress granule, neurexin family protein binding |
| mmu-miR-148a-3p | -0.602 | 0.009 | Cdk19;Cdk5r1;Cdkn1b; | inflammatory process-phosphatase activity; neuron cytoskeleton |
| mmu-miR-376b-3p | -0.590 | 0.003 | Dscam11, Wwtr1 | axonal guidance and brain development, cycle progression and differentiation |
| mmu-miR-101b-3p | -0.590 | 0.004 | Gclc;Nek7 | glutamate metabolism and oxidative stress response; phosphorelation and inflammation |
| mmu-miR-15b-5p | -0.585 | 0.020 | Bcl2,Akt3 | Apoptosis, survival pathway |
| mmu-miR-384-3p | -0.558 | 0.006 | Asap2,Prkacb | inflammatory process-macrophage function; apoptosis signaling pathway |
| mmu-miR-135a-5p | -0.548 | 0.008 | Pik3r2;Cplx2;Sdcbp;Kcnb1 | Apoptosis pathway; synaptic transmission and plasticity, synaptic transmission ;potassium ion transmembrane transport |
| mmu-miR-335-3p | -0.526 | 0.000 | Map3k2,Nrxn1;Arhgap18 | inflammation; synaptic function; regulation of stress fiber assembly |
| mmu-miR-300-3p | -0.480 | 0.017 | Nck2;Il13ra1 | pericyte migration and neovascularization; immunological function-dendrites |
| mmu-miR-22-3p | -0.465 | 0.000 | Grm5;Ddit4;Akt3;Arrb1 | glutamate receptor activity, synaptic transmission, and apoptotic process ; neuron survival; inflammation and apoptosis |

| Downregulated by mino in comparison to SCI+SLN | FC | padj | Target | Function (predicted) |
|--|--------|-------|-----------------|---|
| mmu-miR-582-3p | -0.430 | 0.008 | Cacna1h,NeuroD6 | mediate the entry of Ca(2+), Oxidative stress and neurons differentiation and development |
| mmu-miR-29b-3p | -0.384 | 0.012 | Nav1;Adamts17 | Neuronal migration; metalloproteinases activity |
| mmu-miR-379-3p | -0.327 | 0.041 | Plch1,Smurf1 | intracellular signal transduction-Ca+2 binding, regulation of dendrites extension |

| Upregulated by mino in comparison to SCI+SLN | FC | padj | Target | Function |
|--|-------|-------|----------------------|--|
| mmu-miR-326-3p | 0.775 | 0.000 | Itga5;Parva;Plec | cell adhesion; cell cytoskeleton; cell cytoskeleton |
| mmu-miR-34a-5p | 0.670 | 0.001 | Caps2;Erc1;Satb2 | Apoptosis; synaptic plasticity; neuronal migration |
| mmu-miR-3547-3p | 0.992 | 0.001 | Casp2;Chsy1;Cacna2d2 | Apoptosis; Chondroitin sulfate biosynthesis; voltage-gated calcium channel activity |
| mmu-miR-702-3p | 0.843 | 0.002 | Traf2;Nsg1;Dap3 | Apoptosis; neurotransmitter receptor cycle |
| mmu-miR-667-3p | 0.645 | 0.003 | Prdx6;Mrpl3 | calcium-independent phospholipase A2 and glutathione peroxidase activity; Neurodegeneration |
| mmu-miR-700-5p | 0.686 | 0.002 | Per2,Csgalnact2 | circadian regulation of gene expression, chondroitin sulfate biosynthetic process |
| mmu-miR-490-5p | 0.987 | 0.000 | Cyb5rl;Tmem41b;Rock1 | cytochrome-b5 reductase activity, acting on NAD(P)H, autophagosome assembly and nervous system development; inflammation I-kappaB kinase/NF-kappaB signaling |
| mmu-miR-3102-3p | 0.839 | 0.004 | Adamts17;Ccnv | extracellular matrix organization; Wnt signaling pathway and kinase activity |
| mmu-miR-1224-3p | 0.661 | 0.002 | Cyb561d1;Apln | oxidoreductase activity; G-protein function - angiogenesis and other function |
| mmu-miR-383-5p | 0.506 | 0.005 | Irf1;Ctnnal1;Nckap1 | positive regulation of cell death-apoptosis; Cell cytoskeleton; cell cytoskeleton neuronal development |
| mmu-miR-431-3p | 0.484 | 0.001 | Slc25a12 | Transmembrane transport of glutamate and aspartate and Ca2+ transport |

Table 2.2 The 48 miRNA that changed by SCI and minocycline

2.3.7 Criteria of miRNA selection for confirmation in 7d group

In the 7d survival group, there were fewer miRNAs that were significantly changed than in the 1d group, when SCI+SLN was compared to SCI+mino. The criteria that were used in the 1d group were again applied here, taking the limitations in consideration. There were 14 miRNAs identified in this group. Again, the focus was on the known miRNAs (8 miRNAs, Table B.7 Appendix B) and excluded the novel ones (6 miRNAs, Table B.8 Appendix B). Of the 8 known miRNAs, four of them showed less than 10 copies in total and were not identified in some individual RNAs samples (0 copies). It was determined that the likelihood of not identifying them with RT-qPCR or ddPCR was potentially high. Therefore, the miRNAs with base mean or copies numbering more than 10 (4 miRNAs) were considered and utilized during the confirmatory step. The process of selecting the 4 miRNAs in the 7d group is illustrated in Figure 2.13. The selected miRNAs subsets for both timepoints are shown in Table 2.3.

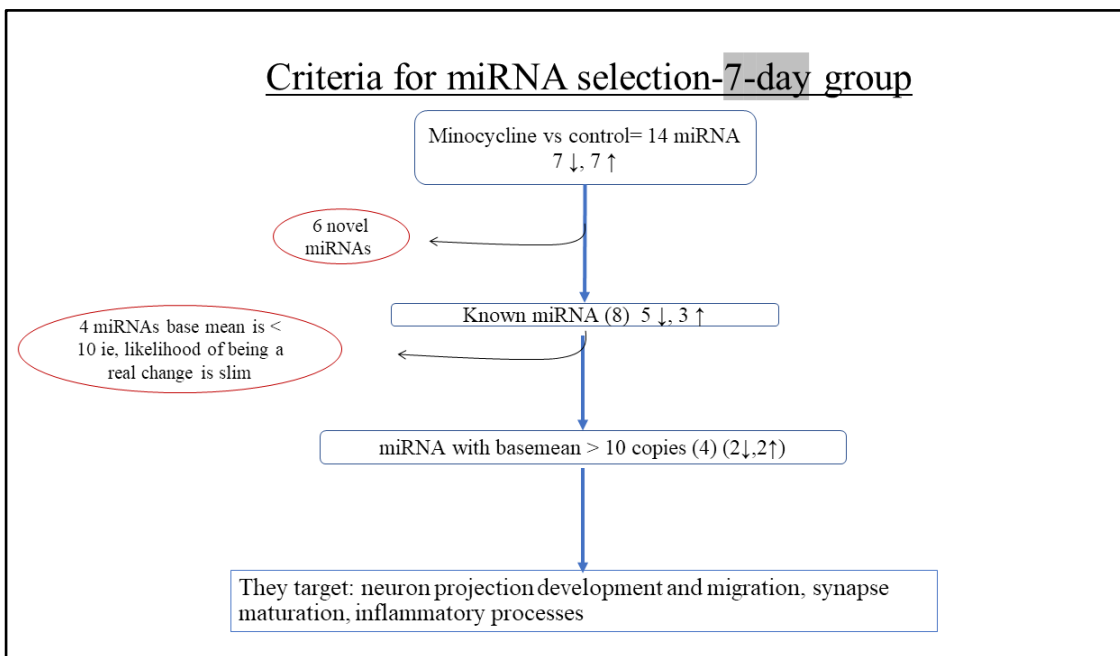


Figure 2.13 Criteria for miRNA selection 7d group

Subsets of miRNAs-1-day & 7-day groups

Downregulated ↓ ↑ Upregulated

| 1d miRNA | Targets | process | 1d miRNA | Targets | process |
|-------------|---------------------------|--|-------------|----------------------|---|
| miR-15b-5p | <i>Akt3, Bcl2, Bcl2l2</i> | Apoptosis, PI3K/AKT Signaling pw | miR-34a-5p | <i>Casp2</i> | Apoptosis, stress-induced apoptosis |
| miR-21a-5p | <i>Pik3r1, Bcl2</i> | Apoptosis, PI3K pathway | miR-702-3p | <i>Traf2</i> | Apoptosis, TNFα downstream pathway |
| miR-486a-3p | <i>Faim2</i> | Apoptosis, Fas& Casp 8 inhibitor | miR-3547-3p | <i>Casp2</i> | Apoptosis, stress-induced apoptosis |
| 7d miRNA | Targets | process | 7d miRNA | Targets | process |
| miR-15b-3p | <i>Srx3, Ptprij</i> | Neuron projection development, Inflammatory process: | miR-96-5p | <i>Nexmif, Prkce</i> | Neuronal migration Negative regulation of mitochondrial calcium ion |
| miR-200b-3p | <i>Gpm6a, Nfia, Errf1</i> | Neuron projection Synaptic maturation Inflammatory process | miR-344e-3p | <i>Pcdh8, Pde4b</i> | synaptic transmission Inflammatory process: positive regulation of IF- |

When miRNA levels ↑ , target mRNA protein product ↓

Table 2.3 The subsets of miRNAs and their targets in 1 day and 7-day groups

2.3.8 Validation processes of primers sets for RT-qPCR and ddPCR experiment

First, the cDNA was synthesized from all samples of both groups. Following, the primer sets were validated (by quality control tests) starting with serial dilutions, temperature gradients, and then the standard (efficiency) curve. The reference or endogenous control small RNA namely RNU6 and SNORD96A worked very well in RT-qPCR experiments (270-272). The validating experiments (quality control tests) for primer sets and endogenous control small RNA were run as well before conducting ddPCR experiments. Technically, the same optimizing conditions that were used in RT-qPCR could be used in ddPCR experiments. However, it was found that RNU6 endogenous control small RNA did not work well under our ddPCR conditions. Additionally, the primer sets of miR-34a and miR-96-5p did not elicit reliable data during the validation process of ddPCR experiments. Therefore, another reference gene SNORD95 was used and successfully

validated. Additionally, the miR-34a and miR-96-5p were not run in the final ddPCR experiments (Figures B.9, B.10 Appendix B).

2.3.9 RT-qPCR and ddPCR for the 1d survival group

In these experiments, six miRNAs were included from the 1d survival group, three downregulated (miR-21a-5p, miR-15b-5p and miR-486a-3p) and three upregulated miRNAs (miR-34a-5p, miR-702-3p, and miR-3547-3p). These experiments were run using 12 RNA samples (collected from each of the 12 experimental animals) for each experimental condition (SCI+SLN and SCI+mino). Two miRNAs (miR-21a-5p and miR-15b-5p) of this subset were found to be significantly changed (Figure 2.14). This confirmed the miRNA sequencing results for miR-21a-5p and miR-15b-5p. Conversely, the other 4 miRNAs were not found to be not significantly changed. These miRNAs were then subjected to another confirmation method, the ddPCR.

The ddPCR experiments were used as another confirmatory step for the miRNAs that did not show significant changes in RT-qPCR. This technique was implemented for the miR-486a-3p, miR-702-3p, and miR-3547-3p. Again, none of these miRNAs was found significantly changed between experimental conditions (Figure 2.15). Unfortunately, miR-34a-5p did not show reliable results during primer set validation steps. Therefore, this miRNA was not run in the final ddPCR run. Of note, in ddPCR experiments for the 1d group there were 11 cDNA samples used for technical consideration.

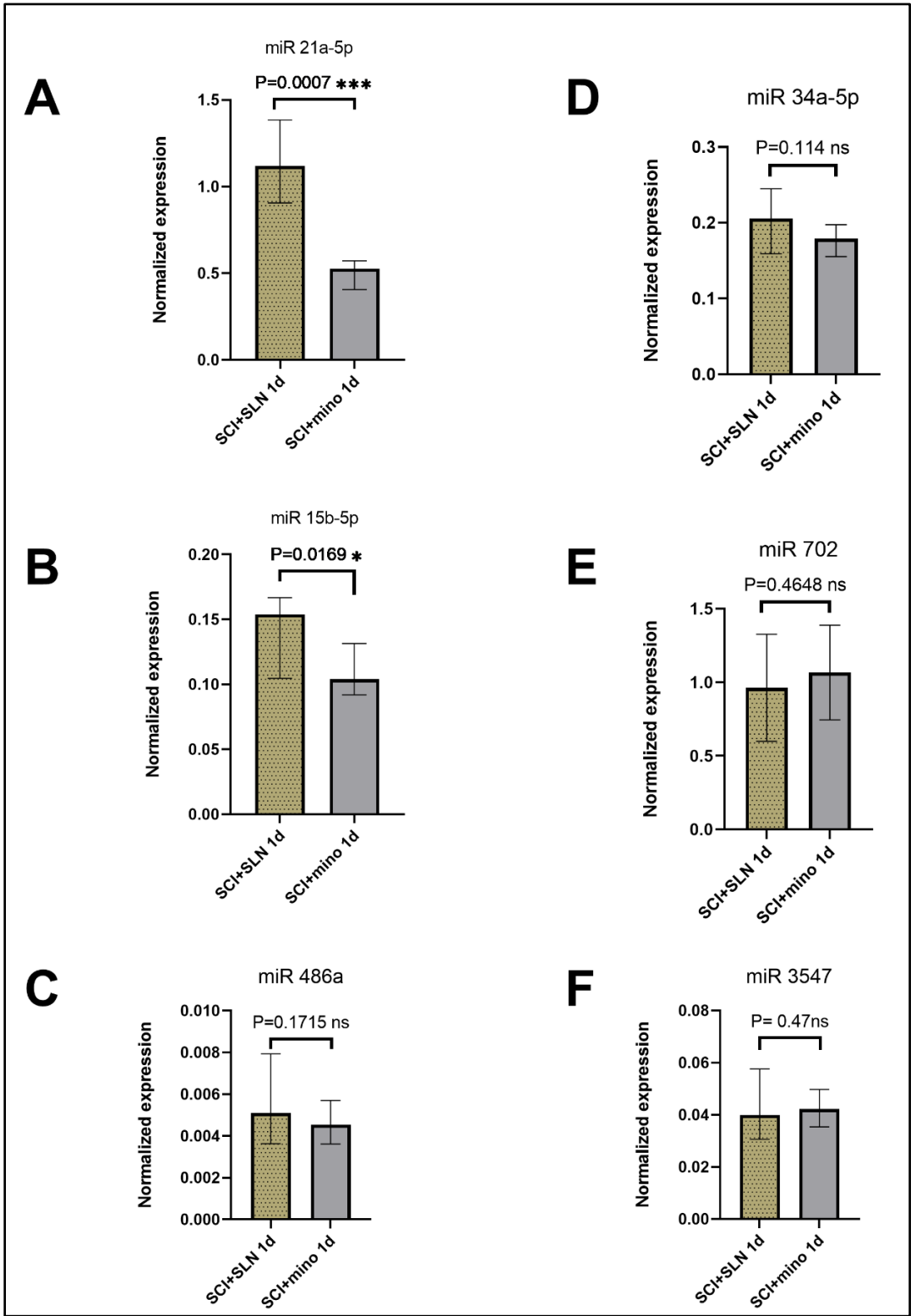


Figure 2.14 RT-qPCR miRNA results in 1d

* Y axis represents normalized fold expression (normalized to 2 endogenous small RNAs)

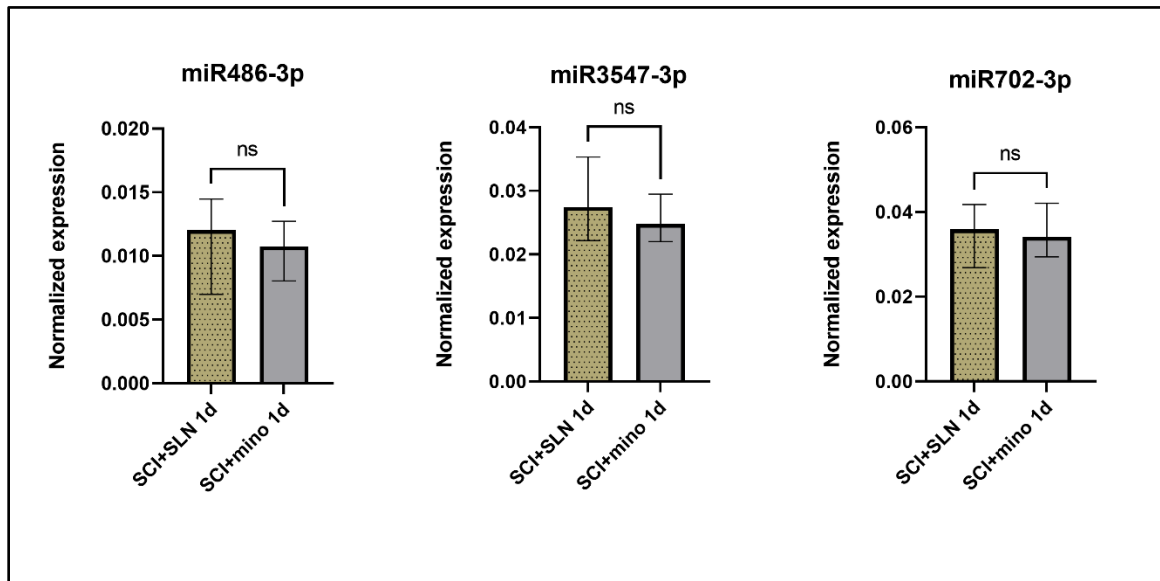


Figure 2.15 Droplet digital PCR miRNA results in 1d group

2.3.10 RT-qPCR and ddPCR for 7d survival group (subacute)

In the 7d group, there were eight cDNA samples for each experimental condition (SCI+SLN and SCI+mino). There was no miRNA from the selected subset (miR-15b-3p, miR-200b-2p, miR-96-5p, and miR-344e-3p) significantly changed after running RT-qPCR test (Figure 2.16). Therefore, ddPCR was used for further confirmation of these miRNAs. Similar to what was observed in the 1d experiments, ddPCR showed no significant difference in expression of miR-15b-3p, miR-200b-2p, and miR-344e-3p (Figure 2.17). Again, miR-96-5p did not pass the validation step (quality control test) and was excluded from the final ddPCR run.

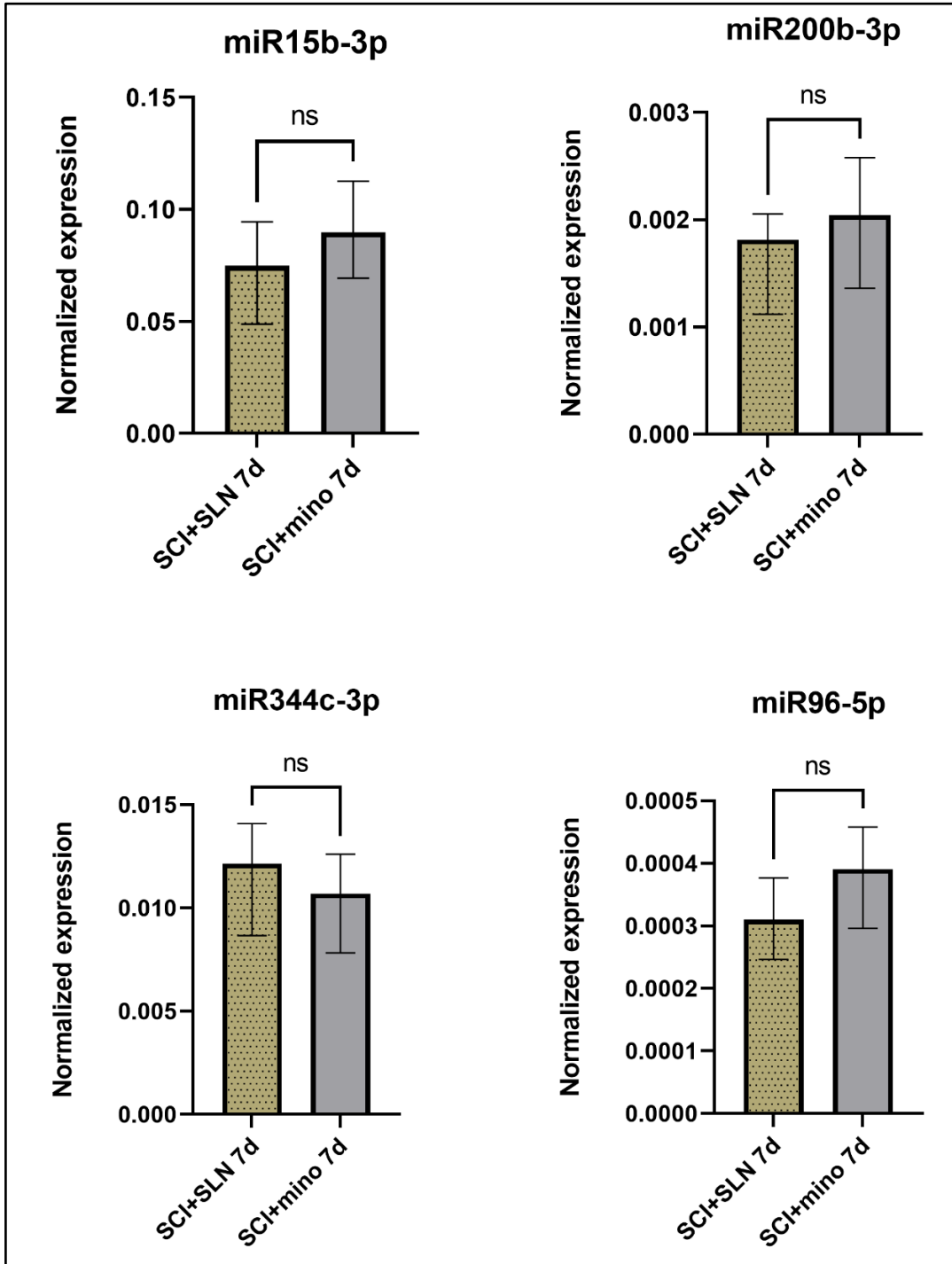


Figure 2.16 RT-qPCR miRNA results in 7d

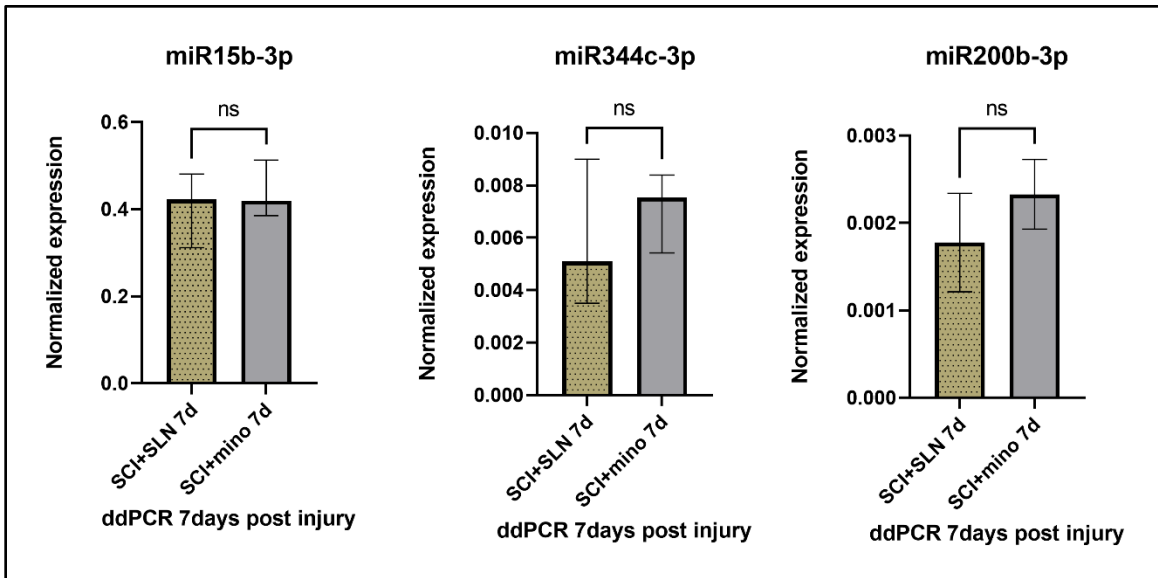


Figure 2.17 ddPCR miRNA results in 7d

2.3.11 Testing the levels of miR-21a-5p and miR-15b-5p in 7d samples

It was known from the miRNA deep sequencing experiments that miR-21a-5p and miR-15b-5p were not significantly changed in the 7d group analysis. Notwithstanding, this negative finding was confirmed by re-testing. RT-qPCR was used to test these miRNAs in the samples of 7d survival group in both experimental conditions (SCI+SLN and SCI+mino). No significant differences between the SCI+SLN and SCI+mino were observed (Figure 2.18).

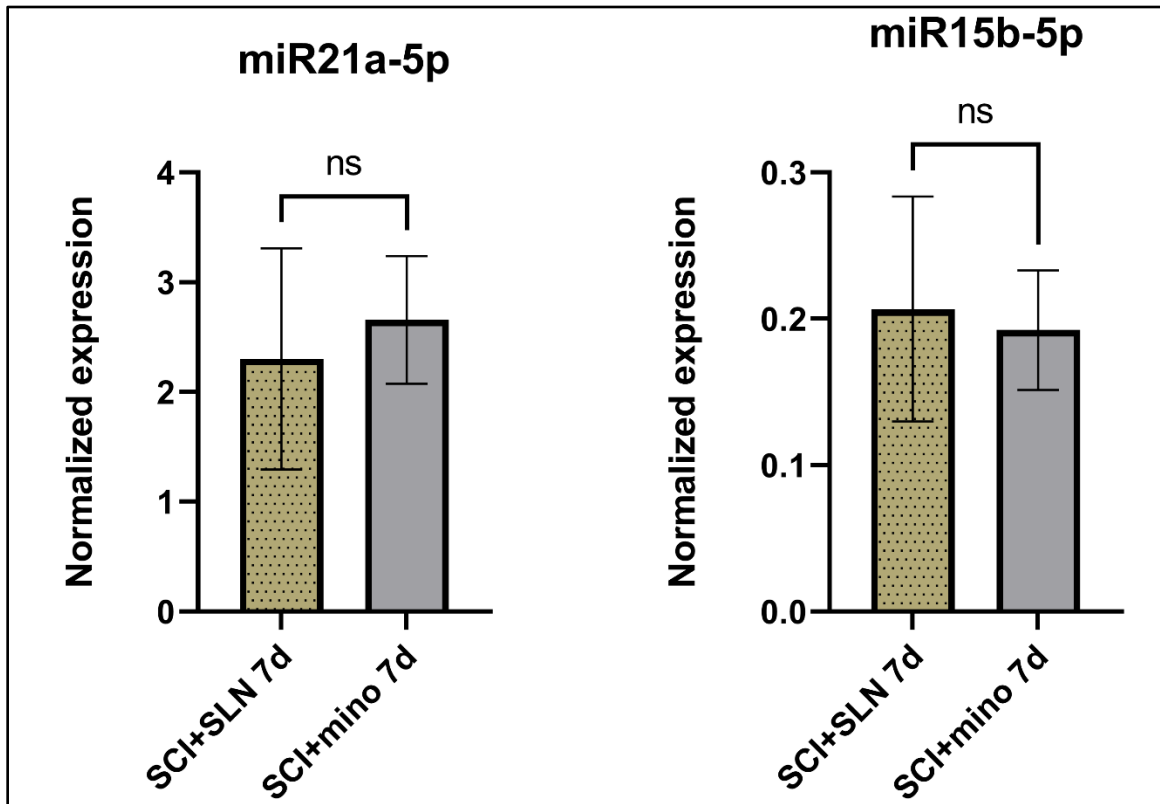


Figure 2.18 RT-qPCR for miR21a-5p&15b-5p in 7d

2.3.12 Were all animals in the experiments exposed to a similar injury impact?

In all experiments, the Infinite Horizon Spinal Cord Impactor, Precision Systems Inc., USA was utilized. A moderate SCI was delivered with a target force of 50 kilodyne (kd) to the lower thoracic area of the SC. The computer recorded the actual force applied and the resultant SC tissue displacement. In the 1d group, the actual force for the two conditions SCI+SLN (n=12) and SCI+mino (n=12) were 50.92 ± 0.484 K dyne (mean \pm SEM) and 52.34 ± 0.732 K dyne respectively (Figure 2.19). Student t-test comparing the two experimental conditions demonstrated no statistical difference (p-value = 0.1206; 95% confidence interval -0.4026 and 3.236). Similarly, there was no statistical difference observed in the SC displacement between the two conditions, with SCI+SLN

displacement 536 ± 61.365 microns (mean \pm SEM) and SCI+mino displacement 522.75 ± 48.95 microns (p-value = 0.8675; 95% confidence interval -176.0 to 149.5).

In the 7d group, the actual force delivered to SC for the two conditions SCI+SLN (n=8) and SCI+mino (n=8) were 51.25 ± 0.526 K dyne (mean \pm SEM) and 51.875 ± 1.043 K dyne respectively. Again, there was no statistical difference in the actual force delivered to the SC between the two experimental conditions (p-value = 0.6009; 95% confidence interval -1.880 and 3.130) (Figure 2.19). Likewise, there was no statistical difference was observed for the SC displacement between the two experimental conditions with SCI+SLN displacement 539.625 ± 63.556 microns (mean \pm SEM) and SCI+mino displacement 442.75 ± 17.133 microns (p-value = 0.1632, 95% confidence interval -238.1 to 44.30).

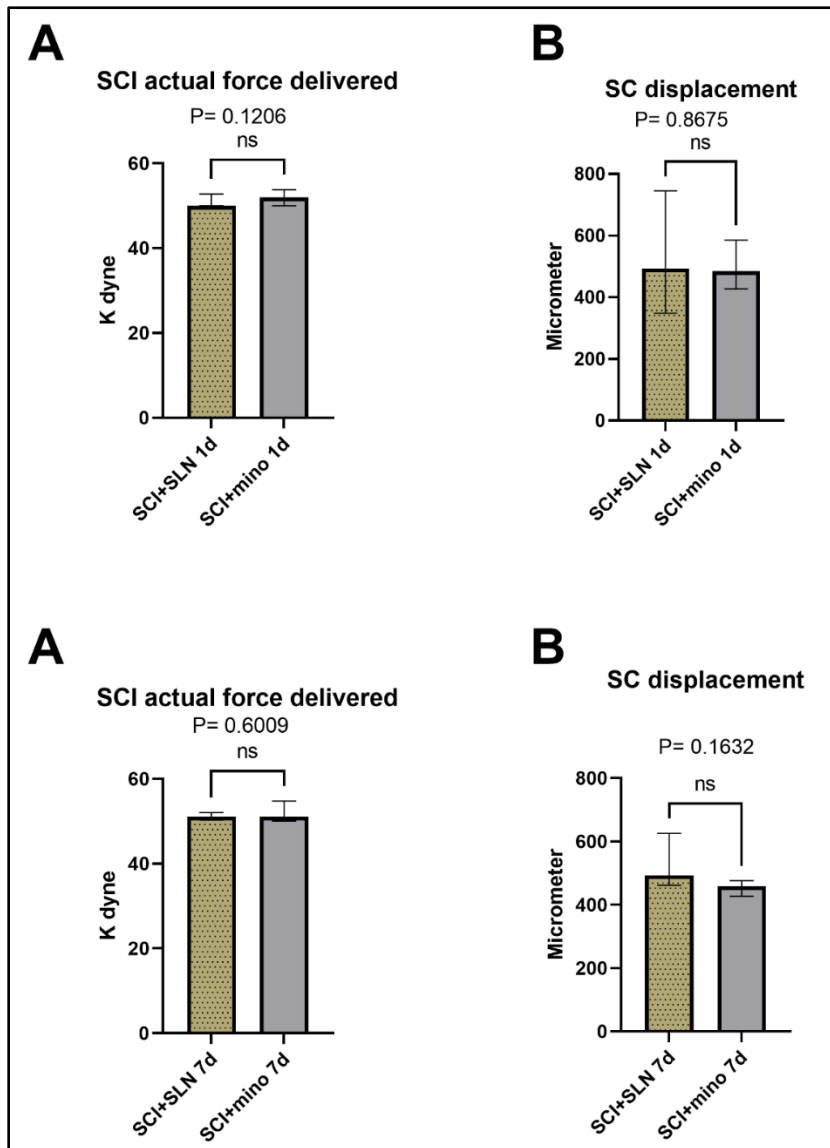


Figure 2.19 Actual force and SC displacement in 1d and 7d groups

2.4 Discussion and interpretation

The sSCI mechanisms can be divided into three major stages: acute, subacute, and chronic SCI. In this study, two main time points were used. The 1d group was representative of acute SCI, while the 7d group was representative of subacute SCI. In the

1d group, there were three experimental conditions: no SCI (laminectomy only) as a baseline; SCI+SLN to examine the miRNAs changes resulting from the injury; and SCI+mino to examine possible effects of a known neuroprotective drug on the expression of miRNAs. In the 7d group, technically there were two experimental conditions the SCI+SLN and SCI+mino. The baseline miRNA data from the no SCI-1d group was used to make comparisons across groups, as it was done between the 1d-experimental conditions. Unfortunately, the PCA failed to show segregated groups when the baseline data from the 1d group was used. In retrospect, for Deep Sequencing runs, the collected RNA samples from all experimental conditions should have been processed at the same time. Otherwise, the results would be incomparable and the likelihood of producing technical error is high. Therefore, the comparison and data analyses in 7d timepoint were conducted between SCI+SLN and SCI+mino only.

The RNA samples are total RNA from the lesion site (6, 227) and the miRNA sequencing reflect the changes in expression from SC tissue which contains different types of cells including neurons, glia, vascular tissue and blood components.

In the 1d-timepoint group, the general pattern of miRNA changes due to SCI was found to be an upregulation of miRNAs expression (80 miRNAs were upregulated and 40 miRNAs were downregulated) when the SCI+SLN condition was compared to no SCI. Nevertheless, the minocycline administration resulted in a different global pattern. Minocycline resulted in a downregulation pattern of the expressed miRNAs (59 miRNAs were downregulated and 22 miRNAs were upregulated) when the SCI+mino condition was compared to SCI+SLN condition. This difference in the general pattern of miRNA expression might reflect the effect of minocycline on changing miRNA expression. Of note, the molecular mechanisms of how minocycline could change the miRNA expression is not clear and it is beyond the scope of this study.

In the 7d-time point group, there were 7 miRNAs upregulated and 7 downregulated. In general, there were fewer miRNAs significantly changed in the 7d time points (14 miRNA) than the number of miRNAs in the 1d-time point group within similar experimental condition (81 miRNAs). It was observed in the 7d group that some of these

miRNAs were not detectable in some total RNA samples, such was the case for miR-6977-3p and miR-669m-3p.

In this exploratory study, the focus was on known miRNAs at this stage of experiments for two reasons. First, the aim was not only to stop following the identification of miRNA *per se*, but also to identify what the miRNAs do in the pathophysiology of SCI. At this time, identifying genes targeted by miRNA is totally based on computational prediction that requires verification via the mRNA and/or their protein products. Therefore, two sequential steps of uncertainty in a multi-step experiment may produce ambiguous data and less reliable results. Secondly, some researchers reported difficulty in verifying novel miRNAs and known miRNAs secondary to quality control issues and validation challenges (269). A similar quality control problem was experienced in the present study during the validation tests of miR-34a-5p, miR-96-5p and RNU6 (endogenous control) primer sets for ddPCR experiments.

Although the sSCI pathophysiology involves inflammatory and oxidative processes in addition to many other reactive cascades, apoptosis is often considered a significant result of sSCI (128, 227, 237). Moreover, this work attempted to identify cellular pathways that are targeted by miRNAs which could lead to neuronal survival. Therefore, the miRNAs that potentially target apoptotic and survival pathways were selected for analysis.

Although there are several online miRNA data base resources, two were used to predict the target genes, namely miRDB (<http://mirdb.org/>) (267) and TargetScan (<http://www.targetscan.org/>) (268). Two subsets of miRNAs were selected for verification by running RT-qPCR.

To address the first aim of this study, to determine whether SCI alters miRNA expression, SCs from animals with and without SCI were examined for changes in miRNA expression with NGS. This analysis afforded 120 discrete miRNAs that were either upregulated (n=80) or downregulated (n=40). Furthermore, contained within these 120 miRNAs were 10 that have not been previously identified. The characterization of these novel miRNAs was beyond the scope of this work, and as such will be addressed in the future. However, it is clear that a traumatic insult to the SC does evoke changes in miRNA expression.

Investigating the second aim, whether administration of a known neuroprotectant could influence miRNA changes, required further experimentation. Minocycline was chosen as the neuroprotectant for study as it is known to exert its action through multiple mechanisms, which was felt to increase the chance of observing a possible effect. Comparing untreated (SCI+SLN) to treated (SCI+mino) injury groups demonstrated a different pattern of miRNA expression, with 81 miRNAs demonstrating significantly different degrees of expression between the groups (59 miRNAs were downregulated and 22 miRNAs were upregulated) in the 1d group, for example. Through the selection process described in Sections 2.3.6 and 2.3.7, ultimately 6 miRNAs from the 1d group and 4 miRNAs from the 7d group were selected for further confirmation. (Figures 2.12 and 2.13) and (Tables B.7 and B.8).

RT-qPCR technique has been described for confirmation of miRNA sequencing (6, 227). For the 1d time point group, the experiments were repeated for SCI+SLN and SCI+mino. Additional 8 new RNA samples for each experimental condition (16 RNA sample in total) were collected. Samples that were initially analyzed for miRNA sequencing were again probed with RT-qPCR for verification of the findings (227). In this study, RT-qPCR experiments included the 4 RNA samples that were sequenced by NGS technique. A total of 12 RNA samples were utilized for RT-qPCR from each experimental condition. Endogenous controls snRNA RNU6B and SNORD96A-11 were used. Both worked well and passed the validation experiments for RT-qPCR. RT-qPCR showed significant decrease in the expression of miR-21a-5p and miR-15b-5p in SCI+mino condition (Figure 2.14). These results are in agreement with NGS and confirmed the sequencing results. The other 4 miRNAs showed no statistical difference in their expression which is incongruent with NGS results. These 4 miRNAs (miR-486a, miR-34a-5p, miR-702, miR-3547) were analysed with a further confirmational approach, namely ddPCR (to confirm previous results by RT-qPCR tests). During the validations process for ddPCR, it was found that miR-34a-5p produced a second band on the histogram (which indicates the primer set failed, thus providing a false positive result despite optimization of the experimental conditions). Additionally, the endogenous control snRNA RNU6B did not show regular amplification, therefore, these two primer sets failed to pass the validation tests and were thus excluded. A new endogenous control

SNORD95 was successfully validated for ddPCR experiments. The ddPCR tests confirmed the negative RT-qPCR results and none of the miRNAs (miR-486a, miR-702, miR-3547) demonstrated significant changes in their expression when samples from the SCI+SLN were compared with samples from the SCI+mino groups. In parallel with these results, miR-96-5p in the 7d group also failed the validating test and were excluded. The other three miRNAs (miR-15b-3p, miR-200b, and miR-344c) showed no significant difference in their expression between the two experimental conditions. Therefore, in the end, only the downregulated expression of miR-21a-5p and miR-15b-5p in the 1d group was confirmed after minocycline administration.

Only 2 out of 10 potential miRNAs were subsequently validated, which corresponded to 2 of the 6 miRNAs identified in the 1d group. The validation was based on the criteria of selecting the subset of miRNAs for confirmation, which was directed to identify apoptotic pathway targets. Only miRNAs with statistically significant dysregulation, regardless of the fold change, were considered. The fold change (FC) was used to select from the same group that target survival and apoptotic pathways. No miRNA in 7d timepoint group showed significant changes. In this group, the base mean (copy number) and fold changes were by far smaller than the pattern that was observed in the 1d group. With respect, to these observations a recent study suggests a relationship between the severity of SCI and the pattern of miRNA expression (273). This study included human SCI patients and analysed the identification of miRNAs in patients' serum and CSF daily for 5 days and correlated these findings to the severity of clinical deficits. It was observed that the number of differentially expressed miRNAs was highest in serum in the first day following the injury and the number of significantly expressed miRNAs was highest in CSF over the first two days then decreased over time depending on the severity of the SCI. The mathematical methods in high-throughput assays are more complex and beyond the scope of this thesis. The results of sequencing are subjected to several corrections and adjustments to show the difference between the experimental groups. In high-throughput technologies, the statistical methods are designed to demonstrate differences between groups as low as two biological replicates per experimental condition. These statistical considerations are well-addressed by Love et al. 2014 (265). In our miRNA NGS, four biological replicates per condition for each timepoint were used. In the experiments to

validate miRNAs, 12 biological replicates per condition in the 1d timepoint group and 8 biological replicates per condition in the 7d timepoint group were used. The number of replicates employed here are similar, if not greater, than those reported in the literature (6, 227, 237).

In conclusion, SCI injury resulted in widespread miRNA dysregulation in the experimental mouse model studied here. The expression of miR-21a-5p and miR-15b-5p were found to be downregulated at 1d following SCI and treatment with the neuroprotective agent minocycline. In contrast, no significant changes in expression of miRNAs were identified at 7d following SCI and treatment with minocycline. It is suggested that these two miRNAs (miR-21a-5p and miR-15b-5p) likely serve a role in reaction cascades within the SC in response to injury, as such bioinformatics may be employed to determine their potential targets and their subsequent downstream effects (see Chapter 3).

CHAPTER 3 : IDENTIFICATION OF THE ROLE OF miR21a-5p AND miR15b-5p FOLLOWING SCI IN CELLULAR PATHWAYS.

3.1 Introduction

Bioinformatic tools are useful in identifying miRNA targets. As described in Chapter 2, several miRNAs were predicted to participate in apoptotic and survival pathways. Two of these miRNAs were validated (miR-21a-5p and miR-15b-5p) and found to be downregulated by minocycline at 1d following SCI. Since a single miRNA can target several genes and influence their protein production, it is important to keep in mind that the prediction depends on the base pairing of the seed areas of the miRNAs to 3'UTR of the mRNA (173). Furthermore, these predictions are computational models (<http://mirdb.org> ; <http://www.targetscan.org>) (267, 268) and as such these predicted targets *in silico* or machine-learning methods require *in vivo* confirmation. To minimize false positive predictions, two popular miRNA data bases were used in addition to the National Center for Biotechnology Information, U.S. National Library of Medicine (<https://www.ncbi.nlm.nih.gov/gene>) to identify the relevant genes. Recognizing the complex interactions of miRNAs and the various target genes they effect, another bioinformatic resource “DAVID” (The **D**atabase for **A**notation, **V**isualization and **I**ntegrated **D**iscovery” v6.8 <https://david.ncifcrf.gov/home.jsp>) (274, 275) has been developed to infer the biological function of these genes and generate the potential cellular pathways of these genes. The significantly enriched genes and proteins that participated in apoptotic and survival pathways were selected. It was hypothesized that the target genes of the downregulated miR-21a-5p and miR-15b-5p were relieved from suppression and their protein products subsequently expressed. This reverse relationship between the miRNAs and their targets mRNA has been well described previously (6, 227). The regulatory mechanisms of gene translation by miRNA can be either via mRNA degradation or mRNA repression or an interplay between these two mechanisms (173).

Regardless of the mechanism of miRNA gene silencing, and the levels of mRNAs, the protein products of these genes were examined. There are fewer published studies of note that correlate miRNA levels to predicted proteins compared to studies that have demonstrated the relationship between the miRNAs and mRNAs (276). Recently, differential changes in miRNAs were examined in the experimental autoimmune encephalomyelitis mouse model (269) and predicted the target genes in several cellular pathways as well as protein expression. However, studying sequential multi-step experiments in SCI is less clear. Thus, expression levels of predicted proteins in two experimental conditions, namely SCI+SLN and SCI+mino were examined.

3.2 Materials and Methods

3.2.1 Identification of miRNAs target genes and their functions

The details for identification of miRNA targets are found in Section 2.2.9. Briefly, miRDB, and TargetScan online data sets and gene online source "<https://www.ncbi.nlm.nih.gov/gene/>" were used to identify miRNAs targets and their protein products. The genes were checked in the ensemble genome database "<http://useast.ensembl.org/index.html>" that provides gene and protein ID. In this study the Ensembl Gene ID was considered.

To understand how the predicted targets are related and how they function, the online bioinformatic tool "DAVID: The Database for Annotation, Visualization and Integrated Discovery" was used (274, 275). This tool is useful in identifying and filtering the targets. The DAVID tool identifies the cellular pathways of these genes as well as their protein products. A list of predicted genes and proteins were analyzed by DAVID software using Ensembl Gene ID. The significantly enriched gene products (proteins) demonstrating a p-value > 0.05 as well as identified as participating in apoptotic or cell survival pathways were selected for verification and confirmation.

3.2.2 Animals And Research Approval

A detailed description is in Section 2.2.1 animals and ethics approval. Six mice each were included in the SCI+mino group and the SCI+SLN group for western blot experiments. The pre-operative care, procedures, and post-operative care followed Dalhousie University policy & the Canadian Council on Animal Care guidelines. Ethics approval (protocols #17-136, 20-060) from the Dalhousie University Committee on Laboratory Animals was obtained .

3.2.3 Experimental Design

The experiments were designed to examine the differential expression of SC proteins 1 day following SCI in two groups, the minocycline (treatment) group and saline (control) group. The details of the experimental conditions and methods of giving IP solutions were described in Section 2.2.2 Experimental design. In short, both groups received moderate grade SCI. One dose of IP minocycline (90 mg/kg in 0.5 ml buffered saline) was given after the surgery for the minocycline group and one dose of IP saline was given to the SCI+SLN condition. The animals were euthanized 1 day after SCI and 5 mm of SC segments centred on the lesion were harvested for protein extraction.

3.2.4 Surgeries

The detailed surgical procedure and anesthesia were described in Section 2.2.3 Surgical procedures and setup.

3.2.5 Protein Extraction

For lysate preparation, mice were euthanized by a lethal dose of pentobarbital. A 5 mm SC segment centred on the injury epicenter was harvested following extraction of the SC by hydraulic ejection with cold sterile PBS. The SC segment was rinsed in sterile cold PBS and transferred into a pre-chilled beadbug tube. Then, 400 ul of RIPA lysis buffer was added with 4 µl (1%) of protease inhibitors cocktail. To lyse the tissue effectively, the SC segment was homogenized inside the cold room for 1 minute. The lysate was

incubated on ice for 10 minutes and then centrifuged at 13 000 rpm for 15 minutes. The supernatant was transferred into a prechilled protease free tube, and the pellet was discarded. The lysate was frozen at -80 °C or used in the same day for further analysis.

To determine protein concentration in each lysate sample the Lowry assay method was used. The reagents (for details see Table C.1 appendix C). In summary, triplicate samples (2µl) of lysate from each mouse were mixed with fixed amounts of BSA (Bovine Serum Albumin) (Bio-Rad, Quick Start Bovine Serum Albumin Standard catalog #5000206) incrementally in 1 µl increments beginning with 0 µl in first row then 7 µl in the 8th row in a 96-well plate. A mixture of buffer A and buffer S were added into each well followed by reagent B and incubated for 15 minutes. The plate was read at 750 nm absorbance using The BMG LABTECH- SPECTROstar Nano system.

3.2.6 Western blotting

After measuring protein concentrations in the lysates, the required volume of the lysate was determined such that 25 µg of protein was contained in each well of the separating gel. SDS-PAGE 10% gel was used in all western blot experiments. All separating gels were made in-house. The lysate was mixed with Laemmli Sample Buffer and heated for 5 minutes at 95 °C.

Pre-stained protein ladder (Bio-Rad) and SCI protein samples were thawed on ice. The electrophoresis cell (core + gel) was assembled and filled with a running buffer. A 10 µl sample of ladder and between 25 and 50 µg of SCI protein samples were loaded into each well. The electrophoresis separation was started at 50 V, set at 300 W for 30 minutes and then adjusted to 100 V until the dye front reached the bottom of the gel. Following a run time of approximately 105 minutes, the gel was removed and dipped in cold 4 °C transfer buffer for 10 minutes.

A transfer sandwich was assembled inside the transfer cassette (sponge-filter paper-PVDF membrane-filter paper-sponge). PVDF was pre-activated with methanol. The transfer cell was assembled and run under cold (4 °C) conditions for 1 hour at 100 V. The

membrane was then washed 3 times with TBST 0.1% for 5 minutes and blocked with 5% milk (milk in TBST) for 1hr. Following blocking, the primary antibodies [Akt (pan) (11E7) Rabbit mAb-Cell signaling tech (CST 4685S); Bcl-2 (D17C4) Rabbit mAb (Mouse Preferred) (CST) 3498S); PI3- kinase p85- α Rabbit polyclonal (Sigma, SAB4502195); Loading control GAPDH (D16H11) XP® Rabbit mAb (CST5174S)] were added GAPDH 1:5000, Akt 1:1000, Bcl2 1:1000, PI3K p85 α 1:1000 (each primary antibody on a separate membrane) and the membranes were kept on shaker overnight at 4°C. The membranes were washed and incubated with appropriate secondary antibody [Secondary Ab Anti-Rabbit IgG, HRP-linked Ab (CST 7074S)] 1:10000 diluted with TBST and 0.05% non-fat milk for 1 hour, washed and developed.

3.2.7 Blots reading and statistical analysis

Membrane signals were developed using a chemiluminescent Pierce ECL 2 Western Blotting Substrate (Thermo Scientific Prod # 80196) and the ECL signals were captured using a Azure 300c Chemidoc system. Electronic images were saved and then analyzed by using ImageJ software v1.53. Briefly, the captured image was opened in ImageJ software. The rectangle function was used to surround one signal band in the membrane starting from the first lane and remaining uniform for all bands to gain a proper reading. Using the analyze function, a first lane order was created. The software created another rectangle that was positioned around the band in the second lane. The rectangle dimensions remained uniform in size. The process was repeated in the same sequence for each lane. In the last lane, the order 'plot the lane' is used to produce intensity histograms based on the intensity of the band. Background signal was subtracted using the line tool for all bands and the intensity of the bands was calculated using the wand function. ImageJ data for the bands signals was collected for all membranes and recorded. The values were analyzed by using GraphPrism 9.0.0. The results were shown in mean \pm SEM.

3.3 Results

3.3.1 Identification of miR-21a-5p and miR-15b-5p target genes and identification of their functions:

For miR-21a-5p, fourteen target genes were determined and uploaded into the DAVID software for analysis. DAVID selected two pathway analysis systems, KEGG_database (Kyoto Encyclopedia of Genes and Genomes) and BIOCARTA pathway analysis. More genes were analyzed by KEGG system then BIOCARTA and were selected. Following analysis 8 genes were discarded and 6 genes were included for further analysis. KEGG analysis produced several pathways. The pathway related to cell survival and/or apoptosis as well as significantly enriched ($p < 0.05$) was selected (JAK-STAT signaling pathway). JAK-STAT pathway was generated by DAVID software and annotated three genes and proteins that participate in cell survival and anti-apoptotic pathways (Table 3.1). The detailed list of genes and output charts generated by DAVID software for miR-21a-5p targets are in Figures C.1 – C.5 (Appendix C).

Similarly, for miR-15b-5p, 46 target genes were uploaded into DAVID software. Again, two-pathway analysis systems were selected by the DAVID software, KEGG and BIOCARTA. KEGG pathway analysis was selected since it provided more predicted targets. Following analysis, 35 targets were excluded. Of note, the PI3K-Akt signaling pathway was among the pathways automatically generated by DAVID ($p < 0.05$). This pathway annotated 6 genes and proteins that are known to participate in anti-apoptotic and cell survival pathways (Table 3.1). The details of the generated DAVID output are in Figures C.6 – C.10 (Appendix C). A simplified illustration of Jak-STAT pathway the miR-21a-5p filtered targets is shown in Figure 3.1.

| miR-21a-5p target products (proteins) | miR-15b-5p target products (proteins) |
|---|---------------------------------------|
| Phosphatidylinositol 3-kinase, regulatory subunit, polypeptide 1 (p85 alpha) (Pik3r1) | B cell leukemia/lymphoma 2(Bcl2) |
| Interleukin 12a(IL12a) | Thymoma viral proto-oncogene 3(Akt3) |
| Interleukin 21(IL21) | Fibroblast growth factor 7(Fgf7) |
| | Fibroblast growth factor 9(Fgf9) |
| | Cyclin D2(Ccnd2) |
| | Cyclin E1(Ccne1) |

Table 3.1 The miR-21a-5p and miR-15b-5p filtered targets by DAVID.

The miR-21a-5p targets participate in cell survival in JAK-STAT signaling pathway.

The miR-15b-5p targets participate in anti-apoptotic and cell survival in PI3K and Akt signaling pathway.

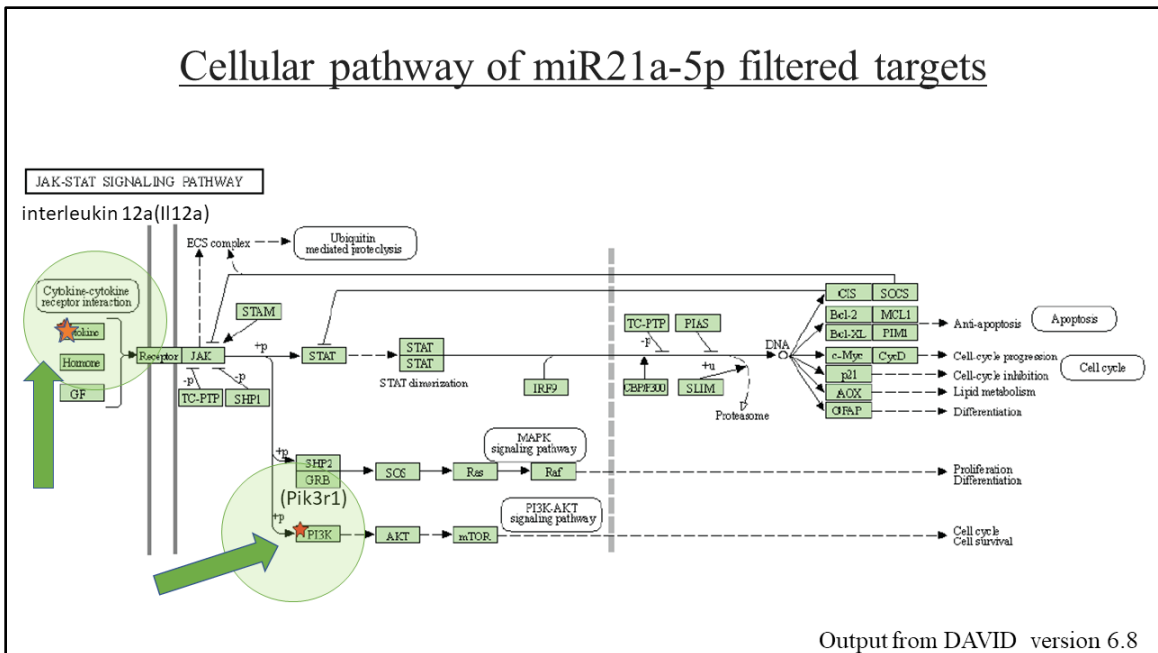


Figure 3.1 A simplified illustration of filtered mi-R21a-5p targets in Jak-STAT pathway. This simplified illustration was automatically generated by DAVID bioinformatic tools. See Appendix C for full illustration. The software annotated the proteins of interest with a red star. The green arrows and circles were added for further clarification. PI3Kp85 α regulatory subunit is a target of miR-21a-5p. This protein is part of PI3K-Akt signaling pathway which is also target by miR-15b-5p. It is not known if they have synergistic effect or not.

3.3.2 Testing the changes in the expression levels of target proteins

From the 9 filtered proteins, three proteins that participate in the anti-apoptotic process were selected, namely Bcl2, Akt as miR-15b-5p target protein products, and PI3Kp85 α as miR-21a-5p target protein product. The expression level of these three proteins is hypothesized to increase in the condition that showed downregulation of miR-21a-5p and miR-15b-5p. All western blot experiments were repeated at least two times (Figure 3.2).

Bcl2 expression level

Bcl2 protein expression levels were tested in 12 mice in total, six SCI+SLN mice and six SCI+mino animals. Western blot showed the expression of Bcl2 increased by 10% in experimental conditions that showed miR-15b-5p downregulation but was not statistically significant ($p = 0.4037$; 95% confidence interval -0.1401 to 0.3387).

Akt expression level

Again, this protein expression level was tested in six mice with SCI+SLN and six SCI+mino mice. Similar to Bcl2, this protein expression increased in SCI+mino group in comparison to SCI+SLN group. It is likely that miR-15b-5p downregulation resulted in a 30% increase in the expression of Akt protein but was not statistically significant ($p = 0.4016$; 95% confidence interval -0.4211 to 1.018).

PI3Kp85 α expression level

The increase in the expression of the protein PI3Kp85 α was the most prominent in the group that showed miR-21a-5p downregulation (SCI+mino). There was a 50% increase in comparison to the SCI+SLN group but not statistically significant ($p = 0.2029$; 95% confidence interval -0.2886 to 1.295).

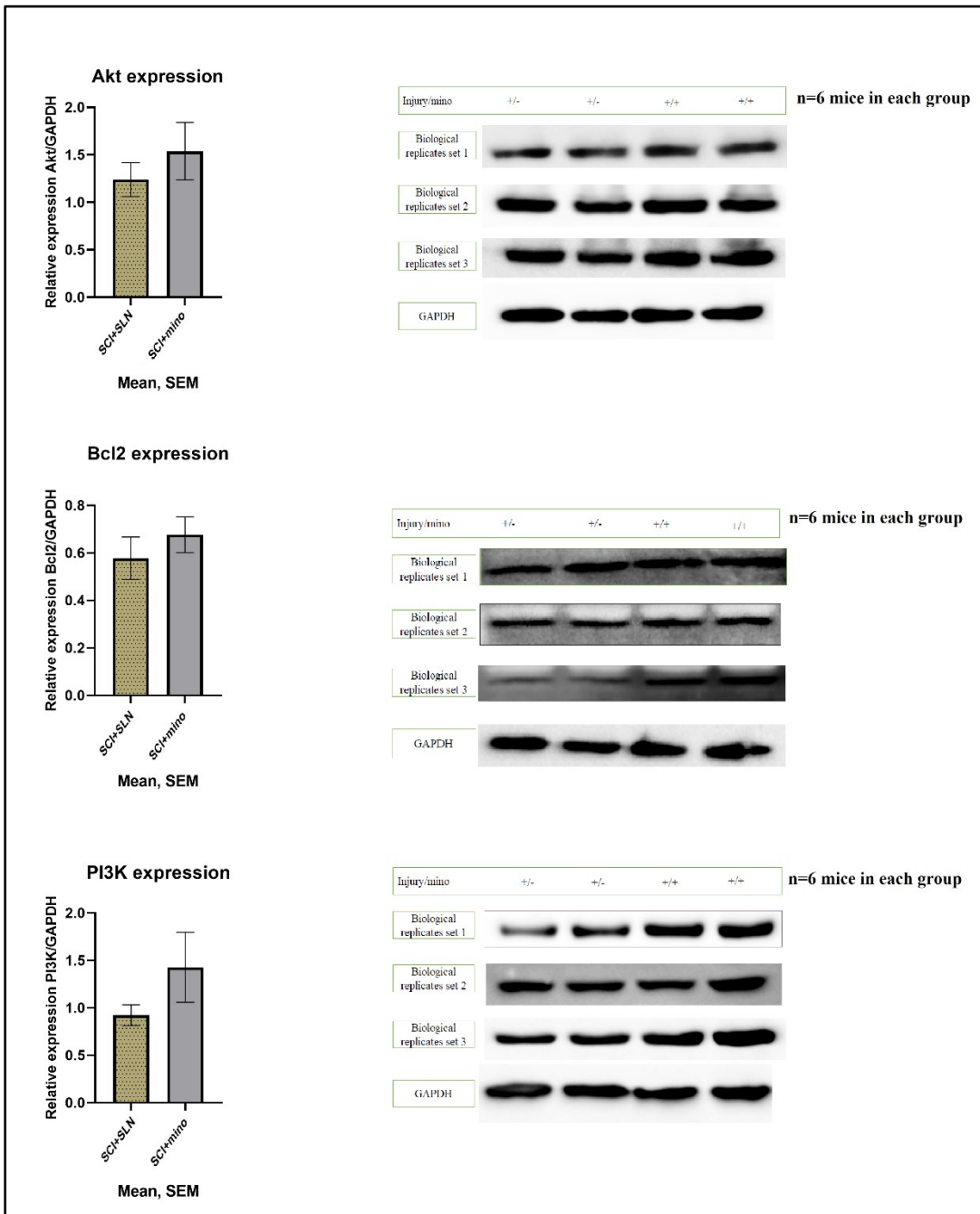


Figure 3.2 Protein levels in 1d survival SCI+SLN and SCI+mino.

Western blot showed that there was increase in the expression of proteins when their corresponding genes are targeted by the downregulated miR-21-5p (PI3Kp85 α) and the downregulated miR-15b-5p (Akt and Bcl2), but this increase was not statistically significant.

3.3.3 SCI impact parameters

All mice (n=12) were subjected to a similar impact injury (Figure C.11, Appendix C). SCIs for WB experiment were done in the 1d group only. There was no statistical difference between the actual force delivered to the two experimental conditions. The actual force for the two conditions SCI+SLN (n=6) and SCI+mino (n=6) were 53.667 ± 0.667 K dyne (mean \pm SEM) and 52 ± 0.865 K dyne respectively (p = 0.1556). Similarly, there was no statistical difference in SC displacement after the impact between the experimental conditions. The SC displacement in SCI+SLN was 423 ± 44.4 microns and the displacement in SCI+mino was 443.33 ± 38.16 microns (p = 0.7356).

3.4 Discussion and interpretation

In this study, currently available bioinformatic tools and databases were used to predict the targets of two identified downregulated miRNAs, miR-21a-5p and miR-15b-5p in mice following SCI. The targets of these miRNAs were identified in miRDB and TargetScan, Gene section of the National Center for Biotechnology Information, U.S. National Library of Medicine Genbank (<https://www.ncbi.nlm.nih.gov/gene/>) with gene ID-ensemble numbers. The DAVID bioinformatic tool was used to filter the predicted genes for both miRNAs of interest and to search for the pathways of these genes. It was determined that for miR-21a-5p, 3 genes play a role in the cell survival pathway (Figure 3.1 and Table 3.2) and miR-15b-5p targeted 6 genes in antiapoptotic and survival pathways (Table 3.1).

The differential protein expression level was examined at 1d after injury between the two experimental conditions, the SCI+mino (that showed downregulation of miRNAs) and the SCI+SLN. Three proteins were selected out of 9 predicted proteins, Akt, Bcl2 as miR-15b-5p targets and PI3Kp85 α as a target of miR-21a-5p. Western blot showed that there was an increase in expression level of these three proteins in SCI+mino condition compared to SCI+SLN condition. Although the increase was not statistically significant,

it is possible that the observed increase in protein expression could be biologically significant at cellular levels. Several previous studies showed significant increases in Bcl2 levels following minocycline administration with a neuroprotective effect (27, 35). Several factors may explain why the results here differ from the literature, such as different animal species or strain, the timing of measuring these proteins and the technique used. For the other two proteins of interest, PI3K and Akt, both participate in the same anti-apoptotic signaling pathway (277, 278). Although the increase in their expression was not statistically significant, both of these proteins are regulated by two different miRNAs. Furthermore, these two proteins in the PI3K-Akt signaling pathway may work synergistically. To test this potential synergistic effect, one could silence one protein translation and test for the proteins level and assess the impact on the neuronal survival.

Regardless, these findings might explain the possibility of increasing Bcl2 expression by relieving the suppression of miR-15b-5p. Additionally, the higher Akt level was correlated to miR-15b-5p downregulation. Regarding PI3K increased expression, this increase was likely due to miR-21a-5p downregulation effect.

In conclusion, this study demonstrated that bioinformatic resources can be very helpful in predicting the targets of the two downregulated miRNAs. Furthermore, our results suggest an increase in the expression of Akt, Bcl2 and PI3K proteins, which may be due to downregulation of the miRNAs that control translation of their genes. To verify that these proteins indeed play a role in neuroprotection, histological evaluation of SC tissue following injury should be undertaken, with the intent to identify evidence supporting enhanced neuronal survival (see Chapter 4).

CHAPTER 4 : POTENTIAL EFFECTS OF DOWNREGULATED miRNA ON THE TARGETED NEURONAL SURVIVAL PATHWAYS

4.1 Introduction

The initial cellular, axonal, and vascular disruption that results from mechanical impact on spinal cord parenchyma is followed by a series of biochemical reactions, the sSCI, that leads to expansion of the lesion size. In addition to necrosis, programmed cell death or the apoptosis has been shown to play a significant role in cellular population loss within and around the injury epicenter (128). Previous studies showed that an increase in Bcl2 protein expression resulted in neuronal cell body preservation but not myelinated axons protection (279). Additionally, Akt and PI3K proteins function as anti-apoptotic molecules and preserve neurons (277). Studies described here demonstrated moderate increase in the levels of these three proteins in conjunction with the downregulation of miR-21a-5p and miR-15b-5p (see Chapter 3). The working hypothesis was that the elevation in the expression of these proteins has a neuroprotective effect. To determine if the expression of these proteins in a mouse model of SCI was biologically significant, SC tissue specimens were examined under two experimental conditions: i) SCI+SLN and ii) SCI+mino (where the miRNAs downregulated and Akt, Bcl2 and PI3K over expressed). A reasonable quantitative method to observe any potential beneficial effect of these overexpressed proteins was to determine if there was any difference in the degenerated neurons between the two experimental conditions. To achieve this, Fluoro-Jade C (FJC) was used to label degenerated neurons. This fluorescent stain selectively labels degenerated neurons regardless the cause of the injury or mechanism of neuronal death (280, 281). FJC dye has high affinity to cell bodies and processes with the highest resolution and displays the best signal to background ratio compared to its predecessors Fluoro-Jade and Fluoro-Jade B. It is also compatible with immunofluorescent double-staining techniques (282).

4.2 Materials and methods

4.2.1 Mice and Ethics Approval

This was described in Section 2.2.1 animals and ethical approval. Briefly, a total of 10 female C57BL/6 mice 10 to 20 weeks old were used for histology experiments. Five animals were used in the minocycline group and five animals were used in the control group. Dalhousie University policy and the Canadian Council on Animal Care guidelines were followed through our experiments. The project (protocols #17-136, 20-060) was approved by the Dalhousie University Committee on Laboratory Animals.

4.2.2 Operative procedures

The surgeries and general anesthesia were described in Section 2.2.3 Surgical procedures and setup.

4.2.3 Spinal cord harvesting and preparation

Mice were euthanized 24 hours following the SCI by administration a lethal dose of IP pentobarbital (see section 2.2.6 for more details). Mice were transcardially perfused via thoracotomy with 7-10 ml of cold (4°C) sterile PBS 1X followed cold 4% paraformaldehyde (PFA). Following fixation, a segment of spinal column approximately 2 cm in length, which included the injury epicenter of the SC, was extracted and immersed in 4% PFA overnight. The following day the SC was dissected from the spinal column and immersed in 15% sucrose for 24 hours, followed by 30% sucrose for another 24 hours. A 5 mm section of injured SC was cut centered around the injury epicenter and embedded in the O.C.T Compound Tissue-Pluse 4585 (Fischer Scientific, catalog # 23-730-571). A cryostat was used to cut 30 µm cross-section of SC tissue, 5 sections were mounted on each chrome gelatin coated slide (Superfrost Plus, catalog # 12-550-15 Fisher brand). The gelatin solution was prepared by mixing 1 L of milli-Q water, 5 g

gelatin (Sigma, G2625) and 0.5 g chromium potassium sulfate dodecahydrate-CrK (SO₄).12H₂O (C337- Fisher scientific) to positively charge the slide and minimize SC sections loss. The SC sections 500 μm caudal to the injury epicenter from both SCI+mino and SCI+SLN groups were stained with Fluoro-Jade C, Hoechst 33342, neuN, and GFAP stains. The injury epicenter was determined as the area of highest blood intensity (visible contusion) and was consistent in all SC specimens (Figure 4.1). Identification of this region has been shown to correlate to the area of maximum damage/disruption resulting from the impact (257).

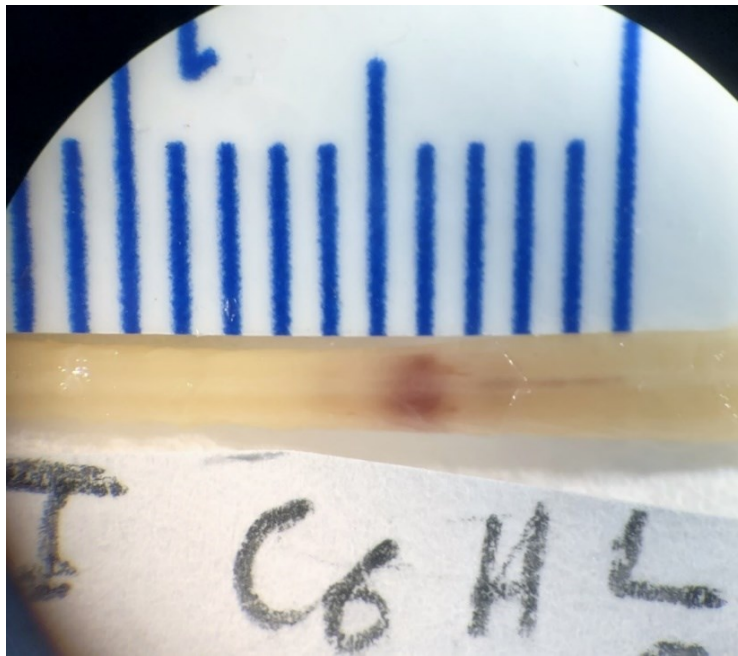


Figure 4.1 Spinal cord specimen collected 1d after the injury. Blood-tinged area represents the area hit by the tip of the impactor. Pictured captured via using Leica dissecting microscope . T=thoracic (rostral), L=lumbar (caudal)

4.2.4 Fluoro-Jade C staining and Hoechst nuclear counter staining

FJC was used to stain the degenerated neurons, whereas Hoechst is a blue fluorescent dye that stains DNA (35). The SC cross-sections were immersed in basic alcohol solution for 5 minutes, followed by 70% ethanol for 2 minutes. The slides were washed with milli-Q water for 2 minutes. The SC sections were incubated in 0.06% potassium permanganate for 15 minutes and rinsed with milli-Q water for 2 minutes. Then, the SC sections were incubated for 20 minutes in 0.0001% FJC solution (Fluoro- Jade C, Histo-chem inc. # US 62290240) or 0.0001% mixture solution of both FJC and Hoechst (Invitrogen, H21492, Hoechst 33342) nuclear counter stain (stock FJC dissolved in 0.1% acetic acid vehicle) (283-285). The slides then were rinsed in milli-Q water twice for 1 minute. The slides were dried on a slide warmer at 50-60° C for at least 10 minutes then cleared by xylene 1 minutes twice. The slides were then covered with coverslips by using a DPX (Sigma, 44581) mounting media. FJC and Hoechst were prepared and applied in dark conditions. The slides were kept in dark place to avoid fading.

4.2.5 Double labelling with immunohistochemistry nuclear anti-neuN antibody and fluoro-Jade C staining:

For further confirmation that FJC selectively stains neurons, a neuronal nuclear stain, anti-neuN antibody was used. This antibody was used to examine if it is colocalized with FJC positive neurons. The sequence of staining is important for the clarity of fluorescent signals (283). Therefore, for double labeling, first immunohistochemistry staining was started using anti-neuN antibody followed by FJC. The antigen retrieval technique was applied where SC sections were incubated with 0.1% Triton 100-X (Sigma, T8787) for 10 minutes, incubated in ~ 95 °C sodium citrate for 10 minutes. (Sodium citrate buffer is prepared by mixing Tri-sodium citrate dihydrate (Fisher Scientific-S279) 2.94 g in 1L milli-Q water and the pH is adjusted to 6 by HCl. Then, 0.5 ml of Tween 20 (Fisher

Scientific BP337) is added. The slides then were rinsed with 1X PBS three times for 5 minutes. Sections of the SC were covered with blocking buffer mixture of normal goat serum (5%) (Sigma, G6767), Triton 100-X (Sigma, T8787) and 1X PBS for 1 hour before the primary mouse anti-neuN antibody (Sigma-Aldrich, MAB377) was added on the slides (1:500) and incubated at 4 °C overnight. Goat anti-mouse IgG secondary antibody (1:500) Alexa Fluor 546 (ThermoFisher Scientific, Invitrogen-A11003) was applied for two hours at room temperature. The sections were subsequently incubated with potassium permanganate for 10-15 minutes and washed with 1X PBS three times for 5 minutes each. Following incubation, the working FJC solution (1: million) was applied to the slides for 20 minutes and then washed with milli-Q water three times and air dried at 50-60 °C for 20 minutes. DPX mountant and coverslip were applied, and the slides were examined.

4.2.6 Double labelling with immunohistochemistry anti-GFAP antibody and fluoro-Jade C staining:

Anti-GFAP antibody labeling has been described as a methodology to detect astrocytes (astrocyte marker) (283). To test for the selectivity of FJC for neurons in the SCI-mouse model, double labelling studies to visualize astrocytes using anti-GFAP was undertaken. Several previous laboratories have demonstrated that FJC is selective for degenerated neurons and does not colocalized with anti-GFAP staining (281, 286).

Immunohistochemistry staining was conducted first, followed by FJC staining (283). Briefly, as described in Section 4.2.6 above, the heat-induced epitope retrieval method was used to retrieve the antigens. The SC cross-sections mounted on the slides were blocked with normal goat serum (Sigma, G6767) mixture including Triton 100-X (Sigma, T8787) and 1X PBS for 60 minutes followed by the addition of the primary rabbit anti-GFAP antibody (abcam, ab7260) (1:1000) overnight at 4 °C. Following overnight incubation with anti-GFAP, secondary goat anti-rabbit IgG antibody conjugated with 594 fluoro-chrome (Invitrogen, Alexa Fluor 594-A11037) was applied (1:500) for 2 hours at room temperature. Following GFAP staining, potassium permanganate was applied for

10-15 minutes and FJC 1: million was applied for 20 minutes. Slides were cover slipped with DPX mounting media and examined histologically.

4.2.7 Imaging, histological quantification and analysis

The analysis was performed on cross-sections of SC tissue specimens collected from minocycline and saline treated groups (n = 5 in each group). Moreover, non-contused SC cross sections were used as controls for comparison. FJC positive cells were visualized in the dorsal horn or Rexed Laminae III-V (laminae III and VI contain nucleus proprius neurons, and lamina V contains interneurons and propriospinal neurons) (257, 287, 288) Fig. 4.2.

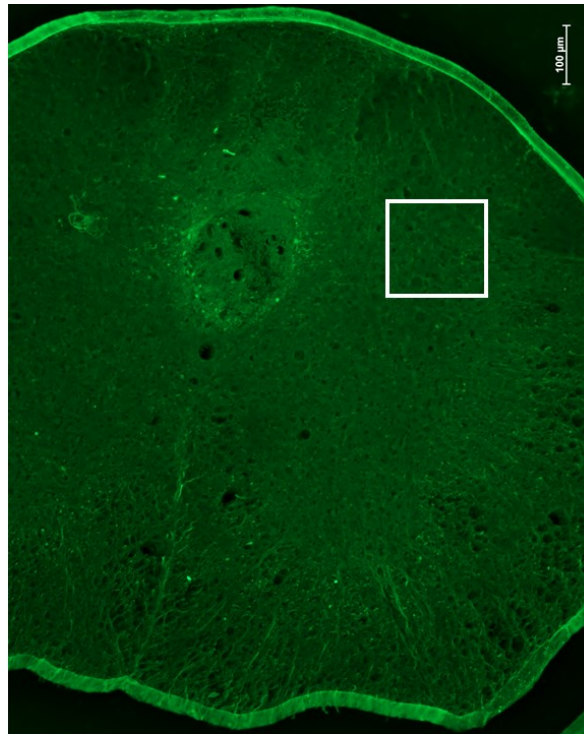


Figure 4.2 Spinal cord cross section at low magnification stained with FJC stain
The white square is showing the area of interest- dorsal horn Rexed laminae III-V.

A Zeiss Axio Imager Z1 was used with Color and Monochrome Camera Systems (Axiocam 506c_S2658 (2752 x 2208 pixels) and Axiocam 506m_S1975 (2752 x 2208 pixels). This Multi-track Image system supported with multi-position, motorized stage and with software: Zen Blue 3.0. Filter set 38 He GFP was used for Fluoro-Jade C dye, 49 DAPI channel for Hoechst stain, and 43 He DsRed was used for the antibodies conjugated with fluorophores 546 and 594. For evaluation of neuroprotection, the FJC positive cells were quantified and compared between the SCI+SLN and SCI+mino groups (284). The images were captured at high magnification (40X optical magnification). To observe if GFAP colocalizes with FJC, and to examine if the neuN antibody stains FJC positive cells, images were captured at high magnification as well (63X optical magnification) (258, 284). ImageJ software v1.52 was utilized for image analysis (257). FJC positive cells were quantified manually due to technical challenges related to automated counting. In automated counting, threshold set up was giving inconsistent results that was corrected by manual counting. The manual quantification was conducted by a blinded observer. Images from both conditions, SCI+SLN and SCI+mino, were captured and coded before, so as to maintain blinding. Images from two different sections, for each animal, were captured and saved in TIFF format. A total of 20 different sections were analyzed (10 section from each experimental condition). The ImageJ multi-point function was utilized for counting the FJC positive neurons in captured images. The same captured and coded images were quantified again by a different reader and inter reader reliability was tested by using Intraclass Correlation Coefficient (ICC) test. ICC was calculated by using IBM SPSS Statistics for Windows, version 28.0.0.0 USA.

4.3 Results

4.3.1 Fluoro-Jade C staining and Hoechst nuclear counter staining

FJC immunohistochemistry selectively stains degenerated neurons, whereas Hoechst nuclear counter stain is a blue, fluorescent dye and stains the nuclear DNA. In our experiments, FJC and Hoechst stains were used in SC sections under three conditions,

normal spinal cord (no injury), SCI+SLN and SCI+mino. Fluor-Jade C did not stain neurons in normal SC sections (Figure 4.3 G, H, and I). Fluor-Jade C labeled the degenerated neurons in control and treatment SCI groups (Figure 4.3 A-F).

Hoechst nuclear counter stain confirmed that neuronal cell bodies were stained with FJC. Similar to previous reports that FJC stains dendrites and axons; our study demonstrated FJC staining primarily within the cell bodies, although it was identified within neuronal processes in a few sections.

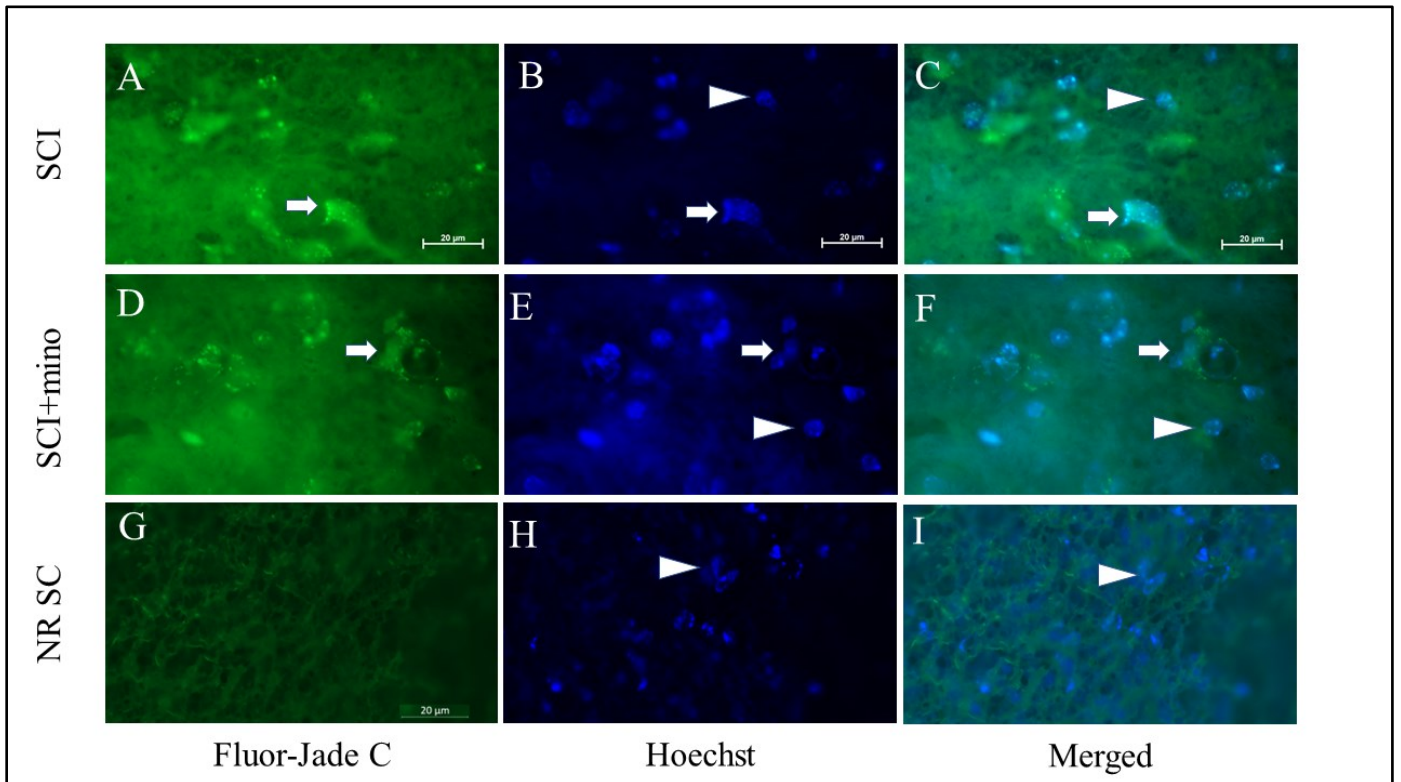


Figure 4.3 Fluoro - Jade C and Hoechst nuclear counter stain in three different experimental conditions.

The top row images A, B, and C represent SCI + saline. The middle row images D, E, and F represent SCI+ minocycline. The bottom row images G, H, and I represent normal SC. The first column is Fluoro-Jade C stain, the second column is Hoechst, and the third column are merged images. In the top row, the arrows in images A, B, and C point to a neuron labeled with FJC and Hoechst. In the middle row, the arrows in the images D, E, and F represent a neuron labeled with both FJC and Hoechst. The arrow heads in these images point to nucleus of a neurons. In the bottom row, the arrow heads point to a nucleus of a neuron. No neuron was stained with FJC in normal SC sections.

4.3.2 Double labelling with immunohistochemistry nuclear anti-neuN antibody and fluoro-Jade C staining:

To confirm that the FJC labeled cells are neurons, anti-neuN antibody immunohistochemistry was used to determine colocalization. Double labeling of FJC and anti-neuN antibody were used in three experiment conditions: normal spinal cord (no injury), SCI+SLN and SCI+mino. In the SCI experimental conditions, neurons that were labeled with FJC were also positive for the anti-neuN antibody. Anti-neuN antibody also labeled neurons that were negative for FJC stain in all experimental conditions, including normal SC. It was interpreted that the FJC negative neurons were normal neurons, as not only they lack FJC staining, but their soma size were larger than the neurons that were FJC positive (Figure 4.4). These results confirm that FJC labeled cells were neurons.

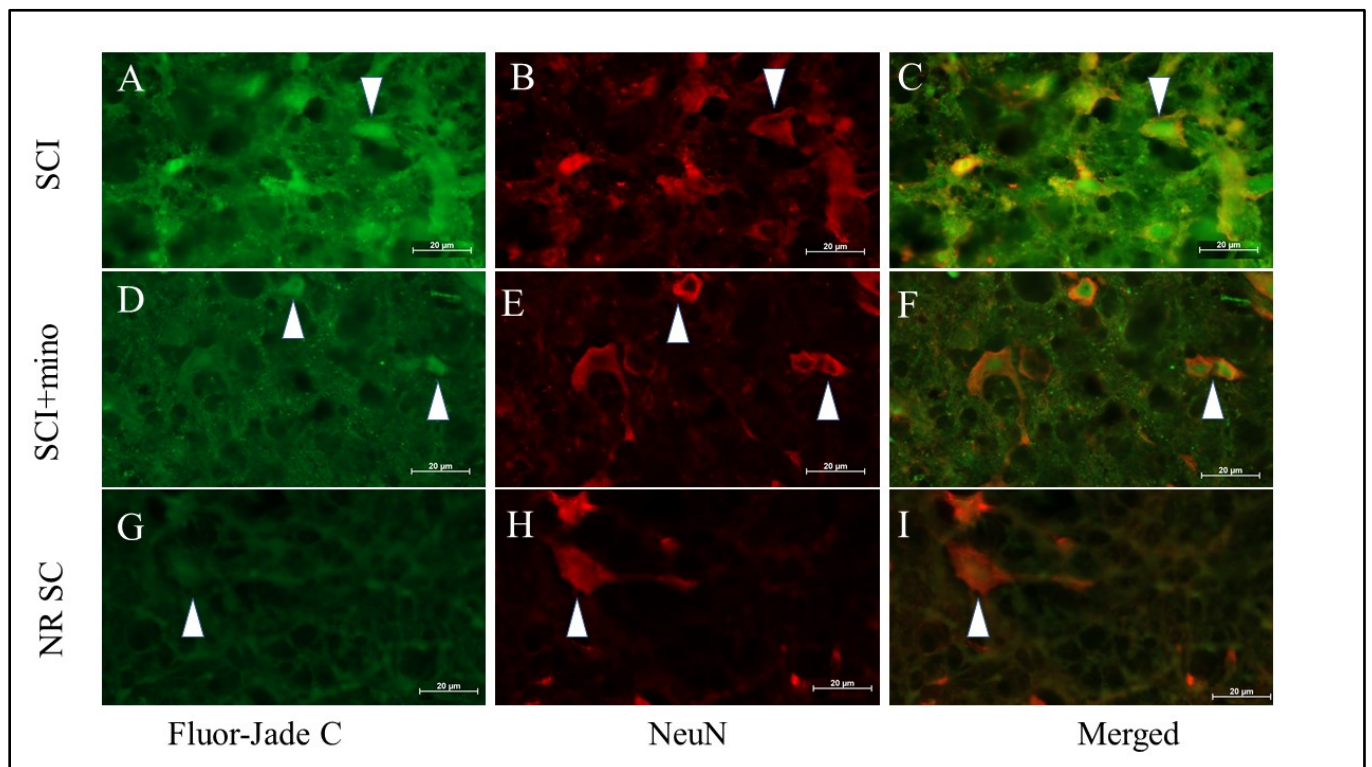


Figure 4.4 Anti-neuN immunohistochemistry and FJC stains in three different experimental conditions.

The top row images A, B, and C represent SCI + saline. The middle row images D, E, and F represent SCI+ minocycline. The bottom row images G, H, and I represent normal SC. The first column is Fluoro-Jade stain, the second column represents anti-neuN

immunohistochemistry, and the third column displays merged images. The arrowheads in A and D highlight neurons labeled with FJC. In B and E, the arrowheads denote the same cells after staining with anti-neuN stain. In C and F, the arrowheads point to the same neurons that are double labeled with both anti-neuN and FJC. FJC-positive neurons were shrunken in size when compared with the neurons that were labeled with Anti-neuN only. This comparison was most obvious when comparing the SCI+saline to no SCI condition.

4.3.3 Double labeling with immunohistochemistry anti-GFAP antibody and fluoro-Jade C staining:

To determine whether the FJC-labeled cells could be astrocytes, double labeling immunohistochemistry was used. FJC and anti-GFAP antibody double labeling was used in SCI+SLN, SCI+mino and normal SC sections (no injury). The Anti-GFAP antibody clearly delineated astrocytes, demonstrating the typical star shape, however it was not identified in the FJC-labeled cells. This lack of colocalization further suggests that the FJC labels neurons and not astrocytes, in the three experimental conditions examined (Figure 4.5 A-I).

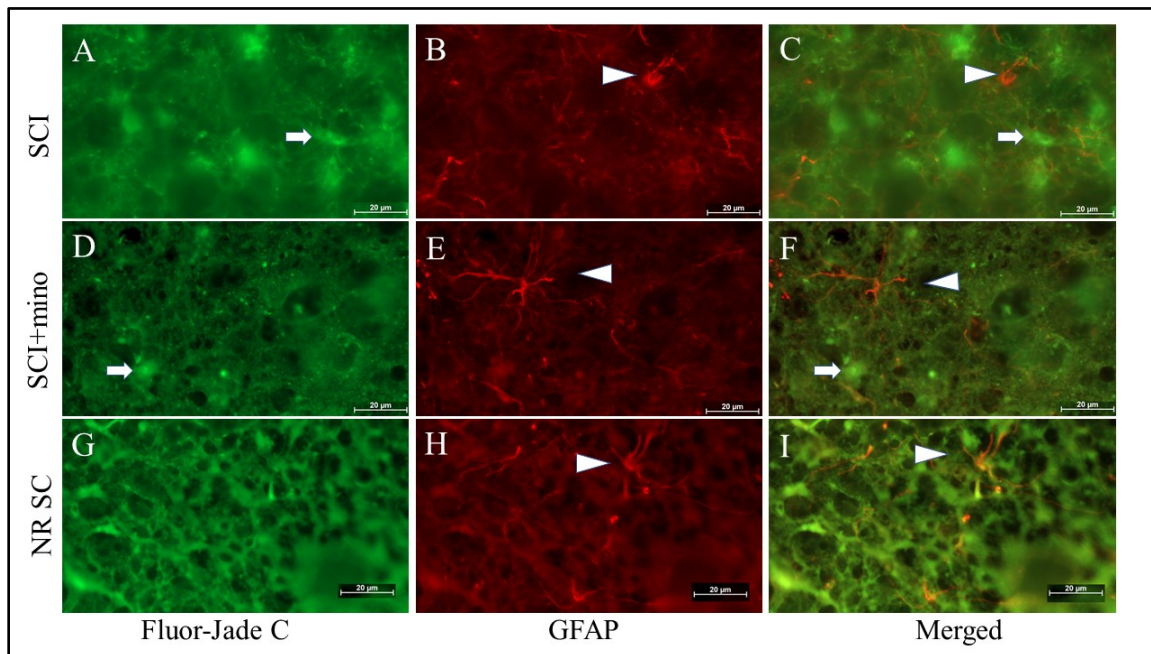


Figure 4.5 Anti-GFAP immunohistochemistry and FJC stains in three different experimental conditions.

The top row images A, B, and C represent SCI + saline. The middle row images D, E, and F represent SCI+ minocycline. The bottom row images G, H, and I represent normal SC. The first column is FJC, the second column is Anti-GFAP immunohistochemistry, and the third column are merged images. The arrows in the images A, C, D and F represent FJC-labeled neurons. The arrow heads in the images B, C, D, F, H, and I point to astrocytes labeled with Anti-GFAP stain. FJC stain clearly did not label astrocytes. The typical astrocytic star shape was more clearly identified in the no SCI and SCI+mino conditions compared to the SCI+saline group, where the astrocytes portrayed a more reactive phenotype.

4.3.4 Quantification analysis

Ten mice included in the analysis, 5 mice in the SCI+SLN and 5 mice in the SCI+mino groups. Two SC sections were read for each animal, total 20 sections. It was observed that conditions where miR-21a-5p and miR-15b-5p were downregulated and Akt, Bcl2, and PI3K proteins overexpressed (SCI+mino) there was significantly fewer FJC positive neurons (more neuronal cell population preservation) than the SCI+SLN condition ($p < 0.0369$, 95% confidence interval -40.97 to -1.435) (Figure 4.6). The same images were

read again by a second reader. The intraclass Correlation Coefficient (ICC) by using agreement function of IBM SPSS Statistics 28.0.0.0 was 0.92 (Cronbach's alpha) with p value < 0.001 and CI (0.81-0.97) .

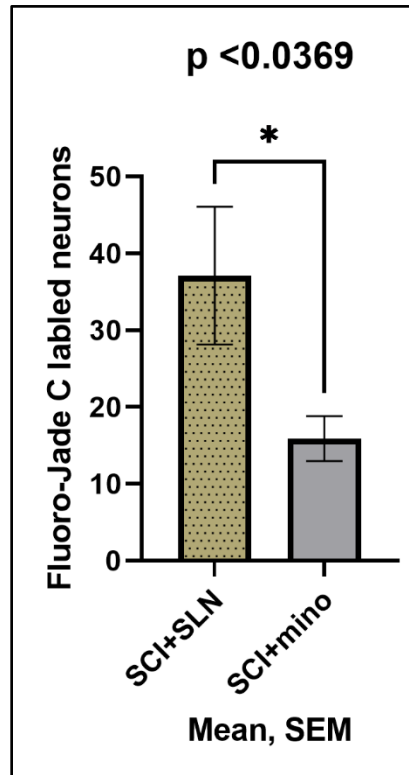


Figure 4.6 Comparison of Fluoro-Jade C positive cells in SCI+SLN and SCI+mino

This bar graph represents a comparison of FJC labeled neurons between two different experimental conditions. There were more degenerated neurons in SCI+SLN (labeled with FJC stain) than SCI+mino and the difference was statistically significant.

4.3.5 SCI impact parameters

There was no significant difference in actual force delivered to the SCs in the two experimental conditions, saline and minocycline (n=10) (Figure D.1; Appendix D). The actual force in the SCI+SLN condition was 51.6 ± 0.365 k dyne (mean \pm SEM), and in SCI+mino condition the actual force was 52.4 ± 0.619 k dyne (p = 0.3394). Likewise,

there was no significant difference in SC displacement after the injury in the two conditions. In the SCI+SLN the SC displacement was 507.4 ± 43.26 micrometer and the displacement in SCI+mino condition was 422.8 ± 16.11 micrometer ($p = 0.1329$).

4.4 Discussion and interpretation

The histological observations in this study included qualitative and quantitative analyses. To determine any potential beneficial effect related to the downregulation of miR-21a-5p and miR-15b-5p, and their respective protein expression (Akt, Bcl2 and PI3K), degenerated neurons were identified in SC sections by using FJC immunohistochemistry, to selectively stain for degenerated neurons. Anti-nuclear Hoechst counter stain was also used to confirm that FJC labeled neuronal cell bodies. The findings showed that FJC primarily labeled neuronal cell body and less often cell processes (Figure 4.3 A-I). These observations are consistent with previous studies by Schmued et al. 2005, Bian et al 2007 and Chen et al 2008 (280, 281, 286).

To confirm that these FJC positive cells were neurons and not other glial cells, a known neuronal marker anti-neuN antibody was used. The anti-neuN antibody colocalized with FJC stain and stained other neurons that were negative for FJC. Additionally, the neurons that were labeled only with anti-neuN antibody were relatively larger than the FJC positive neurons. This might indicate that the FJC positive cells have shrunk in size secondary to apoptosis.

Furthermore, to ensure that FJC did not stain astrocytes, an astrocytic marker (GFAP) was used (283). The results showed that GFAP and FJC did not colocalize. It was observed that FJC positive cells were neurons and GFAP anti-body specifically labeled astrocytes. Consistent with these findings, Bian et al 2007 and Chen et al 2008 showed that FJC does not colocalize with GFAP, and FJC selectively stains degenerated neurons (281, 286). It was noticed here as well that the typical star shape of astrocytes was more identifiable in the experimental conditions of no SCI and in SCI+mino sections when compared to SCI+SLN. It is known that GFAP stains approximately 15% of the actual

astrocyte volume (289), albeit the possible reason for this observation could be due to the fact that astrocytes in SCI+SLN condition were hypertrophied. This observation has been previously reported in the SC and the brain after different types of insults (258, 281). Moreover, Schmued et al. 2005 reported that astrocytes are more swollen when they are adjacent to the degenerated neurons (280).

Following confirmation that the FJC positive cells were neurons, the ratios of degenerated neurons were quantified in the two experimental conditions, SCI+SLN and SCI+mino. There were significantly more degenerated neurons in the SCI+SLN (control) condition than seen in the treatment group, which demonstrated downregulation of miR21a-5p and miR15b-5p and the overexpressed proteins (Akt, Bcl2 and PI3K). This observation may, in part, reflect the beneficial effects of the overexpressed proteins. However, this neuroprotective effect could be due to other beneficial proteins that have not been addressed or examined in this study (35, 258).

In summary, our histological findings suggest that there is a neuroprotective effect when SCI mice are treated with minocycline, and furthermore this effect may be the result of downregulation of miR-21a-5p and miR-15b-5p. These findings could be partly due to the elevation of expression of the proteins Akt, Bcl2, and PI3K. In the previous chapters it was demonstrated how minocycline resulted in downregulation of miR-21a-5p and miR-15b-5p expression. This downregulation resulted in an increase in Akt, Bcl2 and PI3K. These changes might, in part, explain the benefits of downregulation of these two miRNAs. However, other pathways influenced by minocycline cannot be excluded (21).

CHAPTER 5 : DISCUSSION

The findings within this thesis contribute to our insight into the mechanisms of sSCI. Our approach to further decipher this complex series of events following SCI could be viewed as novel. It was the intent to investigate how injury induced changes in upstream post-transcriptional translation pathways could alter downstream molecular events at the cellular level, the primary hypothesis being that modulation of miRNA expression by a neuroprotectant after SCI may attenuate the effects of sSCI.

To our knowledge, when this study was started in 2017, it was the first global analysis of miRNA changes, following SCI in a mouse model, that utilized Next Generation Sequencing (NGS). Additionally, this is the first study that used a known neuroprotective drug (minocycline) to examine alterations in miRNA expression following SCI at a broad level. In this exploratory study, bioinformatic tools were used to correlate the molecular (miRNAs and their target genes) changes with biochemical events (effector proteins) of sSCI. These effector proteins were tested and examined for potential impacts and histological changes. The intent was to determine whether this approach might uncover beneficial molecular (miRNA) pathways that could be targeted to preserve neurons following SCI. The longer-term objective will be to identify particular miRNAs that are either favorable or deleterious to recovery after SCI and subsequently design specific pharmaceuticals to either upregulate or down regulate those miRNAs, respectively, to gain an overall beneficial therapeutic effect. The current series of experiments revealed a number of relevant observations that support this potential novel therapeutic approach.

Firstly, SCI resulted in widespread changes in the expression of miRNA in the acute stage (1d time point) and subacute stage (7d time point). Secondly, for the first time it was demonstrated that a neuroprotective agent (minocycline) resulted in modulation of

miRNA expression following the injury in the acute stage. A subset of altered miRNAs were studied and the changes in miR-21a-5p and miR-15b-5p seen with NGS were subsequently confirmed. Although there are varied reports in the literature as to the observed changes in expression for certain miRNAs following insult, the upregulation of miR-21a-5p following SCI in different animal species is a consistent finding (227). Furthermore, this study supports the previous observation that miR-15b-5p likely regulates Akt protein, an important protein in cell survival (290). Thirdly, there was a relative increase in the expression of Akt, Bcl2, and PI3K proteins in the experimental condition with downregulated miR21a-5p and miR15b-5p expression. These are “beneficial” proteins that play a significant role in neuronal cell survival and anti-apoptotic effects. Fourthly, the observed changes in miRNAs and protein levels were correlated histologically with preservation of neuronal cell populations in the injury penumbra. Finally, it should be emphasized that our findings are based on a subset of miRNAs. The miRNA library constructed still has many significantly altered miRNAs that have yet to be investigated. These miRNAs will be utilized in several future projects. Together, these findings shed the light on the mechanisms of sSCI at upstream level and lend support to these pathways as potential therapeutic opportunities. However, there are several challenges and short comings to this study that need to be acknowledged.

5.1 Global miRNA pattern changes:

In the 1d group (acute phase), there was a general pattern change observed that supported upregulation of miRNA expression following SCI. Minocycline administration resulted in a reverse pattern, i.e. downregulation of 59 miRNAs and upregulation of 22 miRNAs. A review of the literature focused on patterns of miRNA change following SCI revealed different profiles (6, 227). The general profile of miRNA changes solely due to SCI in our study showed a similar pattern of miRNA expression to Lui et al. 2009 in the acute stage (6). These authors showed 30 miRNAs upregulated, 16 miRNAs downregulated. However, in contrast to our study, Yunta et al. 2012 reported two major differences from our results. Firstly, there were no significant changes in miRNA expression at 1d

following SCI, while there were noticeable changes in expression at both 3 and 7 days post-injury (227). Secondly, they observed a general progressive downregulation of miRNA expression following SCI. The pattern of miRNA dysregulation following injury in our study also differed from that reported by Strickland et al. 2011 (237). These authors showed general downregulation of the miRNA profile over various time points following injury.

Moreover, in our study, there was a higher number of miRNA changes identified on the first day compared to 7-days post-injury. This pattern contrasts that reported by Strickland et al. 2011 (237) and Yunta et al. 2012 (227) but is consistent with that reported by Liu et al. 2009 (6). This discrepancy in miRNA expression following the SCI can also be found in another miRNA-global analysis report (291). The explanation for this reported variability is likely multifactorial. Nine different studies addressing global miRNA changes in animals models were appraised by Nieto-Diaz et al 2014 (48). Five of these studies used rat models in their analysis: Liu et al.2009 (6), Strickland et al. 2011 (237), Yunta et al. 2012 (227), Hu et al. 2013a (292), Hu et al. 2013b (293). The other 4 studies, conducted in mouse models, focused their analysis on certain miRNAs, not global analyses (Jee et al. 2012a (294), Jee et al. 2012b (295) , and Im et al. 2012 (296)). Therefore, the hypothesis that there are more miRNA changes in the subacute stage compared to the acute stage may have resulted from the four global miRNAs analyses (by three authors) in a rat model, even though these findings differed from Liu et al 2009, which was also conducted on rats. It is known that miRNAs are tissue and cell specific. Although less likely in this context (due to the work of Liu et al 2009), different species and different strains could be part of the reason for this observed discrepancy. Secondly, in a recent human SCI study, miRNAs were investigated in patients' CSF and sera, with an abundance of miRNAs observed in the acute stage, declining by day 3 post injury and barely detectable in sera after day 5 following the injury (273). The same authors reported that the changes in differential expression of the miRNAs in the CSF was correlated to the severity of the SCI. Similarly, Tigchelaar et al. 2017, concluded in a porcine SCI model that the severity of the injury was related to the number of miRNAs detected in the animal's serum. Furthermore, a severe injury has been correlated with a higher degree of miRNA expression than the moderate or mild injury (248). In our mouse

SCI model, moderate impact was used. Lastly, the model of producing SCI may play a role in influencing miRNA expression (291). Nakanishi et al used forceps compression to create a SCI, which differs from the impact injury delivered herein. Together, these factors (mainly the injury severity and model) may partly explain our findings and the variation observed across studies. The aforementioned rat studies also used microarray technique. RNA sequence technique employed in this study has a higher resolution, down to a single bp, whereas the microarray resolution can be as high as 100 bp. This may allow for further differences in the number and the types of detected miRNAs across these studies.

5.2 miR-21a-5p:

For miR-21a-5p, despite the reported discrepancies in the field of miRNA and SCI, the consistent finding was upregulation of miR-21a-5p following the injury (227). However, Jiang et al. 2017 is an exception, in a rat SCI model these authors reported miR-21 downregulated at 4hr, 8hr and 1d following the injury and upregulated on day 3 and day 7 post injury (297). These findings may reflect their model of SCI or species of animal or some other technical aspect. In our study, the miR-21 was upregulated after SCI and significantly downregulated after minocycline administration. This downregulation is assumed beneficial, based upon the proteomics analysis which predicted the miR-21 targets and was supported in part by the observed increase in the expression of PI3K, which is a miR-21 target protein. Consistent with our findings, Wang et al. 2018 reported that downregulation of miR-21 improved functional recovery in a mouse SCI model (298). They used different proteins targets ((TGF)- β 1 and SMAD) and spinal fibroblast cells. The subsequent work of Xie et al. 2018 (299) and Ning et al 2019 (300) reinforced this concept. Furthermore, the notion of useful effects of downregulation of miR-21 was supported by Mohammed AZ et al 2019 (301). These authors used a proteomic approach to compare miR21 knockdown group vs negative control group (no miR-21 inhibitors) following contusion SCI in a mouse model. Their analysis demonstrated the beneficial pathways of inhibiting miR-21 and that miR-21 could be used as a biomarker for

amyotrophic lateral sclerosis. Again, they showed different targets for miR-21 from the previous studies and they addressed that several pathways could be targeted by this miRNA.

Conversely, Jiang et al. 2017 concluded that miR-21 upregulation is beneficial and enhances SC tissue repair via inducing neurite overgrowth (297). They argued that their finding was due to miR-21 targeting programmed cell death 4 (PDCD4) and decreased its expression. They scrutinized another predicted target, phosphatase and tensin homolog (PTEN), and concluded that the expression of this protein was not changed. There are several critiques for their study methodology. Firstly, they used the antibiotic gentamicin for the first three days after the surgery. The effect of gentamicin on miRNA expression after SCI is not known. Secondly, they overexpressed miR-21 in cultured postnatal rat SC neurons to show PDCD4 downregulation and neurite overgrowth. It is known that the results of in vitro experiments could differ from in vivo experiments. Given these factors, the expression of miR-21 could change as well as protein expression. Similar to Jiang et al. 2017, the concept of beneficial effect of miR-21 was raised by Hu et al. 2013 in a rat SCI contusion model. Yet, they found the protein target was PTEN and not PDCD4, which was the opposite finding to Jiang et al. 2017 (293). These authors also used penicillin G for 5 days in their experiments and reported the beneficial effect of miR-21 upregulation on day 3.

It is quite apparent that there are discrepancies in reports conveying miR-21 benefits. Notwithstanding, it can be gleaned that miR-21 is upregulated following SCI. Additionally, our findings suggest that miR-21 downregulation, following minocycline, may be useful following SCI and could potentially modulate survival pathways via targeting PI3K pathway.

5.3 miR-15b-5p

The present study found that miR-15b-5p was upregulated after SCI and downregulated following minocycline administration. Although little is known about this miRNA

relative to miR-21 in SCI models, the functions of miR-15b-5p have been studied in malignancy and cellular growth studies, albeit with different conclusions regarding its beneficial function when it is either over- or under-expressed (302, 303). Despite this, miR-15b-5p has been shown regulate protein Akt3 (290) similar to that observed herein. Furthermore, the present study demonstrated that miR-15b-5p regulates Bcl2. The beneficial effects of Bcl2 have been shown in several previous SCI studies, specifically the work by Wang et al 2004 (35). Interestingly, Sagot et al 1995 suggested that although Bcl2 promoted survival of neuronal cell bodies, it did not appear to prevent degeneration of myelinated axons. This work complements their findings, regarding the importance of Bcl2, and supports the notion that SCI recovery will require a multifaceted approach, one that targets the multitude of deleterious mechanisms that contribute to sSCI (279).

5.4 Lessons learned and future directions from this project:

There were a few lessons learned that can be addressed in future studies:

1. To further study the changes in miRNA expression during the subacute stage (7d group), consideration should be given to utilizing a more severe SCI model. This could be achieved through delivering a higher impact to the SC, such as ≥ 70 k dyne versus the 50 k dyne force used in this study. Support for this has been shown by Tigchelaar et al. 2019 and Tigchelaar et al. 2017(247, 248), in which the more severe injury resulted in a greater detectable level of miRNA in subacute stage.
2. There are many miRNAs identified in our NGS that require further characterization and subsequent validation. The miRNAs examined herein were selected due to their predicted relationship to neuronal survival, which was the selected target outcome. Another approach would be to select miRNAs for validation and downstream targeting experiments based upon the highest magnitude of expression regardless their potential functions. One potential downside of this approach is that there may be a higher likelihood of having downstream proteins that participate in different, even divergent pathways that require different sets of experiments to confirm. For instance, miRNAs that

target proteins in oxidative stress processes or those that relate to matrix metalloproteinases of sSCI, would need different methods to show the potential biological effects.

3. Further to #2 above, this work identified 10 novel, previously uncharacterized miRNAs that were significantly altered following injury. The role these miRNAs play in sSCI and any potential for therapeutic intervention will require further investigation.

4. The work presented herein demonstrates a correlation between miRNA changes, physiologic effects and a pharmaceutical treatment. To verify that the physiological effects observed are indeed related directly to the intended miRNA modulation, and not to alternative pharmacodynamics, miRNA silencing experiments should be done. Antagomirs are synthetic RNA complements that inactivate target miRNAs. Antagomirs to both miR-15b-5p and miR-21a-5p could be employed to verify that their modulation leads to the observed neuronal protection.

5.5 Conclusion

In conclusion, throughout this thesis sSCI was examined from a different angle than has been typically done in the past. Since there is no outright cure for SCI, and pharmacological agents that appear experimentally promising continue to fail to provide similar successes in clinical settings, novel approaches need to be developed. These studies have attempted to explore the feasibility of miRNAs being prospective future molecules that may be modulated to improve the SCI recovery. To our knowledge, this is the first study that addresses global modulation of the miRNAs following SCI by using a neuroprotective drug (minocycline). This study demonstrated how miRNA expression changes following SCI, and, moreover, it demonstrated that minocycline may influence the expression of miRNAs at two different time points. Specifically, it was found that miR-21a-5p and miR-15b-5p were downregulated after minocycline administration and that these two miRNAs participate in neuronal survival and anti-apoptotic pathways. A positive correlation was identified between the observed molecular changes, predicted

function and histologically confirmed neuronal cell survival. There are still many miRNAs in our library to scrutinize via different approaches in future experiments. The ultimate goal is to control the deleterious reactions characteristic of sSCI, so as to facilitate a local environment that is less hostile and more prone to promote neuronal preservation and regeneration, leading to enhanced functional recovery. This work suggests that targeting miRNAs and altering their expression following injury may be a novel approach worthy of further investigation.

REFERENCES

1. Silva NA, Sousa N, Reis RL, Salgado AJ. From basics to clinical: a comprehensive review on spinal cord injury. *Prog Neurobiol.* 2014;114:25-57.
2. Hayta E, Elden H. Acute spinal cord injury: A review of pathophysiology and potential of non-steroidal anti-inflammatory drugs for pharmacological intervention. *J Chem Neuroanat.* 2018;87:25-31.
3. Hassannejad Z, Zadegan SA, Shakouri-Motlagh A, Mokhatab M, Rezvan M, Sharif-Alhoseini M, et al. The fate of neurons after traumatic spinal cord injury in rats: A systematic review. *Iran J Basic Med Sci.* 2018;21(6):546-57.
4. Taoka Y, Okajima K. Role of leukocytes in spinal cord injury in rats. *J Neurotrauma.* 2000;17(3):219-29.
5. Taoka Y, Okajima K, Uchiba M, Murakami K, Kushimoto S, Johno M, et al. Role of neutrophils in spinal cord injury in the rat. *Neuroscience.* 1997;79(4):1177-82.
6. Liu NK, Wang XF, Lu QB, Xu XM. Altered microRNA expression following traumatic spinal cord injury. *Exp Neurol.* 2009;219(2):424-9.
7. Furlan JC, Craven BC, Fehlings MG. Surgical Management of the Elderly With Traumatic Cervical Spinal Cord Injury: A Cost-Utility Analysis. *Neurosurgery.* 2016;79(3):418-25.
8. Ahuja CS, Wilson JR, Nori S, Kotter MRN, Druschel C, Curt A, et al. Traumatic spinal cord injury. *Nat Rev Dis Primers.* 2017;3:17018.
9. Singh A, Tetreault L, Kalsi-Ryan S, Nouri A, Fehlings MG. Global prevalence and incidence of traumatic spinal cord injury. *Clin Epidemiol.* 2014;6:309-31.
10. Cripps RA, Lee BB, Wing P, Weerts E, Mackay J, Brown D. A global map for traumatic spinal cord injury epidemiology: towards a living data repository for injury prevention. *Spinal Cord.* 2011;49(4):493-501.
11. Ahuja CS, Schroeder GD, Vaccaro AR, Fehlings MG. Spinal Cord Injury-What Are the Controversies? *J Orthop Trauma.* 2017;31 Suppl 4:S7-S13.
12. Spinal Cord Injury Facts and Figures at a Glance. National Spinal Cord Injury Statistical Center. Birmingham, AL: University of Alabama at Birmingham; 2018.
13. Furlan JC, Sakakibara BM, Miller WC, Krassioukov AV. Global incidence and prevalence of traumatic spinal cord injury. *The Canadian journal of neurological sciences / Le journal canadien des sciences neurologiques.* 2013;40(4):456-64.

14. Lenehan B, Street J, Kwon BK, Noonan V, Zhang H, Fisher CG, et al. The epidemiology of traumatic spinal cord injury in British Columbia, Canada. *Spine (Phila Pa 1976)*. 2012;37(4):321-9.
15. DeVivo MJ, Chen Y. Trends in new injuries, prevalent cases, and aging with spinal cord injury. *Arch Phys Med Rehabil*. 2011;92(3):332-8.
16. Chen Y, He Y, DeVivo MJ. Changing Demographics and Injury Profile of New Traumatic Spinal Cord Injuries in the United States, 1972-2014. *Arch Phys Med Rehabil*. 2016;97(10):1610-9.
17. Seidl SE, Potashkin JA. The promise of neuroprotective agents in Parkinson's disease. *Front Neurol*. 2011;2:68.
18. Dunnett SB, Bjorklund A. Prospects for new restorative and neuroprotective treatments in Parkinson's disease. *Nature*. 1999;399(6738 Suppl):A32-9.
19. Andersen JK. Oxidative stress in neurodegeneration: cause or consequence? *Nat Med*. 2004;10 Suppl:S18-25.
20. Casson RJ, Chidlow G, Ebner A, Wood JP, Crowston J, Goldberg I. Translational neuroprotection research in glaucoma: a review of definitions and principles. *Clin Exp Ophthalmol*. 2012;40(4):350-7.
21. Shultz RB, Zhong Y. Minocycline targets multiple secondary injury mechanisms in traumatic spinal cord injury. *Neural Regen Res*. 2017;12(5):702-13.
22. Varma AK, Das A, Wallace Gt, Barry J, Vertegel AA, Ray SK, et al. Spinal cord injury: a review of current therapy, future treatments, and basic science frontiers. *Neurochem Res*. 2013;38(5):895-905.
23. Geisler FH, Coleman WP, Grieco G, Poonian D, Sygen Study G. The Sygen multicenter acute spinal cord injury study. *Spine (Phila Pa 1976)*. 2001;26(24 Suppl):S87-98.
24. Ahuja CS, Nori S, Tetreault L, Wilson J, Kwon B, Harrop J, et al. Traumatic Spinal Cord Injury-Repair and Regeneration. *Neurosurgery*. 2017;80(3S):S9-S22.
25. Ulndreaj A, Badner A, Fehlings MG. Promising neuroprotective strategies for traumatic spinal cord injury with a focus on the differential effects among anatomical levels of injury. *F1000Res*. 2017;6:1907.
26. Wilson JR, Forgione N, Fehlings MG. Emerging therapies for acute traumatic spinal cord injury. *CMAJ*. 2013;185(6):485-92.
27. Stirling DP, Koochesfahani KM, Steeves JD, Tetzlaff W. Minocycline as a neuroprotective agent. *Neuroscientist*. 2005;11(4):308-22.

28. Chopra I, Roberts M. Tetracycline antibiotics: mode of action, applications, molecular biology, and epidemiology of bacterial resistance. *Microbiol Mol Biol Rev.* 2001;65(2):232-60 ; second page, table of contents.
29. Feldman S, Careccia RE, Barham KL, Hancox J. Diagnosis and treatment of acne. *Am Fam Physician.* 2004;69(9):2123-30.
30. Stirling DP, Khodarahmi K, Liu J, McPhail LT, McBride CB, Steeves JD, et al. Minocycline treatment reduces delayed oligodendrocyte death, attenuates axonal dieback, and improves functional outcome after spinal cord injury. *J Neurosci.* 2004;24(9):2182-90.
31. Lee SM, Yune TY, Kim SJ, Park DW, Lee YK, Kim YC, et al. Minocycline reduces cell death and improves functional recovery after traumatic spinal cord injury in the rat. *J Neurotrauma.* 2003;20(10):1017-27.
32. Sanchez Mejia RO, Ona VO, Li M, Friedlander RM. Minocycline reduces traumatic brain injury-mediated caspase-1 activation, tissue damage, and neurological dysfunction. *Neurosurgery.* 2001;48(6):1393-9; discussion 9-401.
33. Chen M, Ona VO, Li M, Ferrante RJ, Fink KB, Zhu S, et al. Minocycline inhibits caspase-1 and caspase-3 expression and delays mortality in a transgenic mouse model of Huntington disease. *Nat Med.* 2000;6(7):797-801.
34. Wang X, Zhu S, Drozda M, Zhang W, Stavrovskaya IG, Cattaneo E, et al. Minocycline inhibits caspase-independent and -dependent mitochondrial cell death pathways in models of Huntington's disease. *Proc Natl Acad Sci U S A.* 2003;100(18):10483-7.
35. Wang J, Wei Q, Wang CY, Hill WD, Hess DC, Dong Z. Minocycline up-regulates Bcl-2 and protects against cell death in mitochondria. *J Biol Chem.* 2004;279(19):19948-54.
36. Scarabelli TM, Stephanou A, Pasini E, Gitti G, Townsend P, Lawrence K, et al. Minocycline inhibits caspase activation and reactivation, increases the ratio of XIAP to smac/DIABLO, and reduces the mitochondrial leakage of cytochrome C and smac/DIABLO. *J Am Coll Cardiol.* 2004;43(5):865-74.
37. Lee SM, Yune TY, Kim SJ, Kim YC, Oh YJ, Markelonis GJ, et al. Minocycline inhibits apoptotic cell death via attenuation of TNF-alpha expression following iNOS/NO induction by lipopolysaccharide in neuron/glia co-cultures. *J Neurochem.* 2004;91(3):568-78.
38. Kremlev SG, Roberts RL, Palmer C. Differential expression of chemokines and chemokine receptors during microglial activation and inhibition. *J Neuroimmunol.* 2004;149(1-2):1-9.

39. Ambrosini E, Aloisi F. Chemokines and glial cells: a complex network in the central nervous system. *Neurochem Res.* 2004;29(5):1017-38.
40. Pruzanski W, Greenwald RA, Street IP, Laliberte F, Stefanski E, Vadas P. Inhibition of enzymatic activity of phospholipases A2 by minocycline and doxycycline. *Biochem Pharmacol.* 1992;44(6):1165-70.
41. Kim SS, Kong PJ, Kim BS, Sheen DH, Nam SY, Chun W. Inhibitory action of minocycline on lipopolysaccharide-induced release of nitric oxide and prostaglandin E2 in BV2 microglial cells. *Arch Pharm Res.* 2004;27(3):314-8.
42. Yrjanheikki J, Tikka T, Keinanen R, Goldsteins G, Chan PH, Koistinaho J. A tetracycline derivative, minocycline, reduces inflammation and protects against focal cerebral ischemia with a wide therapeutic window. *Proc Natl Acad Sci U S A.* 1999;96(23):13496-500.
43. Pang T, Wang J, Benicky J, Saavedra JM. Minocycline ameliorates LPS-induced inflammation in human monocytes by novel mechanisms including LOX-1, Nur77 and LITAF inhibition. *Biochim Biophys Acta.* 2012;1820(4):503-10.
44. Krady JK, Basu A, Allen CM, Xu Y, LaNoue KF, Gardner TW, et al. Minocycline reduces proinflammatory cytokine expression, microglial activation, and caspase-3 activation in a rodent model of diabetic retinopathy. *Diabetes.* 2005;54(5):1559-65.
45. Ryu JK, Franciosi S, Sattayaprasert P, Kim SU, McLarnon JG. Minocycline inhibits neuronal death and glial activation induced by beta-amyloid peptide in rat hippocampus. *Glia.* 2004;48(1):85-90.
46. McPhail LT, Stirling DP, Tetzlaff W, Kwiecien JM, Ramer MS. The contribution of activated phagocytes and myelin degeneration to axonal retraction/dieback following spinal cord injury. *Eur J Neurosci.* 2004;20(8):1984-94.
47. Giuliani F, Hader W, Yong VW. Minocycline attenuates T cell and microglia activity to impair cytokine production in T cell-microglia interaction. *J Leukoc Biol.* 2005;78(1):135-43.
48. Nieto-Diaz M, Esteban FJ, Reigada D, Munoz-Galdeano T, Yunta M, Caballero-Lopez M, et al. MicroRNA dysregulation in spinal cord injury: causes, consequences and therapeutics. *Front Cell Neurosci.* 2014;8:53.
49. Song G, Cechvala C, Resnick DK, Dempsey RJ, Rao VL. GeneChip analysis after acute spinal cord injury in rat. *J Neurochem.* 2001;79(4):804-15.
50. Popovic N, Schubart A, Goetz BD, Zhang SC, Linington C, Duncan ID. Inhibition of autoimmune encephalomyelitis by a tetracycline. *Ann Neurol.* 2002;51(2):215-23.

51. Brundula V, Rewcastle NB, Metz LM, Bernard CC, Yong VW. Targeting leukocyte MMPs and transmigration: minocycline as a potential therapy for multiple sclerosis. *Brain*. 2002;125(Pt 6):1297-308.
52. Power C, Henry S, Del Bigio MR, Larsen PH, Corbett D, Imai Y, et al. Intracerebral hemorrhage induces macrophage activation and matrix metalloproteinases. *Ann Neurol*. 2003;53(6):731-42.
53. Wells JE, Rice TK, Nuttall RK, Edwards DR, Zekki H, Rivest S, et al. An adverse role for matrix metalloproteinase 12 after spinal cord injury in mice. *J Neurosci*. 2003;23(31):10107-15.
54. Tikka T, Fiebich BL, Goldsteins G, Keinanen R, Koistinaho J. Minocycline, a tetracycline derivative, is neuroprotective against excitotoxicity by inhibiting activation and proliferation of microglia. *J Neurosci*. 2001;21(8):2580-8.
55. Suk K. Minocycline suppresses hypoxic activation of rodent microglia in culture. *Neurosci Lett*. 2004;366(2):167-71.
56. Amin AR, Patel RN, Thakker GD, Lowenstein CJ, Attur MG, Abramson SB. Post-transcriptional regulation of inducible nitric oxide synthase mRNA in murine macrophages by doxycycline and chemically modified tetracyclines. *FEBS Lett*. 1997;410(2-3):259-64.
57. Amin AR, Attur MG, Thakker GD, Patel PD, Vyas PR, Patel RN, et al. A novel mechanism of action of tetracyclines: effects on nitric oxide synthases. *Proc Natl Acad Sci U S A*. 1996;93(24):14014-9.
58. Sonmez E, Kabatas S, Ozen O, Karabay G, Turkoglu S, Ogus E, et al. Minocycline treatment inhibits lipid peroxidation, preserves spinal cord ultrastructure, and improves functional outcome after traumatic spinal cord injury in the rat. *Spine (Phila Pa 1976)*. 2013;38(15):1253-9.
59. Aras M, Altas M, Motor S, Dokuyucu R, Yilmaz A, Ozgiray E, et al. Protective effects of minocycline on experimental spinal cord injury in rats. *Injury*. 2015;46(8):1471-4.
60. Garcia-Martinez EM, Sanz-Blasco S, Karachitos A, Bandez MJ, Fernandez-Gomez FJ, Perez-Alvarez S, et al. Mitochondria and calcium flux as targets of neuroprotection caused by minocycline in cerebellar granule cells. *Biochem Pharmacol*. 2010;79(2):239-50.
61. Wu Y, Chen Y, Wu Q, Jia L, Du X. Minocycline inhibits PARP1 expression and decreases apoptosis in diabetic retinopathy. *Mol Med Rep*. 2015;12(4):4887-94.
62. Casha S, Zygun D, McGowan MD, Bains I, Yong VW, Hurlbert RJ. Results of a phase II placebo-controlled randomized trial of minocycline in acute spinal cord injury. *Brain*. 2012;135(Pt 4):1224-36.

63. Casha S, Rice T, Stirling DP, Silva C, Gnanapavan S, Giovannoni G, et al. Cerebrospinal Fluid Biomarkers in Human Spinal Cord Injury from a Phase II Minocycline Trial. *J Neurotrauma*. 2018;35(16):1918-28.
64. Patestas MAG, Leslie P. *A Textbook of Neuroanatomy*. Malden, MA, USA Blackwell Science Ltd; 2006.
65. Harrison M, O'Brien A, Adams L, Cowin G, Ruitenber MJ, Sengul G, et al. Vertebral landmarks for the identification of spinal cord segments in the mouse. *Neuroimage*. 2013;68:22-9.
66. Gould DJ. *Neuroanatomy, Board Review Series*. Fifth edition ed. Philadelphia, PA, USA: Wolters Kluwer, Lippincott Williams & Wilkins; 2014.
67. Van De Graaff KM, Rhees RW. *Human anatomy and physiology*: New York: McGraw-Hill, Inc; 1987.
68. Vander AJ, Sherman JH, Luciano DS, Van Wynsberghe DM. *Human physiology: the mechanisms of body function*: McGraw-Hill Boston;; 1998.
69. Watson C, Paxinos G, Puelles L. *The mouse nervous system*. 1st ed. Amsterdam ; Boston: Elsevier Academic Press; 2012. xvii, 795 p. p.
70. Alstermark B, Ogawa J. In vivo recordings of bulbospinal excitation in adult mouse forelimb motoneurons. *J Neurophysiol*. 2004;92(3):1958-62.
71. Watson C, Paxinos G, Kayalioglu G, Heise C. *Atlas of the mouse spinal cord. The spinal cord*: Elsevier; 2008. p. 308-79.
72. Watson C, Paxinos G, Kayalioglu G, Heise C. *Atlas of the rat spinal cord. The spinal cord*: Elsevier; 2008. p. 238-306.
73. Watson C, Paxinos G, Kayalioglu G. *The spinal cord: a Christopher and Dana Reeve Foundation text and atlas*: Academic press; 2009.
74. Rivlin AS, Tator CH. Effect of duration of acute spinal cord compression in a new acute cord injury model in the rat. *Surg Neurol*. 1978;10(1):38-43.
75. Schuld C, Franz S, Bruggemann K, Heutehaus L, Weidner N, Kirshblum SC, et al. International standards for neurological classification of spinal cord injury: impact of the revised worksheet (revision 02/13) on classification performance. *J Spinal Cord Med*. 2016;39(5):504-12.
76. Greenberg MS. General Information, Neurologic Assessment, Whiplash and Sports-Related Injuries, Pediatric Spine Injuries. In: Greenberg MS, editor. *Handbook of Neurosurgery*. Eighth ed. New York: Thieme; 2016. p. 930-48.

77. Kirshblum SC, Waring W, Biering-Sorensen F, Burns SP, Johansen M, Schmidt-Read M, et al. Reference for the 2011 revision of the International Standards for Neurological Classification of Spinal Cord Injury. *J Spinal Cord Med.* 2011;34(6):547-54.
78. Zhang N, Fang M, Chen H, Gou F, Ding M. Evaluation of spinal cord injury animal models. *Neural Regen Res.* 2014;9(22):2008-12.
79. Kijima K, Kubota K, Hara M, Kobayakawa K, Yokota K, Saito T, et al. The acute phase serum zinc concentration is a reliable biomarker for predicting the functional outcome after spinal cord injury. *EBioMedicine.* 2019;41:659-69.
80. Ghasemlou N, Kerr BJ, David S. Tissue displacement and impact force are important contributors to outcome after spinal cord contusion injury. *Exp Neurol.* 2005;196(1):9-17.
81. Sharif-Alhoseini M, Khormali M, Rezaei M, Safdarian M, Hajjghadery A, Khalatbari MM, et al. Animal models of spinal cord injury: a systematic review. *Spinal Cord.* 2017;55(8):714-21.
82. Byrnes KR, Fricke ST, Faden AI. Neuropathological differences between rats and mice after spinal cord injury. *J Magn Reson Imaging.* 2010;32(4):836-46.
83. Ma M, Basso DM, Walters P, Stokes BT, Jakeman LB. Behavioral and histological outcomes following graded spinal cord contusion injury in the C57Bl/6 mouse. *Exp Neurol.* 2001;169(2):239-54.
84. Nishimura S, Sasaki T, Shimizu A, Yoshida K, Iwai H, Koya I, et al. Global gene expression analysis following spinal cord injury in non-human primates. *Exp Neurol.* 2014;261:171-9.
85. Alizadeh A, Dyck SM, Karimi-Abdolrezaee S. Traumatic Spinal Cord Injury: An Overview of Pathophysiology, Models and Acute Injury Mechanisms. *Front Neurol.* 2019;10:282.
86. Gruner JA. A monitored contusion model of spinal cord injury in the rat. *J Neurotrauma.* 1992;9(2):123-6; discussion 6-8.
87. Behrmann DL, Bresnahan JC, Beattie MS, Shah BR. Spinal cord injury produced by consistent mechanical displacement of the cord in rats: behavioral and histologic analysis. *J Neurotrauma.* 1992;9(3):197-217.
88. Cheriyan T, Ryan DJ, Weinreb JH, Cheriyan J, Paul JC, Lafage V, et al. Spinal cord injury models: a review. *Spinal Cord.* 2014;52(8):588-95.
89. Bottai D, Cigognini D, Madaschi L, Adami R, Nicora E, Menarini M, et al. Embryonic stem cells promote motor recovery and affect inflammatory cell infiltration in spinal cord injured mice. *Exp Neurol.* 2010;223(2):452-63.

90. Scheff SW, Rabchevsky AG, Fugaccia I, Main JA, Lumpp JE, Jr. Experimental modeling of spinal cord injury: characterization of a force-defined injury device. *J Neurotrauma*. 2003;20(2):179-93.
91. Marcol W, Slusarczyk W, Gzik M, Larysz-Brysz M, Bobrowski M, Gryniewicz-Bylina B, et al. Air gun impactor--a novel model of graded white matter spinal cord injury in rodents. *J Reconstr Microsurg*. 2012;28(8):561-8.
92. Stokes BT. Experimental spinal cord injury: a dynamic and verifiable injury device. *J Neurotrauma*. 1992;9(2):129-31; discussion 31-4.
93. Fehlings MG, Tator CH. The relationships among the severity of spinal cord injury, residual neurological function, axon counts, and counts of retrogradely labeled neurons after experimental spinal cord injury. *Exp Neurol*. 1995;132(2):220-8.
94. Tarlov IM, Klinger H, Vitale S. Spinal cord compression studies. I. Experimental techniques to produce acute and gradual compression. *AMA Arch Neurol Psychiatry*. 1953;70(6):813-9.
95. Fukuda S, Nakamura T, Kishigami Y, Endo K, Azuma T, Fujikawa T, et al. New canine spinal cord injury model free from laminectomy. *Brain Res Brain Res Protoc*. 2005;14(3):171-80.
96. Nesathurai S, Graham WA, Mansfield K, Magill D, Sehgal P, Westmoreland SV, et al. Model of traumatic spinal cord injury in *Macaca fascicularis*: similarity of experimental lesions created by epidural catheter to human spinal cord injury. *J Med Primatol*. 2006;35(6):401-4.
97. Blight AR. Morphometric analysis of a model of spinal cord injury in guinea pigs, with behavioral evidence of delayed secondary pathology. *J Neurol Sci*. 1991;103(2):156-71.
98. Plemel JR, Duncan G, Chen KW, Shannon C, Park S, Sparling JS, et al. A graded forceps crush spinal cord injury model in mice. *J Neurotrauma*. 2008;25(4):350-70.
99. da Costa ES, Carvalho AL, Martinez AM, De-Ary-Pires B, Pires-Neto MA, de Ary-Pires R. Strapping the spinal cord: an innovative experimental model of CNS injury in rats. *J Neurosci Methods*. 2008;170(1):130-9.
100. Cloud BA, Ball BG, Chen BK, Knight AM, Hakim JS, Ortiz AM, et al. Hemisection spinal cord injury in rat: the value of intraoperative somatosensory evoked potential monitoring. *J Neurosci Methods*. 2012;211(2):179-84.
101. Dabney KW, Ehrenshteyn M, Agresta CA, Twiss JL, Stern G, Tice L, et al. A model of experimental spinal cord trauma based on computer-controlled intervertebral distraction: characterization of graded injury. *Spine (Phila Pa 1976)*. 2004;29(21):2357-64.

102. Seifert JL, Bell JE, Elmer BB, Sucato DJ, Romero MI. Characterization of a novel bidirectional distraction spinal cord injury animal model. *J Neurosci Methods*. 2011;197(1):97-103.
103. Choo AM, Liu J, Liu Z, Dvorak M, Tetzlaff W, Oxland TR. Modeling spinal cord contusion, dislocation, and distraction: characterization of vertebral clamps, injury severities, and node of Ranvier deformations. *J Neurosci Methods*. 2009;181(1):6-17.
104. Watson BD, Prado R, Dietrich WD, Ginsberg MD, Green BA. Photochemically induced spinal cord injury in the rat. *Brain Res*. 1986;367(1-2):296-300.
105. Liu NK, Zhang YP, Titsworth WL, Jiang X, Han S, Lu PH, et al. A novel role of phospholipase A2 in mediating spinal cord secondary injury. *Ann Neurol*. 2006;59(4):606-19.
106. Liu D, Xu GY, Pan E, McAdoo DJ. Neurotoxicity of glutamate at the concentration released upon spinal cord injury. *Neuroscience*. 1999;93(4):1383-9.
107. Oyinbo CA. Secondary injury mechanisms in traumatic spinal cord injury: a nugget of this multiply cascade. *Acta Neurobiol Exp (Wars)*. 2011;71(2):281-99.
108. Chen K, Deng S, Lu H, Zheng Y, Yang G, Kim D, et al. RNA-seq characterization of spinal cord injury transcriptome in acute/subacute phases: a resource for understanding the pathology at the systems level. *PLoS One*. 2013;8(8):e72567.
109. Shi LL, Zhang N, Xie XM, Chen YJ, Wang R, Shen L, et al. Transcriptome profile of rat genes in injured spinal cord at different stages by RNA-sequencing. *BMC Genomics*. 2017;18(1):173.
110. Kalsi-Ryan S, Karadimas SK, Fehlings MG. Cervical spondylotic myelopathy: the clinical phenomenon and the current pathobiology of an increasingly prevalent and devastating disorder. *Neuroscientist*. 2013;19(4):409-21.
111. Karadimas SK, Moon ES, Yu WR, Satkunendrarajah K, Kallitsis JK, Gatzounis G, et al. A novel experimental model of cervical spondylotic myelopathy (CSM) to facilitate translational research. *Neurobiol Dis*. 2013;54:43-58.
112. Karadimas SK, Gatzounis G, Fehlings MG. Pathobiology of cervical spondylotic myelopathy. *Eur Spine J*. 2015;24 Suppl 2:132-8.
113. Rowland JW, Hawryluk GW, Kwon B, Fehlings MG. Current status of acute spinal cord injury pathophysiology and emerging therapies: promise on the horizon. *Neurosurg Focus*. 2008;25(5):E2.
114. Mauter AE, Weinzierl MR, Donovan F, Noble LJ. Vascular events after spinal cord injury: contribution to secondary pathogenesis. *Phys Ther*. 2000;80(7):673-87.

115. Maikos JT, Shreiber DI. Immediate damage to the blood-spinal cord barrier due to mechanical trauma. *J Neurotrauma*. 2007;24(3):492-507.
116. Ito T, Oyanagi K, Wakabayashi K, Ikuta F. Traumatic spinal cord injury: a neuropathological study on the longitudinal spreading of the lesions. *Acta Neuropathol*. 1997;93(1):13-8.
117. Pineau I, Lacroix S. Proinflammatory cytokine synthesis in the injured mouse spinal cord: multiphasic expression pattern and identification of the cell types involved. *J Comp Neurol*. 2007;500(2):267-85.
118. Stone WL, Basit H, Burns B. Pathology, Inflammation. StatPearls. Treasure Island (FL)2021.
119. Epelman S, Lavine KJ, Randolph GJ. Origin and functions of tissue macrophages. *Immunity*. 2014;41(1):21-35.
120. Streit WJ, Semple-Rowland SL, Hurley SD, Miller RC, Popovich PG, Stokes BT. Cytokine mRNA profiles in contused spinal cord and axotomized facial nucleus suggest a beneficial role for inflammation and gliosis. *Exp Neurol*. 1998;152(1):74-87.
121. Popovich PG, Wei P, Stokes BT. Cellular inflammatory response after spinal cord injury in Sprague-Dawley and Lewis rats. *J Comp Neurol*. 1997;377(3):443-64.
122. Popovich PG. Immunological regulation of neuronal degeneration and regeneration in the injured spinal cord. *Prog Brain Res*. 2000;128:43-58.
123. Blight AR. Effects of silica on the outcome from experimental spinal cord injury: implication of macrophages in secondary tissue damage. *Neuroscience*. 1994;60(1):263-73.
124. Popovich PG, Guan Z, Wei P, Huitinga I, van Rooijen N, Stokes BT. Depletion of hematogenous macrophages promotes partial hindlimb recovery and neuroanatomical repair after experimental spinal cord injury. *Exp Neurol*. 1999;158(2):351-65.
125. Mabon PJ, Weaver LC, Dekaban GA. Inhibition of monocyte/macrophage migration to a spinal cord injury site by an antibody to the integrin alphaD: a potential new anti-inflammatory treatment. *Exp Neurol*. 2000;166(1):52-64.
126. Donnelly DJ, Popovich PG. Inflammation and its role in neuroprotection, axonal regeneration and functional recovery after spinal cord injury. *Exp Neurol*. 2008;209(2):378-88.
127. Klusman I, Schwab ME. Effects of pro-inflammatory cytokines in experimental spinal cord injury. *Brain Res*. 1997;762(1-2):173-84.
128. Beattie MS, Farooqui AA, Bresnahan JC. Review of current evidence for apoptosis after spinal cord injury. *J Neurotrauma*. 2000;17(10):915-25.

129. Wu KL, Chan SH, Chao YM, Chan JY. Expression of pro-inflammatory cytokine and caspase genes promotes neuronal apoptosis in pontine reticular formation after spinal cord transection. *Neurobiol Dis.* 2003;14(1):19-31.
130. Hains BC, Black JA, Waxman SG. Primary cortical motor neurons undergo apoptosis after axotomizing spinal cord injury. *J Comp Neurol.* 2003;462(3):328-41.
131. Beattie MS, Harrington AW, Lee R, Kim JY, Boyce SL, Longo FM, et al. ProNGF induces p75-mediated death of oligodendrocytes following spinal cord injury. *Neuron.* 2002;36(3):375-86.
132. Crowe MJ, Bresnahan JC, Shuman SL, Masters JN, Beattie MS. Apoptosis and delayed degeneration after spinal cord injury in rats and monkeys. *Nat Med.* 1997;3(1):73-6.
133. Dumont RJ, Okonkwo DO, Verma S, Hurlbert RJ, Boulos PT, Ellegala DB, et al. Acute spinal cord injury, part I: pathophysiologic mechanisms. *Clin Neuropharmacol.* 2001;24(5):254-64.
134. Jamme I, Petit E, Divoux D, Gerbi A, Maixent JM, Nouvelot A. Modulation of mouse cerebral Na⁺,K⁽⁺⁾-ATPase activity by oxygen free radicals. *Neuroreport.* 1995;7(1):333-7.
135. McAdoo DJ, Xu GY, Robak G, Hughes MG. Changes in amino acid concentrations over time and space around an impact injury and their diffusion through the rat spinal cord. *Exp Neurol.* 1999;159(2):538-44.
136. Verkhratsky A, Steinhauser C. Ion channels in glial cells. *Brain Res Brain Res Rev.* 2000;32(2-3):380-412.
137. Gottlieb M, Matute C. Expression of ionotropic glutamate receptor subunits in glial cells of the hippocampal CA1 area following transient forebrain ischemia. *J Cereb Blood Flow Metab.* 1997;17(3):290-300.
138. Karadottir R, Attwell D. Neurotransmitter receptors in the life and death of oligodendrocytes. *Neuroscience.* 2007;145(4):1426-38.
139. Xu GY, Hughes MG, Zhang L, Cain L, McAdoo DJ. Administration of glutamate into the spinal cord at extracellular concentrations reached post-injury causes functional impairments. *Neurosci Lett.* 2005;384(3):271-6.
140. Couillard-Despres S, BL, Vogl M. Pathophysiology of Traumatic Spinal Cord Injury. In: Weidner N. RR, Tansey K., editor. *Neurological Aspects of Spinal Cord Injury.* Switzerland: Springer, Cham; 2017.
141. Fernyhough P, Calcutt NA. Abnormal calcium homeostasis in peripheral neuropathies. *Cell Calcium.* 2010;47(2):130-9.

142. Pivovarova NB, Andrews SB. Calcium-dependent mitochondrial function and dysfunction in neurons. *FEBS J.* 2010;277(18):3622-36.
143. Verkhratsky A, Toescu EC. Endoplasmic reticulum Ca(2+) homeostasis and neuronal death. *J Cell Mol Med.* 2003;7(4):351-61.
144. Dingledine R, Borges K, Bowie D, Traynelis SF. The glutamate receptor ion channels. *Pharmacol Rev.* 1999;51(1):7-61.
145. Faden AI, Simon RP. A potential role for excitotoxins in the pathophysiology of spinal cord injury. *Ann Neurol.* 1988;23(6):623-6.
146. Li S, Stys PK. Na(+)-K(+)-ATPase inhibition and depolarization induce glutamate release via reverse Na(+)-dependent transport in spinal cord white matter. *Neuroscience.* 2001;107(4):675-83.
147. Stys PK, Waxman SG, Ransom BR. Ionic mechanisms of anoxic injury in mammalian CNS white matter: role of Na⁺ channels and Na(+)-Ca²⁺ exchanger. *J Neurosci.* 1992;12(2):430-9.
148. LoPachin RM, Gaughan CL, Lehning EJ, Kaneko Y, Kelly TM, Blight A. Experimental spinal cord injury: spatiotemporal characterization of elemental concentrations and water contents in axons and neuroglia. *J Neurophysiol.* 1999;82(5):2143-53.
149. Regan RF, Choi DW. Glutamate neurotoxicity in spinal cord cell culture. *Neuroscience.* 1991;43(2-3):585-91.
150. Agrawal SK, Fehlings MG. Mechanisms of secondary injury to spinal cord axons in vitro: role of Na⁺, Na(+)-K(+)-ATPase, the Na(+)-H⁺ exchanger, and the Na(+)-Ca²⁺ exchanger. *J Neurosci.* 1996;16(2):545-52.
151. Chandra J, Sheerin F, Lopez de Heredia L, Meagher T, King D, Belci M, et al. MRI in acute and subacute post-traumatic spinal cord injury: pictorial review. *Spinal Cord.* 2012;50(1):2-7.
152. Hagg T, Oudega M. Degenerative and spontaneous regenerative processes after spinal cord injury. *J Neurotrauma.* 2006;23(3-4):264-80.
153. Sofroniew MV. Molecular dissection of reactive astrogliosis and glial scar formation. *Trends Neurosci.* 2009;32(12):638-47.
154. Gurtner GC, Werner S, Barrandon Y, Longaker MT. Wound repair and regeneration. *Nature.* 2008;453(7193):314-21.
155. Wanner IB, Deik A, Torres M, Rosendahl A, Neary JT, Lemmon VP, et al. A new in vitro model of the glial scar inhibits axon growth. *Glia.* 2008;56(15):1691-709.

156. Giger RJ, Hollis ER, 2nd, Tuszynski MH. Guidance molecules in axon regeneration. *Cold Spring Harb Perspect Biol.* 2010;2(7):a001867.
157. Falci SP, Indeck C, Lammertse DP. Posttraumatic spinal cord tethering and syringomyelia: surgical treatment and long-term outcome. *J Neurosurg Spine.* 2009;11(4):445-60.
158. Liu M, Wu W, Li H, Li S, Huang LT, Yang YQ, et al. Necroptosis, a novel type of programmed cell death, contributes to early neural cells damage after spinal cord injury in adult mice. *J Spinal Cord Med.* 2015;38(6):745-53.
159. Wang Y, Wang H, Tao Y, Zhang S, Wang J, Feng X. Necroptosis inhibitor necrostatin-1 promotes cell protection and physiological function in traumatic spinal cord injury. *Neuroscience.* 2014;266:91-101.
160. Wang Y, Wang J, Yang H, Zhou J, Feng X, Wang H, et al. Necrostatin-1 mitigates mitochondrial dysfunction post-spinal cord injury. *Neuroscience.* 2015;289:224-32.
161. Cramer SC, Lastra L, Lacourse MG, Cohen MJ. Brain motor system function after chronic, complete spinal cord injury. *Brain.* 2005;128(12):2941-50.
162. Jones LL, Margolis RU, Tuszynski MH. The chondroitin sulfate proteoglycans neurocan, brevican, phosphacan, and versican are differentially regulated following spinal cord injury. *Exp Neurol.* 2003;182(2):399-411.
163. Fawcett JW, Asher RA. The glial scar and central nervous system repair. *Brain Res Bull.* 1999;49(6):377-91.
164. Anderson MA, Burda JE, Ren Y, Ao Y, O'Shea TM, Kawaguchi R, et al. Astrocyte scar formation aids central nervous system axon regeneration. *Nature.* 2016;532(7598):195-200.
165. Bush TG, Puvanachandra N, Horner CH, Polito A, Ostefeld T, Svendsen CN, et al. Leukocyte infiltration, neuronal degeneration, and neurite outgrowth after ablation of scar-forming, reactive astrocytes in adult transgenic mice. *Neuron.* 1999;23(2):297-308.
166. Marinelli S, Vacca V, Angelis F, Pieroni L, Orsini T, Parisi C, et al. Innovative mouse model mimicking human-like features of spinal cord injury: efficacy of Docosahexaenoic acid on acute and chronic phases. *Sci Rep.* 2019;9(1):8883.
167. Siddall PJ, McClelland JM, Rutkowski SB, Cousins MJ. A longitudinal study of the prevalence and characteristics of pain in the first 5 years following spinal cord injury. *Pain.* 2003;103(3):249-57.
168. Masri R, Keller A. Chronic pain following spinal cord injury. *Adv Exp Med Biol.* 2012;760:74-88.

169. Hains BC, Johnson KM, Eaton MJ, Willis WD, Hulsebosch CE. Serotonergic neural precursor cell grafts attenuate bilateral hyperexcitability of dorsal horn neurons after spinal hemisection in rat. *Neuroscience*. 2003;116(4):1097-110.
170. Drew GM, Siddall PJ, Duggan AW. Responses of spinal neurones to cutaneous and dorsal root stimuli in rats with mechanical allodynia after contusive spinal cord injury. *Brain Res*. 2001;893(1-2):59-69.
171. Di Giovanni S, Knobloch SM, Brandoli C, Aden SA, Hoffman EP, Faden AI. Gene profiling in spinal cord injury shows role of cell cycle in neuronal death. *Ann Neurol*. 2003;53(4):454-68.
172. Ha M, Kim VN. Regulation of microRNA biogenesis. *Nat Rev Mol Cell Biol*. 2014;15(8):509-24.
173. Jonas S, Izaurralde E. Towards a molecular understanding of microRNA-mediated gene silencing. *Nat Rev Genet*. 2015;16(7):421-33.
174. Storz G. An expanding universe of noncoding RNAs. *Science*. 2002;296(5571):1260-3.
175. Fatica A, Bozzoni I. Long non-coding RNAs: new players in cell differentiation and development. *Nat Rev Genet*. 2014;15(1):7-21.
176. Batista PJ, Chang HY. Long noncoding RNAs: cellular address codes in development and disease. *Cell*. 2013;152(6):1298-307.
177. Sun X, Wong D. Long non-coding RNA-mediated regulation of glucose homeostasis and diabetes. *Am J Cardiovasc Dis*. 2016;6(2):17-25.
178. Rinn JL, Chang HY. Genome regulation by long noncoding RNAs. *Annu Rev Biochem*. 2012;81:145-66.
179. Cooper GM. *The Cell*. Washington, DC: ASM Press; 2003.
180. Wirta V. *Mining the transcriptome - methods and applications*. Stockholm: School of Biotechnology, Royal Institute of Technology; 2006.
181. Ruvkun G. Molecular biology. Glimpses of a tiny RNA world. *Science*. 2001;294(5543):797-9.
182. Bartel DP. MicroRNAs: target recognition and regulatory functions. *Cell*. 2009;136(2):215-33.
183. Huntzinger E, Izaurralde E. Gene silencing by microRNAs: contributions of translational repression and mRNA decay. *Nat Rev Genet*. 2011;12(2):99-110.

184. Ameres SL, Zamore PD. Diversifying microRNA sequence and function. *Nat Rev Mol Cell Biol.* 2013;14(8):475-88.
185. Kim VN, Han J, Siomi MC. Biogenesis of small RNAs in animals. *Nat Rev Mol Cell Biol.* 2009;10(2):126-39.
186. Krol J, Loedige I, Filipowicz W. The widespread regulation of microRNA biogenesis, function and decay. *Nat Rev Genet.* 2010;11(9):597-610.
187. Chiang HR, Schoenfeld LW, Ruby JG, Auyeung VC, Spies N, Baek D, et al. Mammalian microRNAs: experimental evaluation of novel and previously annotated genes. *Genes Dev.* 2010;24(10):992-1009.
188. Ozsolak F, Poling LL, Wang Z, Liu H, Liu XS, Roeder RG, et al. Chromatin structure analyses identify miRNA promoters. *Genes Dev.* 2008;22(22):3172-83.
189. Cai X, Hagedorn CH, Cullen BR. Human microRNAs are processed from capped, polyadenylated transcripts that can also function as mRNAs. *RNA.* 2004;10(12):1957-66.
190. Lee Y, Ahn C, Han J, Choi H, Kim J, Yim J, et al. The nuclear RNase III Drosha initiates microRNA processing. *Nature.* 2003;425(6956):415-9.
191. Lund E, Guttinger S, Calado A, Dahlberg JE, Kutay U. Nuclear export of microRNA precursors. *Science.* 2004;303(5654):95-8.
192. Ketting RF, Fischer SE, Bernstein E, Sijen T, Hannon GJ, Plasterk RH. Dicer functions in RNA interference and in synthesis of small RNA involved in developmental timing in *C. elegans*. *Genes Dev.* 2001;15(20):2654-9.
193. Park JE, Heo I, Tian Y, Simanshu DK, Chang H, Jee D, et al. Dicer recognizes the 5' end of RNA for efficient and accurate processing. *Nature.* 2011;475(7355):201-5.
194. Macrae IJ, Zhou K, Li F, Repic A, Brooks AN, Cande WZ, et al. Structural basis for double-stranded RNA processing by Dicer. *Science.* 2006;311(5758):195-8.
195. Yoda M, Kawamata T, Paroo Z, Ye X, Iwasaki S, Liu Q, et al. ATP-dependent human RISC assembly pathways. *Nat Struct Mol Biol.* 2010;17(1):17-23.
196. Hammond SM, Boettcher S, Caudy AA, Kobayashi R, Hannon GJ. Argonaute2, a link between genetic and biochemical analyses of RNAi. *Science.* 2001;293(5532):1146-50.
197. Kawamata T, Tomari Y. Making RISC. *Trends Biochem Sci.* 2010;35(7):368-76.
198. Song JJ, Smith SK, Hannon GJ, Joshua-Tor L. Crystal structure of Argonaute and its implications for RISC slicer activity. *Science.* 2004;305(5689):1434-7.

199. Parker JS, Roe SM, Barford D. Structural insights into mRNA recognition from a PIWI domain-siRNA guide complex. *Nature*. 2005;434(7033):663-6.
200. Forstemann K, Horwich MD, Wee L, Tomari Y, Zamore PD. Drosophila microRNAs are sorted into functionally distinct argonaute complexes after production by dicer-1. *Cell*. 2007;130(2):287-97.
201. Jannot G, Boisvert ME, Banville IH, Simard MJ. Two molecular features contribute to the Argonaute specificity for the microRNA and RNAi pathways in *C. elegans*. *RNA*. 2008;14(5):829-35.
202. Dueck A, Ziegler C, Eichner A, Berezikov E, Meister G. microRNAs associated with the different human Argonaute proteins. *Nucleic Acids Res*. 2012;40(19):9850-62.
203. Betancur JG, Tomari Y. Dicer is dispensable for asymmetric RISC loading in mammals. *RNA*. 2012;18(1):24-30.
204. Rand TA, Petersen S, Du F, Wang X. Argonaute2 cleaves the anti-guide strand of siRNA during RISC activation. *Cell*. 2005;123(4):621-9.
205. Liu Y, Ye X, Jiang F, Liang C, Chen D, Peng J, et al. C3PO, an endoribonuclease that promotes RNAi by facilitating RISC activation. *Science*. 2009;325(5941):750-3.
206. Ryan BM, Robles AI, Harris CC. Genetic variation in microRNA networks: the implications for cancer research. *Nat Rev Cancer*. 2010;10(6):389-402.
207. Nam Y, Chen C, Gregory RI, Chou JJ, Sliz P. Molecular basis for interaction of let-7 microRNAs with Lin28. *Cell*. 2011;147(5):1080-91.
208. Heo I, Joo C, Cho J, Ha M, Han J, Kim VN. Lin28 mediates the terminal uridylation of let-7 precursor MicroRNA. *Mol Cell*. 2008;32(2):276-84.
209. Heo I, Ha M, Lim J, Yoon MJ, Park JE, Kwon SC, et al. Mono-uridylation of pre-microRNA as a key step in the biogenesis of group II let-7 microRNAs. *Cell*. 2012;151(3):521-32.
210. Kawahara Y, Zinshteyn B, Chendrimada TP, Shiekhattar R, Nishikura K. RNA editing of the microRNA-151 precursor blocks cleavage by the Dicer-TRBP complex. *EMBO Rep*. 2007;8(8):763-9.
211. Xhemalce B, Robson SC, Kouzarides T. Human RNA methyltransferase BCDIN3D regulates microRNA processing. *Cell*. 2012;151(2):278-88.
212. Elkayam E, Kuhn CD, Tocilj A, Haase AD, Greene EM, Hannon GJ, et al. The structure of human argonaute-2 in complex with miR-20a. *Cell*. 2012;150(1):100-10.
213. Schirle NT, MacRae IJ. The crystal structure of human Argonaute2. *Science*. 2012;336(6084):1037-40.

214. Suzuki HI, Arase M, Matsuyama H, Choi YL, Ueno T, Mano H, et al. MCPIP1 ribonuclease antagonizes dicer and terminates microRNA biogenesis through precursor microRNA degradation. *Mol Cell*. 2011;44(3):424-36.
215. Upton JP, Wang L, Han D, Wang ES, Huskey NE, Lim L, et al. IRE1alpha cleaves select microRNAs during ER stress to derepress translation of proapoptotic Caspase-2. *Science*. 2012;338(6108):818-22.
216. Das SK, Sokhi UK, Bhutia SK, Azab B, Su ZZ, Sarkar D, et al. Human polynucleotide phosphorylase selectively and preferentially degrades microRNA-221 in human melanoma cells. *Proc Natl Acad Sci U S A*. 2010;107(26):11948-53.
217. Ruegger S, Grosshans H. MicroRNA turnover: when, how, and why. *Trends Biochem Sci*. 2012;37(10):436-46.
218. Cazalla D, Yario T, Steitz JA. Down-regulation of a host microRNA by a Herpesvirus saimiri noncoding RNA. *Science*. 2010;328(5985):1563-6.
219. Desvignes T, Batzel P, Berezikov E, Eilbeck K, Eppig JT, McAndrews MS, et al. miRNA Nomenclature: A View Incorporating Genetic Origins, Biosynthetic Pathways, and Sequence Variants. *Trends Genet*. 2015;31(11):613-26.
220. Okamura K, Hagen JW, Duan H, Tyler DM, Lai EC. The mirtron pathway generates microRNA-class regulatory RNAs in *Drosophila*. *Cell*. 2007;130(1):89-100.
221. Ruby JG, Jan CH, Bartel DP. Intronic microRNA precursors that bypass Drosha processing. *Nature*. 2007;448(7149):83-6.
222. Xie M, Li M, Vilborg A, Lee N, Shu MD, Yartseva V, et al. Mammalian 5'-capped microRNA precursors that generate a single microRNA. *Cell*. 2013;155(7):1568-80.
223. Ender C, Krek A, Friedlander MR, Beitzinger M, Weinmann L, Chen W, et al. A human snoRNA with microRNA-like functions. *Mol Cell*. 2008;32(4):519-28.
224. Yang JS, Maurin T, Robine N, Rasmussen KD, Jeffrey KL, Chandwani R, et al. Conserved vertebrate mir-451 provides a platform for Dicer-independent, Ago2-mediated microRNA biogenesis. *Proc Natl Acad Sci U S A*. 2010;107(34):15163-8.
225. Yoda M, Cifuentes D, Izumi N, Sakaguchi Y, Suzuki T, Giraldez AJ, et al. Poly(A)-specific ribonuclease mediates 3'-end trimming of Argonaute2-cleaved precursor microRNAs. *Cell Rep*. 2013;5(3):715-26.
226. Bak M, Silahdaroglu A, Moller M, Christensen M, Rath MF, Skryabin B, et al. MicroRNA expression in the adult mouse central nervous system. *RNA*. 2008;14(3):432-44.

227. Yunta M, Nieto-Diaz M, Esteban FJ, Caballero-Lopez M, Navarro-Ruiz R, Reigada D, et al. MicroRNA dysregulation in the spinal cord following traumatic injury. *PLoS One*. 2012;7(4):e34534.
228. Smirnova L, Grafe A, Seiler A, Schumacher S, Nitsch R, Wulczyn FG. Regulation of miRNA expression during neural cell specification. *Eur J Neurosci*. 2005;21(6):1469-77.
229. Zhao X, He X, Han X, Yu Y, Ye F, Chen Y, et al. MicroRNA-mediated control of oligodendrocyte differentiation. *Neuron*. 2010;65(5):612-26.
230. Ruan W, Ning G, Feng S, Gao S, Hao Y. MicroRNA381/Hes1 is a potential therapeutic target for spinal cord injury. *Int J Mol Med*. 2018;42(2):1008-17.
231. Krichevsky AM. MicroRNA profiling: from dark matter to white matter, or identifying new players in neurobiology. *ScientificWorldJournal*. 2007;7:155-66.
232. Saugstad JA. MicroRNAs as effectors of brain function with roles in ischemia and injury, neuroprotection, and neurodegeneration. *J Cereb Blood Flow Metab*. 2010;30(9):1564-76.
233. Kosik KS. The neuronal microRNA system. *Nat Rev Neurosci*. 2006;7(12):911-20.
234. Meza-Sosa KF, Valle-Garcia D, Pedraza-Alva G, Perez-Martinez L. Role of microRNAs in central nervous system development and pathology. *J Neurosci Res*. 2012;90(1):1-12.
235. Li F, Zhou MW. MicroRNAs in contusion spinal cord injury: pathophysiology and clinical utility. *Acta Neurol Belg*. 2019;119(1):21-7.
236. Martirosyan NL, Carotenuto A, Patel AA, Kalani MY, Yagmurlu K, Lemole GM, Jr., et al. The Role of microRNA Markers in the Diagnosis, Treatment, and Outcome Prediction of Spinal Cord Injury. *Front Surg*. 2016;3:56.
237. Strickland ER, Hook MA, Balaraman S, Huie JR, Grau JW, Miranda RC. MicroRNA dysregulation following spinal cord contusion: implications for neural plasticity and repair. *Neuroscience*. 2011;186:146-60.
238. Ning B, Gao L, Liu RH, Liu Y, Zhang NS, Chen ZY. microRNAs in spinal cord injury: potential roles and therapeutic implications. *Int J Biol Sci*. 2014;10(9):997-1006.
239. Dong J, Lu M, He X, Xu J, Qin J, Cheng Z, et al. Identifying the role of microRNAs in spinal cord injury. *Neurol Sci*. 2014;35(11):1663-71.
240. Fu X, Shen Y, Wang W, Li X. MiR-30a-5p ameliorates spinal cord injury-induced inflammatory responses and oxidative stress by targeting Neurod 1 through MAPK/ERK signalling. *Clin Exp Pharmacol Physiol*. 2018;45(1):68-74.

241. Xu Y, An BY, Xi XB, Li ZW, Li FY. MicroRNA-9 controls apoptosis of neurons by targeting monocyte chemoattractant protein-1 expression in rat acute spinal cord injury model. *Brain Res Bull.* 2016;121:233-40.
242. Liu D, Huang Y, Jia C, Li Y, Liang F, Fu Q. Administration of antagomir-223 inhibits apoptosis, promotes angiogenesis and functional recovery in rats with spinal cord injury. *Cell Mol Neurobiol.* 2015;35(4):483-91.
243. Liu S, Ren C, Qu X, Wu X, Dong F, Chand YK, et al. miR-219 attenuates demyelination in cuprizone-induced demyelinated mice by regulating monocarboxylate transporter 1. *Eur J Neurosci.* 2017;45(2):249-59.
244. Shin D, Shin JY, McManus MT, Ptacek LJ, Fu YH. Dicer ablation in oligodendrocytes provokes neuronal impairment in mice. *Ann Neurol.* 2009;66(6):843-57.
245. Scholz J, Woolf CJ. The neuropathic pain triad: neurons, immune cells and glia. *Nat Neurosci.* 2007;10(11):1361-8.
246. Wang Y, Ye F, Huang C, Xue F, Li Y, Gao S, et al. Bioinformatic Analysis of Potential Biomarkers for Spinal Cord-injured Patients with Intractable Neuropathic Pain. *Clin J Pain.* 2018;34(9):825-30.
247. Tigchelaar S, Gupta R, Shannon CP, Streijger F, Sinha S, Flibotte S, et al. MicroRNA Biomarkers in Cerebrospinal Fluid and Serum Reflect Injury Severity in Human Acute Traumatic Spinal Cord Injury. *J Neurotrauma.* 2019.
248. Tigchelaar S, Streijger F, Sinha S, Flibotte S, Manouchehri N, So K, et al. Serum MicroRNAs Reflect Injury Severity in a Large Animal Model of Thoracic Spinal Cord Injury. *Sci Rep.* 2017;7(1):1376.
249. Shao Y, Chen Y. Roles of Circular RNAs in Neurologic Disease. *Front Mol Neurosci.* 2016;9:25.
250. Wang K. The Ubiquitous Existence of MicroRNA in Body Fluids. *Clin Chem.* 2017;63(3):784-5.
251. Chakraborty C, Sharma AR, Sharma G, Lee SS. Therapeutic advances of miRNAs: A preclinical and clinical update. *J Adv Res.* 2021;28:127-38.
252. Fiore R, Siegel G, Schratt G. MicroRNA function in neuronal development, plasticity and disease. *Biochim Biophys Acta.* 2008;1779(8):471-8.
253. Hutchison ER, Okun E, Mattson MP. The therapeutic potential of microRNAs in nervous system damage, degeneration, and repair. *Neuromolecular Med.* 2009;11(3):153-61.

254. Behjati S, Tarpey PS. What is next generation sequencing? *Arch Dis Child Educ Pract Ed.* 2013;98(6):236-8.
255. Lacroix S, Hamilton LK, Vaugeois A, Beaudoin S, Breault-Dugas C, Pineau I, et al. Central canal ependymal cells proliferate extensively in response to traumatic spinal cord injury but not demyelinating lesions. *PLoS One.* 2014;9(1):e85916.
256. Orr MB, Simkin J, Bailey WM, Kadambi NS, McVicar AL, Veldhorst AK, et al. Compression Decreases Anatomical and Functional Recovery and Alters Inflammation after Contusive Spinal Cord Injury. *J Neurotrauma.* 2017;34(15):2342-52.
257. Squair JW, Ruiz I, Phillips AA, Zheng MMZ, Sarafis ZK, Sachdeva R, et al. Minocycline Reduces the Severity of Autonomic Dysreflexia after Experimental Spinal Cord Injury. *J Neurotrauma.* 2018;35(24):2861-71.
258. Teng YD, Choi H, Onario RC, Zhu S, Desilets FC, Lan S, et al. Minocycline inhibits contusion-triggered mitochondrial cytochrome c release and mitigates functional deficits after spinal cord injury. *Proc Natl Acad Sci U S A.* 2004;101(9):3071-6.
259. Taylor SC, Nadeau K, Abbasi M, Lachance C, Nguyen M, Fenrich J. The Ultimate qPCR Experiment: Producing Publication Quality, Reproducible Data the First Time. *Trends Biotechnol.* 2019;37(7):761-74.
260. New-England-Biolabs. Protocol for use with NEBNext Small RNA Library Prep Set for Illumina (E7300, E7580, E7560, E7330) Canada 2019 [Available from: https://www.neb.ca/neb_protocols.php?p=protocols/2018/03/27/protocol-for-use-with-nebnext-small-rna-library-prep-set-for-illumina-e7300-e7580-e7560-e7330].
261. Kozomara A, Griffiths-Jones S. miRBase: annotating high confidence microRNAs using deep sequencing data. *Nucleic Acids Res.* 2014;42(Database issue):D68-73.
262. Barturen G, Rueda A, Hamberg M, Alganza A, Lebron R, Kotsyfakis M, et al. sRNAbench: profiling of small RNAs and its sequence variants in single or multi-species high-throughput experiments. *Methods Next-Generation Seq.* 2014;1:21-31.
263. Friedlander MR, Mackowiak SD, Li N, Chen W, Rajewsky N. miRDeep2 accurately identifies known and hundreds of novel microRNA genes in seven animal clades. *Nucleic Acids Res.* 2012;40(1):37-52.
264. Babraham Bioinformatics. [Available from: <http://www.bioinformatics.babraham.ac.uk>].
265. Love MI, Huber W, Anders S. Moderated estimation of fold change and dispersion for RNA-seq data with DESeq2. *Genome Biol.* 2014;15(12):550.
266. Kozomara A, Birgaoanu M, Griffiths-Jones S. miRBase: from microRNA sequences to function. *Nucleic Acids Res.* 2019;47(D1):D155-D62.

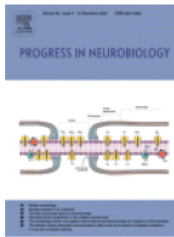
267. Liu W, Wang X. Prediction of functional microRNA targets by integrative modeling of microRNA binding and target expression data. *Genome Biol.* 2019;20(1):18.
268. Agarwal V, Bell GW, Nam JW, Bartel DP. Predicting effective microRNA target sites in mammalian mRNAs. *Elife.* 2015;4.
269. Juzwik CA, Drake S, Lecuyer MA, Johnson RM, Morquette B, Zhang Y, et al. Neuronal microRNA regulation in Experimental Autoimmune Encephalomyelitis. *Sci Rep.* 2018;8(1):13437.
270. Sperveslage J, Hoffmeister M, Henopp T, Kloppel G, Sipos B. Establishment of robust controls for the normalization of miRNA expression in neuroendocrine tumors of the ileum and pancreas. *Endocrine.* 2014;46(2):226-30.
271. Kumar V, Kumar V, Chaudhary AK, Coulter DW, McGuire T, Mahato RI. Impact of miRNA-mRNA Profiling and Their Correlation on Medulloblastoma Tumorigenesis. *Mol Ther Nucleic Acids.* 2018;12:490-503.
272. Shen J, Wang Q, Gurvich I, Remotti H, Santella RM. Evaluating normalization approaches for the better identification of aberrant microRNAs associated with hepatocellular carcinoma. *Hepatoma Res.* 2016;2:305-15.
273. Tigchelaar S, Gupta R, Shannon CP, Streijger F, Sinha S, Flibotte S, et al. MicroRNA Biomarkers in Cerebrospinal Fluid and Serum Reflect Injury Severity in Human Acute Traumatic Spinal Cord Injury. *J Neurotrauma.* 2019;36(15):2358-71.
274. Huang da W, Sherman BT, Lempicki RA. Systematic and integrative analysis of large gene lists using DAVID bioinformatics resources. *Nat Protoc.* 2009;4(1):44-57.
275. Huang da W, Sherman BT, Lempicki RA. Bioinformatics enrichment tools: paths toward the comprehensive functional analysis of large gene lists. *Nucleic Acids Res.* 2009;37(1):1-13.
276. Hu J, Ni S, Cao Y, Zhang T, Wu T, Yin X, et al. The Angiogenic Effect of microRNA-21 Targeting TIMP3 through the Regulation of MMP2 and MMP9. *PLoS One.* 2016;11(2):e0149537.
277. Kanekura K, Hashimoto Y, Kita Y, Sasabe J, Aiso S, Nishimoto I, et al. A Rac1/phosphatidylinositol 3-kinase/Akt3 anti-apoptotic pathway, triggered by AlsinLF, the product of the ALS2 gene, antagonizes Cu/Zn-superoxide dismutase (SOD1) mutant-induced motoneuronal cell death. *J Biol Chem.* 2005;280(6):4532-43.
278. Franke TF, Kaplan DR, Cantley LC. PI3K: downstream AKTion blocks apoptosis. *Cell.* 1997;88(4):435-7.
279. Sagot Y, Dubois-Dauphin M, Tan SA, de Bilbao F, Aebischer P, Martinou JC, et al. Bcl-2 overexpression prevents motoneuron cell body loss but not axonal degeneration in a mouse model of a neurodegenerative disease. *J Neurosci.* 1995;15(11):7727-33.

280. Schmued LC, Stowers CC, Scallet AC, Xu L. Fluoro-Jade C results in ultra high resolution and contrast labeling of degenerating neurons. *Brain Res.* 2005;1035(1):24-31.
281. Bian GL, Wei LC, Shi M, Wang YQ, Cao R, Chen LW. Fluoro-Jade C can specifically stain the degenerative neurons in the substantia nigra of the 1-methyl-4-phenyl-1,2,3,6-tetrahydro pyridine-treated C57BL/6 mice. *Brain Res.* 2007;1150:55-61.
282. Saadoun S, Bell BA, Verkman AS, Papadopoulos MC. Greatly improved neurological outcome after spinal cord compression injury in AQP4-deficient mice. *Brain.* 2008;131(Pt 4):1087-98.
283. Ehara A, Ueda S. Application of Fluoro-Jade C in acute and chronic neurodegeneration models: utilities and staining differences. *Acta Histochem Cytochem.* 2009;42(6):171-9.
284. Crowley LC, Marfell BJ, Waterhouse NJ. Analyzing Cell Death by Nuclear Staining with Hoechst 33342. *Cold Spring Harb Protoc.* 2016;2016(9).
285. Gutierrez IL, Gonzalez-Prieto M, Garcia-Bueno B, Caso JR, Leza JC, Madrigal JLM. Alternative Method to Detect Neuronal Degeneration and Amyloid beta Accumulation in Free-Floating Brain Sections With Fluoro-Jade. *ASN Neuro.* 2018;10:1759091418784357.
286. Chen LW, Wang YQ, Bian GL, Wei LC, Yung KL. Neurokinin-3 peptide instead of neurokinin-1 synergistically exacerbates kainic acid-inducing degeneration of neurons in the substantia nigra of mice. *J Neurochem.* 2008;105(1):203-16.
287. Xiao W, Wen J, Huang YC, Yu BS. Development of a modified model of spinal cord ischemia injury by selective ligation of lumbar arteries in rabbits. *Spinal Cord.* 2017;55(11):1028-32.
288. Puls B, Ding Y, Zhang F, Pan M, Lei Z, Pei Z, et al. Regeneration of Functional Neurons After Spinal Cord Injury via in situ NeuroD1-Mediated Astrocyte-to-Neuron Conversion. *Front Cell Dev Biol.* 2020;8:591883.
289. Bushong EA, Martone ME, Jones YZ, Ellisman MH. Protoplasmic astrocytes in CA1 stratum radiatum occupy separate anatomical domains. *J Neurosci.* 2002;22(1):183-92.
290. Zhu LP, Zhou JP, Zhang JX, Wang JY, Wang ZY, Pan M, et al. MiR-15b-5p Regulates Collateral Artery Formation by Targeting AKT3 (Protein Kinase B-3). *Arterioscler Thromb Vasc Biol.* 2017;37(5):957-68.
291. Nakanishi K, Nakasa T, Tanaka N, Ishikawa M, Yamada K, Yamasaki K, et al. Responses of microRNAs 124a and 223 following spinal cord injury in mice. *Spinal Cord.* 2010;48(3):192-6.

292. Hu JR, Lv GH, Yin BL. Altered microRNA expression in the ischemic-reperfusion spinal cord with atorvastatin therapy. *J Pharmacol Sci.* 2013;121(4):343-6.
293. Hu JZ, Huang JH, Zeng L, Wang G, Cao M, Lu HB. Anti-apoptotic effect of microRNA-21 after contusion spinal cord injury in rats. *J Neurotrauma.* 2013;30(15):1349-60.
294. Jee MK, Jung JS, Choi JI, Jang JA, Kang KS, Im YB, et al. MicroRNA 486 is a potentially novel target for the treatment of spinal cord injury. *Brain.* 2012;135(Pt 4):1237-52.
295. Jee MK, Jung JS, Im YB, Jung SJ, Kang SK. Silencing of miR20a is crucial for Ngn1-mediated neuroprotection in injured spinal cord. *Hum Gene Ther.* 2012;23(5):508-20.
296. Im YB, Jee MK, Choi JI, Cho HT, Kwon OH, Kang SK. Molecular targeting of NOX4 for neuropathic pain after traumatic injury of the spinal cord. *Cell Death Dis.* 2012;3:e426.
297. Jiang Y, Zhao S, Ding Y, Nong L, Li H, Gao G, et al. MicroRNA21 promotes neurite outgrowth by regulating PDCD4 in a rat model of spinal cord injury. *Mol Med Rep.* 2017;16(3):2522-8.
298. Wang W, Liu R, Su Y, Li H, Xie W, Ning B. MicroRNA-21-5p mediates TGF-beta-regulated fibrogenic activation of spinal fibroblasts and the formation of fibrotic scars after spinal cord injury. *Int J Biol Sci.* 2018;14(2):178-88.
299. Xie W, Yang SY, Zhang Q, Zhou Y, Wang Y, Liu R, et al. Knockdown of MicroRNA-21 Promotes Neurological Recovery After Acute Spinal Cord Injury. *Neurochem Res.* 2018;43(8):1641-9.
300. Ning SL, Zhu H, Shao J, Liu YC, Lan J, Miao J. MiR-21 inhibitor improves locomotor function recovery by inhibiting IL-6R/JAK-STAT pathway-mediated inflammation after spinal cord injury in model of rat. *Eur Rev Med Pharmacol Sci.* 2019;23(2):433-40.
301. Mohammed AZ, Du HX, Song HL, Gong WM, Ning B, Jia TH. Comparative proteomes change and possible role in different pathways of microRNA-21a-5p in a mouse model of spinal cord injury. *Neural Regen Res.* 2020;15(6):1102-10.
302. Wu B, Liu G, Jin Y, Yang T, Zhang D, Ding L, et al. miR-15b-5p Promotes Growth and Metastasis in Breast Cancer by Targeting HPSE2. *Front Oncol.* 2020;10:108.
303. Lovat F, Fassan M, Gasparini P, Rizzotto L, Cascione L, Pizzi M, et al. miR-15b/16-2 deletion promotes B-cell malignancies. *Proc Natl Acad Sci U S A.* 2015;112(37):11636-41.

APPENDIX A: COPYRIGHT AGREEMENT LETTER

The permission letter was obtained to use modified figure 1.1



From basics to clinical: A comprehensive review on spinal cord injury

Author: Nuno A. Silva, Nuno Sousa, Rui L. Reis, António J. Salgado

Publication: Progress in Neurobiology

Publisher: Elsevier

Date: March 2014

Copyright © 2013 Elsevier Ltd. All rights reserved.

License Number 5176210625991

[Printable Details](#)

License date Oct 25, 2021

Licensed Content

| | |
|------------------------------|---|
| Licensed Content Publisher | Elsevier |
| Licensed Content Publication | Progress in Neurobiology |
| Licensed Content Title | From basics to clinical: A comprehensive review on spinal cord injury |
| Licensed Content Author | Nuno A. Silva, Nuno Sousa, Rui L. Reis, António J. Salgado |
| Licensed Content Date | Mar 1, 2014 |
| Licensed Content Volume | 114 |
| Licensed Content Issue | n/a |
| Licensed Content Pages | 33 |

Order Details

| | |
|--|--------------------------------|
| Type of Use | reuse in a thesis/dissertation |
| Portion | figures/tables/illustrations |
| Number of figures/tables/illustrations | 2 |
| Format | both print and electronic |
| Are you the author of this Elsevier article? | No |
| Will you be translating? | No |

APPENDIX B: SUPPLEMENTARY FIGURES AND TABLES OF CHAPTER 2

Figure B1. Surgical room set up.

This figure illustrates the major elements of the surgical theatre for animal surgery to produce SCI model. The microscope is essential to perform laminectomy and avoid inadvertent SC injury to minimize the confounding factors. Heat is of paramount significance as the small animal can lose their temperature quickly and this can influence their gene expression and may increase their mortality. The position of the impactor should be as close to the surgical area to keep the connection with the anesthesia machine during the injury. *Nadi, 2019.*

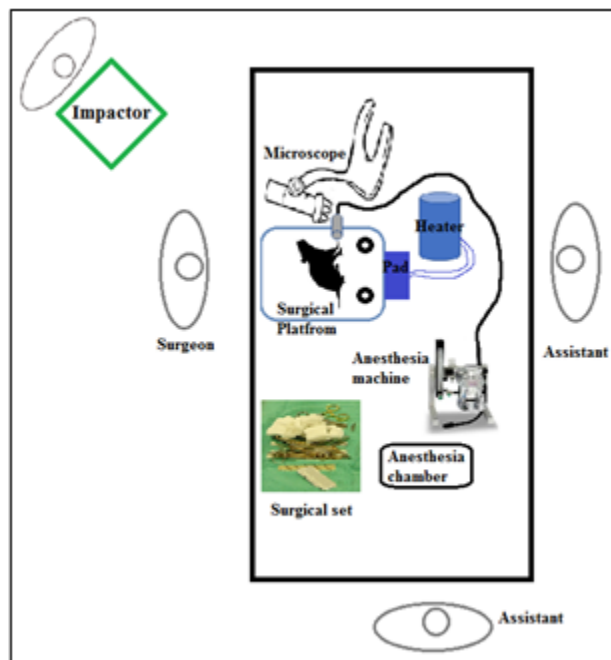


Figure B2. PCA-1 vs PCA2 of miRNA expression of three experimental conditions in the 7d group.

PCA1 vs PCA2 of miRNA expression in the 7d SCI group including three experimental conditions: SCI+SLN in the 7d group = D7C#, SCI+mino in the 7d group = D7R#, and Sham, no SCI, only laminectomy = S, baseline from the 1d group. This figure demonstrates that there was no relationship of miRNA expression among the three conditions when we compared PCA1 (principal component analysis) and PCA2. The three experimental conditions cannot really be segregated into distinctive groups.

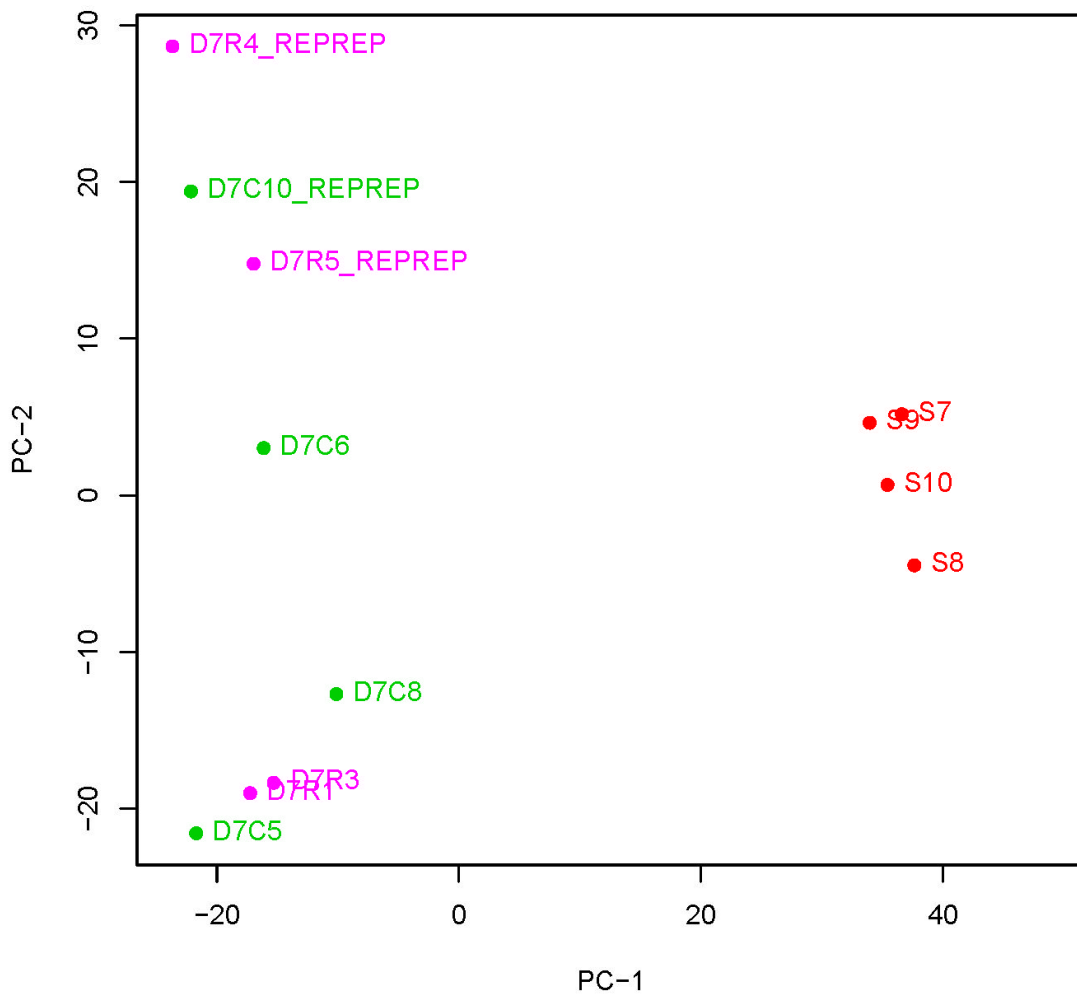


Figure B3. PCA2 vs PCA3 of miRNA expression of three experimental conditions in the 7d group.

PCA2 vs PCA3 of miRNA expression in the 7d SCI group including three experimental conditions: SCI+SLN in the 7d group = D7C#, SCI+mino in the 7d group = D7R#, and Sham, no SCI, only laminectomy = S, baseline from the 1d group. This figure shows that there was no relationship of miRNA expression amongst the three conditions when we compared PCA2 and PCA3. The three experimental conditions cannot really be segregated.

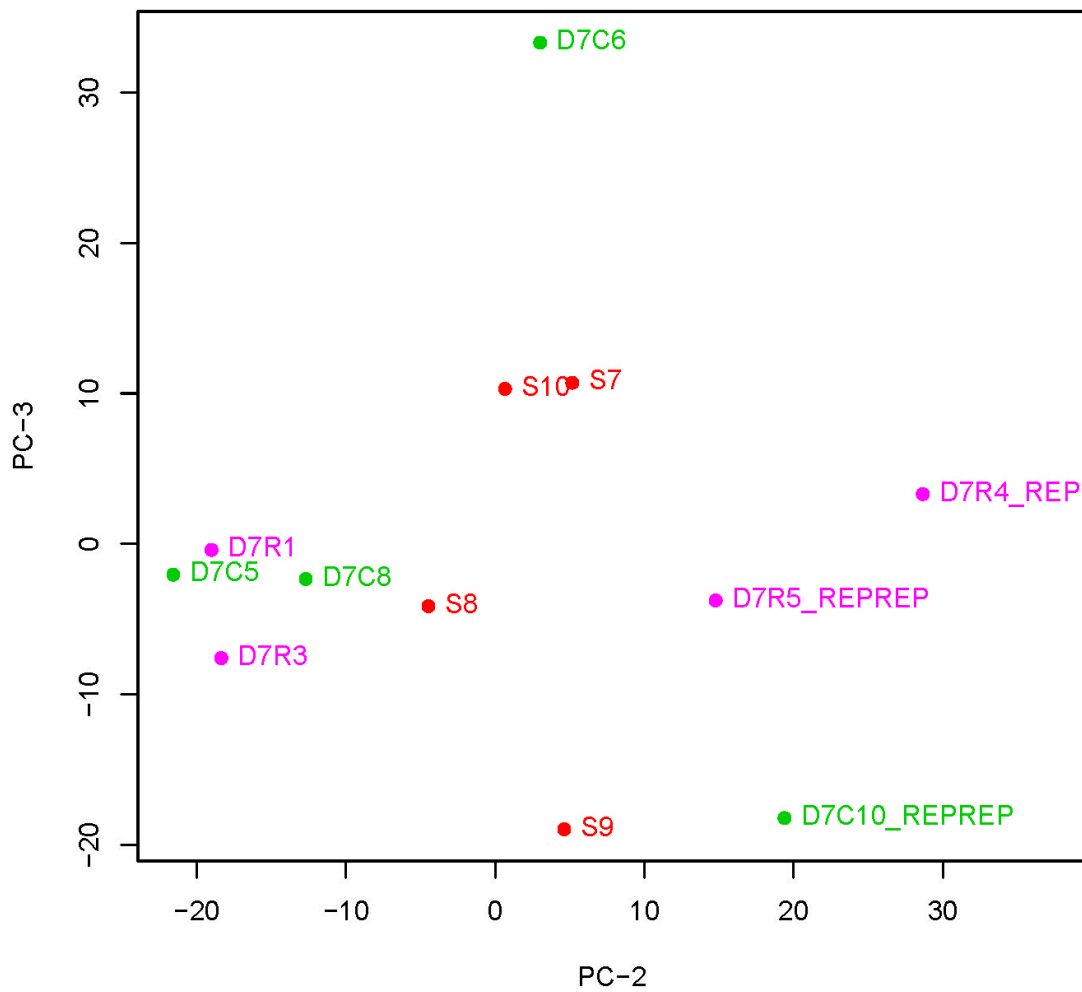


Figure B4. PCA3 vs PCA4 of miRNA expression of three experimental conditions in the 7d group.

PCA3 vs PCA4 of miRNA expression in the 7d SCI group including three experimental conditions: SCI+SLN in the 7d group = D7C#, SCI+mino in the 7d group = D7R#, and Sham, no SCI, only laminectomy = S, baseline from the 1d group. This figure shows that there was no relationship of miRNA expression amongst the three conditions when we compared PCA3 and PCA4.

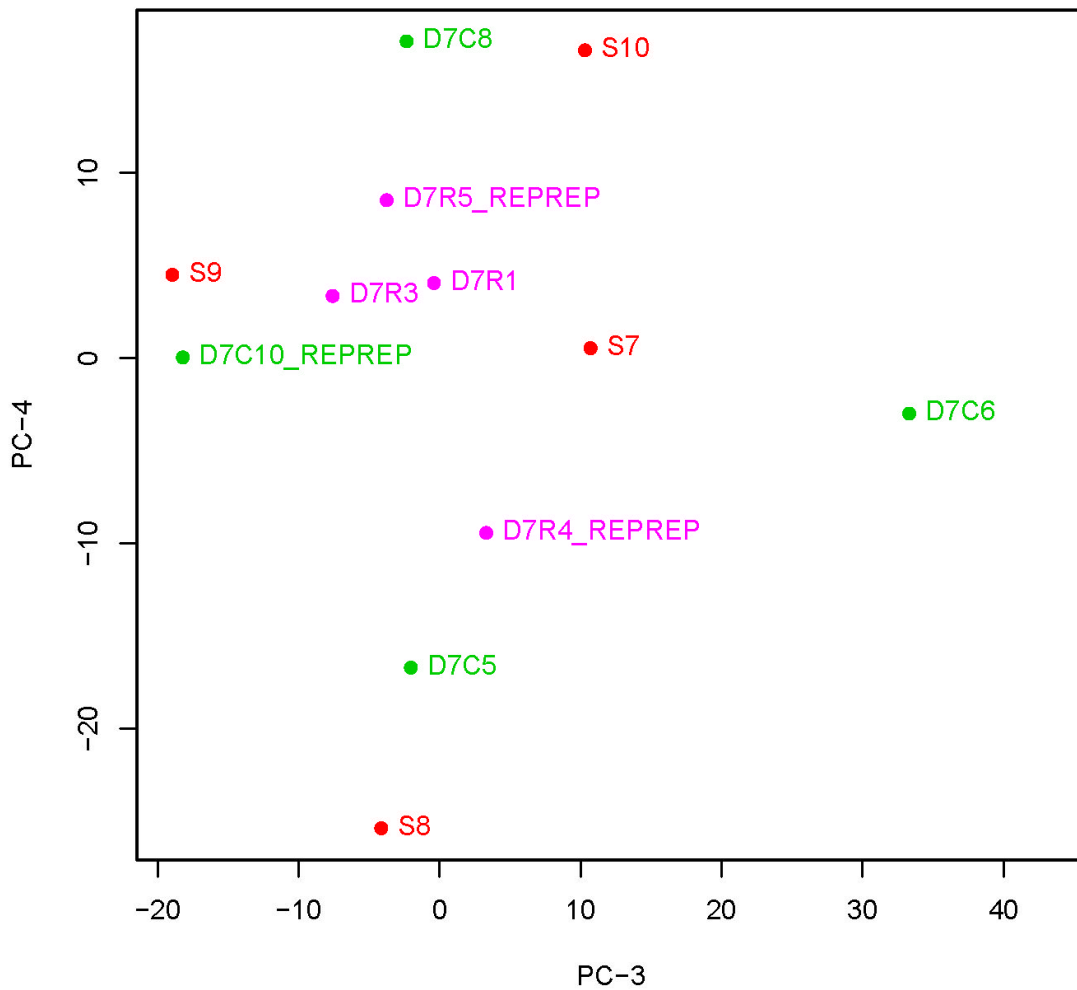


Figure B5. PCA1 vs PCA2 of miRNA expression of two experimental conditions in the 7d group.

PCA1 vs PCA2 of miRNA expression in the 7d SCI group including two experimental conditions: SCI+SLN in the 7d group = D7C#, SCI+mino in the 7d group = D7R#. This figure illustrates that there was no relationship of miRNA expression between the two conditions.

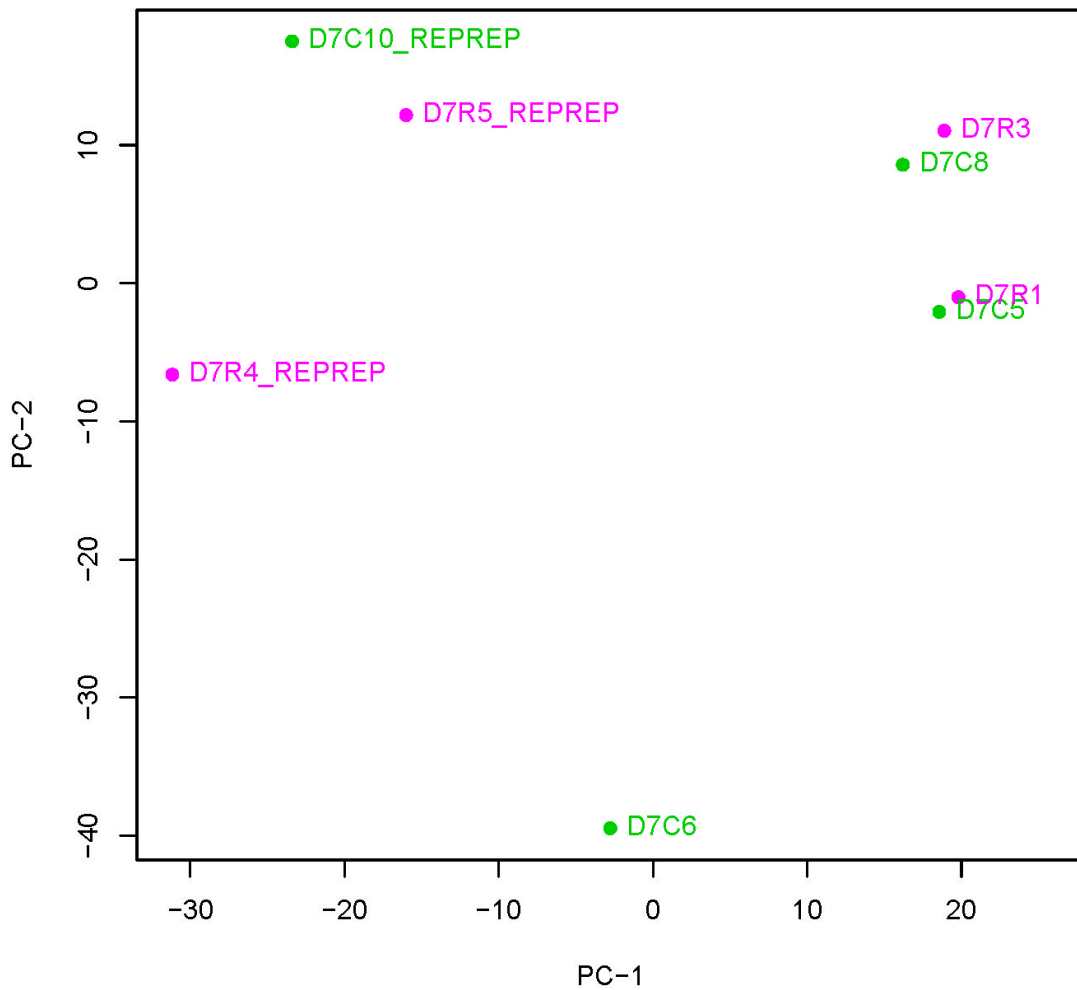


Figure B6. PCA2 vs PCA3 of miRNA expression of two experimental conditions in the 7d group.

PCA2 vs PCA3 of miRNA expression in the 7d SCI group including two experimental conditions: SCI+SLN in the 7d group = D7C#, SCI+mino in the 7d group = D7R#. This figure explains that there was no relationship of miRNA expression between the two conditions.

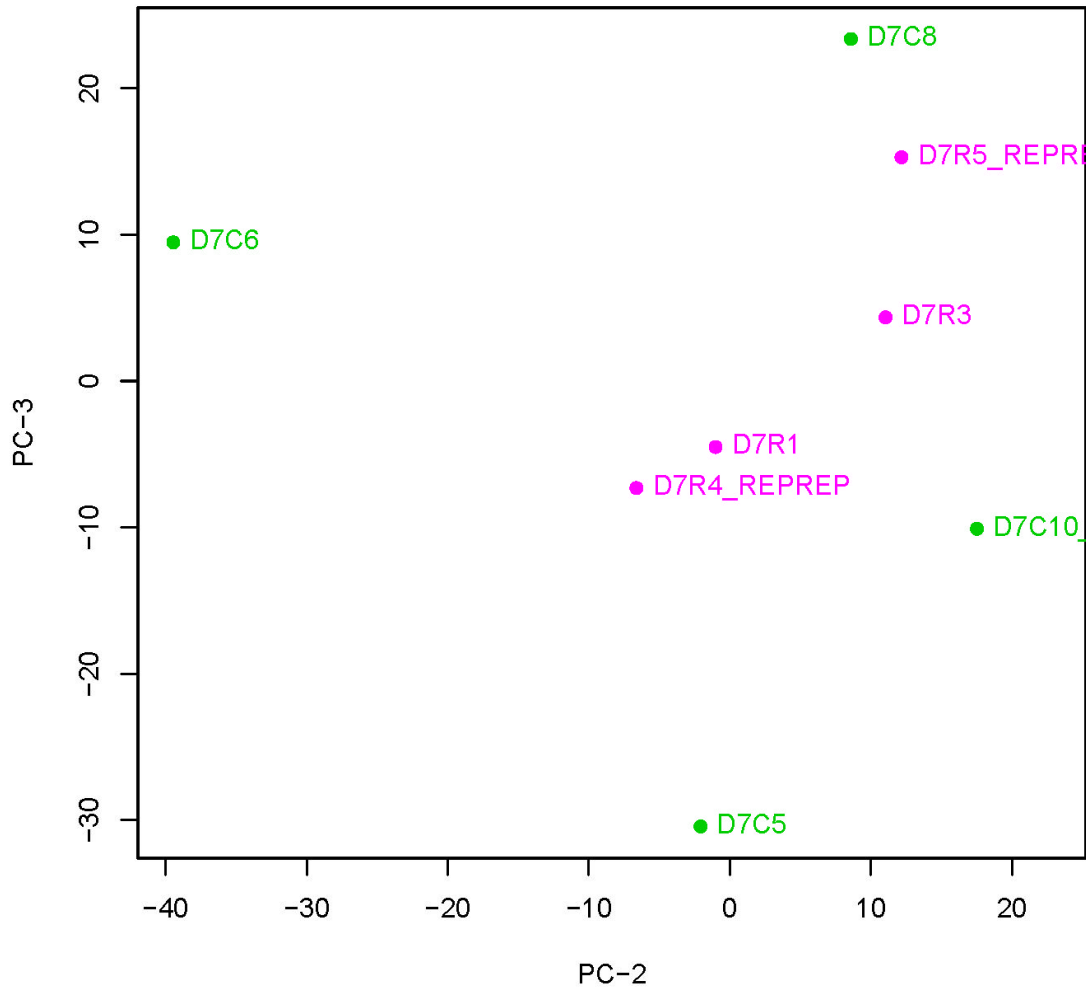


Figure B7. Heatmap: no SCI vs SCI+SLN 1d demonstrating the changes of miRNAs after one day of SCI.

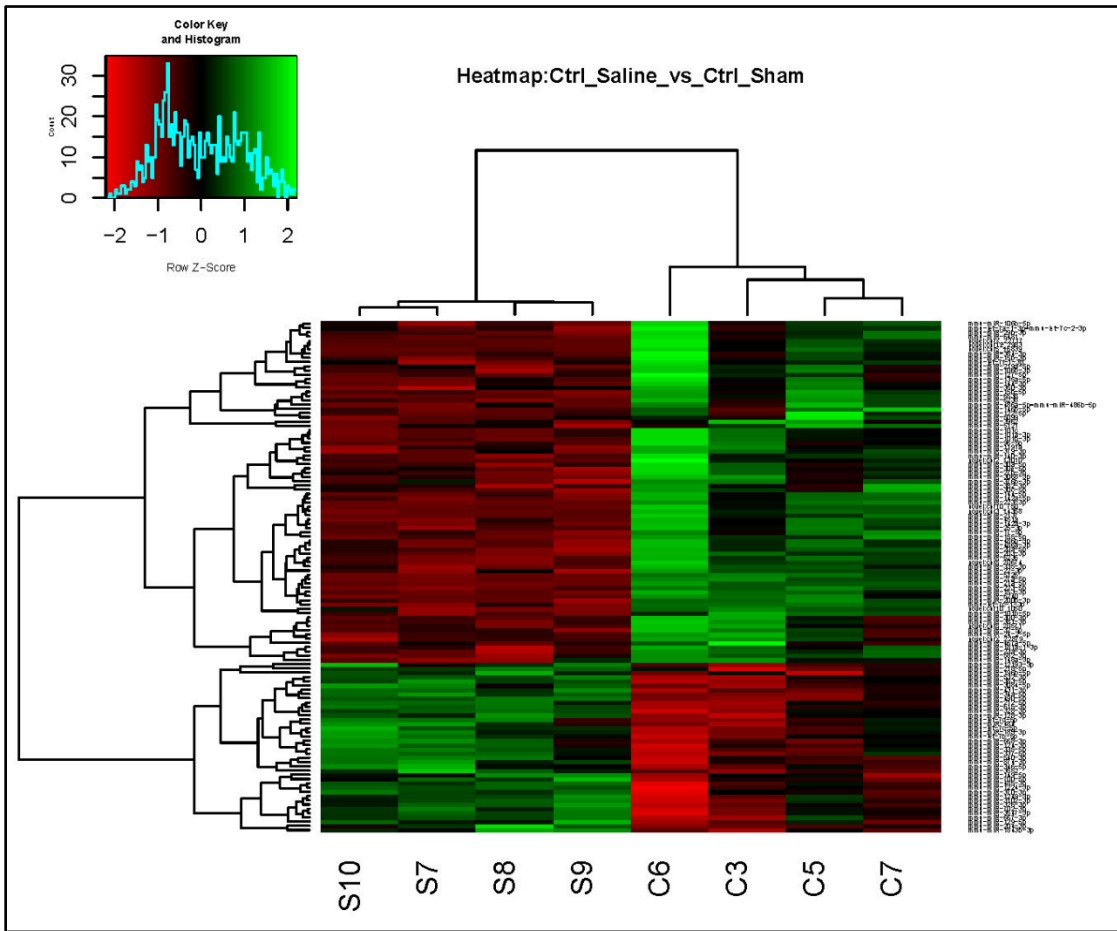


Figure B9. Heatmap: SCI+mino vs noSCI 1d demonstrates the miRNA pattern changes following minocycline administration in comparison to no SCI condition after 1d of SCI.

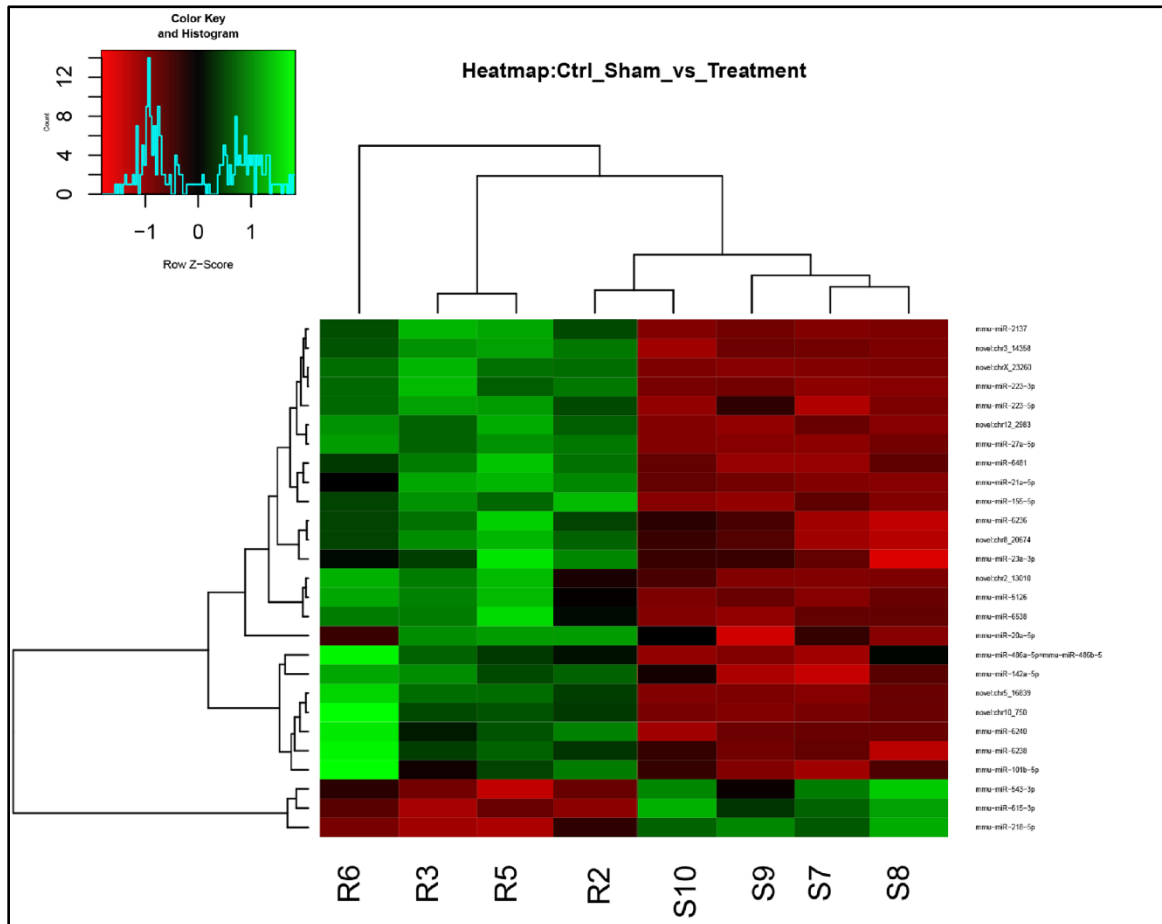


Figure B10. Heatmap: SCI+SLN vs SCI+mino 7d demonstrates the changes of miRNA expression following minocycline administration and SCI (treatment) in comparison to SCI+ saline (control) tested 7 days after SCI.

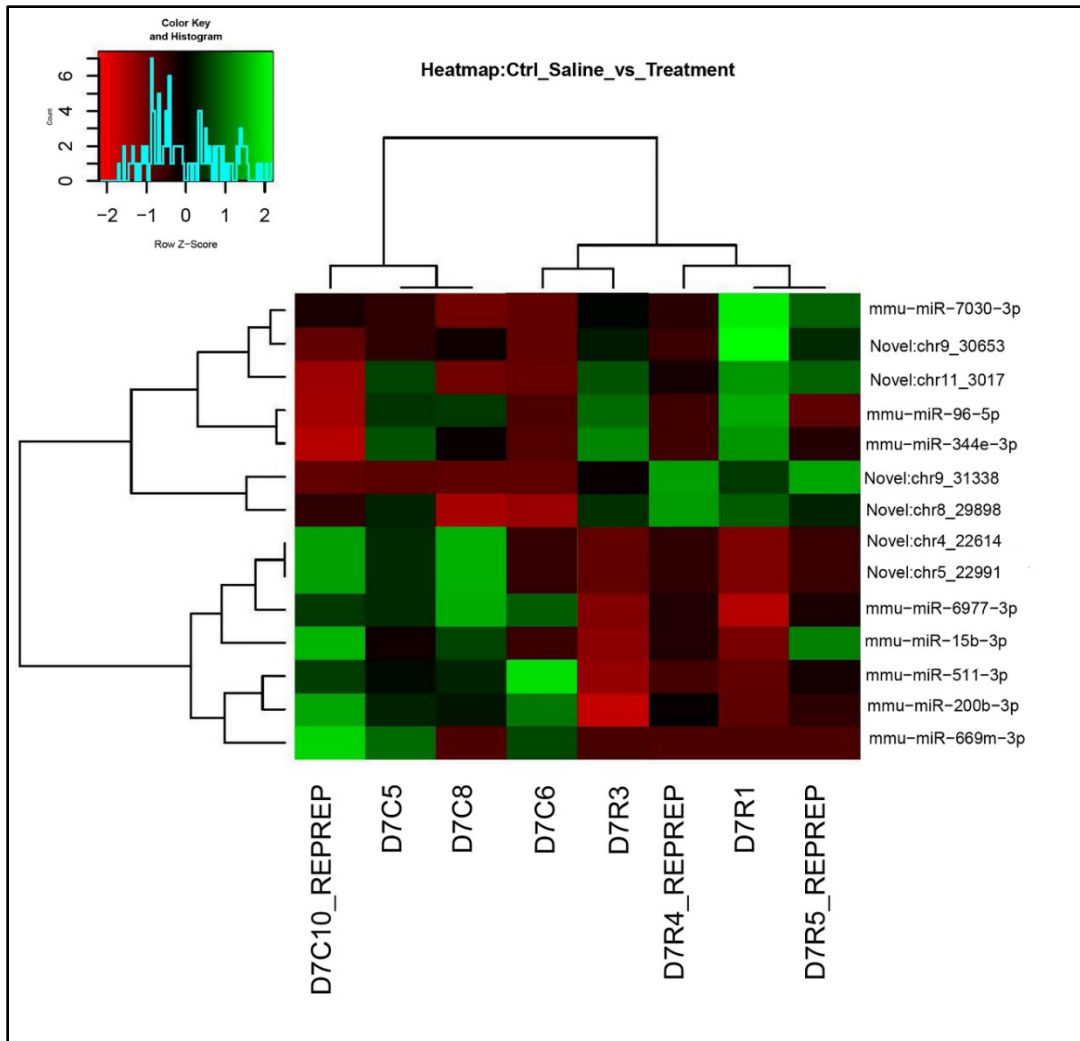


Figure B11. Efficiency curve in the 1d group RT-qPCR validation experiments.

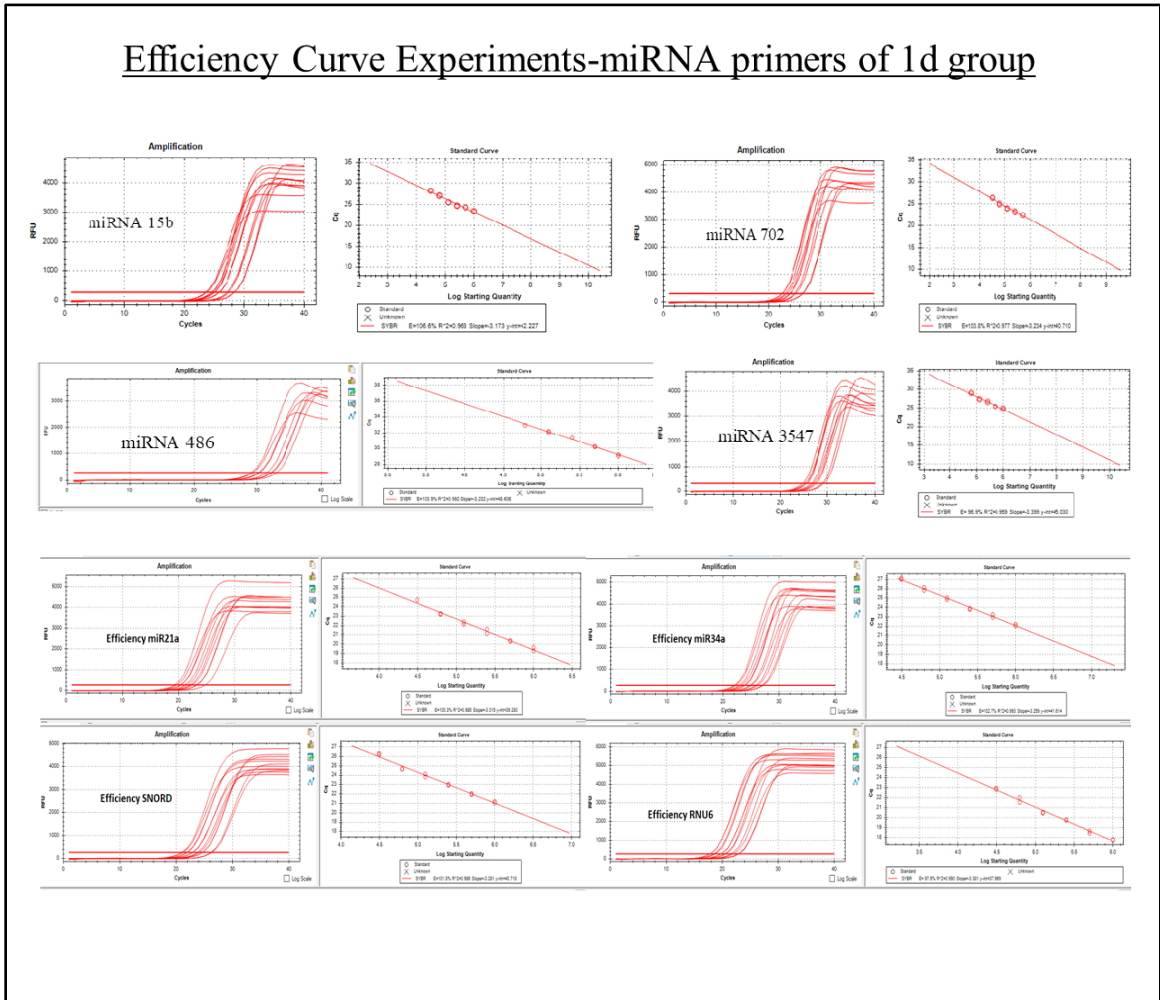


Figure B12. Efficiency curve in the 7d group RT-qPCR validation experiments.

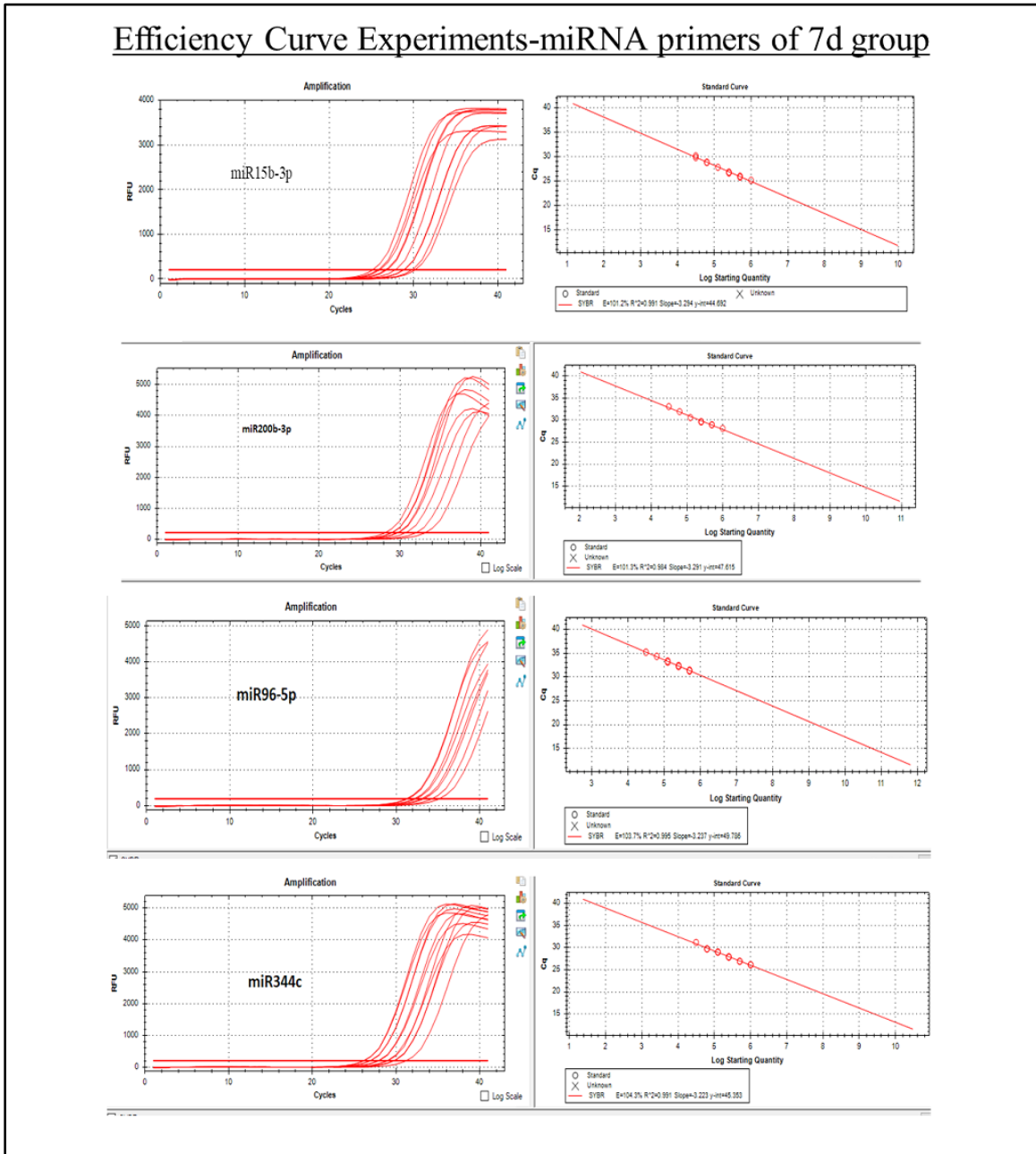


Table B-1 Significantly Expressed miRNAs in SCI+SLN vs no SCI experimental conditions in the 1d group.

| Downregulated miRNAs | log2FoldChange | padj |
|-----------------------------|-----------------------|-------------|
| mmu-miR-490-5p | -1.406763741 | 2.20066E-09 |
| mmu-miR-615-3p | -1.172605701 | 4.80444E-09 |
| mmu-miR-34a-5p | -0.960048377 | 5.63114E-08 |
| mmu-miR-326-3p | -0.760032154 | 2.4478E-05 |
| mmu-miR-431-3p | -0.553257926 | 9.83489E-05 |
| mmu-miR-383-5p | -0.614274295 | 0.00022314 |
| mmu-miR-1843b-3p | -0.629695486 | 0.000903909 |
| mmu-miR-328-3p | -0.717072126 | 0.001810849 |
| mmu-miR-185-3p | -0.634540219 | 0.002645357 |
| mmu-miR-532-3p | -0.747138918 | 0.003768639 |
| mmu-miR-874-3p | -0.567230429 | 0.004159201 |
| mmu-miR-128-3p | -0.541532547 | 0.004598227 |
| mmu-miR-204-3p | -0.693800019 | 0.005064516 |
| mmu-miR-1224-3p | -0.571058857 | 0.007570014 |
| mmu-miR-3102-3p | -0.787221916 | 0.007626617 |
| mmu-miR-485-3p | -0.412217632 | 0.007798225 |
| mmu-miR-3547-3p | -0.834705056 | 0.008142446 |
| mmu-miR-196b-5p | -0.531584695 | 0.008575566 |
| mmu-miR-337-5p | -0.489051727 | 0.013011979 |
| mmu-miR-702-3p | -0.68049696 | 0.014789496 |
| mmu-miR-3552 | -1.035148171 | 0.016163916 |
| mmu-let-7c-5p | -0.360417099 | 0.018926731 |
| mmu-miR-700-5p | -0.544287259 | 0.019957738 |
| mmu-miR-124-3p | -0.409160789 | 0.019957738 |
| mmu-miR-1249-3p | -0.625881128 | 0.019973185 |
| mmu-miR-149-5p | -0.447804621 | 0.020159641 |
| mmu-miR-129-5p | -0.39084824 | 0.021287985 |
| mmu-miR-484 | -0.507366538 | 0.022597015 |
| mmu-miR-335-5p | -0.47559207 | 0.022597015 |
| mmu-miR-212-5p | -0.360048196 | 0.023360915 |
| mmu-miR-218-5p | -0.302428123 | 0.023865219 |
| mmu-miR-12193-3p | -1.655092536 | 0.025119066 |
| mmu-miR-667-3p | -0.504294581 | 0.025119066 |
| mmu-let-7d-5p | -0.426367407 | 0.027511949 |
| mmu-miR-668-3p | -0.353428762 | 0.027511949 |
| mmu-let-7b-5p | -0.334935199 | 0.027511949 |
| mmu-miR-346-5p | -0.386333251 | 0.029995841 |
| mmu-miR-540-3p | -0.363506619 | 0.040567394 |

| Downregulated miRNAs | log2FoldChange | padj |
|-----------------------------|-----------------------|-------------|
| mmu-miR-3084-5p | -0.830962197 | 0.044312614 |
| mmu-miR-370-3p | -0.325701714 | 0.048943824 |

| Upregulated miRNAs | log2FoldChange | padj |
|---------------------------------|-----------------------|-------------|
| mmu-miR-21a-5p | 2.396786354 | 4.26368E-28 |
| mmu-miR-223-3p | 4.140075503 | 8.49426E-28 |
| mmu-miR-27a-5p | 2.793120586 | 3.18811E-25 |
| novel:chr3_14358 | 3.802388503 | 1.02076E-20 |
| mmu-miR-6240 | 2.789284918 | 3.1814E-16 |
| mmu-miR-223-5p | 2.894867646 | 3.6108E-14 |
| mmu-miR-142a-5p | 1.866129181 | 2.46582E-13 |
| mmu-miR-6538 | 3.976650426 | 4.69218E-13 |
| mmu-miR-5126 | 5.352490484 | 8.8465E-12 |
| mmu-miR-2137 | 5.475932218 | 1.91262E-11 |
| mmu-miR-144-5p | 2.188833549 | 3.39651E-11 |
| novel:chr8_20674 | 3.051428411 | 1.58629E-09 |
| novel:chr10_750 | 5.996926616 | 6.73589E-09 |
| mmu-miR-142a-3p | 2.29349848 | 8.04593E-09 |
| mmu-miR-6481 | 3.041210144 | 3.50622E-08 |
| mmu-miR-203-3p | 1.090133837 | 1.1186E-07 |
| mmu-miR-6236 | 2.402448241 | 1.44841E-07 |
| novel:chr5_16839 | 5.373599321 | 2.91432E-07 |
| mmu-miR-451a | 2.541918076 | 5.32392E-07 |
| mmu-miR-486a-3p | 1.51901031 | 7.9975E-07 |
| mmu-miR-20a-5p | 1.211181686 | 1.39744E-06 |
| mmu-miR-486b-3p | 1.506983983 | 1.39744E-06 |
| mmu-miR-582-3p | 0.687883473 | 2.64722E-06 |
| novel:chrX_22879 | 1.120308562 | 3.70194E-06 |
| novel:chr12_2983 | 5.710358995 | 1.06449E-05 |
| mmu-miR-6238 | 2.51480821 | 1.30544E-05 |
| novel:chrX_22717 | 5.486188349 | 2.81755E-05 |
| mmu-miR-25-3p | 0.665423835 | 4.03224E-05 |
| mmu-miR-23a-3p | 0.617436136 | 8.53675E-05 |
| mmu-miR-15b-5p | 0.900518487 | 9.05366E-05 |
| mmu-miR-486a-5p=mmu-miR-486b-5p | 1.164932566 | 0.000146005 |

| Upregulated miRNAs | log2FoldChange | padj |
|---------------------------------|-----------------------|-------------|
| mmu-miR-155-5p | 0.744768802 | 0.000189824 |
| mmu-miR-101b-3p | 0.713513634 | 0.000191615 |
| mmu-miR-101a-3p | 0.708126902 | 0.000263926 |
| mmu-miR-101c | 0.707992839 | 0.000268017 |
| mmu-miR-335-3p | 0.49335811 | 0.00035942 |
| mmu-miR-144-3p | 2.613300668 | 0.000393143 |
| novel:chr8_20571 | 1.071838507 | 0.000773834 |
| mmu-miR-101b-5p | 1.485238986 | 0.000903909 |
| mmu-miR-24-2-5p | 0.905376176 | 0.001126284 |
| novel:chr2_13010 | 4.709717009 | 0.001126284 |
| mmu-miR-17-5p | 0.807543354 | 0.001194682 |
| mmu-miR-153-3p | 0.723356233 | 0.00167928 |
| mmu-let-7c-1-3p | 0.832353778 | 0.002987331 |
| mmu-miR-148a-3p | 0.636108723 | 0.004763975 |
| mmu-miR-5099 | 0.70125507 | 0.004772748 |
| mmu-miR-381-3p | 0.578869547 | 0.004832061 |
| mmu-miR-5121 | 0.682722229 | 0.004957726 |
| mmu-miR-29b-3p | 0.414252028 | 0.005112975 |
| mmu-miR-379-3p | 0.411639467 | 0.006231946 |
| mmu-miR-3068-3p | 0.567189366 | 0.006527645 |
| mmu-miR-22-3p | 0.316840743 | 0.008575566 |
| mmu-miR-146b-5p | 0.557899877 | 0.010201228 |
| mmu-miR-122-5p | 1.740664101 | 0.013672715 |
| mmu-miR-27b-3p | 0.386614267 | 0.014789496 |
| mmu-let-7a-1-3p=mmu-let-7c-2-3p | 0.73560972 | 0.014789496 |
| novel:chr10_1050 | 1.047311103 | 0.014789496 |
| mmu-miR-140-3p | 0.298548845 | 0.01782472 |
| mmu-miR-300-3p | 0.469139617 | 0.018036412 |
| mmu-miR-30a-5p | 0.415234532 | 0.018392455 |
| mmu-miR-1191a | 0.614929197 | 0.0184692 |
| mmu-miR-30c-5p | 0.349055557 | 0.019266052 |
| mmu-miR-181a-1-3p | 0.414423166 | 0.019831178 |
| mmu-miR-200b-3p | 1.479574246 | 0.019831178 |
| mmu-miR-32-5p | 0.804691208 | 0.020481222 |
| mmu-miR-96-5p | 0.520911795 | 0.021287985 |
| mmu-miR-350-3p | 0.651150029 | 0.022597015 |
| mmu-miR-106b-5p | 0.755222372 | 0.023360915 |
| mmu-miR-3962 | 0.945991659 | 0.023360915 |
| mmu-miR-106b-3p | 0.37869889 | 0.025119066 |
| mmu-miR-127-5p | 0.559010742 | 0.025709096 |

| Upregulated miRNAs | log2FoldChange | padj |
|---------------------------|-----------------------|-------------|
| mmu-miR-376b-3p | 0.452223441 | 0.027511949 |
| mmu-miR-30e-5p | 0.36502483 | 0.029995841 |
| mmu-miR-15b-3p | 1.020892438 | 0.029995841 |
| mmu-let-7f-1-3p | 0.778303852 | 0.037136332 |
| mmu-miR-384-3p | 0.436654499 | 0.03973835 |
| mmu-miR-135a-5p | 0.437621275 | 0.040064415 |
| mmu-miR-467a-5p | 0.645414592 | 0.04297113 |
| mmu-miR-382-3p | 0.365238463 | 0.046760409 |
| mmu-miR-219a-5p | 0.575703611 | 0.047414026 |

Table B-2 Significantly Expressed Novel miRNAs in SCI+SLN vs no SCI conditions in the 1d group.

| Novel miRNAs-provisional ID | log2FoldChange | padj | mature sequence |
|------------------------------------|-----------------------|-------------|--------------------------|
| novel:chr3_14358 | 3.802388503 | 1.02076E-20 | ccaggaguggagccugc |
| novel:chr8_20674 | 3.051428411 | 1.58629E-09 | uucuuaguugguggagc |
| novel:chr10_750 | 5.996926616 | 6.73589E-09 | uuccggagcgggaggaau |
| novel:chr5_16839 | 5.373599321 | 2.91432E-07 | cggcggcggcggcucug |
| novel:chrX_22879 | 1.120308562 | 3.70194E-06 | agugugcuuggaauaaaa |
| novel:chr12_2983 | 5.710358995 | 1.06449E-05 | gcccggcgggagcgcug |
| novel:chrX_22717 | 5.486188349 | 2.81755E-05 | aggauagaagucuuacag |
| novel:chr8_20571 | 1.071838507 | 0.000773834 | cgugggcacauuacccgucugaca |
| novel:chr2_13010 | 4.709717009 | 0.001126284 | aggacaauaguagguaag |
| novel:chr10_1050 | 1.047311103 | 0.014789496 | ggagaggaacaacucugagu |

Table B-3 Significantly Expressed miRNAs in SCI+mino VS SCI+SLN conditions in the 1d group.

| Upregulated miRNAs | log2FoldChange | padj |
|---------------------------|-----------------------|-------------|
| mmu-miR-326-3p | 0.775202407 | 6.75405E-05 |
| mmu-miR-490-5p | 0.986854246 | 0.000230539 |
| mmu-miR-34a-5p | 0.669754197 | 0.000780876 |
| mmu-miR-3547-3p | 0.991681947 | 0.001449665 |
| mmu-miR-431-3p | 0.484010407 | 0.00148652 |
| mmu-miR-702-3p | 0.843252652 | 0.001679895 |
| mmu-miR-1224-3p | 0.661281733 | 0.001679895 |
| mmu-miR-700-5p | 0.686062728 | 0.001795167 |
| mmu-miR-667-3p | 0.64482345 | 0.003182194 |
| mmu-miR-3102-3p | 0.838838978 | 0.00445857 |
| mmu-miR-342-3p | 0.612976741 | 0.00445857 |
| mmu-miR-383-5p | 0.505786373 | 0.00472027 |
| mmu-miR-132-3p | 0.3672234 | 0.005081216 |
| mmu-miR-150-5p | 0.312804446 | 0.005081216 |
| mmu-miR-1224-5p | 0.498019457 | 0.0065258 |
| mmu-miR-145a-5p | 0.504800432 | 0.019167138 |
| mmu-miR-491-5p | 0.842688408 | 0.031430284 |
| mmu-miR-212-3p | 0.493479764 | 0.036625813 |
| mmu-miR-877-3p | 0.458415773 | 0.038413889 |
| mmu-miR-1839-5p | 0.224414178 | 0.041196441 |
| mmu-miR-133a-3p | 0.312249049 | 0.04704245 |
| mmu-miR-744-5p | 0.405428994 | 0.049493662 |

| Downregulated miRNAs | log2FoldChange | padj |
|-----------------------------|-----------------------|-------------|
| mmu-miR-30e-5p | -0.666528095 | 6.75405E-05 |
| mmu-miR-140-5p | -0.780823956 | 6.75405E-05 |
| mmu-miR-153-3p | -0.920571257 | 6.75405E-05 |
| mmu-miR-219a-5p | -1.082693637 | 6.75405E-05 |
| novel:chrX 22879 | -1.08859275 | 6.75405E-05 |
| mmu-miR-22-3p | -0.465409307 | 6.99127E-05 |
| mmu-miR-21a-5p | -0.970651951 | 0.000191803 |
| mmu-miR-335-3p | -0.525531318 | 0.000276442 |
| mmu-miR-101a-3p | -0.739993267 | 0.000276442 |
| mmu-miR-101c | -0.740852517 | 0.000276442 |
| mmu-miR-144-5p | -1.282935504 | 0.000292712 |

| Downregulated miRNAs | log2FoldChange | padj |
|---------------------------------|-----------------------|-------------|
| mmu-miR-142a-5p | -1.025981708 | 0.000374902 |
| mmu-miR-29a-3p | -0.488077249 | 0.00039223 |
| mmu-miR-136-5p | -0.53693542 | 0.000479813 |
| mmu-miR-96-5p | -0.718910675 | 0.000981089 |
| mmu-miR-381-3p | -0.665635479 | 0.001349175 |
| mmu-miR-29c-3p | -0.688845839 | 0.001694767 |
| mmu-let-7a-1-3p=mmu-let-7c-2-3p | -0.914338805 | 0.001694767 |
| mmu-miR-32-5p | -1.051383937 | 0.001694767 |
| mmu-miR-142a-3p | -1.296627056 | 0.001694767 |
| mmu-miR-24-2-5p | -0.890523032 | 0.001780252 |
| novel:chr8_20571 | -1.016217864 | 0.001795167 |
| mmu-miR-376b-3p | -0.590265491 | 0.00299895 |
| mmu-miR-1191a | -0.721905699 | 0.004069559 |
| mmu-miR-101b-3p | -0.589800429 | 0.004217304 |
| mmu-miR-203-3p | -0.637350139 | 0.005627752 |
| mmu-miR-384-3p | -0.557681108 | 0.006317215 |
| mmu-miR-582-3p | -0.429812721 | 0.007892912 |
| mmu-miR-135a-5p | -0.548135935 | 0.007892912 |
| mmu-miR-148a-3p | -0.602391075 | 0.009436649 |
| mmu-miR-30d-5p | -0.259753313 | 0.012304961 |
| mmu-miR-29b-3p | -0.384159613 | 0.012304961 |
| novel:chr10_403 | -1.459211628 | 0.012304961 |
| mmu-miR-186-5p | -0.491823547 | 0.014434065 |
| mmu-miR-300-3p | -0.480315033 | 0.01692456 |
| mmu-miR-7043-3p | -0.915046839 | 0.01692456 |
| mmu-miR-135b-5p | -0.569283244 | 0.017400456 |
| mmu-miR-33-5p | -1.366715547 | 0.017400456 |
| mmu-miR-455-5p | -0.52576836 | 0.018686403 |
| mmu-miR-15b-5p | -0.58533984 | 0.020028382 |
| mmu-miR-6240 | -0.945916438 | 0.02075819 |
| mmu-miR-223-5p | -0.807339439 | 0.022345672 |
| mmu-miR-338-3p | -0.417334953 | 0.022907303 |
| novel:chr3_14358 | -0.923337333 | 0.022907303 |
| mmu-miR-136-3p | -0.492472429 | 0.023838533 |
| mmu-miR-872-5p | -0.374210267 | 0.023846726 |
| mmu-let-7f-1-3p | -0.828420366 | 0.023846726 |
| mmu-miR-467a-5p | -0.710796645 | 0.025204786 |
| mmu-miR-27a-3p | -0.371255522 | 0.02641181 |
| mmu-miR-486a-3p | -0.738433502 | 0.031152424 |
| mmu-miR-486b-3p | -0.749549907 | 0.031152424 |

| Downregulated miRNAs | log2FoldChange | padj |
|-----------------------------|-----------------------|-------------|
| mmu-miR-144-3p | -1.71871538 | 0.033441325 |
| mmu-miR-24-1-5p | -0.655696883 | 0.034445367 |
| mmu-miR-434-5p | -0.445917465 | 0.04051662 |
| mmu-miR-379-3p | -0.327215215 | 0.040547708 |
| mmu-miR-3068-5p | -0.505703891 | 0.041196441 |
| mmu-miR-451a | -1.238290632 | 0.042013898 |
| mmu-miR-6236 | -0.895206657 | 0.046897087 |
| mmu-miR-194-5p | -0.327649549 | 0.047435366 |

Table B-4 Significantly Expressed Novel miRNAs in SCI+mino vs SCI+SLN conditions 1d group.

| Novel miRNAs-provisional ID | log2FoldChange | padj | mature sequence |
|------------------------------------|-----------------------|-------------|--------------------------|
| novel:chr10_403 | -1.459211628 | 0.012305 | ggaagagcacaugucua |
| novel:chr3_14358 | -0.923337333 | 0.022907 | ccaggaguggagccugc |
| novel:chr8_20571 | -1.016217864 | 0.001795 | cgugggcacauuacccgucugaca |
| novel:chrX_22879 | -1.08859275 | 6.75E-05 | agugugcuuggaauaaaa |

Table B-5 Significantly Expressed miRNA in SCI+mino vs no SCI conditions in the 1d group.

| Upregulated miRNA | log2FoldChange | padj |
|---------------------------------|-----------------------|-------------|
| novel:chr10_750 | 5.53252972 | 3.51E-07 |
| novel:chr5_16839 | 5.249302249 | 1.18E-06 |
| mmu-miR-2137 | 4.959733676 | 5.35E-09 |
| novel:chr12_2983 | 4.672034558 | 0.001836 |
| novel:chrX_23260 | 4.599433425 | 0.007149 |
| mmu-miR-5126 | 4.557610401 | 3.5E-08 |
| novel:chr2_13010 | 4.29623779 | 0.010735 |
| mmu-miR-223-3p | 3.593552026 | 2.06E-20 |
| mmu-miR-6538 | 3.010942721 | 3.73E-07 |
| novel:chr3_14358 | 2.87905117 | 2.54E-11 |
| mmu-miR-6481 | 2.435764525 | 4.81E-05 |
| novel:chr8_20674 | 2.319458003 | 2.58E-05 |
| mmu-miR-27a-5p | 2.282671637 | 1.76E-16 |
| mmu-miR-6238 | 2.131564682 | 0.000981 |
| mmu-miR-223-5p | 2.087528207 | 4.02E-07 |
| mmu-miR-6240 | 1.84336848 | 6.13E-07 |
| mmu-miR-6236 | 1.507241583 | 0.010166 |
| mmu-miR-21a-5p | 1.426134403 | 1.13E-09 |
| mmu-miR-101b-5p | 1.293987985 | 0.012155 |
| mmu-miR-155-5p | 0.914821458 | 1.2E-06 |
| mmu-miR-486a-5p=mmu-miR-486b-5p | 0.884048685 | 0.019825 |
| mmu-miR-142a-5p | 0.840147473 | 0.012155 |
| mmu-miR-20a-5p | 0.726319092 | 0.029866 |
| mmu-miR-23a-3p | 0.499006122 | 0.007256 |

| Downregulated miRNA | log2FoldChange | padj |
|----------------------------|-----------------------|-------------|
| mmu-miR-218-5p | -0.361529077 | 0.014042 |
| mmu-miR-543-3p | -0.602042072 | 0.012155 |
| mmu-miR-615-3p | -0.698011311 | 0.005191 |

Table B-6 Significantly Expressed Novel miRNA in SCI+mino vs no SCI conditions at the 1d timepoint.

| Novel miRNAs-provisional ID | log2FoldChange | padj | mature sequence |
|------------------------------------|-----------------------|-------------|------------------------|
| novel:chr10_750 | 5.53252972 | 3.51E-07 | uuccggagcgggaggaau |
| novel:chr12_2983 | 4.672034558 | 0.001836 | gcccgggcggagcgug |
| novel:chr2_13010 | 4.29623779 | 0.010735 | aggaacauguagguaag |
| novel:chr3_14358 | 2.87905117 | 2.54E-11 | ccaggaguggagccugc |
| novel:chr5_16839 | 5.249302249 | 1.18E-06 | cggcggcggcggcug |
| novel:chr8_20674 | 2.319458003 | 2.58E-05 | uucuuaguuggugagc |
| novel:chrX_23260 | 4.599433425 | 0.007149 | gggccucgcuccacccccac |

Table B-7 known miRNA in SCI+mino vs SCI+SLN condition at the 7d timepoint.

| Downregulated miRNA | log2FoldChange | P value |
|----------------------------|-----------------------|----------------|
| mmu-miR-669m-3p | -3.981279841 | 0.03273211 |
| mmu-miR-6977-3p | -2.152363017 | 0.025535938 |
| mmu-miR-511-3p | -1.468967638 | 0.029153666 |
| mmu-miR-200b-3p | -0.802564095 | 0.011146122 |
| mmu-miR-15b-3p | -0.711019935 | 0.01590731 |

| Upregulated miRNA | log2FoldChange | P value |
|--------------------------|-----------------------|----------------|
| mmu-miR-96-5p | 0.430949724 | 0.030018103 |
| mmu-miR-344e-3p | 0.751202457 | 0.018296892 |
| mmu-miR-7030-3p | 1.73534393 | 0.043422181 |

Table B-8 Novel miRNA in SCI+mino vs SCI+SLN conditions at the 7d timepoint.

| ID | log2FoldChange | p value | mature sequence |
|------------------|-----------------------|----------------|-------------------------|
| Novel:chr9_31338 | -3.647202686 | 0.041724681 | uucacaguggacuccagcacagg |
| Novel:chr9_30653 | -3.063817737 | 0.021489132 | ucucugcugcuuuccuccuaga |
| Novel:chr8_29898 | -1.047128703 | 0.020149608 | uucuuaguugguggagc |
| Novel:chr11_3017 | -0.524794829 | 0.014587425 | agccauccucugcuacca |
| Novel:chr5_22991 | 2.439037417 | 0.001182245 | cugucucuggcugggccu |
| Novel:chr4_22614 | 2.439037417 | 0.001182245 | cugucucuggcugggccu |

Table B-9 The 29 miRNAs that were excluded because they were not from the miRNAs that were found the miRNA in SCI+SLN compared to baseline.

| Downregulated | Fold change | padj |
|----------------------|--------------------|-------------|
| mmu-miR-135b-5p | -0.569283244 | 0.0174 |
| mmu-miR-136-3p | -0.492472429 | 0.023839 |
| mmu-miR-136-5p | -0.53693542 | 0.00048 |
| mmu-miR-140-5p | -0.780823956 | 6.75E-05 |
| mmu-miR-186-5p | -0.491823547 | 0.014434 |
| mmu-miR-194-5p | -0.327649549 | 0.047435 |
| mmu-miR-24-1-5p | -0.655696883 | 0.034445 |
| mmu-miR-27a-3p | -0.371255522 | 0.026412 |
| mmu-miR-29a-3p | -0.488077249 | 0.000392 |
| mmu-miR-29c-3p | -0.688845839 | 0.001695 |
| mmu-miR-3068-5p | -0.505703891 | 0.041196 |
| mmu-miR-30d-5p | -0.259753313 | 0.012305 |
| mmu-miR-33-5p | -1.366715547 | 0.0174 |
| mmu-miR-338-3p | -0.417334953 | 0.022907 |
| mmu-miR-434-5p | -0.445917465 | 0.040517 |
| mmu-miR-455-5p | -0.52576836 | 0.018686 |
| mmu-miR-7043-3p | -0.915046839 | 0.016925 |
| mmu-miR-872-5p | -0.374210267 | 0.023847 |

| Upregulated | Fold change | padj |
|--------------------|--------------------|-------------|
| mmu-miR-1224-5p | 0.498019 | 0.006526 |
| mmu-miR-132-3p | 0.367223 | 0.005081 |
| mmu-miR-133a-3p | 0.312249 | 0.047042 |
| mmu-miR-145a-5p | 0.5048 | 0.019167 |
| mmu-miR-150-5p | 0.312804 | 0.005081 |
| mmu-miR-1839-5p | 0.224414 | 0.041196 |
| mmu-miR-212-3p | 0.49348 | 0.036626 |
| mmu-miR-342-3p | 0.612977 | 0.004459 |
| mmu-miR-491-5p | 0.842688 | 0.03143 |
| mmu-miR-744-5p | 0.405429 | 0.049494 |
| mmu-miR-877-3p | 0.458416 | 0.038414 |

APPENDIX C: SUPPLEMENTARY FIGURES AND TABLE OF CHAPTER 3

Figure C1. List of genes miR-21-5p uploaded to DAVID software

The screenshot shows the DAVID Gene Name Batch Viewer interface. The top navigation bar includes links for Home, Start Analysis, Shortcut to DAVID Tools, Technical Center, Downloads & APIs, Term of Service, About DAVID, and About LHRI. The main content area is titled 'Gene List Report' and shows the current gene list as 'List_1' and the background as 'Mus musculus'. There are 14 DAVID IDs listed. A table on the right displays the gene details, including ENSEMBL_GENE_ID, Gene Name, Related Genes, and Species. The species for all genes is Mus musculus.

| ENSEMBL_GENE_ID | Gene Name | Related Genes | Species |
|--------------------|--|--------------------|------------------------------|
| ENSMUSG00000020702 | chemokine (C-C motif) ligand 1 (Ccl1) | RG | Mus musculus |
| ENSMUSG00000021772 | NFkB inhibitor interacting Bas-like protein 1(Nkiras1) | RG | Mus musculus |
| ENSMUSG00000025880 | SMAD family member 7(Smad7) | RG | Mus musculus |
| ENSMUSG00000027718 | interleukin 21(Il21) | RG | Mus musculus |
| ENSMUSG00000027776 | interleukin 12a(Il12a) | RG | Mus musculus |
| ENSMUSG00000029438 | B cell CLL/lymphoma 7A(Bcl7a) | RG | Mus musculus |
| ENSMUSG00000035493 | transforming growth factor, beta induced(Tofib) | RG | Mus musculus |
| ENSMUSG00000039990 | erythroid differentiation regulatory factor 1(Edrf1) | RG | Mus musculus |
| ENSMUSG00000041417 | phosphatidylinositol 3-kinase, regulatory subunit, polypeptide 1 (p85 alpha)(Pik3r1) | RG | Mus musculus |
| ENSMUSG00000048249 | CREB3 regulatory factor(Crebrf) | RG | Mus musculus |
| ENSMUSG00000048251 | B cell leukemia/lymphoma 11B(Bcl11b) | RG | Mus musculus |
| ENSMUSG00000049001 | neuron-derived neurotrophic factor(Ndnf) | RG | Mus musculus |
| ENSMUSG00000049107 | neurotrophin 3(Ntf3) | RG | Mus musculus |
| ENSMUSG00000057967 | fibroblast growth factor 18(Fgf18) | RG | Mus musculus |

Figure C2. DAVID_ Functional Annotation Tools miR-21-5p – step 1

The screenshot shows the DAVID Analysis Wizard interface. At the top, there is a blue header with the DAVID logo and the text "Analysis Wizard" and "DAVID Bioinformatics Resources 6.8, NIAID/NIH". Below the header is a navigation bar with links: Home, Start Analysis, Shortcut to DAVID Tools, Technical Center, Downloads & APIs, Term of Service, About DAVID, and About LHRI.

The main content area is divided into two sections. On the left is the "Gene List Manager" sidebar, which includes a "List" tab. It contains a dropdown menu for species selection, currently set to "Mus musculus(14)". Below this is a "List Manager" section with a dropdown showing "List_1" and a "Select List to:" section with buttons for "Use", "Rename", "Remove", "Combine", and "Show Gene List".

The main content area is titled "Analysis Wizard" and contains the following steps:

- Step 1. Successfully submitted gene list
 - Current Gene List: List_1
 - Current Background: Mus musculus
- Step 2. Analyze above gene list with one of DAVID tools
 - Which DAVID tools to use?
 - [Functional Annotation Tool](#)
 - [Functional Annotation Clustering](#)
 - [Functional Annotation Chart](#)
 - [Functional Annotation Table](#)
 - [Gene Functional Classification Tool](#)
 - [Gene ID Conversion Tool](#)
 - [Gene Name Batch Viewer](#)

Figure C3. DAVID_ Functional Annotation Result Summary miR-21-5p – step 2

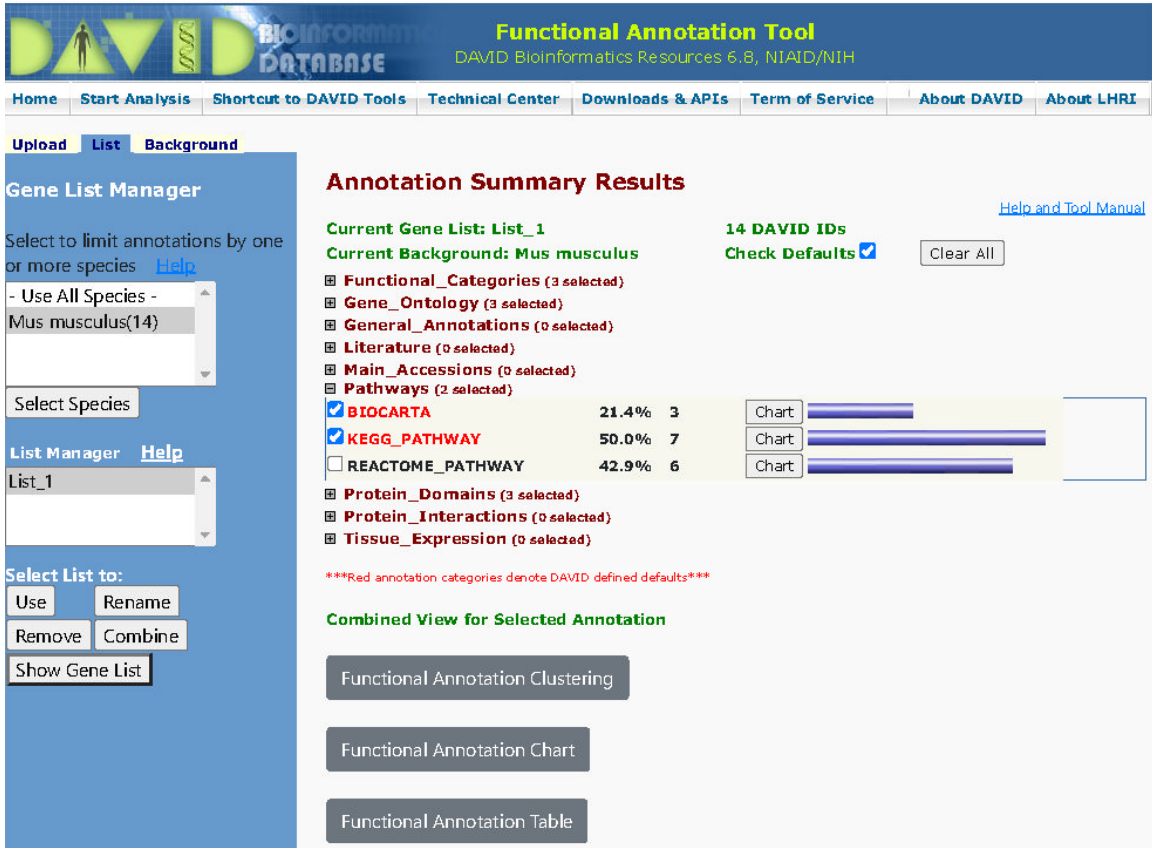



Figure C4. DAVID output – step 3


DAVID Bioinformatics Resources 6.8
Laboratory of Human Retrovirology and Immunoinformatics (LHRI)

Functional Annotation Chart

[Help and Manual](#)

Current Gene List: List_1
Current Background: Mus musculus
14 DAVID IDs
Options

3 chart records
[Download File](#)

| Sublist | Category | Term | RT | Genes | Count | % | P-Value | Benjamini |
|--------------------------|--------------|---|----|---|-------|------|---------|-----------|
| <input type="checkbox"/> | KEGG_PATHWAY | Iak-STAT signaling pathway | RT | <div style="width: 100%; height: 10px; background-color: #0056b3;"></div> | 3 | 21.4 | 5.0E-3 | 4.1E-1 |
| <input type="checkbox"/> | KEGG_PATHWAY | Cytokine-cytokine receptor interaction | RT | <div style="width: 100%; height: 10px; background-color: #0056b3;"></div> | 3 | 21.4 | 1.4E-2 | 5.6E-1 |
| <input type="checkbox"/> | KEGG_PATHWAY | Inflammatory bowel disease (IBD) | RT | <div style="width: 100%; height: 10px; background-color: #0056b3;"></div> | 2 | 14.3 | 4.5E-2 | 9.3E-1 |
| <input type="checkbox"/> | KEGG_PATHWAY | Melanoma | RT | <div style="width: 100%; height: 10px; background-color: #0056b3;"></div> | 2 | 14.3 | 5.4E-2 | 9.3E-1 |
| <input type="checkbox"/> | KEGG_PATHWAY | Toll-like receptor signaling pathway | RT | <div style="width: 100%; height: 10px; background-color: #0056b3;"></div> | 2 | 14.3 | 7.6E-2 | 9.3E-1 |
| <input type="checkbox"/> | KEGG_PATHWAY | Chagas disease (American trypanosomiasis) | RT | <div style="width: 100%; height: 10px; background-color: #0056b3;"></div> | 2 | 14.3 | 7.8E-2 | 9.3E-1 |
| <input type="checkbox"/> | KEGG_PATHWAY | Amoebiasis | RT | <div style="width: 100%; height: 10px; background-color: #0056b3;"></div> | 2 | 14.3 | 8.8E-2 | 9.3E-1 |
| <input type="checkbox"/> | KEGG_PATHWAY | Neurotrophin signaling pathway | RT | <div style="width: 100%; height: 10px; background-color: #0056b3;"></div> | 2 | 14.3 | 9.2E-2 | 9.3E-1 |

from your list are not in the output.

Figure C5. Pathway miR-21-5p – step 4

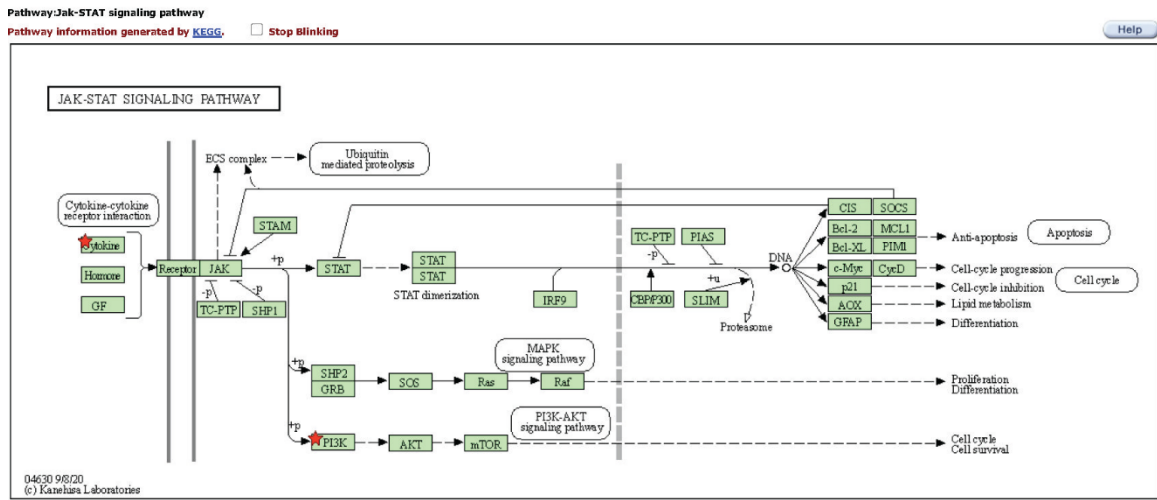


Figure C6. miR-15b-5p target analysis - uploaded targets to DAVID software

3/15/2021 DAVID: Database for Annotation, Visualization, and Integrated Discovery (Laboratory of Human Retrovirology and Immunoinformatics (LHRI), National Institute of Allergies and Infectious Diseases (NIAID))

Gene Name Batch Viewer
DAVID Bioinformatics Resources 6.8, NIAID/NIH

[Home](#) | [Start Analysis](#) | [Shortcut to DAVID Tools](#) | [Technical Center](#) | [Downloads & APIs](#) | [Term of Service](#) | [About DAVID](#) | [About LHRI](#)

Upload | **List** | **Background**

Gene List Manager

Select to limit annotations by one or more species [Help](#)

- Use All Species -
Mus musculus(46)

Select Species

List Manager [Help](#)

List_1

Select List to:

Use

Gene List Report

[Help and Manual](#)

Current Gene List: List_1
Current Background: Mus musculus
46 DAVID IDs

[Download File](#)

| ENSEMBL_GENE_ID | Gene Name | Related Genes | Species |
|--------------------|---|---------------|--------------|
| ENSMUSG00000000184 | cavin_D2(Ccnd2) | RG | Mus musculus |
| ENSMUSG00000001089 | leucine zipper protein 1(Luzo1) | RG | Mus musculus |
| ENSMUSG00000002068 | cavin E1(Ccne1) | RG | Mus musculus |
| ENSMUSG00000009905 | 3-ketodihydrospingosine reductase(Kdsr) | RG | Mus musculus |
| ENSMUSG00000013033 | adhesion G protein-coupled receptor L1(Adgrl1) | RG | Mus musculus |
| ENSMUSG00000016619 | nucleoporin 50(Nup50) | RG | Mus musculus |
| ENSMUSG00000016664 | protein kinase C and casein kinase substrate in neurons 2(Pacsin2) | RG | Mus musculus |
| ENSMUSG00000019699 | thymoma viral proto-oncogene 3(Akt3) | RG | Mus musculus |
| ENSMUSG00000020015 | cyclin-dependent kinase 17(Cdk17) | RG | Mus musculus |
| ENSMUSG00000020151 | protein tyrosine phosphatase, receptor type, R(Ptprr) | RG | Mus musculus |
| ENSMUSG00000020152 | ARP2 actin-related protein 2(Actr2) | RG | Mus musculus |
| ENSMUSG00000021974 | fibroblast growth factor 9(Fgf9) | RG | Mus musculus |
| ENSMUSG00000024944 | ADP-ribosylation factor-like 2(Arl2) | RG | Mus musculus |
| ENSMUSG00000025217 | beta-transducin repeat containing protein(Btrc) | RG | Mus musculus |
| ENSMUSG00000025234 | ariadne RBR E3 ubiquitin protein ligase 1(Arh1) | RG | Mus musculus |
| ENSMUSG00000026764 | kinesin family member 5C(Kif5c) | RG | Mus musculus |
| ENSMUSG00000026873 | PHD finger protein 19(Phf19) | RG | Mus musculus |
| ENSMUSG00000027208 | fibroblast growth factor 7(Fgf7) | RG | Mus musculus |
| ENSMUSG00000028370 | pregnancy-associated plasma protein A(Pappa) | RG | Mus musculus |
| ENSMUSG00000028960 | ubiquitination factor E4B(Ube4b) | RG | Mus musculus |
| ENSMUSG00000029287 | transforming growth factor, beta receptor III(Tgbr3) | RG | Mus musculus |
| ENSMUSG00000029765 | plexin A4(Plxna4) | RG | Mus musculus |
| ENSMUSG00000029772 | S-adenosylhomocysteine hydrolase-like 2(Aheyl2) | RG | Mus musculus |
| ENSMUSG00000030870 | ubiquitin family domain containing 1(Ubfd1) | RG | Mus musculus |
| ENSMUSG00000031652 | NEED4 binding protein 1(N4bp1) | RG | Mus musculus |
| ENSMUSG00000032012 | nectin cell adhesion molecule 1(Nectn1) | RG | Mus musculus |
| ENSMUSG00000032601 | protein kinase, cAMP dependent regulatory, type II alpha(Prkar2a) | RG | Mus musculus |
| ENSMUSG00000036863 | synapse defective 1, Rho GTPase, homolog 2 (C. elegans)(Syde2) | RG | Mus musculus |
| ENSMUSG00000037010 | anelin(Anln) | RG | Mus musculus |
| ENSMUSG00000038696 | mitogen-activated protein kinase associated protein 1(Makap1) | RG | Mus musculus |
| ENSMUSG00000039782 | cytoplasmic polyadenylation element binding protein 2(Cpeb2) | RG | Mus musculus |
| ENSMUSG00000040929 | regulatory factor X, 3 (influences HLA class II expression)(Rfx3) | RG | Mus musculus |
| ENSMUSG00000041695 | potassium inwardly-rectifying channel, subfamily J, member 2(Kcnj2) | RG | Mus musculus |
| ENSMUSG00000044364 | transmembrane protein 74B(Tmem74b) | RG | Mus musculus |
| ENSMUSG00000044617 | zinc finger and BTB domain containing 39(Zbtb39) | RG | Mus musculus |
| ENSMUSG00000047888 | trinucleotide repeat containing 6b(Tnrc6b) | RG | Mus musculus |
| ENSMUSG00000048249 | CREB3 regulatory factor(Crebrf) | RG | Mus musculus |
| ENSMUSG00000049354 | DOB1 and CUL4 associated factor 7(Dcaf7) | RG | Mus musculus |
| ENSMUSG00000053626 | toll-like receptor 1(Tlr1) | RG | Mus musculus |
| ENSMUSG00000055567 | unc-80, NALCN activator(Unc80) | RG | Mus musculus |
| ENSMUSG00000057329 | B cell leukemia/lymphoma 2(Bcl2) | RG | Mus musculus |
| ENSMUSG00000063317 | ubiquitin specific peptidase 31(Usp31) | RG | Mus musculus |
| ENSMUSG00000063415 | cytochrome P450, family 26, subfamily b, polypeptide 1(Cyp26b1) | RG | Mus musculus |
| ENSMUSG00000074785 | plexin C1(Plxnc1) | RG | Mus musculus |
| ENSMUSG00000089682 | RCL2-like 2(Rcl2l2) | RG | Mus musculus |
| ENSMUSG00000089809 | RIKEN cDNA A930011G23 gene(A930011G23Rik) | RG | Mus musculus |

Figure C7. miR-15b-5p target analysis – step 1

The screenshot shows the DAVID Functional Annotation Tool interface. The browser address bar displays `dauid.ncicrf.gov/summary.jsp`. The page header includes the DAVID logo and the text "Functional Annotation Tool" and "DAVID Bioinformatics Resources 6.8, NIAID/NIH". A navigation menu contains links for Home, Start Analysis, Shortcut to DAVID Tools, Technical Center, Downloads & APIs, Term of Service, About DAVID, and About LHRI.

The main content area is divided into two sections:

- Gene List Manager (Left Sidebar):** Contains options to "Select to limit annotations by one or more species" (with a "Help" link), a dropdown menu currently set to "Mus musculus(46)", a "Select Species" button, a "List Manager" section with a dropdown for "List_1", and a "Select List to:" section with buttons for "Use", "Rename", "Remove", "Combine", and "Show Gene List".
- Annotation Summary Results (Main Area):** Displays "Current Gene List: List_1" and "Current Background: Mus musculus". It shows "46 DAVID IDs" and a "Check Defaults" checkbox (checked) next to a "Clear All" button. A list of annotation categories is shown with checkboxes and counts: Functional_Categories (3 selected), Gene_Ontology (3 selected), General_Annotations (0 selected), Literature (0 selected), Main_Accessions (0 selected), Pathways (2 selected), Protein_Domains (3 selected), Protein_Interactions (0 selected), and Tissue_Expression (0 selected). A red note states: "***Red annotation categories denote DAVID defined defaults***". Below this is a section titled "Combined View for Selected Annotation" with three buttons: "Functional Annotation Clustering", "Functional Annotation Chart", and "Functional Annotation Table".

Figure C8. miR-15b-5p target analysis – step 2

The screenshot shows the DAVID Functional Annotation Tool interface. The browser address bar displays `dauid.ncifcrf.gov/summary.jsp`. The page title is "Functional Annotation Tool" with the subtitle "DAVID Bioinformatics Resources 6.8, NIAID/NIH". The navigation menu includes "Home", "Start Analysis", "Shortcut to DAVID Tools", "Technical Center", "Downloads & APIs", "Term of Service", "About DAVID", and "About LHRI".

The main content area is titled "Annotation Summary Results" and includes a "Help and Tool Manual" link. The current gene list is "List_1" with 46 DAVID IDs. The current background is "Mus musculus". There are options to "Check Defaults" (checked) and "Clear All".

The "Gene List Manager" on the left allows selecting species (currently "Mus musculus(46)") and lists the current list as "List_1". It includes buttons for "Use", "Rename", "Remove", "Combine", and "Show Gene List".

The "Annotation Summary Results" section shows a table of selected annotations:

| Annotation Category | Percentage | Count | Chart |
|---|------------|-------|-------|
| <input checked="" type="checkbox"/> BIOCARTA | 17.4% | 8 | |
| <input type="checkbox"/> EC_NUMBER | 21.7% | 10 | |
| <input checked="" type="checkbox"/> KEGG_PATHWAY | 45.7% | 21 | |
| <input type="checkbox"/> REACTOME_PATHWAY | 52.2% | 24 | |

Other selected annotations include Functional_Categories (3), Gene_Ontology (3), Protein_Domains (3), and Pathways (2). Unselected categories include Literature, Main_Accessions, Protein_Interactions, and Tissue_Expression.

A note states: "***Red annotation categories denote DAVID defined defaults***".

At the bottom, there is a "Combined View for Selected Annotation" section with a "Functional Annotation Clustering" button.

Figure C9. miR-15b-5p target analysis – step 3

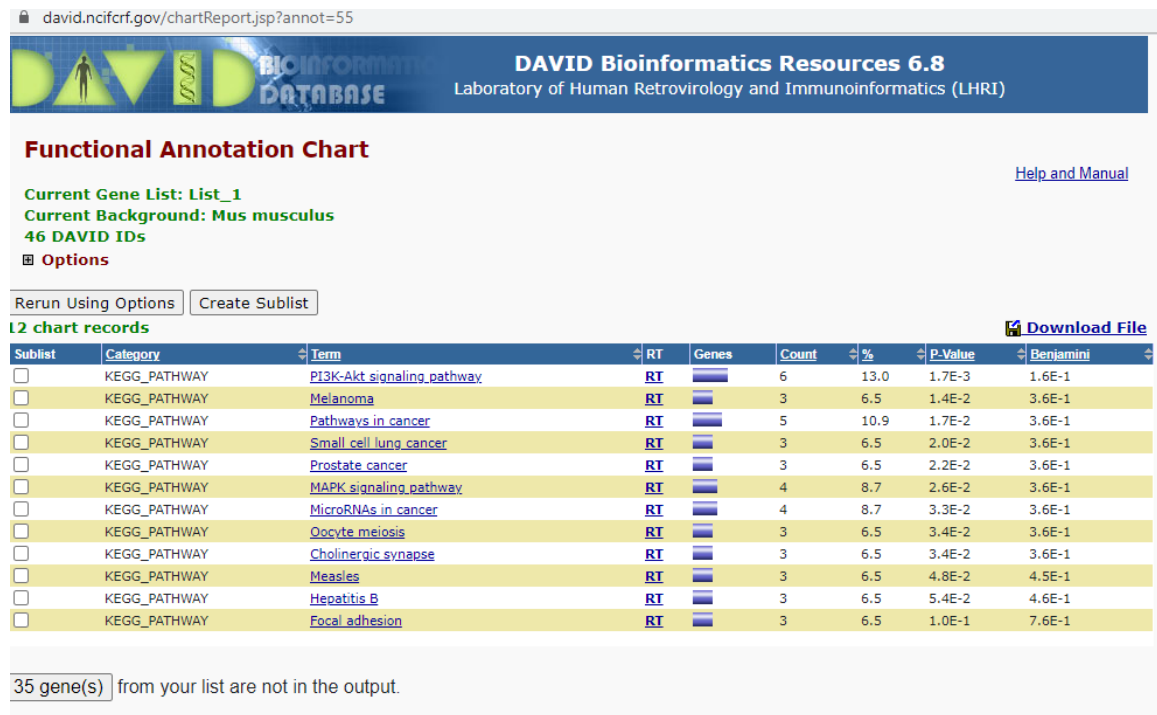


Figure C10. miR-15b-5p target analysis – step 4

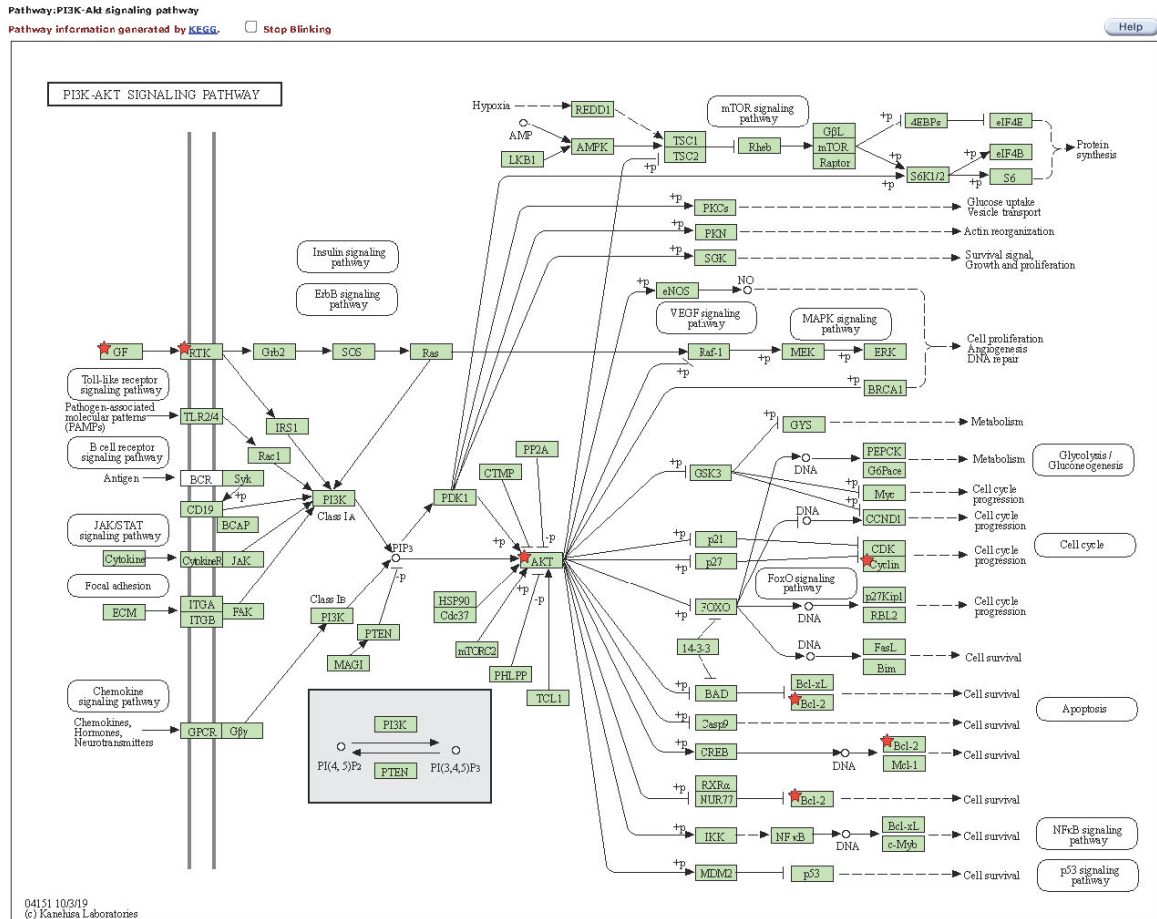


Figure C11. SCI parameters in proteins experiment-western blot.

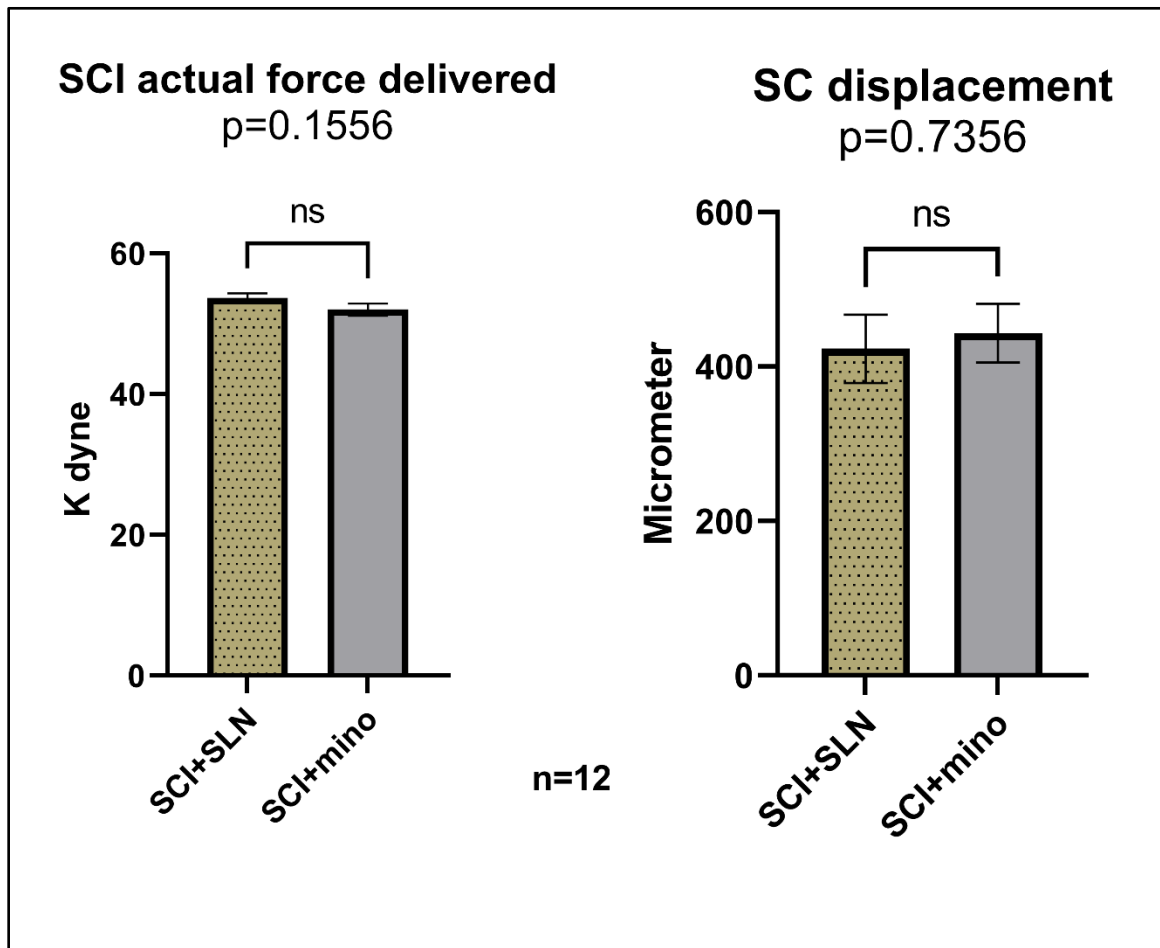


Table C-1 The reagents that were used in western blot experiments

1X PBS: 100 ml of 10x PBS (Sigma P5493-1L) + 900 ml milli Q H₂O
Ladder: (Bio-Rad, precision plus catalog # 1610374).
Glycine (Fisher BP381-500)
Tris-base (Fisher Bp152-1)
SDS (sodium dodecyl sulfate) (Bio-Rad, catalog # 161-0302)
Tween 20 (Fisher BP337-500)
Sodium deoxycholate (Sigma D-6750)
EDTA (Sigma E-5134)
Tris-HCl (OmniPur-9310)
Nonidet P-40 substitute (Fluka biochemika 74385)
Sodium azide (Sigma S2002-500)
4x Laemmli Sample buffer (Bio-Rad catalog # 1610747)
DC Protein Assay Reagent A (Bio-Rad catalog # 5000113)
Protein Assay Reagent B (Bio-Rad catalog # 5000114)
DC Protein Assay Reagent S (Bio-Rad catalog # 500-0115)
Pierce ECL 2 Western Blotting Substrate (Thermo Scientific Prod # 80196)
Polyacrylamide= 30% acrylamide/Bis-Solution 29:1 (Bio-Rad catalog # 1610156)
TEMED (Sigma T9281)
Ammonium persulfate (Bio-Rad catalog # 161-0700)
BSA standard solution (Bio-Rad, Quick Start Bovine Serum Albumin Standard catalog #5000206)
Protease inhibitors cocktail, EDTA free (abcam, ab270055)

APPENDIX D: SUPPLEMENTARY FIGURES OF CHAPTER 4

Figure D1. SCI parameters in histology experiments

